SCIENCE & TECHNOLOGY

ARS JOURNAL

A PUBLICATION OF THE AMERICAN ROCKET SOCIETY

VOLUME 30 NUMBER 10 OCTOBER 1960

LOS ANGELES PUBLIC LIBRARY

JAN 13 1961

STACKS

SURVEY ARTICLE

The Image Furnace as a Research Tool . . Nevin K. Hiester and R. E. De La Rue 928

CONTRIBUTED ARTICLES

Astronomical Constants and Their Importance in Lunar Trajectory Determination . . . C. Tross 938

Heat Diffusion . . . Reaction . . . C. Frederick Hansen 942

Gyro . . . Henry J. Kelley 947

Optimum . . . Rocket Vehicles in a . . . C. R. Faulders 954

Specific Impulse . . . Ralph E. Amster, Evan C. Noonan and George J. Bryan 960

Solid . . . Thrust Rocket . . . J. J. Gordon and R. J. Pollak 964

TECHNICAL NOTES

Effect of Different . . . Radio Telemetry . . . A. T. Bublitz and M. H. Nichols 969

Gyro Time Constants . . . Allen Lange 971

Satellite Librations . . . C. F. Bentinger 973

Dynamic Stabilization of a Small Body Between Two Equal Rotating Masses . . . Howard D. Graybar 975

Fifth Harmonic of Earth's Gravitational Field . . . Herman F. Michielsen 976

High Temperature Equilibria Involving Metallic Halides . . . L. J. Gordon 978

Heat Storage System for Satellite Powerplants . . . C. L. Walker, J. D. Matchett and R. J. Hanold 979

Shock Tube Design for Producing High Gas Temperatures . . . Hugh N. Powell 980

Optimum Contours for Propulsion Nozzles . . . Elden L. Keuth 983

DEPARTMENTS

Book Reviews 984

Technical Literature Digest 988

ANNOUNCEMENT OF VOLUME 1 OF ARS PROGRESS SERIES . . . 927

FORECAST

Major space age role for fluorine rocket fuel oxidizers

25,000 POUNDS OF LIQUID FLUORINE, from General's Metropolis, Ill., Works — ready for over-the-highway shipment in tank trucks of our own design to rocket and missile research centers throughout the nation.

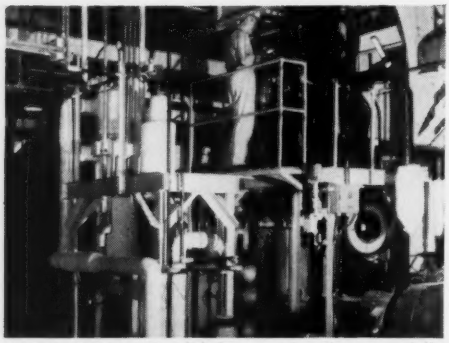

CHLORINE TRIFLUORIDE has been produced commercially by General Chemical for the past 10 years. Reactors like this one, located at General's Baton Rouge Works, have a capacity of more than 100 tons of CTF per year.

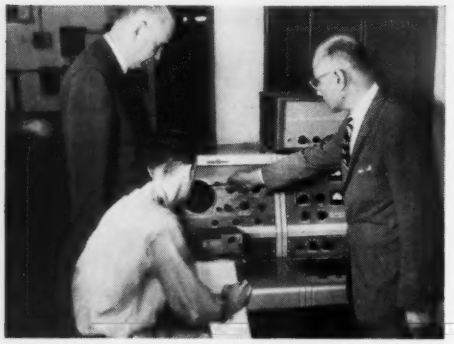

GENERAL CHEMICAL SCIENTISTS make use of the most advanced scientific equipment to investigate fluorine compounds as high energy oxidizers for solid propellants.

Potential applications for fluorine in rocketry extend over the entire propellant spectrum—from cryogenics to storable liquid to solid propellants

As America's primary producer of fluorine and halogen fluorides and leader in fluorochemical research, General Chemical helps support America's rocket and missile development programs in three key areas.

For investigation of cryogenic systems in the super-high energy range, General supplies large quantities of liquid fluorine. For investigation of advanced, high-energy storable liquid propellant systems, General supplies chlorine trifluoride (CTF) and other halogen fluorides. To serve both these areas, General has large existing production capacity, and can meet volume requirements.

In solid propellant systems, General is conducting intensive investigation under Government contract. Incorporation of the fluorine atom in the oxidizing molecule is part of this research.

If you would like technical data, we will be glad to send you our free bulletins, "Fluorine" and "Chlorine Trifluoride." Simply request them on company letterhead.

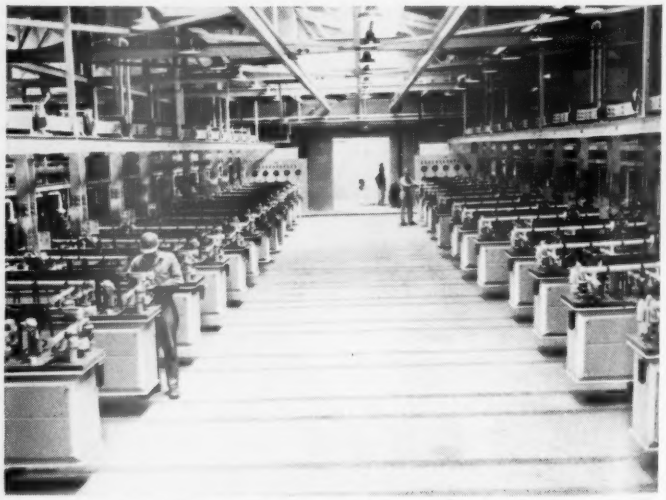

PART OF THE GIANT FLUORINE CELL ROOM at General Chemical's Metropolis, Ill., Works. This is the largest privately owned fluorine production facility in the world.

First in fluorine chemistry

Allied Chemical

GENERAL CHEMICAL DIVISION

40 Rector Street, New York 6, N. Y.

For data on the environment of space, the

JOURNAL OF GEOPHYSICAL RESEARCH

is a most important source of basic information. The *Journal of Geophysical Research* publishes more articles containing basic data on the environment provided by the Earth, its atmosphere, and the space beyond than any other journal. In addition to basic scientific data on the environment, it contains articles on the relevant physics. For example, during 1959 papers were published on the following subjects: Van Allen radiation, cosmic radiation, atmospheric density, temperature and composition at satellite altitudes, magnetic fields in space, solar radiation, and many other subjects of value in systems design.

Papers in other areas traditional to the broad field of geophysics are also included. In 1959 the *Journal* contained over 2400 pages; it is anticipated that substantially more material will be published in 1960.

Groups of papers presented at symposia are frequently and promptly published in the *Journal*, making the summaries and opinions of leading scientists quickly available in print. In 1959, the *Journal* contained the proceedings of symposia on Scientific Effects of Artificially Introduced Radiations at High Altitudes (Argus results), Exploration of Space, and Fluid Mechanics in the Ionosphere.

Monthly—$20.00 for calendar year 1960 on subscription

AMERICAN GEOPHYSICAL UNION
Department M2
1515 Massachusetts Avenue, N. W., Washington 5, D. C.

Other publications of the AGU . . .

TRANSACTIONS: quarterly, including IGY Bulletin, $4.00 for the calendar year

GEOPHYSICAL MONOGRAPH SERIES: No. 5 now available, *Physics of Precipitation,* 435 pp., $12.50

IZVESTIYA, Academy of Sciences, USSR, English edition: monthly, available for 1957, 1958, 1959, and 1960, $25.00 for each calendar year

GEODEZIYA I KARTOGRAFIYA (Geodesy and Cartography): monthly, 1959 series, $20.00

TRUDY, Geophysics Institute, Academy of Sciences, USSR: Nos. 37–40 (in cooperation with Consultants Bureau), prices range from $6.00 to $8.00

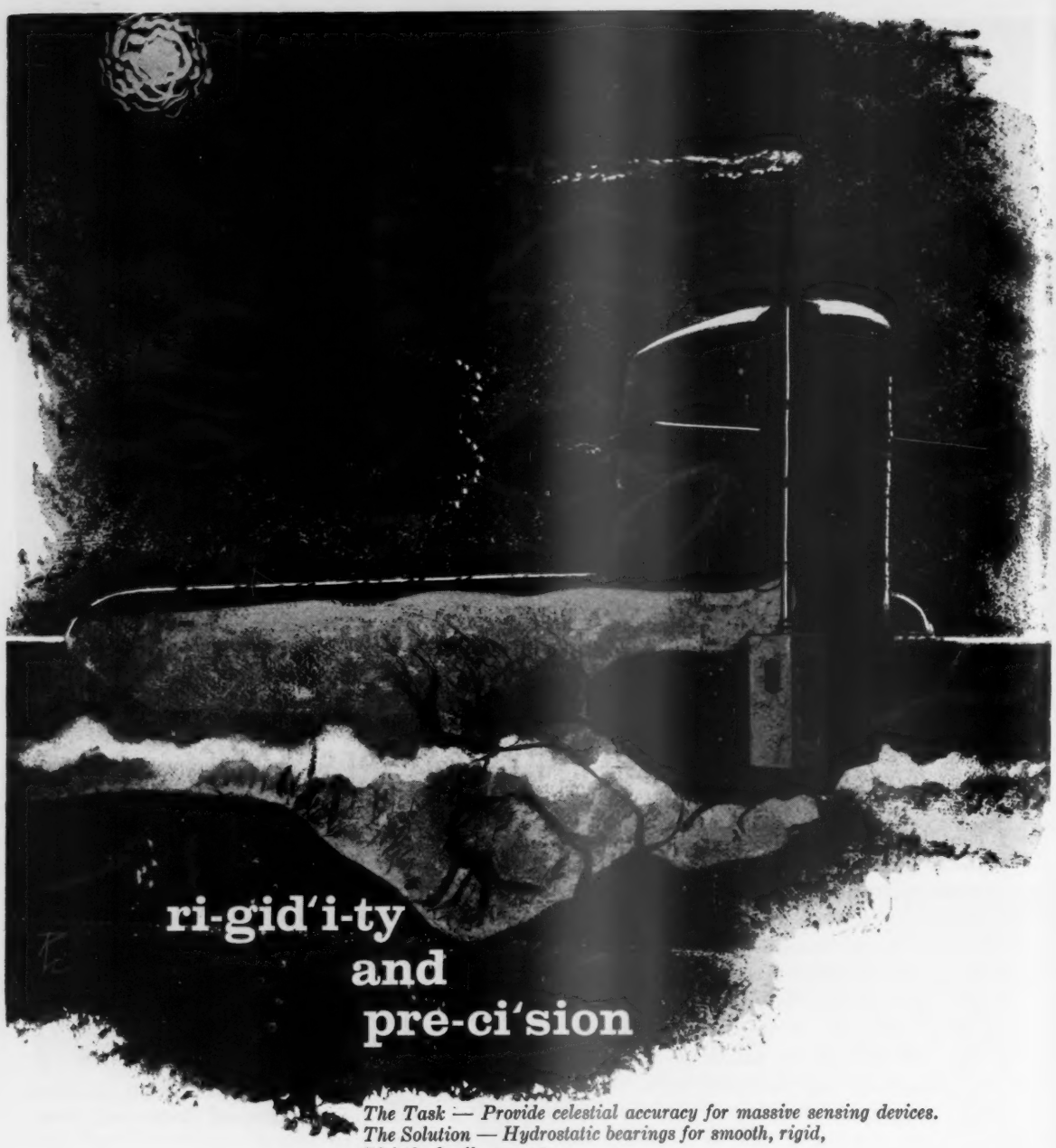

The Task — Provide celestial accuracy for massive sensing devices. The Solution — Hydrostatic bearings for smooth, rigid, "frictionless" support.

In Polaris submarines and other military applications, these hydrostatic bearings, developed by Nortronics, are particularly suited to virtually frictionless support of a large structure, which can be positioned accurately by a servo system with no unevenness, runout or binding — yet extremely stiff under applied loads.

A NOTE FOR TALENTED ENGINEERS:
We invite your inquiry as to important positions at Nortronics' Precision Products Department. Excellent salaries for qualified men in both our Systems and Component Groups.

Contact E. P. Reardon
PRECISION PRODUCTS DEPARTMENT
NORWOOD, MASSACHUSETTS
Field Offices

Highway #46
Teterboro, New Jersey
Telephone: ATlas 8-1750
TWX-Hasbrouck Heights 871-U

2486 Huntington Drive
San Marino, California
Telephone: ATlantic 7-0461
TWX-Alhambra 9619-U

NORTRONICS
A Division of
NORTHROP CORPORATION

ARS JOURNAL

A PUBLICATION OF THE AMERICAN ROCKET SOCIETY

EDITOR — Martin Summerfield
ASSOCIATE TECHNICAL EDITOR — Irvin Glassman
MANAGING EDITOR — Barbara Nowak
ART EDITOR — John Culin

ASSOCIATE EDITORS

Ali Bulent Cambel, *Northwestern University, Book Reviews;* Igor Jurkevich, *G. E. Space Sciences Laboratory, Russian Supplement;* George F. McLaughlin, *Patents;* Charles J. Mundo Jr., *Raytheon Co., Guidance;* Bernard H. Paiewonsky, *Aeronautical Research Associates of Princeton, Flight Mechanics;* M. H. Smith, *Princeton University, Technical Literature Digest*

ASSISTANT EDITORS

Julie Hight, Carol Rubenstein, Estelle Viertel

ADVERTISING SALES MANAGER
Owen Kean

ADVERTISING PROMOTION MANAGER
Robert M. Lamb

ADVERTISING PRODUCTION MANAGER
Walter Brunke

ADVERTISING REPRESENTATIVES

New York
D. C. Emery and Associates
400 Madison Ave., New York, N. Y.
Telephone: Plaza 9-7460

Los Angeles
James C. Galloway and Co.
6535 Wilshire Blvd., Los Angeles, Calif.
Telephone: Olive 3-3223

Chicago
Jim Summers and Associates
35 E. Wacker Dr., Chicago, Ill.
Telephone: Andover 3-1154

Detroit
R. F. Pickrell and Vincent Purcell
318 Stephenson Bldg., Detroit, Mich.
Telephone: Trinity 1-0790

Boston
Robert G. Melendy
17 Maugus Ave., Wellesley Hills, Mass.
Telephone: Cedar 5-6503

Pittsburgh
C. F. Livingston
17 Canterbury Rd., Pittsburgh 2, Pa.
Telephone: Poplar 6-8639

American Rocket Society

500 Fifth Avenue, New York 36, N. Y.

Founded 1930

OFFICERS

President — Howard S. Seifert
Vice-President — Harold W. Ritchey
Executive Secretary — James J. Harford
Treasurer — Robert M. Lawrence
General Counsel — Andrew G. Haley
Director of Publications — Irwin Hersey

BOARD OF DIRECTORS

Terms expiring on dates indicated

Ali B. Cambel	1962	William H. Pickering	1961
Richard B. Canright	1962	Simon Ramo	1960
James R. Dempsey	1961	William L. Rogers	1960
Herbert Friedman	1962	David G. Simons	1961
Robert A. Gross	1962	John L. Sloop	1961
Samuel K. Hoffman	1960	Martin Summerfield	1962
A. K. Oppenheim	1961	Wernher von Braun	1960
		Maurice J. Zucrow	1960

TECHNICAL COMMITTEE CHAIRMEN

G. Daniel Brewer, Solid Rockets
Ali B. Cambel, Magnetohydrodynamics
William H. Dorrance, Hypersonics
James S. Farrior, Guidance and Navigation
Herbert Friedman, Physics of the Atmosphere and Space
George Gerard, Structures and Materials
Martin Goldsmith, Liquid Rockets
Andrew G. Haley, Space Law and Sociology
Samuel Herrick, Astrodynamics
Maxwell W. Hunter, Missiles and Space Vehicles
David B. Langmuir, Ion and Plasma Propulsion
Max A. Lowy, Communications
Irving Michelson, Education
Peter L. Nichols Jr., Propellants and Combustion
Eugene Perchonok, Ramjets
Richard A. Schmidt, Test, Operations and Support
C. J. Wang, Nuclear Propulsion
Stanley C. White, Human Factors and Bioastronautics
George F. Wislicenus, Underwater Propulsion
John E. Witherspoon, Instrumentation and Control
Abe M. Zarem, Power Systems

Your complete guide to the *new* language of space exploration

AEROSPACE DICTIONARY

by Frank Gaynor

with an introduction by Wernher von Braun

As man probes further into space, a vital new language comes swiftly into being. This up-to-the-minute reference work answers the needs of the student and general reader, as well as those in government and industry who require a knowledge of the essential terminology in space exploration.

Thousands of clear, concise entries, alphabetically arranged, present the most authoritative information on the language of rocketry and astronautics, guidance systems, satellites, telemetering devices, manned space flight, re-entry phenomena, celestial mechanics and aeronautic science.

The dictionary's editor, *Frank Gaynor*, had the assistance of the United States Department of Defense as well as civilian agencies and research centers in preparing the book's entries. America's most distinguished authority on rocketry and space travel, Dr. Wernher von Braun, has also assisted in the work's preparation and contributed a provocative introduction "The Why of Space Travel."

AD-7

PHILOSOPHICAL LIBRARY, *Publishers*
15 East 40th Street, New York 16, N. Y.

Please send me .... copies of AEROSPACE DICTIONARY @ $6.00 per copy. To expedite shipment I enclose

☐ Check ☐ Money Order

☐ Check here if you wish C.O.D.

Name .....

Address .....

City .....Zone ....State .....

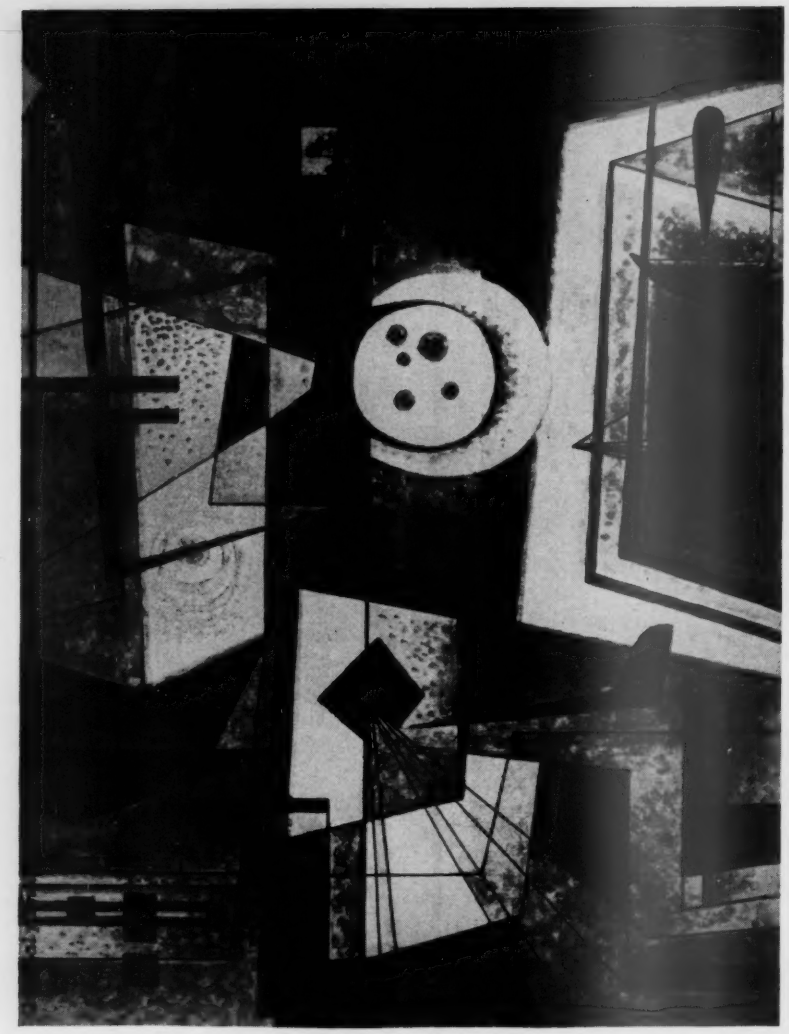

ORIENTATION LECTURES

GRADUATE TRAINING CENTER

FREQUENT SCIENTIFIC COLLOQUIA

ASSOCIATION WITH LEADING SCIENTISTS

GRADUATE THESIS PROGRAM

ADVANCE STUDY PROGRAM

SUMMER GRADUATE STUDENT PROGRAM

. . . these are some of the Doorways to Knowledge at Los Alamos.

For employment write to Personnel Director Division 60-91

los alamos
scientific laboratory
OF THE UNIVERSITY OF CALIFORNIA
LOS ALAMOS, NEW MEXICO

Scope of ARS JOURNAL

This Journal is devoted to the advancement of astronautics through the dissemination of original papers disclosing new scientific knowledge and basic applications of such knowledge. The sciences of astronautics are understood here to embrace selected aspects of jet and rocket propulsion, spaceflight mechanics, high speed aerodynamics, flight guidance, space communications, atmospheric and outer space physics, materials and structures, human engineering, overall system analysis, and possibly certain other scientific areas. The selection of papers to be printed will be governed by the pertinence of the topic to the field of astronautics, by the current or probable future significance of the research, and by the importance of distributing the information to the members of the Society and to the profession at large.

Information for Authors

Manuscripts must be as brief as the proper presentation of the ideas will allow. Exclusion of dispensable material and conciseness of expression will influence the Editors' acceptance of a manuscript. In terms of standard-size double-spaced typed pages, a typical maximum length is 22 pages of text (including equations), 1 page of references, 1 page of abstract and 12 illustrations. Fewer illustrations permit more text, and vice versa. Greater length will be acceptable only in exceptional cases.

Short manuscripts, not more than one quarter of the maximum length stated for full articles, may qualify for publication as Technical Notes or Technical Comments. They may be devoted to new developments requiring prompt disclosure or to comments on previously published papers. Such manuscripts are published within a few months of the date of receipt.

Sponsored manuscripts are published occasionally as an ARS service to the industry. A manuscript that does not qualify for publication, according to the above-stated requirements as to subject, scope or length, but which nevertheless deserves widespread distribution among jet propulsion engineers, may be printed as an extra part of the Journal or as a special supplement, if the author or his sponsor will reimburse the Society for actual publication costs. Estimates are available on request. Acknowledgment of such financial sponsorship appears as a footnote on the first page of the article. Publication is prompt since such papers are not in the ordinary backlog.

Manuscripts must be double spaced on one side of paper only with wide margins to allow for instructions to printer. Include a 100 to 200 word abstract. State the authors' positions and affiliations in a footnote on the first page. Equations and symbols may be handwritten or typewritten; clarity for the printer is essential. Greek letters and unusual symbols should be identified in the margin. If handwritten, distinguish between capital and lower case letters, and indicate subscripts and superscripts. References are to be grouped at the end of the manuscript and are to be given as follows. For journal articles: Authors first, then title, journal, volume, year, page numbers; for books: Authors first, then title, publisher, city, edition and page or chapter numbers. Line drawings must be clear and sharp to make clear engravings. Use black ink on white paper or tracing cloth. Lettering should be large enough to be legible after reduction. Photographs should be glossy prints, not matte or semi-matte. Each illustration must have a legend; legends should be listed in order on a separate sheet.

Manuscripts must be accompanied by written assurance as to security clearance in the event the subject matter lies in a classified area or if the paper originates under government sponsorship. Full responsibility rests with the author.

Preprints of papers presented at ARS meetings are automatically considered for publication.

Submit manuscripts in duplicate (original plus first carbon, with two sets of illustrations) to the Managing Editor, ARS JOURNAL, 500 Fifth Avenue, New York 36, N.Y.

ARS JOURNAL is published monthly by the American Rocket Society, Inc. and the American Interplanetary Society at 20th & Northampton Sts., Easton, Pa., U. S. A. Editorial offices: 500 Fifth Ave., New York 36, N. Y. Price: $12.50 per year, $2.00 per single copy. Second-class postage paid at Easton, Pa., with additional entry at New York, N. Y. This publication is authorized to be mailed at the special rates of postage prescribed by Section 132.122. Notice of change of address should be sent to the Secretary, ARS, at least 30 days prior to publication. Opinions expressed herein are the authors' and do not necessarily reflect the views of the Editors or of the Society.
© Copyright 1960 by the American Rocket Society, Inc.

EXCELCO

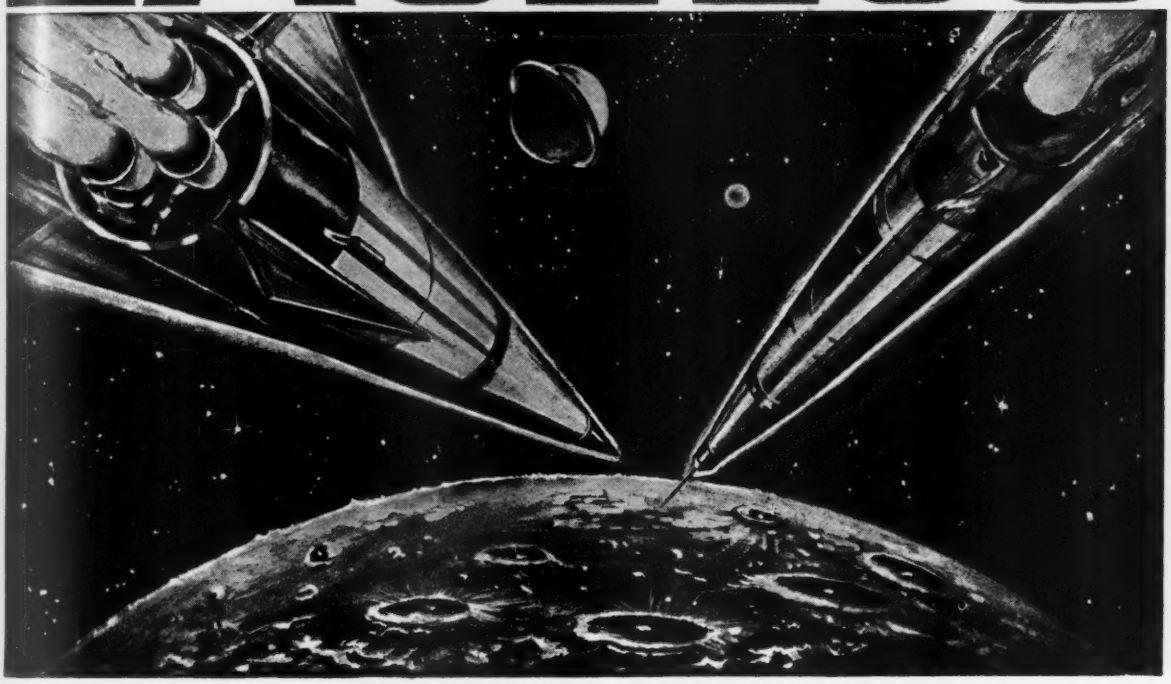

RV-A-10 • SERGEANT
AIR FORCE — RE-ENTRY X-17
POLARIS — RE-ENTRY X-36
JUPITER JR. • JUPITER SR.
POLARIS O • POLARIS A
POLARIS AIX • POLARIS A2-MOD 1-2-3
NIKE HERCULES • NIKE ZEUS
MINUTEMAN • PERSHING
N.A.S.A. PROGRAMS • SCOUT
LITTLE JOE

•

and many other classified projects

Builders of more large, thin wall, high strength solid propellant rocket engine cases and nozzles for development purposes than any other company in America.

A small experienced organization geared to handle your development and prototype requirements for static and flight tests in the shortest possible time.

Call or write:

EXCELCO DEVELOPMENTS

MILL STREET • SILVER CREEK, NEW YORK

New Books from ACADEMIC PRESS

INTRODUCTION TO ASTRODYNAMICS

By ROBERT M. L. BAKER, JR. *and* MAUD W. MAKEMSON
University of California at Los Angeles

September 1960, 358 pp., illus., $7.50

This is the first introductory textbook based on a university course in astrodynamics. In concise, clear language it describes all of the practical problems and methods encountered in the field. The nomenclature is carefully defined in a glossary of over three hundred terms.

The book will serve as a textbook for introductory undergraduate courses and as a reference and handbook of astrodynamical techniques for engineers and scientists involved in space technology. It differs from classical texts in celestial mechanics by relating theory and techniques directly to contemporary space vehicle problems.

HYPERSONIC FLOW THEORY

WALLACE D. HAYES
Princeton University and Space Technology Laboratories
RONALD F. PROBSTEIN
Brown University and Avco Research Laboratory

1959, 464 pp., illus., $11.50

"... the nature of the present volume makes it an important contribution to the contemporary scene as well as a book that will remain vital for many future years."
—*ARS Journal*

"Those readers familiar with the other work of the authors will not be surprised to note that, in presenting a comprehensive picture of hypersonic flow theory, Prof. Hayes and Probstein have also succeeded in presenting some aspects of general compressible flow theory in a new and stimulating light.

"... it will long be regarded as the authoritative text on the theoretical foundations of the subject. It can be strongly recommended to anyone directly concerned with problems of high speed gas dynamics." —*Aircraft Engineering*

SPACEFLIGHT TECHNOLOGY

The First Commonwealth Spaceflight Symposium
Organized by the British Interplanetary Society, 1959

Edited by KENNETH W. GATLAND
The British Interplanetary Society

November 1960, about 400 pp., illus., approx. $12.00

The important spaceflight research in progress throughout the British Commonwealth is thoroughly discussed by active participants in space science from Woomera to Jodrell Bank. The subjects covered include equipment necessary for manned satellites, satellite tracking, space navigation, satellite recovery, nuclear thermal fission rockets, scientific instrumentation, and heating problems of entry into planetary atmospheres.

Advances in SPACE SCIENCE

Edited by FREDERICK I. ORDWAY, III
George C. Marshall Space Flight Center
National Aeronautics and Space Administration

Editorial Advisory Board

WERHNER VON BRAUN, FREDERICK C. DURANT, III, EUGEN SÄNGER, LESLIE R. SHEPHERD, GEORGE P. SUTTON, and ÊTIENNE VASSY

"... the scientists who function in this field must be competent specialists who have a moderately complete knowledge of the subject as a whole. *Advances in Space Science* should be extremely helpful to specialists for securing information concerning recent contributions made in their specialty to astronautics as well as for obtaining a general picture of the subject as a whole." —*Science* (Review of Volume 1)

VOLUME 1 *1959, 412 pp., illus., $12.00*

VOLUME 2 *1960, 450 pp., illus., $13.00*

Experimental Physics Using Space Vehicles, by CHARLES P. SONETT
Tracking Artificial Satellites and Space Vehicles, by KARL G. HENIZE
Materials in Space, by FREDERICK L. BAGBY
Plasma Propulsion Devices, by MORTON CAMAC
Electrostatic Propulsion Systems for Space Vehicles, by ERNST STUHLINGER and ROBERT N. SEITZ
Attitude Control of Satellites and Space Vehicles, by ROBERT E. ROBERSON
AUTHOR INDEX—SUBJECT INDEX.

VOLUME 3 *1961, in preparation*

SPACE TRAJECTORIES

A Symposium Sponsored by
The American Astronautical Society,
The Advanced Research Projects Agency,
and Radiation Incorporated

Chairman of the Symposium:
T. C. HELVEY, *Radiation Incorporated*

September 1960, 298 pp., illus., $12.00

This symposium was planned to achieve a comprehensive survey of the field and the widest possible exchange of ideas between the leading scientists who participated. The area to be covered by each paper was carefully outlined beforehand in order to provide a truly comprehensive treatment of the entire field. This volume, therefore, will be useful to specialists in the field and will serve as a valuable reference book for those working in related sciences.

ACADEMIC PRESS, New York and London

111 Fifth Avenue, New York 3 **17 Old Queen Street, London, S.W. 1**

ACADEMIC PRESS, *Publishers*

are pleased to announce a new serial publication

Progress in Astronautics and Rocketry

Sponsored by the American Rocket Society

Series Editor: MARTIN SUMMERFIELD,
Princeton University

With this Progress series, the American Rocket Society is inaugurating a new approach to the basic task of publishing the scientific output of an association with many diverse specialties. Each Progress volume will be focused on a single specialty.

Volume I: Solid Propellant Rocket Research

A Selection of Technical Papers based mainly on a Symposium of the American Rocket Society held at Princeton, New Jersey, January 28, 29, 1960

Edited by MARTIN SUMMERFIELD

October 1960, 692 pp., illus., $6.50.

MECHANICAL PROPERTIES OF GRAINS

A. B. Boyd, W. M. Burkes, and J. E. Medford, Grain Design and Development Problems for Very Large Rocket Motors
A. M. Freudenthal, and L. A. Henry, On "Poisson's Ratio" in Linear Viscoelastic Propellants
M. L. Williams, Mechanical Properties and the Design of Solid Propellant Motors
N. N. Au, A Method of Strength Analysis of Solid Propellant Rocket Grains
J. Vandenkerckhove, and G. Lampens, Stress and Strain Analysis of Cylindrical Case-Bonded Grains

STEADY-STATE BURNING MECHANISMS

Martin Summerfield, G. S. Sutherland, M. J. Webb, H. J. Taback, and K. P. Hall, Burning Mechanism of Ammonium Perchlorate Propellants
D. W. Blair, E. K. Bastress, C. E. Hermance, K. P. Hall, and M. Summerfield, Some Research Problems in the Steady-State Burning of Composite Solid Propellants
W. Nachbar, A Theoretical Study of the Burning of a Solid Propellant Sandwich
R. F. Chaiken, and W. H. Andersen, The Role of Binder in Composite Propellant Combustion

COMBUSTION OF METALS

Irvin Glassman, Combustion of Metals: Physical Considerations
W. M. Fassell, C. A. Papp, D. L. Hildenbrand, and R. P. Sernka, The Experimental Nature of the Combustion of Metallic Powders
Derck A. Gordon, Combustion Characteristics of Metal Particles
Claude P. Talley, The Combustion of Elemental Boron
William A. Wood, Metal Combustion in Deflagrating Propellant

THEORIES OF UNSTABLE COMBUSTION

F. T. McClure, R. W. Hart, and J. F. Bird, Solid Propellant Rocket Motors as Acoustic Oscillators
Reuel Shinnar, and Menachem Dishon, Heat Transfer Stability Analysis of Solid Propellant Rocket Motors
A. G. Smith, A Theory of Oscillatory Burning of Solid Propellants Assuming a Constant Surface Temperature
Sin-I Cheng, Combustion Instability in Solid Rockets Using Propellants with Reactive Additives
R. W. Hart, J. F. Bird, and F. T. McClure, The Influence of Erosive Burning on Acoustic Instability in Solid Propellant Rocket Motors

EXPERIMENTS ON UNSTABLE BURNING

W. Grant Brownlee, and Frank E. Marble, An Experimental Investigation of Unstable Combustion in Solid Propellant Rocket Motors
E. M. Landsbaum, W. C. Kuby, and F. W. Spaid, Experimental Investigations of Unstable Burning in Solid Propellant Rocket Motors
T. A. Angelus, Unstable Burning Phenomenon in Double-Base Propellants
E. W. Price, Review of Experimental Research on Combustion Instability of Solid Propellants
R. H. Wall, Resonant Burning of Solid Propellants: Review of Causes, Cures and Effects

SOLID PROPELLANT IGNITION

R. F. McAlevy, III, P. L. Cowan, and M. Summerfield, The Mechanism of Ignition of Composite Solid Propellants by Hot Gases
A. D. Baer, N. W. Ryan, and D. L. Salt, Propellant Ignition by High Convective Heat Fluxes
Rodney B. Beyer, and Norman Fishman, Solid Propellant Ignition Studies with High Flux Radiant Energy as a Thermal Source

---

In preparation:

Volume II: **Liquid Rockets and Propellants**
Edited by Loren E. Bollinger, Martin Goldsmith, and Alexis W. Lemmon, Jr.

Volume III: **Space Power Systems**
Edited by Nathan W. Snyder

Volume IV: **Electrostatic Propulsion**
Edited by David Langmuir, Ernst Stuhlinger, and J. M. Sellen

ACADEMIC PRESS, New York and London

111 Fifth Avenue, New York 3 **17 Old Queen Street, London S.W. 1**

The Image Furnace as a Research Tool

NEVIN K. HIESTER and R. E. DE LA RUE

Stanford Research Institute
Menlo Park, Calif.

THE CONCENTRATION of radiant energy by optical means has been known since antiquity. In Aristophanes' comedy "The Clouds," Stepsiades explains to Socrates how he intends to defeat his creditors by aiming a burning glass properly as he meets them, so as to melt the wax tablets on which the debt is recorded (1).[1]

The first military use of this principle is attributed to Archimedes during the siege of Syracuse in 212 B.C. He is reputed to have "set fire to the invading ships of Marcellus' Navy by means of a burning glass composed of small square mirrors moving every way upon hinges, which, when placed in the sun's rays, were directed upon the Roman fleet, so as to reduce it to ashes at the distance of a bow shot" (1). Archimedes' activities in defense of his home city are probably also the first case of the use of science to devise new weapons for the armed forces, and resulted in prolongation of the campaign for 3 years.

Nearly two millennia were to pass before the concept was to be used for research purposes. In 1695, Averoni and Targioni of Florence used a burning glass to decompose a diamond, a substance previously considered inalterable (2). During the next 50 years, Tschirnhauss in Germany, Parker in England, and Geoffroy and Homberg in France found the lens (or solar image) furnace an invaluable tool in their studies of the properties of matter and fire (2–4). Its use as a high temperature tool of the new science of chemistry was climaxed by Lavoisier's construction of a large double lens furnace in 1774 to demonstrate that diamond was just another form of carbon (5).

One of the laboratory demonstrations used by Tyndall during his lecture on the properties of radiant energy was probably among the first examples of the arc image furnace (6). Fig. 1 illustrates the ignition of a chlorine-hydrogen mixture by an electric arc through a double parabolic mirror system.

The preceding application of radiant energy concentration exemplifies one of the important advantages of image furnaces, i.e., their ability to supply uncontaminated heat at a point remote from the source. This, coupled with the fact that the materials being studied can be enclosed in a transparent envelope and heated rapidly either in a vacuum or in a precisely controlled atmosphere without crucible contamination, has led to the recently increased interest in such devices.

Modern solar furnace research probably started in Germany in 1909, and sporadic activity, at about 10-year intervals, has continued since then in Germany, the United States and France (2). A more intensive effort has been under way at several laboratories in recent years.

Some completed research work has been reported by Trombe and Foex and their co-workers at Mont Louis in France (7) and by Mii's group in Japan (8), but very little actual results have been published in this country.

This has probably been due to several factors, the most important of which is that expected high temperatures were not attained. This is possibly because many of these furnaces are built around war surplus searchlight mirrors whose optical qualities leave something to be desired, and because of the added complexity of a sun tracking mechanism whose continued precise performance is a must. In addition, the vagaries of weather and the requirement that the sun not be too near the horizon also limit the working period.

For these reasons emphasis has recently shifted to arc image furnaces where one has a relatively stationary source of radiant energy, and where the device can be used at any time and yet provide a flux and irradiation area comparable to that from a solar image furnace based on searchlight mirrors. For example, Stanford Research Institute's solar furnace with an unusually good paraboloid of a 60-in. aperture and a heliostat sun follower can, under the best weather conditions, provide an irradiance of 160 cal/cm²/sec over a 6-mm diameter focus (9). At the same time, the SRI arc image furnace using a double ellipsoidal set of mirrors of 16-in. aperture can supply a flux of 160 cal/cm²/sec and a focal diameter of 9 mm, with an

Received Sept. 1, 1960.

[1] Numbers in parentheses indicate References at end of paper.

Dr. Hiester is Manager of the Chemical Engineering Section. He received his B.S. and M.S. degrees in chemical engineering from the University of Washington in 1941 and 1946, respectively. His Ph.D., in chemical engineering, was received from the University of California at Berkeley in 1949. Since then, the author has been at Stanford Research Institute. Other papers published have been on fluid-solid mass transfer theory and the production and utilization of high temperature. He was co-chairman of the symposium on "High Temperature—A Tool for the Future," held at Berkeley, Calif., in 1956, and chairman of the International Symposium on High Temperature Technology held at Asilomar, Calif., in 1959. Dr. Hiester is an ARS member.

Mr. De La Rue is a member of the Chemical Engineering Section, which is engaged in research in the areas of propellant, ceramic and high temperature technologies, also, chemical engineering and fine particle technologies. He received his B.S. and M.S. degrees in chemical engineering from the University of California at Berkeley in 1950 and 1955, respectively. Before joining Stanford Research Institute in 1954, he was with the University of California Radiation Laboratory. He has had papers published on electrochemistry and image furnaces.

input of near 9 kw (10). The 160 cal/cm²/sec radiant flux corresponds to a black-body temperature of 3250 K. As a result the trend toward arc image furnaces as research tools has recently accelerated.

The purpose of this paper is to provide a guide to the literature covering some of the important theoretical and practical aspects of image furnaces and their operation. In addition, some of the research areas where these devices have been used will be briefly described in the hope that it may trigger ideas for other ways in which they can be used to solve research problems.

Theory

In an image furnace, regardless of whether the radiating source is the sun, the crater of a carbon arc or a luminescent flame, the optical system does no more than collect as much of the emitted energy as possible and focus it in a concentrated form in a single region. The furnace itself is at the plane of maximum radiant flux per unit area. The prediction of the size of the focal spot and of the flux is the goal of image furnace theory. The optics used govern the theoretical degree of concentration, but the actual concentration depends on many practical factors.

The majority of solar furnaces in the United States are single continuous paraboloidal mirrors, either following the sun directly or through a heliostat. The theory for these types of furnaces has been well worked out (2, 11–18), including the effects of such sources of thermal losses to the radiant energy as: Atmospheric absorption, glass absorption, imperfect reflectivity of reflecting surface, geometrical imperfections of reflecting surface, shadowing effects and imperfections in reflector alignments.

These theories show, disregarding inefficiencies, that the highest flux in the focal plane is a function of paraboloid aperture to focal length ratio (or opening expressed in terms of the rim angle θ) and covers an image whose diameter is a function of the focal length. Thus, for a sun of uniform flux intensity, the maximum theoretical flux is 46,100 times $\sin^2\theta$ times incident solar flux, and the image diameter d is 0.0093 times focal length. The variation of flux, outside the image, in the focal plane has been calculated by Le Phat Vinh (17), Mii et al. (16) and Simon (19); and the first two have also calculated flux variations in planes parallel to the focal plane.

In actuality the sun is brighter in the center—the so-called limb-darkening effect—and this must be taken into account. De La Rue et al. (20), Mii et al. (16) and Jose (21) have calculated the flux through the focal spot for the nonuniform case, and the first two have also considered the distribution for planes adjacent to the focal plane.

As pointed out earlier, there are factors which contribute to a lower performance of a solar furnace than theory would predict. This design point has been considered seriously by Hiester et al. (2, 14, 22) and Bliss (13, 15).

In connection with the large solar furnace proposed by the Air Force for construction at Cloudcroft, N. Mex., a number of theoretical studies were undertaken for the Air Force Missile Development Center at Holloman AFB. Several of these were concerned with the effect on performance of using mosaics of spherical (or toroidal) mirror segments to approximate a paraboloid (18,23,24). This was necessitated by the impracticality of fabricating a continuous, geometrically perfect, curved surface of the aperture desired. Baum and Strong (25) considered another approach to the system, reduction of the aperture by finding an optical system that places more of the intercepted radiant energy in the central sun image on the focal plane. They show that double mirror systems, having continuously curved surfaces (but where the geometry of each changes from point to point, in a related manner), do provide some small improvement.[2] The other key paper in this series is by Jose (26) covering the theory for matching the heliostat to its paraboloid.

Although, as pointed out earlier, arc image furnaces are providing considerably more experimental results, to date the only theoretical discussion of their performance is that of Null and Lozier (27).[3]

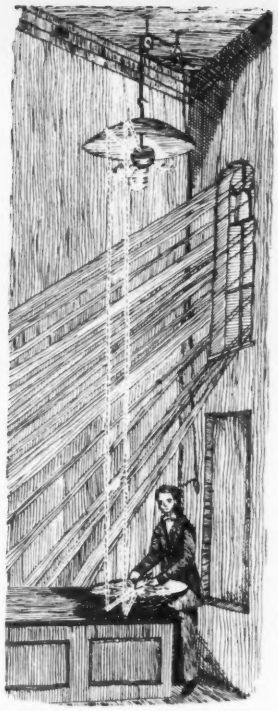

Fig. 1 Tyndall demonstrating an arc image furnace. (Redrawn by D. Lew)

Solar Image Furnace

The types of solar furnaces can be classified in a number of ways:

Optics
- A Single paraboloid
- B Double paraboloid with focusing lens
- C Double lens
- D Paraboloid with ellipsoid
- E Combined variable mirrors
- F Cylindro-paraboloid

Concentrating Surface
- 1 Continuous geometric curved surface
- 2 Flat segments tangent to the surface
- 3 Curved segments approximating and tangent to the geometric surface
- 4 Oriented flat segments (analogous to a Fresnel lens)

Energy Collection
- a Concentrator movable, follows sun directly
- b Concentrator fixed, heliostat follows sun

Thus the French solar furnace shown in Fig. 2 might be classified as type A3b.

Most of the high temperature furnaces built recently are continuous paraboloidal mirrors, either following the sun directly or through a heliostat, types A1a and A1b. The only important exceptions are the C1a lens-type furnace at

[2] This, of course, would be at the expense of increased fabrication difficulties.

[3] Additional work in this area is under way at Stanford Research Institute.

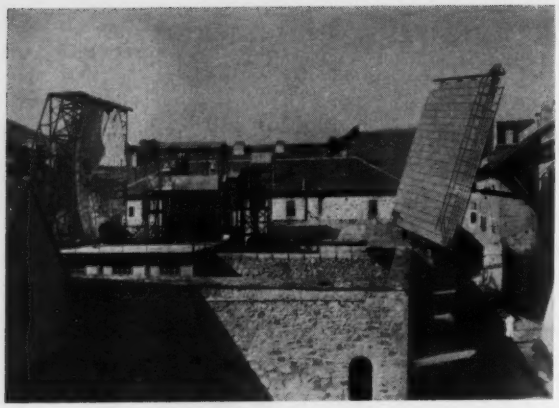

Fig. 2 General view of the 35-ft furnace located at Mont Louis in the Pyrenees

California Institute of Technology, which utilizes an array of 19 lenses that ultimately concentrate the radiations at a unique focus (28), the type A4a segmented flat plate furnace at Massachusetts Institute of Technology (29), and the type A3b segmented spherical concentrator furnace at the Quartermaster Research and Development Laboratories (30).

Usually, in large units auxiliary mirrors are used to facilitate access to a stationary focus (30,31). Auxiliary mirrors in this case are usually simpler to operate and actually less expensive than the delicate and sturdy mechanisms that must be provided to rotate accurately the entire paraboloid and focus.

Considerable effort has been extended in various design studies for solar furnaces in the past few years. Most of these design studies have been in connection with the large solar furnace proposed by the Air Force for construction at Cloudcroft, N. Mex. These studies include such topics as optical design principles (15), basic optical considerations in the choice of a design for a solar furnace (25), the loss of energy by absorption and reflection in the heliostat and parabolic condenser (32), a solar furnace using a horizontal heliostat array (33), design of a solar furnace and the calculations of concentration using spherical-mirror elements (23), thermal effects on solar furnace mirrors (34), design of a heliostat mirror for a solar furnace (26), design of the condenser of a solar furnace using nonparabolic elements (18), and the economic factors in furnace design (22). Other studies concerning mechanical factors and operating aspects are contained in (35 and 36).

The choice of reflector materials is governed by reflectivity and corrosion resistance, as well as by the optics and the spectrum desired. A discussion of reflectivity of metals and the corrosion characteristics has been given elsewhere (35,37,38). Those in use today are silver, aluminum, rhodium and stellite surfaces. Back-silvered glass has been determined to be the most favorable. The spectral distribution for the Stanford Research Institute solar furnace has been measured by Marcus and Wohlers (9).

As important as the optical design of a solar furnace is the guiding system, or sun tracking mechanism. When a solar furnace is used for high temperature research, it is essential that the position of the hot zone on the target be very stable. This can be achieved by keeping the concentrator or heliostat focused on the sun. Manual focusing results in jerky motion and is therefore unsatisfactory. Mechanical rotation has to be guided so as to follow precisely the apparent motion of the sun. Various guiding systems have been described in the literature (8,39,40,41).

Control of temperatures and flux is invaluable if proper use of the solar furnaces is to be made. In operation of a solar furnace, there is little control over the flux received by the target, except by use of various mechanical methods. Among these methods would be: Using a control shutter placed between the focal plane and the concentrator; shading a portion of the concentrator and/or heliostat; or, if possible, changing the focal length by adjustment and deformation of the individual mirror segments of the concentrator. Laszlo (42) used a unique Venetian-blind-type shutter to control the temperature and flux. Conn (43) used a shutter in the form of a cylinder which moves along the axis of a paraboloidal mirror focus. In addition to the mechanical method of controlling flux, flux control can be attained by off-focus operations (20).

With the increased use of image furnaces for research, the measurement of high temperatures and fluxes is becoming more important. Conn (44) points out the necessity of shutting off, by two rotating sectors, the incident and reflected energy from the sample, so that the true temperature of the specimen can be measured with a disappearing-filament pyrometer. Kostkowski (45), Blau (46) and Brenden et al. (47) have also reviewed recent developments in this field. In an article discussing proposed instrumentation for the large solar furnace planned for construction at Cloudcroft, Shank (48) has discussed temperature measurement in solar furnaces.

The development of fluxmeters for high intensity thermal radiation has been reported by Farber (49) and Gardon (50), and Hughes (51) has described the pertinent factors in the design of such instruments. Blau (46) also reports on two flux measuring devices as well as equipment for measuring emissivities at high temperatures. He, Gardon (50), Loh et al. (52) and Laszlo (42) give flux distributions across the focal spots of various solar furnaces. Overall flux measurements at the focus as a function of rim angle are given by Farber (49).

In recent years a number of solar furnaces have been built. A survey of these installations in the United States, and of their research plans, is available in references (53 to 55). Reference (22) contains a table of estimated overall furnace efficiencies for actual furnaces. These workers, and others (13), have concluded that, in general, an overall furnace factor of 70 per cent is probably the highest efficiency that can be reached.

A survey of the European solar furnaces is contained in (44). The world's largest solar furnace, located at Mont Louis in France, is described by Trombe (31). Several furnaces have been built in Japan by the Government Industrial Research Institute, and are described in (56).

A directory of world activities and bibliography of significant literature on solar furnaces is given in (57). Development in the field of solar furnaces is also reported in the *Journal of Solar Sciences and Engineering*, and new furnaces are normally announced by *The Sun at Work*, a news publication of the Association for Applied Solar Energy.

Arc Image Furnaces

Developments in arc image furnaces have been closely associated with advances in the lamp projectors and carbons used in the motion picture industry. As the demand for brighter light sources increased, the manufacturers developed a variety of carbons, lens, reflectors and accessories for the industry. Today, from this wide choice of component parts, various types of arc image furnaces can be assembled.

Arc image furnaces are generally classified by the optics. A diagram of each type is shown in Fig. 3. The relative merits of each are discussed by Null and Lozier (27); therefore, the characteristics of each type will only be summarized.

Type I—Single elliptical mirror: This is the simplest form of an image furnace giving a large area of low irradiance or a small area of high irradiance, depending on whether the arc crater is located at the first or second focus.

Type II—Double elliptical mirror: This provides continuous exposures, and is one of the most practical systems, producing the highest irradiances with the furnace

aperture facing either up or down. It has shuttering advantage over type III.

Type III—Double parabolic mirrors: This provides essentially the same performance as type II. These have been widely used because of the availability of surplus Army and Navy searchlight mirrors.

Type IV—Condenser-relay lenses: This has the largest exposure area, and, as in type I, there is no restriction on the size of the exposure equipment. The level of radiation is the lowest of all types described.

A modification of type III has been proposed by Ploetz (58). The device consists of two identical reflecting paraboloids mounted face to face, so that the focal point of each falls at the vertex of the other. This arrangement allows both the source and image to be external to the optical system.

A survey of some arc image furnaces and their uses is given by Davis (59) and Butler (60). Operating and performance data for carbon arc, double elliptical mirror-image furnace and a comparison of other furnaces are given in (27 and 61).

At present, the flux, temperature and size of the image spot is limited by characteristics of the commercial lamps and carbons. For commercially available arc sources and carbons, the maximum image diameter is about 10 mm and flux about 225 cal/cm²/sec (62). It has been reported (27) that the Gretener Super Vent arc lamp does produce an image diameter 10 to 50 per cent larger in proportion to the carbon diameter than other lamps. Fluxes as high as 350 cal/cm²/sec, equivalent to a black-body temperature of about 4000 K, utilizing this lamp and experimental positive carbons have been obtained.

Experiments have been conducted both here and in Europe in operating arcs at very high currents (63,64). In the future, higher fluxes over much larger areas should be realized by the use of larger cored carbon.

Experiments have also been conducted utilizing pressurized tungsten electrodes (65). Plans with this furnace at the University of California include operating in pressurized argon.

Calculations based on plasma temperatures of high current argon arcs indicate fluxes up to 2000 cal/cm²/sec may be obtained (60).

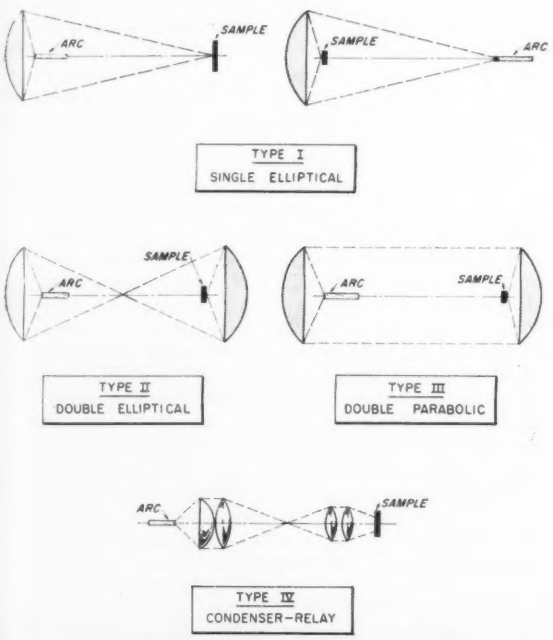

Fig. 3 Types of arc image furnaces

Work is also being conducted at Southwest Research Institute on a double parabolic image furnace, in which the source is an air blown,high current arc (66) which should result in high irradiances.

The life of a single carbon, commercially available, is from 20 to 30 min when operated at the prescribed voltage and current. If continuous operation is required, the use of two lamps and a quick changeover device (similar to that used for motion picture theaters) can be used (27). One of the authors (67) has successfully used this method for the growth of single crystals. The use of a continuous-burning lamp could also accomplish the same purpose. Such carbon arc lamps have been described (68–70). At present, no commercial units are available. As the operating voltages and currents are raised to gain further increases in radiation outputs, the burning rates of the carbon go up. Burning rates of 140 to 160 in. per hr have been reported (27). For the normal length carbon this would allow operating time of about 5 min, a period sufficiently long for some experiments.

Control of the flux and temperature in an arc image furnace can be obtained by a number of methods. For commercial lamps a number of types of carbons are available which can be operated at different voltages and currents, thereby giving different arc intensities. Also, the voltage and current can be varied over a wide range for individual carbons to give a range of arc intensities. Various mechanical methods, as described for solar furnaces, can also be used. For example, with the double ellipsoidal system, a rotating shutter can be placed at the common focus (10). Flux and temperature control can be achieved by defocusing either the source or the image receiver. Both modes of defocusing produce about 10 per cent decrease in central brightness per millimeter of axial movement off-focus with the rotating-type lamp and carbons (27).

Reasonable temperature control at a given temperature can be expected in an arc image furnace. Fluctuations in the irradiance of an arc image furnace owing to nonhomogenous regions in the carbon are often as small as ±5 per cent. This is only possible with the best feed and control mechanism (60). Sobon (71) describes an automatic system for this purpose. This system has been installed on the furnace reported in (67).

A comparison has been made of the distribution of irradiance and illuminance across the image with three different types of optical systems utilizing elliptical mirrors and high intensity carbons (61). Fig. 4 shows this irradiance information in watts per mm. (The flux conversion factor is 1 w per mm equals 23.9 cal/cm²/sec.) Also reported is the spectral distribution

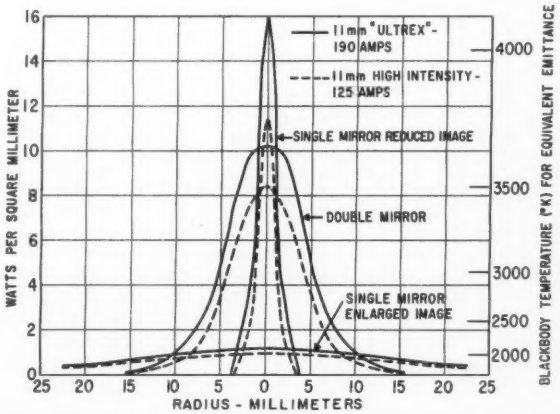

Fig. 4 Distribution of irradiance across focal spot of arc image furnaces

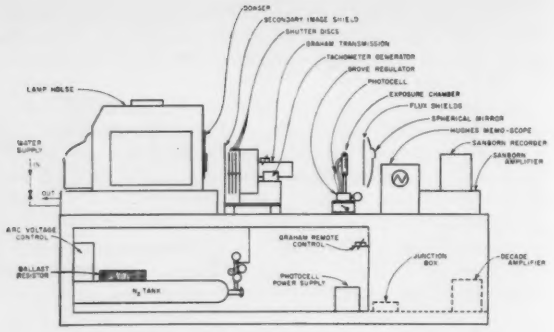

Fig. 5 Schematic diagram of ignition equipment

of irradiance at center of the focal spot for a double elliptical mirror furnace. Brown (72) measured the absolute spectral intensity distribution at the center of the focused image of a carbon arc in the region of 3000–9000 Å.

Research With Solar Image Furnaces

The results reported from solar furnace experiments have predominantly involved oxide systems, and the majority of this work has been performed at the Solar Energy Laboratory at Mont Louis. Trombe (73), at the Tucson Conference on the Use of Solar Energy—The Scientific Basis, outlined some of their experiments on the fusion of refractory oxides and their treatment of minerals. He describes the large-scale fusion of alumina and sand, and experiments on the fritting and stabilization of zirconia. Trombe also used the large solar furnace to prepare citrate-soluble phosphate by the defluorination of apatite through fusion. Refractory minerals were also broken down by the intense heat, and zirconia was prepared from zircon, and forsterite from serpentines. More recent results are contained in a survey of high temperature research in France, reported by Trombe and Foex (7).

Similar but less extensive work on oxides has been under way in Japan and is described by Mii (8). Laszlo (74) used a solar furnace to melt mullite and zirconia. Duwez and Loh used the California Institute of Technology solar furnace to melt specimens in their studies of the zirconia-thoria phase relationships (75).

Conn (76) describes and reviews the work on the production of molten zirconia in a solar furnace. A number of devices for permitting the measurement of high temperature properties of materials, such as thermal conductivity, and expansion, heat content and emissivity are described by Glaser (77), who also makes brief reference to the behavior of metal samples heated in air in the solar furnace.

An entirely new approach to the use of the solar image furnace in research has been made by Marcus and Wohlers (78). Image furnaces are really radiant energy collectors, and, in the case of solar concentrators, a large fraction of the collected energy lies in the visible and ultraviolet region where photochemical reactions occur. Such reactions are not, in general, very efficient, but if the photon flux can be greatly increased by such a concentration technique, the total conversion might also be increased.

An experimental study was therefore undertaken to determine whether photochemical reactions would proceed by the same mechanisms in the focus of a solar image furnace as they do at lower light intensities. The first experiment in this new field was the study of the photoreduction of the ceric ion at the higher irradiances provided by the solar furnace at Stanford Research Institute. The collector of this concentrator faces down directly over the heliostat, so that liquids can be irradiated in open or closed vessels placed at the focus. Based on the results of many runs at different irradiances, it was concluded that stoichiometry and kinetics of the photoreduction of ceric ion in perchloric acid solution is the same at these high light intensities as observed with low light levels at room temperature. It was also found that, although there is local boiling at the location of the focus, the remainder of the liquid system, even that portion through which the energy is transmitted, stays cool, and therefore, it is possible to undertake liquid phase reactions in such a device.

Research With Arc Image Furnaces

Considerably more detailed information is available in the open literature on a variety of uses for arc image furnaces. A brief summary for each of the more pertinent is provided in the following paragraphs.

Solid Propellant Ignition

The ease of ignition of a solid propellant is dependent upon many factors; important ones are the amount of energy supplied to the material, and the duration of its application. In the classical methods of dropping the propellant in a molten metal or using a weighed amount of black powder to ignite it, the results are essentially relative, since it is impossible to determine the amount of heat actually transferred to the material. Image furnaces are known to provide measurable quantities of radiant energy at very high flux rates, instantaneously over a small area, with the energy pulse accurately controlled, and to give several advantages for studies of the ignition behavior of such materials.

Stanford Research Institute has designed and utilized an arc image furnace installation in which a specimen of solid propellant can be irradiated with a predetermined amount of energy (10). A schematic drawing of the double ellipsoidal mirror image furnace used for this purpose is shown in Fig. 5. An Asheraft high intensity motion picture projection lamp house supplies up to 120 cal/cm²/sec on the propellant specimen inside the glass-faced exposure chamber. (This is equivalent to a black-body temperature of approximately 3000 K or 5000 F.)

High speed motion pictures taken of propellant ignition occurring at atmospheric pressure, show that voluminous quantities of particulate material are evolved from the surface during and after the pyrolysis brought about by exposure to the high flux radiant energy. The initial reaction occurs in the vapor phase, and the exothermic energy resulting is then transferred back to the surface. If the exposure is of sufficient length to supply a required minimum amount of this energy, a steady-state condition is brought about and sustained burning occurs.

Ignition of a particular propellant requires a certain amount of energy known as the threshold energy. When less than this threshold energy is supplied, ignition does not occur. Variations of the time of exposure, with constant irradiance, is used to bracket the threshold energy. The variables affecting propellant ignitibility, such as pressure, temperature, thermal flux and exposure time, surface condition, environmental gas composition, and past history can readily be studied. Typical results when several of these are varied are shown in Figs. 6 and 7. Fig. 6 shows that, at reduced pressures, for example, a minimum duration of energy transfer (about 400 millisec) is necessary for ignition to succeed, regardless of flux. This is related to the kinetics of the gas phase reaction. Fig. 7 shows that the threshold ignition energy is markedly affected by the presence of an external source of oxidizer. The authors suggest that both this effect and that of pressure provide strong support for the gas phase theory of propellant ignition.

Radiation Ignition of Fine Fuels

The combustion of organic solids, in the absence of self-contained oxidizer, involves two distinct processes: The

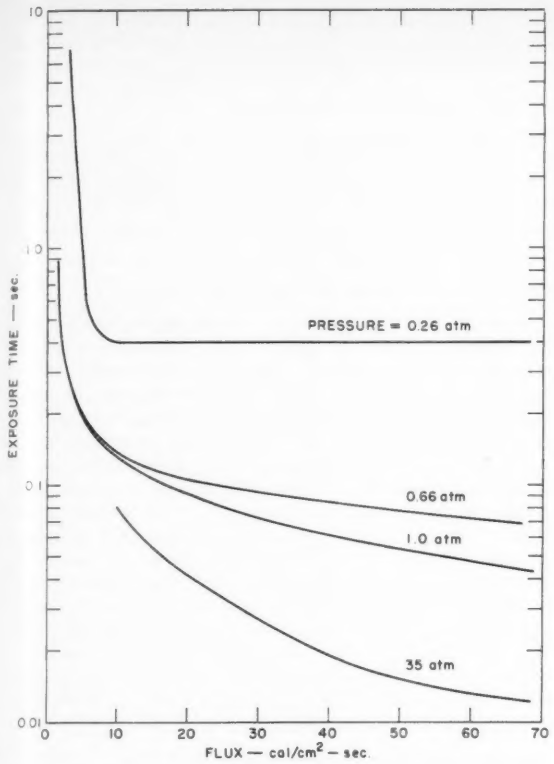

Fig. 6 **Dependence of exposure time for threshold ignition on flux**

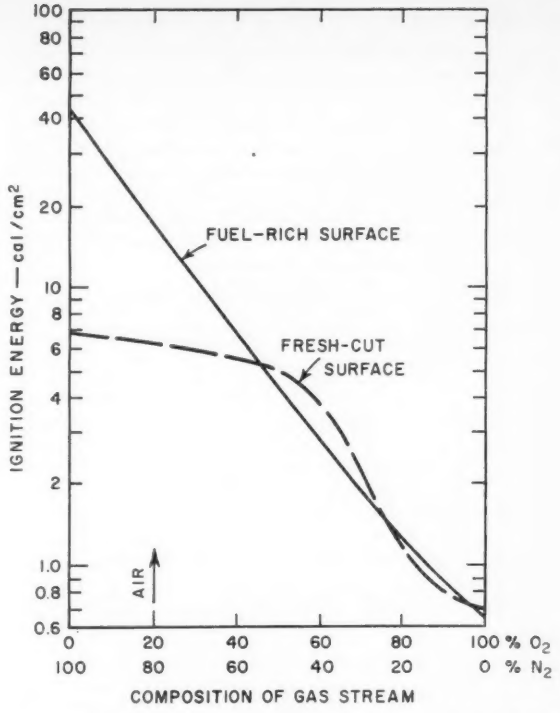

Fig. 7 **Effect of gas composition on ignition energy (atmospheric pressure)**

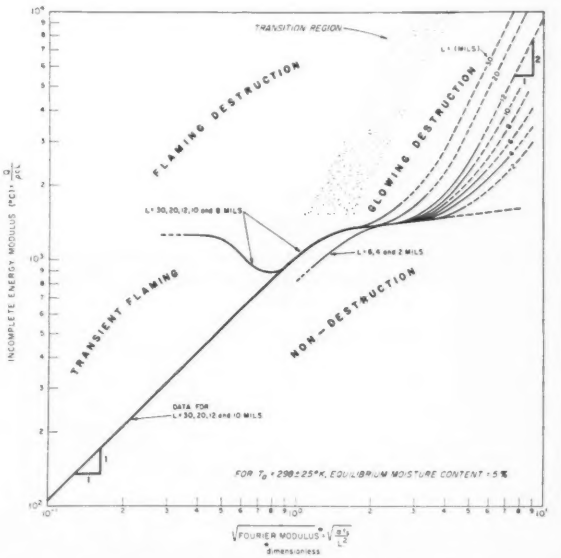
TRANSITION REGION
FLAMING DESTRUCTION
GLOWING DESTRUCTION
TRANSIENT FLAMING
NON-DESTRUCTION
DATA FOR L = 30, 20, 12, 10 and 8 MILS
L = 6, 4 and 2 MILS
FOR T0 = 298±25°K, EQUILIBRIUM MOISTURE CONTENT = 5 %
FOURIER MODULUS

Fig. 8 **Generalized ignition behavior patterns for cellulosic materials**

decomposition of a solid into volatile products, followed by the gas phase oxidation of these products. When a material such as cellulose is irradiated in an image furnace, the high temperatures produced near the surface provide volatiles at high rates. Ignition of this air-gas mixture will take place when, and only when, the gaseous fuel has a high degree of reactivity, and the relative concentration of the fuel and oxygen lie between two well-defined limits.

The work at the Naval Radiological Defense Laboratory on the ignition of fine fuels by irradiation has been done with condenser relay, lens system, arc image furnace (79). The fine fuels are simulated with a series of experimental papers manufactured from pure alpha cellulose in two densities, many different thicknesses, and with varying amounts of carbon black.

Three distinct types of ignition were soon recognized, each characterized by well-defined phenomena.

Glowing ignition: A bright red glow appears under low irradiances and long exposure times throughout a constant equilibrium temperature rise.

Spontaneous flaming ignition: There is a sudden appearance of a flame front which lasts only over the duration of the exposure produced with high irradiances and short times. It is independent of thickness.

Sustained flaming ignition: Continued burning, necessarily preceded by spontaneous flaming, is as in the preceding case. This type of flaming depends upon the thickness of the material, in which not only must the temperature rise be rapid, but high equilibrium temperatures must be maintained within the material.

Correlation procedures have been developed, as shown in Fig. 8, to successfully relate the ignition of fuels whose thickness varied by a factor of 10, densities by a factor of 2, and over a wide range of irradiances and exposure times. In this figure, the ordinate is in dimensionless units of energy, the abscissa in dimensionless time units, and the individual curves are in thickness units. Such a correlation pattern as this on the fundamental processes of flash pyrolysis is essential to provide a basis for new methods of inhibiting ignition and extinguishing the resulting fire.[4]

[4] Stanford Research Institute is actively developing a modification of the arc image furnace for fundamental investigations in the area of fire research.

Thermal Diffusivity of Metals at High Temperatures

If an insulated infinite slab is irradiated on one side only in an image furnace, it is possible to theoretically calculate the gross disposition of heat at any point within the slab from a knowledge of the thermal properties of the material (80). The adaptation of this concept to an experimental technique requires that the area of irradiance must be approximately 1 in. in diameter, and that the flux be sufficiently high so that the specimens can be raised to 1000 C. The condenser relay, carbon arc image furnace at Naval Radiological Laboratory provides such an area with a maximum irradiance of approximately 6 cal/cm²/sec. The temperature rise at two points in a cylindrical specimen of the metal or alloy, mounted so that it simulates a portion of an infinite insulated slab, is measured during the time the front is irradiated.

From the changes in temperature at the front and back of the specimen and heat transfer theory, the thermal diffusivity data are calculated. An example of the results obtained for steel is shown in Fig. 9. It should be noted that the method is sensitive to phase changes, such as the sudden change in slope at the Curie temperature.

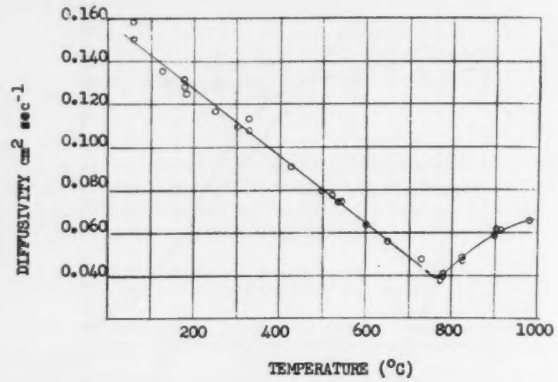

Fig. 9 Thermal diffusivity of steel measured with image furnace

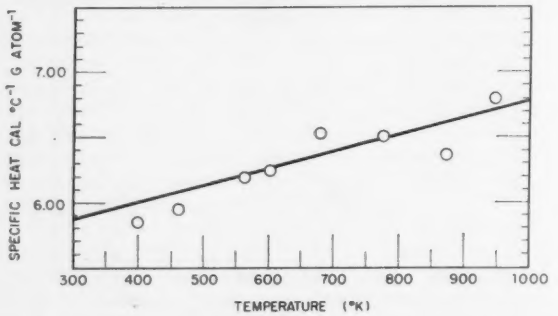

Fig. 10 Specific heat of molybdenum compared with data (solid line) in American Institute of Physics Handbook, 1957, section 4, p. 42

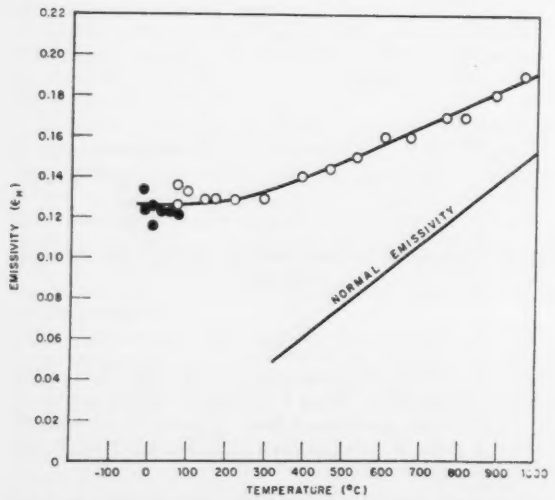

Fig. 11 Total hemispherical emissivity for polished platinum (normal emissivity values from Armour Research Institute)

Specific Heat of Metals at High Temperatures

A novel method has been developed at the Naval Radiological Defense Laboratory (81) for the determination of the heat capacity of metals and alloys based on the use of the arc image furnace. A small, thin test specimen is suspended by its own fine thermocouple wires in an evacuated chamber, the walls of which are optically black on the inside and water-cooled, and irradiated through a double quartz window at one end of the test chamber. If the temperature of the specimen is higher than the walls, if the pressure is lower than that at which convective losses occur, and if the conduction of heat through the supporting wires is negligible, all heat losses are by radiation. If, now, the specimen has been treated so that its surface is optically black, it will radiate with a Planck spectral distribution, with a hemispherical emissivity of 1.0. Since the heat loss is proportional to three quantities—the mass, the rate of temperature change with time and the specific heat—this specific heat can be calculated. Results for molybdenum are shown in Fig. 10.

Hemispherical Emissivity of Metals

Hemispherical emissivity is defined as the ratio of the total thermal energy radiated from unit area of a solid surface, at a given temperature, to that radiated by a black body at the same temperature. It is clear that hemispherical emissivity will be different than the normal, but there is no simple relationship between the two.

The experimental arrangement for the direct measurement of total hemispherical emissivity, as developed by Butler and his co-workers at the Naval Radiological Defense Laboratory, is to suspend a specimen of the metal in an evacuated chamber whose walls are optically black and are maintained at a constant temperature (82). Enclosed shutters inside the chamber can be opened to admit radiation through a quartz window for heating the specimen, and subsequently closed during the cooling, when the measurements are made.

Typical results for the hemispherical emissivity of polished platinum are shown in Fig. 11. It is to be noted that the values are consistently higher than for a similarly polished specimen when measured in the customary normal manner. Measurements made in the same way with polished copper indicated a similar departure from normal values. Butler suggests that the differences in the two sets of data are more indicative of the basic difference in the definition of the measured quantities than in any definite differences in specimen preparation.

Oxidation—Erosion Behavior of Graphite

The National Carbon Research Laboratory has conducted an extensive program for WADD to determine weight loss and decrease in length of impregnated graphite at high temperatures and moving streams of air (83). The method is to place the specimen of graphite, in rod or hemispherical cone form, at the focus of double elliptical mirror arc image furnace, and to irradiate the end of the material which has been carefully positioned. A stream of air is directed on the end of the sample from a tube protruding through the center of a collecting mirror.

With an arc current of approximately 190 amp the irradiance over an area of 1 in. in diameter is 61.5 cal/cm²/sec, as

measured with a calorimeter. Standard exposure times are 30 sec. Weight and length measurements before and after exposure in the furnace are made for each specimen, and in some cases profiles of the eroded specimens recorded.

Reflectivity and Emissivity of Graphite at 3800 K

A method for the measurement of the reflectivity of graphite near the sublimation point has been developed for WADD at the National Carbon Research Laboratory (84).

The radiation from a high current, carbon arc furnace is focused by a double elliptical mirror system on the anode of a standard pyrometric arc in the image plane of a second mirror. These arcs employ spectroscopic electrodes and operate at a brightness temperature close to 3800 K, which is measured with a photocell having a spectral response corresponding to that of the human eye. Two shutters are synchronized to separate the emitted from the reflected energy, as shown in Fig. 12. With both shutters open, both the emitted and reflected energies are recorded by the detector. With the first shutter closed, and the second open, only the emitted energy is recorded. The difference between the two readings gives the reflected illuminance of the burning arc. Comparative measurements of reflected energy are made by observing the freshly coated surface of magnesium oxide. It was concluded from these studies that the crater surface, at the operating temperature of the arc, reflected 2 per cent of the incident light, and hence the emissivities were 98 per cent (83).

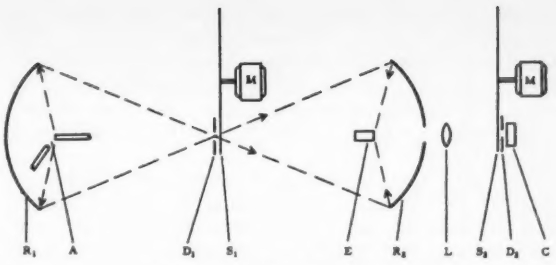

A - Image Furnace Arc, D_1 and D_2 - Diaphragms
S_1 and S_2 - Synchronous Shutters, L - Lens, C - Photocell
E - Exposed Sample, M - Motor, R_1 and R_2 - Furnace Reflectors

Fig. 12 Schematic diagram for reflectance measurements at 3800 K

Crystal Growing in an Arc Image Furnace

Two of the greatest problems in the growth of single crystals of refractory materials are preventing contamination and changes in stoichiometry at elevated temperatures. At the temperatures required for crystal growth these materials are usually extremely reactive, so that they cannot be contained in crucibles without introducing considerable contamination. When this problem has been overcome, for example in the Verneuil or flame fusion process, the atmosphere produced by the heat source is such that oxidation or reduction of the material occurs, and stoichiometry cannot be adequately controlled.

A crystal growing facility has been developed at Stanford Research Institute (67) which employs the Verneuil technique for crystal growth, but which utilizes an arc image furnace as the heat source. Such furnaces are uniquely suited for this application, since the energies required to melt most refractory compounds can be obtained at sharply defined zones. Since the heat is concentrated directly on the crystal, no other furnace elements reach high temperatures, minimizing out-gassing. By employing a glass furnace chamber, highly purified and precisely controlled oxidizing, reducing or neutral atmospheres, as well as vacuum, can be

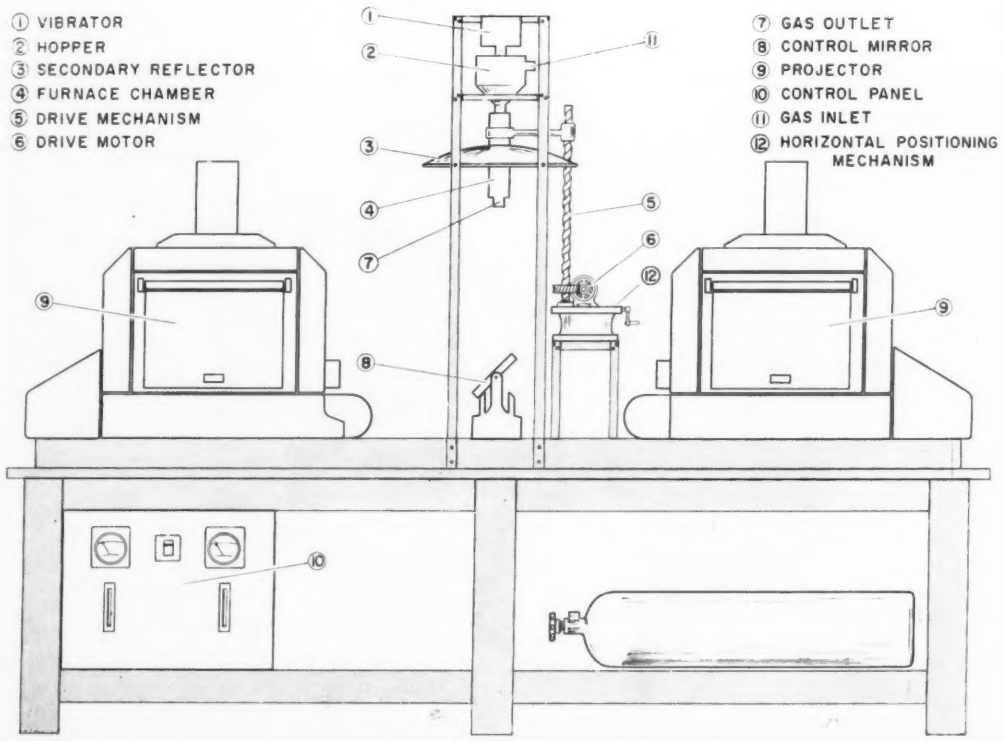

Fig. 13 Diagrammatic sketch of arc image crystal growing furnace

provided to permit close control of crystal stoichiometry at elevated temperatures. Contamination is virtually eliminated, since there is no crucible, and once high purity powders are obtained, purities can be maintained, and in some cases, improved during crystal growth. The glass chamber also permits continuous observation of the crystal during growth.

The arc image, crystal growing furnace is illustrated schematically in Fig. 13. Two commercial arc image sources, each provided with an elliptical mirror, are positioned facing each other, so that their common focus can coincide in one plane. A water-cooled mirror in this position directs either of the beams vertically to another similar elliptical mirror which concentrates the energy downward to the crystal mount. The flux at the focus is approximately 60 to 80 cal/cm²/sec over an area $\frac{1}{4}$ in. in diameter in the furnace chamber. With this system a continuous operation can be maintained by alternating the sources when recarboning is necessary.

The crystals are grown on the tip of a $\frac{1}{4}$-in. diameter refractory rod mounted inside a Pyrex cylinder and partially shielded by an alumina tube. The powder of the refractory compound is fed through a fine orifice, just above the focal plane, from a tube extending through the center of the mirror to a feed hopper driven by a variable amplitude vibrator. The desired environmental gas flowing down the tube directs the powder onto the molten surface. The pedestal is rotated and is drawn downward at the same rate as the crystal grows.

High Temperature Microscopy

An entirely new concept in high temperature microscopy has been reported by Newkirk and Brenden (85). An arc image furnace was constructed for use with a microscope having a working distance of 7.25 in. and a numerical aperture of 0.1. A drawing of the equipment is shown in Fig. 14.

Maximum irradiance of the specimen while under observation is 90 cal/cm²/sec. The interaction of uranium dioxide with silicon or silicon carbide was photographed at 2200 C under a magnification of 22 × with a motion picture camera. Plus X or Kodachrome-type film were used with exposures made at the rate of 24 frames per sec, each lasting $\frac{1}{20}$ sec. Analysis of the motion picture film can provide rate information on the stability of solids in various atmospheres and in contact with other reactive solids.

Ablation

The success of reinforced plastics as heat shields for short-time hypothermal environments has resulted in a large number of studies on the mechanism of ablation. Mixer and Marynowski (86) concerned themselves with the chemical reactions involved. They viewed the total hypothermal effect as the resultant of three components—a velocity effect, a thermal effect and a plasma effect, and used a plasma jet for providing all three of these. The separate effects of the second and third components were simulated by exposure in the arc image furnace and an RF discharge, respectively. They used the same furnace as developed for the propellant ignition studies previously described, with one modification to permit a sampling of the gaseous decomposition products evolved in the exposure chamber. Mass spectrometric analyses of these products were helpful in deducing some of the chemistry involved in ablation.

Acknowledgments

The authors wish to express their appreciation to C. P. Butler of the Naval Radiological Defense Laboratory, whose survey (60) of arc image furnaces eased their task of gathering information on this subject.

References

1 Dutens, L., "An Inquiry into the Origin of the Discoveries Attributed to the Moderns," 1769, available at Stanford University, p. 34.

2 Benveniste, G. and Hiester, N. K., "The Solar Furnace—New Tool for High Temperature Work," *Mech. Engng.*, vol. 78, 1956, pp. 915–920.

3 Geoffroy, M., "Experiences sur les Mètaus Faites Avec le Verre Ardent du Palais Royal." Mèmoire de L'Acadèmie Royale des Sciences, Paris, 1709, p. 162.

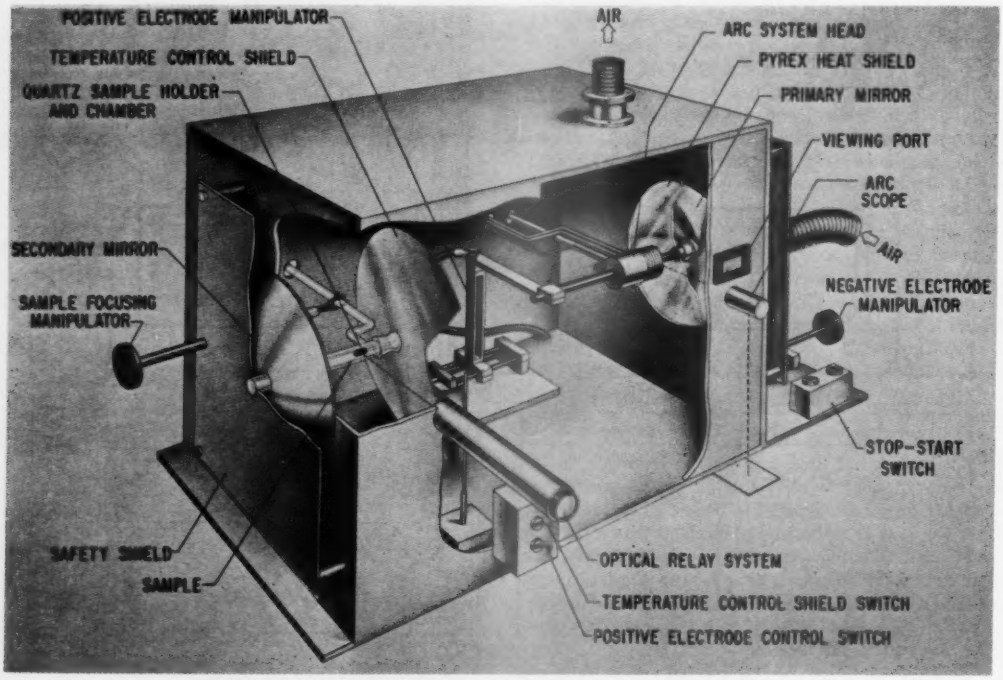

Fig. 14 Arc image furnace for high temperature microscopy

4 Homberg, M., "Observations sur le Fer au Verre Ardent," Mèmoire de L'Acadèmie Royale des Sciences, Paris, 1702, p. 158.

5 Lavoisier, A. L., "Premier Essai du Grand Verre Ardent," Mèmoire de L'Acadèmie Royale des Sciences, Paris, 1782, p. 62.

6 Tyndall, J., "Heat as a Mode of Motion," Appleton Co., N. Y. 1866, p. 281.

7 Trombe, F. and Foex, M., "Recent French Contributions to High Temperature Research," High Temperature Technology Symposium, McGraw-Hill Book Co., Inc., N. Y., 1960, pp. 253–271.

8 Mii, H., "High Temperature Research in Japan," in "High Temperature Technology Symposium," McGraw-Hill Book Co., Inc., N. Y., 1960, pp. 277–291.

9 Marcus, R. J. and Wohlers, H. C., "Photochemistry in the Solar Furnace. Parallel Light and Spectral Distribution," *Ind. Engng. Chem.*, vol. 52, 1960, pp. 377–378.

10 Beyer, R. B. and Fishman, N., "Solid Propellant Ignition Studies with High Flux Radiant Energy as a Thermal Source," in "ARS Progress Series, Vol. 1," in press.

11 Cabannes, F. and Le Phat Vinh, A., "Calcul de la Répartition de L'Énergie Solaire Réfléchie par un Miroir Parabolique," *J. Phys. Rad.*, vol. 15, 1954, p. 817.

12 Farber, J. and Davis, B. I., "Analysis of Large Aperture Parabolic Mirrors for Solar Furnaces," *J. Optical Soc. Amer.*, vol. 47, 1957, pp. 216–220.

13 Bliss, R. W., "Notes on Performance Design of Parabolic Solar Furnaces," *J. Solar Energy Sci. Engng.*, vol. 1, no. 1, 1957, p. 22.

14 Hiester, N. K., Tietz, T. E., Loh, E. and Duwez, P., "Theoretical Considerations on Performance Characteristics of Solar Furnaces," JET PROPULSION, vol. 27, no. 5, 1957, p. 507.

15 Bliss, R. W., "Designing Solar Furnaces for Specific Performance," *J. Solar Energy Sci. Engng.*, vol. 1, no. 2–3, 1957, pp. 55–62.

16 Hukuo, N. and Mii, H., "Design Problems of a Solar Furnace," *J. Solar Energy Sci. Engng.*, vol. 1, no. 2–3, 1957, p. 108.

17 Le Phat Vinh, A., in "Proc. Mont Louis Solar Energy Symposium," June, 1958, in press.

18 Jose, P. D., "The Design of the Condenser of a Solar Furnace Using Non Parabolic Elements," Solar Furnace Support Studies, Air Force Missile Development Center, Holloman Air Force Base, N. Mex., AFMDC-TR-59-15, AD 213260, vol. 2, 1959, pp. 219–260.

19 Simon, A. W., "Calculation of the Concentration of the Solar Radiation Through the Focal Spot of a Parabolic Mirror," *J. Solar Energy Sci. Engng.*, vol. 2, no. 2, 1958, p. 25; *see also* "Calculation of the Concentration of Energy at Points Outside the Focal Spot of a Parabolic Condenser," *J. Solar Energy Sci. Engng.*, vol. 3, no. 4, 1959, p. 67.

20 De La Rue, R., Jr., Loh, E., Brenner, J. L. and Hiester, N. K., "Flux Distribution Near the Focal Plane," *J. Solar Energy Sci. Engng.*, vol. 1, no. 2–3, 1957, p. 94.

21 Jose, P. D., "The Flux Through the Focal Spot of a Solar Furnace," *J. Solar Energy Sci. Engng.*, vol. 1, no. 4, 1957, p. 19.

22 Hiester, N. K., Tietz, T. E. and De La Rue, R., Jr., "Economic Factors in Furnace Design," *J. Solar Energy Sci. Engng.*, vol. 1, no. 2–3, 1957, p. 28.

23 Allison, F., Carr, H. and Hughes, G., "Notes on the Potential Performance of the Clouderoft Solar Furnace," Solar Furnace Support Studies, Air Force Missile Development Center, Holloman Air Force Base, N. Mex., AFMDC-TR-58-7, AD 135014, vol. 1, 1958, p. 23.

24 Foote, J. R. and Adney, J. E., "Some Remarks on the Design of a Solar Furnace and the Calculation of Concentration Using Spherical-Mirror Elements," Solar Furnace Support Studies, Air Force Missile Development Center, Holloman Air Force Base, N. Mex., AFMDC-TR-59-15, AD 213260, vol. 2, 1959, p. 1.

25 Baum, W. A. and Strong, J. D., "Basic Optic Considerations in the Choice of a Design for a Solar Furnace," *J. Solar Energy Sci. Engng.*, vol. 2, no. 3–4, 1958, p. 37.

26 Jose, P. D., "The Design of the Heliostat Mirror for a Solar Furnace," *J. Solar Energy Sci. Engng.*, vol. 1, no. 2–3, 1957, p. 23.

27 Null, M. R. and Lozier, W. W., "Carbon Arc Image Furnaces," *Rev. Sci. Instr.*, vol. 29, 1958, p. 163.

28 Duwez, P., Tietz, T. E., Loh, E. and Hiester, N. K., "The Operation and Use of a Lens-Type Solar Furnace," in "Trans. Conf. on the Use of Solar Energy, Thermal Processes," vol. 2, part I, sect. B, University of Arizona Press, Tucson, 1958, pp. 213–221.

29 Gardon, R., "A Segmented-Mirror Solar Furnace for High-Intensity Thermal Radiation Studies," *Rev. Sci. Instr.*, vol. 25, 1954, pp. 459–463.

30 Davis, J. M. and Cotton, E. S., "Design of the Quartermaster Solar Furnace," *J. Solar Energy Sci. Engng.*, vol. 1, no. 2–3, 1957, pp. 16–22.

31 Trombe, F., "Development of Large Scale Solar Furnaces," in "Solar Energy Research," F. Daniels, Ed., Univ. of Wisconsin Press, Madison, 1955, pp. 169–171.

32 Simon, A. W., "The Loss of Energy and Parabolic Condenser of a Solar Furnace," *J. Solar Energy Sci. Engng.*, vol. 2, no. 2, 1958, pp. 30–33.

33 Hughes, G., "A Solar Furnace Using a Horizontal Heliostat Array," *J. Solar Energy Sci. Engng.*, vol. 2, no. 3–4, 1958, p. 49.

34 Toong, T. Y., "Studies on Thermal Effects on Solar Furnace Mirrors," Solar Furnace Support Studies, Air Force Missile Development Center, Air Force Base, N. Mex., AFMDC-TR-59-15, AD 213260, vol. 2, 1959, pp. 133–144.

35 Solar Furnace Support Studies, Air Force Missile Development Center, Holloman Air Force Base, N. Mex., AFMDC-TR-58-7, AD 135014, 1958.

36 Solar Furnace Support Studies, Air Force Missile Development Center, Holloman Air Force Base, N. Mex., AFMDC-TR-59-15, AD 213260, vol. 2, 1959.

37 Ghai, M. L., "Design of Reflector-Type Direct Solar Cooker," *J. Sci. Ind. Res.*, vol. 12A, no. 4, 1953, p. 168.

38 Wight, R. H., "Materials and Surfaces for Solar Furnaces," *J. Solar Energy Sci. Engng.*, vol. 1, no. 2–3, 1957, p. 84.

39 Laszlo, T. S., de Dufour, W. F. and Erdell, J., "A Guiding System for Solar Furnaces," *J. Solar Energy Sci. Engng.*, vol. 2, no. 1, 1959, pp. 18–20.

40 Moore, J. G. and St. Amand, P., "A Guidance System for a Solar Furnace," *J. Solar Energy Sci. Engng.*, vol. 1, no. 4, 1957, pp. 27–29.

41 Trombe, F., "Self-Regulating Automatic Heliostat Reflecting Mirror Device," U. S. Patent 2,712,772, July 12, 1955.

42 Laszlo, T., "Temperature and Flux vs. Geometrical Perfection," *J. Solar Energy Sci. Engng.*, vol. 1, no. 2–3, 1957, pp. 78–83.

43 Conn, W. M., "A Solar Furnace of 120″ Diameter for Studying Highly Refractory Substances," *Rev. Sci. Instr.*, vol. 22, 1951, p. 945.

44 Conn, W. M., "Obtaining Very High Temperatures by Solar Furnaces," in "High Temperature Technology," I. E. Campbell, ed., John Wiley and Sons, Inc., N. Y., 1956, pp. 319–332.

45 Kostkowski, H. J., "The Accuracy and Precision of Measuring Temperatures Above 1000K," in "High Temperature Technology Symposium," McGraw-Hill Book Co., Inc., N. Y., 1960, pp. 33–44.

46 Blau, H. H., "Measurement of Flux, Emittance and Related Properties," in "High Temperature Technology Symposium," McGraw-Hill Book Co., Inc., N. Y., 1960, pp. 45–53.

47 Brenden, B. B., Newkirk, H. W. and Woodcock, S. H., "A Study of Temperature Measurements in a Solar Furnace," *J. Solar Energy Sci. Engng.*, vol. 2, no. 1, 1958, pp. 13–17.

48 Shank, M. E., "Instrumentation for the 108-Foot Diameter Cloudcroft Solar Furnace," Solar Furnace Support Studies, Air Force Missile Development Center, Holloman Air Force Base, N. Mex., AFMDC-TR-59-15, AD 213260, 1959, pp. 161–186.

49 Farber, J., "Images of Very High Temperature Sources," Proc. Symposium High Temperature, Stanford Research Institute, Menlo Park, Calif., 1956, pp. 1–9.

50 Gardon, R., "An Instrument for the Direct Measurement of Intense Thermal Radiation," *Rev. Sci. Instr.*, vol. 24, 1953, pp. 366–370.

51 Hughes, G., "A Radiation Fluxmeter for High Intensity Applications," Solar Furnace Support Studies, Air Force Missile Development Center, Holloman Air Force Base, N. Mex., AFMDC-TR-59-15, AD 213260, vol. 2, 1959, pp. 145–159.

52 Loh, E., Hiester, N. K. and Tietz, T. E., "Heat Flux Measurements at the Sun Image of the California Institute of Technology Lens-Type Solar Furnace," *J. Solar Energy Sci. Engng.*, vol. 1, no. 4, 1957, pp. 23–26.

53 Cohen, R. K. and Hiester, N. K., "A Survey of Solar Furnace Installations in the United States," *J. Solar Energy Sci. Engng.*, vol. 1, no. 2–3, 1957, pp. 115–117.

54 "A Survey of Solar Furnace Installations in the United States," *Supplement, J. Solar Energy Sci. Engng.*, vol. 1, no. 4, 1957, p. 35.

55 "A Survey of Solar Furnace Installations in the United States," *J. Solar Energy Sci. Engng.*, vol. 2, no. 3–4, 1958, p. 55.

56 Noguchi, T., "Solar Furnace Research in Japan," *J. Solar Energy Sci. Engng.*, vol. 3, no. 3, 1959, pp. 44–46.

57 Jensen, J. J., Ed., "Applied Solar Energy Research, a Directory of World Activities and Bibliography of Significant Literature," Assoc. Appl. Solar Energy, Phoenix, Ariz., 1959.

58 Ploetz, G. P., "The 'Clam Shell' Thermal Image Device," Air Force Cambridge Research Center, Bedford, Mass., AFCRC-TN-59-759, Sept. 1959.

59 Davis, T. P., "The Carbon Arc Image Furnace," Proc. Symposium High Temperature, Stanford Research Institute, Menlo Park, Calif., 1956, pp. 10–15.

60 Butler, C. P., "Image Furnace Research," in "High Temperature Technology Symposium," McGraw-Hill Book Co., Inc. N. Y., 1960, pp. 1–28.

61 Null, M. R. and Lozier, W. W., "Carbon-Arc Image Furnace," *J. Soc. Motion Pic. & Tv. Engrs.*, vol. 68, 1959, p. 80.

62 "Performance Data Sheet on ADL-Strong Arc Imaging Furnace," Bulletin of A. D. Little, Inc., Cambridge, Mass., 1959.

63 Finkelnburg, W., "The High Current Carbon Arc," FIAT Final Rep. 1052, OTS, Dept. of Commerce, Washington, D. C., PB-81644, 1947.

64 "Symposium on Searchlights," Illuminating Engineering Society, 32 Victoria Street, London, 1948.

65 Horning, D. O., "Arc Image Furnace," ARDC Contract AF 18(603)-123, University of California, 1959. [See ref. (59), Fig. 3).]

66 Todd, F. C., Project no. 790–4, NASA, Southwest Research Institute, 1958.

67 De La Rue, R. E., Jr. and Halden, F. A., "Arc Image Furnace for Growth of Single Crystals," *Rev. Sci. Instr.*, vol. 31, 1960, p. 35.

68 Finkelnburg, W. and Latil, J. P., "A Fully Automatic Continually Operating, Very High-Intensity Carbon Arc Lamp," *J. Optical Soc. Amer.*, vol. 44, 1954, pp. 1–5.

69 Gretener, E., "An Improved Carbon-Arc Light Source for Three-Dimensional and Wide-Screen Projectors," *J. Soc. Motion Pic. & Tv. Engrs.*, vol. 61, 1953, pp. 516–524.

70 Latil, J. P., "Automatic Recarboning of Carbon-Arc Lamps," *J. Soc. Motion Pic. & Tv. Engrs.*, vol. 66, 1957, pp. 338–339.

71 Sobon, L. E. and Halden, F. A., "Preparation and Evaluation of Single Crystals of High Temperature Semiconductors," Stanford Research Institute, Menlo Park, Calif., Contract no. NOnr-2620(00), NR 032-447, Quarterly Status Rep. no. VII, March 15 to June 15, 1960.

72 Brown, F. W., "Measurement of the Spectral Intensity Distribution of a Convergent High Intensity Light Beam with a Magnesium-Oxide-Smoked Plate," *J. Solar Energy Sci. Engng.*, vol. 1, no. 2–3, 1957, pp. 104–107.

73 Trombe, F. and Foex, M., "Traitements á Haute Tempèrature au moyen de Fours Centrifuges Chauffès par L'Energie Solaire," in "Trans. Conf. on the Use of Solar Energy, Thermal Processes," vol. 2, part 1, sect. B, University of Arizona Press, Tucson, 1958, p. 146.

74 Laszlo, T., "Some Considerations for the Selection of Materials for Containing High Temperatures," Proc. Symposium High Temperature, Stanford Research Institute, Menlo Park, Calif., 1956, p. 116.

75 Duwez, P. and Loh, E., "Phase Relationship in the System Zirconia-Thoria," *J. Amer. Ceram. Soc.*, vol. 40, 1957, p. 321.

76 Conn, W. M., "A Review of the Production of Molten Zirconia in the Solar Furnace," *J. Solar Energy Sci. Engng.*, vol. 3, no. 3, 1959, p. 39.

77 Glaser, P. E., "Engineering Research with a Solar Furnace," *J. Solar Energy Sci. Engng.*, vol. 2, no. 2, 1958, p. 7.

78 Marcus, R. J. and Wohlers, H. C., "Photochemistry in the Solar Furnace," *Ind. Engng. Chem.*, vol. 51, 1959, p. 1335.

79 Martin, S. B. and Lai, W., "Ignition by Thermal Radiation," Proc. Fire Res. Conf., Natl. Acad. Sci. Publ. no. 475, 1956, pp. 84–92.

80 Butler, C. P. and Inn, E. C. Y., "Thermal Diffusivity of Metals at Elevated Temperatures," in "Thermodynamic and Transport Properties of Gases, Liquids, and Solids," McGraw-Hill Book Co., Inc., N. Y., 1959, pp. 377–390.

81 Butler, C. P. and Inn, E. C. Y., "A Radiometric Method for Determining Specific Heat at Elevated Temperatures," Naval Radiological Defense Laboratories, USNRDL-TR-235, 1958, AD 200857, 30 pp.
82 Butler, C. P. and Inn, E. C. Y., "The Total Hemispherical Emissivity of Metals," Naval Radiological Defense Laboratories, USNRDL-TR-327, 1959, AD 225997.
83 Janes, M., "Graphite-Based Materials for High Temperature Applications," Natl. Carbon Co., Cleveland, Ohio, WADC-TR-57-602, 1958, AD 150962, 59 pp.
84 Null, M. R. and Lozier, W. W., "Measurement of Reflectance and Emissivity of Graphite at Arc Temperature with a Carbon Arc Image Furnace," *J. Appl. Phys.*, vol. 29, 1958, p. 1605.
85 Newkirk, H. W. and Brenden, B. B., "A Carbon Arc Image Furnace and Microscope for Studies at High Temperatures," UC 25, HW-59323, TID-4500, 14th ed., OTS, U.S. Dept. of Commerce, Washington, D. C., 1959.
86 Mixer, R. Y. and Marynowski, C. W., "A Study of the Mechanism of Ablation of Reinforced Plastics," WADC-TR-59-668, part 1, 1959, p. 30.

Astronomical Constants and Their Importance in Lunar Trajectory Determination

C. TROSS[1]

Aeronutronic Div.,
Ford Motor Co.
Newport Beach, Calif.

Whenever the problem of calculating orbits for space vehicles arises, the accuracy of such calculations receives close scrutiny. No matter what technique is adopted for the orbit calculation, uncertainties enter into the calculations which cannot be eliminated by numerical techniques and mathematical representations. These uncertainties result from insufficient accuracy in the constants utilized for the representation of such effects as Earth's bulge and equatorial radius, the lunar and solar masses and their position coordinates. In this paper an attempt is made to appraise the effects astronomical constants have on lunar vehicle impacts. This study shows that lunar impacts can only be predicted to fall into an area of about 78 miles in radius. More accurate predictions can only be made when the terrestrial and astronomical constants are improved.

ALTHOUGH concentrated efforts are being directed to improve the geocentric and selenocentric constants at the present time, only limited contributions can be made until such time as the existing and future satellite data can be analyzed completely. Until the time when these constants are improved, the present values with their respective uncertainties must remain the basis for orbit determination activities. It is very important, however, to appraise the significance of each constant and the effect of all known uncertainties on some quantity, such as the impact point of a ballistic trajectory. The results of such an investigation on lunar trajectories are presented in this report, and the constants to which lunar trajectories are most sensitive are identified.

Perturbation Effects and Their Importance in Precision Lunar Trajectories

What perturbations must be included in the equations of motion for accurate lunar trajectory calculations? Everyone who has ever faced the problem of writing equations of motion has had to answer this question. In this section some of the considerations which should enter into such an analysis are discussed.

A convenient form in which the equations of motion may be considered is to add accelerations resulting from perturbations to the two-body equation of motion for a lunar vehicle, whose mass is negligible, moving under the influence of Earth's gravitational field only. Thus the equation of motion takes the form (3 and 7)[2]

$$\ddot{\mathbf{r}}_{2,1} = -m_2(\mathbf{r}_{2,1}/r_{2,1}^3) + P \qquad [1]$$

where

$\mathbf{r}_{i,j}$ = vectorial distance from body i to body j
m_i = mass of body i
P = those perturbations not yet identified

Numerical subscripts used in this paper to identify bodies are: 1, vehicle; 2, Earth; 3, moon; 4, sun; 5, 6, . . ., n, solar bodies.

A lunar vehicle experiences accelerations caused by the masses of the moon, sun and other solar bodies. The perturbative accelerations resulting from these effects take the form

$$P_I = \sum_{i=3}^{n} m_i \left(\frac{\mathbf{r}_{i,2}}{r_{i,2}^3} - \frac{\mathbf{r}_{i,1}}{r_{i,1}^3} \right) \qquad [2]$$

Maximum values for the differential accelerations are given in Table 1. From these tabulated values it is noted that perturbations resulting from planets other than Earth are quite small and may therefore be ignored even in a high precision lunar trajectory determination procedure.

The Earth is an oblate spheroid, a fact not taken into account in the two-body equations of motion. Therefore, another perturbation owing to Earth's bulge must be con-

Received March 24, 1960.
[1] Senior Staff Member.
[2] Numbers in parentheses indicate References at end of paper.

sidered. Bulge perturbations are obtained through the relation

$$P_{II} = \frac{m_2 \mathbf{r}_{2,1}}{r_{2,1}^5} JA(\mathbf{r}) + \frac{m_2 \mathbf{r}_{2,1}}{6 r_{2,1}^7} KB(\mathbf{r}) \qquad [3]$$

where J and K are related to the DeSitter constant and are the second and fourth harmonic terms in Earth's gravitational potential. Their respective coefficients may be given as

$$A(x) = A(y) = A(z) - 2 = 1 - 5U^2$$

$$B(x) = B(y) = B(z) - 12 + 28U^2 = 3 - 42U^2 + 63U^4$$

where U is a function of z.

The rectangular geocentric inertial coordinates are defined so that the x-y plane identifies the Equator plane with x directed toward the vernal equinox, z directed toward the north pole, and y completing the right-hand system. Accelerations resulting from the terrestrial harmonic terms as a function of r have been tabulated in Table 2. From this table it is apparent that the bulge harmonics of the second order are quite important for the entire lunar trajectory calculation, but the fourth-order harmonics become negligible after the vehicle is more than 8 g-radii away from the geocenter, so that these terms are not needed beyond that distance.

Thus far, solar system perturbations have been analyzed and identified. It is of interest to determine the effect these perturbations have on the lunar impact point. To analyze this effect a standard trajectory[3] is calculated in which the nominal values of all constants are employed. Subsequent trajectories called "altered trajectories" are considered in which all parameters are the same as those used in the standard trajectory, only the perturbative term under consideration is set to zero. The impact point of the standard trajectory is then compared with the impact point of the altered trajectory[4] and displacement on the lunar surface is determined. See Table 3.

It will also be of interest to determine maximum relative accelerations imposed on the vehicle by various perturbations during its transit to the moon. For this purpose Table 4 has been prepared.

Thus far the perturbations caused by the terrestrial bulge, the sun, solar system planets and the moon have been considered. The moon's effect upon lunar vehicles is, of course, not only that of a point mass, but its figure may well be a contributor of additional perturbations. A number of authors, such as Jeffreys (10), think that the moon's figure may be a triaxial ellipsoid whose longest axis is directed toward Earth. Based on this assumption, estimates for the lengths of the longest, the intermediate and the shortest axes, represented by a, b and c respectively, can be made (2)

$$a = 1738.57 \pm 0.07 \text{ km}$$
$$b = 1738.21 \pm 0.07 \text{ km}$$
$$c = 1737.49 \pm 0.07 \text{ km}$$

The moments of inertia about each axis are symbolized by A, B and C, respectively, and experimentally determined values for their ratios are (10)

$$(C - A)/C = 0.6269 \times 10^{-3} \pm 2.7 \times 10^{-6}$$
$$(B - A)/C = 0.2081 \times 10^{-3} \pm 9 \times 10^{-7}$$

The acceleration owing to the moon's triaxiality is then written

$$\frac{\partial \phi}{\partial \mathbf{r}_{3,1}} = -\frac{3}{2 r_{3,1}^4} K(\mathbf{r}_{3,1}) C \times \left[\frac{C - A}{C} U_1(\mathbf{r}_{3,1}) + \frac{B - A}{C} U_2(\mathbf{r}_{3,1})\right]$$

[3] A standard trajectory is one for which the velocity vector at impact intersects the lunar surface at normal incidence.

[4] In the event the altered trajectory does not impact on the moon's surface the point of nearest approach is used in place of the impact point.

Table 1 Solar system perturbations on lunar vehicles

Object	Perturbative Acceleration on vehicle (Earth g's) geocenter vehicle distance — 32 g-radii	64 g-radii
Sun	16.5×10^{-7}	33.0×10^{-7}
Moon	0.1×10^{-4}	0.16
Venus	0.15×10^{-9}	0.30×10^{-9}
Mars	0.25×10^{-11}	0.53×10^{-11}
Jupiter	0.21×10^{-10}	0.43×10^{-10}

Table 2 Accelerations resulting from terrestrial harmonics

r	$\ddot{x}_2/\ddot{x}_0$	$\ddot{x}_4/\ddot{x}_0$
1	0.6494×10^{-2}	0.7232×10^{-4}
4	0.4058×10^{-3}	0.2824×10^{-6}
8	0.1015×10^{-3}	0.1766×10^{-7}
64	0.1585×10^{-5}	0.4310×10^{-11}

where $\ddot{x}_0 = -\frac{1}{r^2}$; $\ddot{x}_2 = \frac{4J}{r^4}$; $\ddot{x}_4 = -\frac{8K}{r^6}$

$(U^2 = \sin^2 \delta = 1)$

Table 3 Perturbational effects on lunar impact

Constant	Deviation from standard trajectory impact, nautical miles
J	368.0
K	9.83
m_4	374.0
J, K, m_4, m_3 (i.e., two-body orbit)	5500.0

Table 4 Maximum accelerations resulting from various perturbations

Perturbing object	Acceleration relative to geocenter, Earth g's — At Earth	32 g-radii	At moon (64 g-radii)
Earth	1.0	0.1×10^{-2}	0.2×10^{-3}
Second terrestrial harmonic	0.6×10^{-2}	0.6×10^{-7}	0.4×10^{-8}
Fourth terrestrial harmonic	0.7×10^{-4}	0.7×10^{-13}	0.1×10^{-14}
Moon	...	0.1×10^{-4}	0.16
Sun	...	0.16×10^{-5}	0.33×10^{-5}
Venus	...	0.15×10^{-9}	0.30×10^{-9}
Mars	...	0.25×10^{-11}	0.5×10^{-11}
Jupiter	...	0.2×10^{-10}	0.4×10^{-10}
Centrifugal force owing to precession	...	...	0.3×10^{-14}

Table 5 Impact deviations owing to uncertainty in astronomical constants

Constant	Value used (1)	Maximum deviation from standard impact, nautical miles	Remarks
J	$(1623.41 \pm 4) \times 10^{-6}$	8.5	
m_4	$(332488 \pm 43)m_2$	0	
m_3	$(122888 \pm 39)10^{-7}m_2$	0.016	
π_3	Ephemeris value[a] $\pm$ 0.0154 sec	4.6	
a_e	6.378270 ($\pm$ 11 $\times$ 10^{-6}) megameters	47.41	from velocity uncertainty
		32.67	from altitude uncertainty
		78.32	from altitude and velocity uncertainty

[a] The apparent value from the "American Nautica Almanac and Lunar Ephemeris" (8) is used in the calculation, and the uncertainty $\pm$0.0154 sec is added.

where $\mathbf{r}_{3,1}$ is the vector from the selenocenter to the vehicle and $K(\mathbf{r}_{3,4})$, $U_1(\mathbf{r}_{3,1})$ and $U_2(\mathbf{r}_{3,1})$ are functions of the direction cosines of $\mathbf{r}_{3,1}$. From these values of the ratio of the moments of inertia an upper bound for the bulge perturbation can be calculated. At the moon's surface this bulge perturbation is 1.3×10^{-5} Earth g's; halfway between Earth and the moon it is about 5×10^{-10} Earth g's, and at Earth's surface it is about 1.2×10^{-10} Earth g's. It can therefore be concluded that the lunar bulge should be considered as a perturbation in computing orbits for lunar satellites, but for Earth-moon trajectories this perturbation may be ignored.

Since the equations of motion may be written to apply to a nonrotating system of axes, the question of the axis rotating slowly owing to precession and nutation is next considered. The value of the precession is about 50 sec per year. The centrifugal acceleration at the distance of the moon (64 g-radii approximately) is then about 1.4×10^{-17} g-radii/min^2 (Table 4).

Planetary and solar position coordinates are referred to the mean equinox of 1950.0. Thus these coordinates are referred to a rotating coordinate system; its rate is about 50 sec of arc per year. The precession displacement for the sun will be 2.4×10^{-5} times the perturbation terms of the sun, which is small. The nutational terms are even of a lesser order of magnitude and can be neglected. The largest of the short-period nutational terms gives rise to a maximum acceleration of 2×10^{-15} Earth g's. Thus, it can be seen that sufficient justification exists for treating a system, which in reality is rotating, as inertial, for the practical purposes of calculation.

Constants

For the purpose of this study, every effort has been made to utilize the latest and most reliable constants possible. The values of the astronomical constants employed in the lunar vehicle orbit determinations discussed in this report are:

Sun's mass (1)

$$m_4 = 332488(1 \pm 0.00013)\ m_2 = 332488 \pm 43\ m_2$$

Moon's mass (1)

$$m_3 = [1/81.375(1 \pm 0.0003)]\ m_2 = (122888 \pm 39)10^{-7}\ m_2$$

Second harmonic in Earth's gravitational potential (9)

$$J = (1623.41 \pm 4)10^{-6}$$

Fourth harmonic in Earth's gravitational potential (9)

$$K = (6.37 \pm 0.23)10^{-6}$$

Geocentric gravitational constant (1)

$$k_e = 0.07436574\ g\text{-radii}^{3/2}/\text{min}$$

$$k_e^{-1}\ \text{min} = 13.447052\ \text{min}$$

Earth's equatorial radius[5] (1,6)

$$a_e = (6.378270)\ (\pm 10 \times 10^{-6})\ \text{megameters}$$

Earth's mass is chosen as unity.

Uncertainty in the Constants

A procedure similar to that outlined previously in determining the effect perturbations have on the lunar impact point is employed to determine the effect uncertainties in the astronomical constants have on lunar trajectories.

Variations in lunar trajectory impact sites resulting from the uncertainties in the constants are determined by first adopting a standard reference trajectory determined on the basis of the nominal value of the constant. Deviations from the reference trajectory impact are then determined by altering the constant under consideration to its limiting value within the recorded uncertainty; trajectories so determined are called "altered trajectories." Thus, the trajectory variations owing to the uncertainties in m_3, m_4, J' and π_4 are determined.[6] The uncertainty in Earth's equatorial radius a_e is reflected in the gravitational constant and in the conversion of burnout velocity and altitude from laboratory units into astronomical units. Earth's radius is given as $a_e = 6.37827\ (\pm 11 \times 10^{-6})$ megameters $= 20926040.8229 \pm 230.1865$ ft. With this value it is found that 1 g-radius/$k_e^{-1} = 25936.342 \pm 0.2853$ fps. Suppose that a burnout velocity of $\dot{s} = 34704.2391$ fps is given; then, upon converting this velocity it is found that

$$1.338069202\ g\text{-radii}/k_e^{-1} \geqslant \dot{s} \geqslant 1.338039796\ g\text{-radii}/k_e^{-1}$$

Thus the uncertainty in Earth's equatorial radius may result in an error in conversion of the burnout velocity units, thereby causing the vehicle to follow an altered trajectory whose impact differs from the design impact point. The maximum impact deviation resulting from a velocity uncertainty is about 47 nautical miles. See Table 5.

In converting the burnout altitude from laboratory units to

[5] At the time these calculations were performed, the latest value of a_e which is $a_e = 6.378145\ (1 \pm 11 \times 10^{-6})$ megameters had not been determined. Consequently the calculations discussed in this paper are based on the older value.

[6] π_4 is the moon's horizontal parallax.

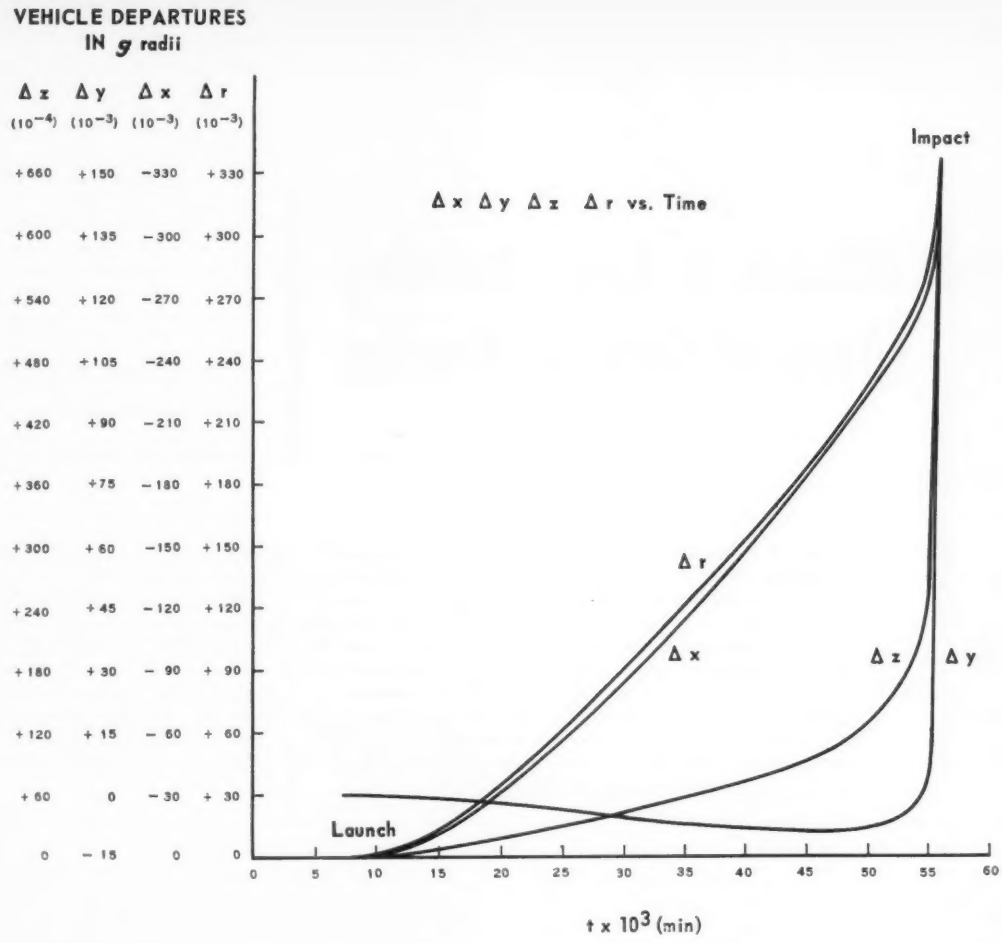

Fig. 1 Maximum trajectory deviations owing to uncertainties in Earth's gravitational radius

astronomical units, the uncertainty in Earth's equatorial radius is again reflected. Suppose the burnout altitude is given as $h = 2092604.08229$ ft, then upon converting this altitude into astronomical units it is found that

$$1.1000121\ g\text{-radii} \geq h \geq 1.0999879\ g\text{-radii}$$

The nominal value is $h = 1.1$ g-radii. The maximum impact deviation owing to an altitude uncertainty is about 33 nautical miles. See Table 5. Combined, the maximum deviation resulting from both altitude and velocity uncertainty is about 78 miles, in contrast to other uncertainties, such as the second harmonic term in Earth's potential, the sun's mass, the moon's mass and the moon's horizontal parallax, all causing impact variations which never exceed 10 nautical miles. It is, therefore, evident that the uncertainty in Earth's gravitational radius may cause the most significant impact variations.

A summary of the maximum impact point variations owing to the uncertainty in the astronomical constants is given in Table 5.

Orbit Deviations

It has been shown that the uncertainty in the astronomical constants causes an uncertainty in the orbit the vehicle follows from Earth to the moon. To illustrate how a maximum deviated orbit may vary from the nominal orbit, differences between two such $3\frac{1}{4}$-day trajectories were computed, and the results are shown graphically in Fig. 1.

References

1 Herrick, S., Baker, R. M. L., Jr. and Hilton, C., "Gravitational and Related Constants for Accurate Space Navigation," presented at VIIIth International Astronautical Congress, Barcelona, 1957.

2 Alexandrov, I., "The Lunar Potential," Aeronutronic Div., Newport Beach, Calif., Publication no. U-377, Dec. 12, 1958.

3 Herrick, S., "Astrodynamics," Van Nostrand Co., Inc., N. Y., to be published, chaps. VI and XIV.

4 Moulton, F. R., "Celestial Mechanics," MacMillan Co., N. Y., 1914, chaps. VI, VIII and X.

5 Baker, R. M. L., Jr., "Treatment of Third Harmonic of the Earth's Potential Field by Method of Special Perturbations," Aeronutronic Div., Newport Beach, Calif., Publication no. C-365, Jan. 1959.

6 Tross, C., Baker, R. M. L., Jr. and Westrom, G., "Gravitational Constants," Aeronutronic Div., Newport Beach, Calif., Publication no. U-380, March 6, 1959.

7 Tross, C. and Liu, A., "Free Flight Trajectory for a Lunar Mission," Aeronutronic Div., Newport Beach, Calif., Publication no. U-329a, March 6, 1959.

8 "The American Ephemeris and Nautical Almanac," U. S. Naval Observatory, Washington, D. C., published yearly.

9 Hilton, C., "Gravitational Constants," Aeronutronic Div., Newport Beach, Calif., Appendix A to Aeronutronic Publication no. C-365, Sept. 1959.

10 Jeffreys, H., "The Earth as a Planet," University of Chicago Press, Chicago, Ill., 1959, pp. 48–50.

Heat Diffusion in Gases, Including Effects of Chemical Reaction

C. FREDERICK HANSEN[1]

Ames Research Center,
NASA
Moffett Field, Calif.

The diffusion of heat through gases is treated where the coefficients of thermal conductivity and diffusivity are functions of temperature. The diffusivity is taken proportional to the integral of thermal conductivity, where the gas is ideal, and is considered constant over the temperature interval in which a chemical reaction occurs. The heat diffusion equation is then solved numerically for a semi-infinite gas medium with constant initial and boundary conditions. These solutions are in a dimensionless form applicable to gases in general, and they are used, along with measured shock velocity and heat flux through a shock reflecting surface, to evaluate the integral of thermal conductivity for air up to 5000 K. This integral has the properties of a heat flux potential and replaces temperature as the dependent variable for problems of heat diffusion in media with variable coefficients. Examples are given in which the heat flux at the stagnation region of blunt hypersonic bodies is expressed in terms of this potential.

THIS paper will consider some aspects of heat conduction through gases. Specifically, it will be confined to the case of pure diffusion; that is, heat transfer by mass convection and by radiation will not be treated. Finally, it will consider briefly the role of the diffusion process in heat transfer to the stagnation region of high speed vehicles.

Heat Diffusion in Ideal Gases

The classical solutions to the heat diffusion equation have generally made use of the assumption that the coefficient of thermal conductivity is a constant [see (1 and 2) for example].[2] However, for the problem of interest here, the conduction of heat through gases, thermal conductivity must be treated as a strong function of temperature (3). In such a case, it is useful to replace the usual dependent variable, temperature, with a quantity φ

$$\varphi = \int_0^T k dT \qquad [1]$$

which is the coefficient of thermal conductivity integrated over temperature. Then the differential equation of heat conduction takes the usual form of the diffusion equation

$$\partial\varphi/\partial t - a\nabla^2\varphi = 0 \qquad [2]$$

where a is the thermal diffusivity. The dependent variable φ will be called the heat flux potential, since the heat flux at any point in the medium is just the gradient of φ

$$q = \text{grad } \varphi \qquad [3]$$

Note that just as the reference level used for temperature is arbitrary, so the lower limit of the integral (Eq. [1]) is arbitrary. However, it will prove convenient to choose this lower limit somewhere near absolute zero for the case of conduction in gases.

Consider now the one-dimensional heat flow through a semi-infinite gas medium, where the initial conditions and the boundary conditions are constants. The initial potential throughout the gas will be designated by φ_∞ and the boundary value by φ_0, the diffusivities by a_∞ and a_0, respectively (see Fig. 1). Normalized coordinates will be used such that φ_0 and a_0 are both taken to be unity. The results can easily be generalized to account for arbitrary units of these boundary conditions, of course.

The idealization of constant initial and boundary conditions will be approximately realized in a physical situation where the reservoir is a slab of material with a very large heat capacity and a large thermal conductivity, such as a metal. Then the wall can soak up heat fast enough to maintain nearly constant conditions at the interface. The slab might be suddenly immersed in a constant temperature gas, for example, or, alternatively, the gas might be heated suddenly by a plane shock wave reflecting from the solid interface.

Boltzmann (4) has shown that the solution to this problem may be expressed with perfect generality as a function of $x/\sqrt{t}$. Therefore, the time and distance variables are transformed to the single dimensionless parameter y

$$y = x/\sqrt{4a_0 t} \qquad [4]$$

where a_0 is the diffusivity of the gas at the boundary. The coefficient a_0 is unity, of course, in the present normalized coordinate system, but this is not an essential feature of the transformation. In terms of this parameter y, the partial differential equation of heat conduction becomes the dimen-

Presented at the ARS Semi-Annual Meeting, June 8–11, 1959, San Diego, Calif.

[1] Chief, Physics Branch. Member ARS.

[2] Numbers in parentheses indicate References at end of paper.

sionless, total differential equation

$$a\frac{d^2\varphi}{dy^2} + 2y\frac{d\varphi}{dy} = 0 \qquad [5]$$

The factor 4 in the parameter y (Eq. [4]) is an arbitrary stretching factor. It is chosen merely so that the solutions to Equation [5] reduce to the usual error function form when the diffusivity is constant, that is when a equals a_0. The merit in using the normalized form for the potential φ (that is, ϕ/ϕ_0) is that one set of integrations for Equation [5] will suffice for all possible boundary conditions. All that is required before one proceeds with the integration is that the diffusivity a be evaluated. Two cases will be considered, one in which the gas is ideal and inert, and the second in which the gas is in local equilibrium but is chemically active with a large heat of reaction.

According to the kinetic theory of inert gases (5), the coefficient of thermal conductivity is approximately proportional to a power n of the temperature, where n is close to $\frac{1}{2}$. Thus the integral of thermal conductivity is proportional to the $n + 1$ power of temperature

$$\int k dT \propto T^{n+1} \qquad [6]$$

Now the thermal diffusivity equals the conductivity divided by the heat capacity per unit volume $C\rho$. Since the density ρ is inversely proportional to temperature, for an ideal gas, the diffusivity is proportional to the $n + 1$ power of temperature also

$$k/C\rho \propto T^{n+1} \qquad [7]$$

It follows that diffusivity is proportional to the potential φ, and in the present normalized coordinates this means that

$$a = \varphi \qquad [8]$$

Sometimes a linear relation between a and φ with a finite intercept will best fit measured values, but this can always be transformed to the direct proportionality of Equation [8] by appropriate adjustment of the lower limit of the integral, Equation [1]. Generally, this limit will be close to absolute zero.

It may be remarked that even if one accounts for the variations of heat capacity which occur in a real gas, the preceding relations are valid to the order of approximation that Prandtl number is a constant. This can be seen from the fact that diffusivity is just the kinematic viscosity divided by the Prandtl number

$$a = \frac{\mu/\rho}{Pr} \qquad [9]$$

and the kinematic viscosity is again approximately proportional to the $n + 1$ power of temperature, at least in gases composed of neutral particles.

When the result of Equation [8] is used, the heat diffusion equation takes the simple but nonlinear form

$$\varphi\frac{d^2\varphi}{dy^2} + 2y\frac{d\varphi}{dy} = 0 \qquad [10]$$

Analytic solutions to Equation [10] are known, but none which satisfy the boundary conditions, namely

$$\varphi(0) = 1 \qquad [11a]$$

$$\lim_{y\to\infty} \varphi \to \varphi_\infty \qquad [11b]$$

However, it is relatively easy to integrate the equation numerically, starting from a given value of the boundary derivative $\varphi_0' = (d\varphi/dy)_0$, and terminating as the solution asymptotically approaches a limit φ_∞. The solutions are something like error functions stretched slightly out of shape. Three of these solutions are shown in Fig. 2 as functions of

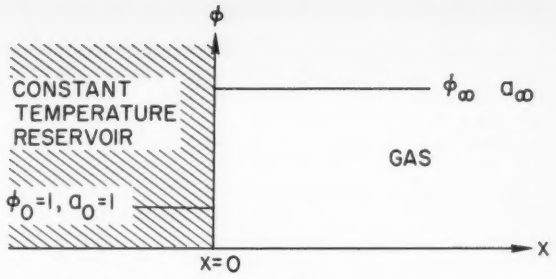

Fig. 1 One-dimensional heat diffusion

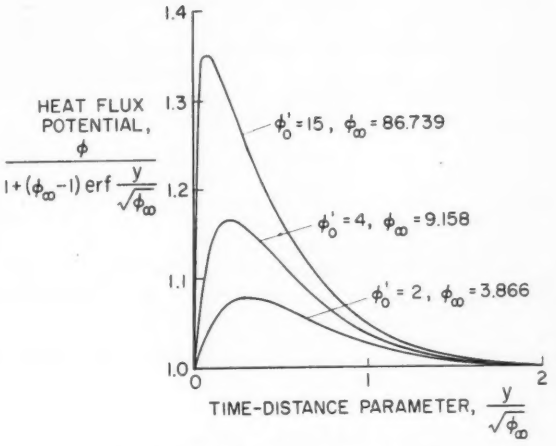

Fig. 2 Heat potentials in inert gases

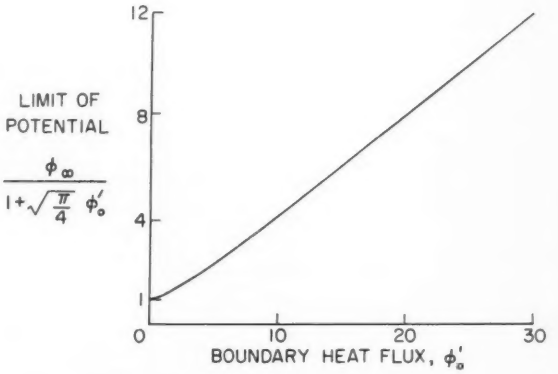

Fig. 3 Heat diffusion in inert gases

$y/\sqrt{\varphi_\infty}$. The solutions φ are shown divided by the error functions, $1 + (\varphi_\infty - 1)$ erf $(y/\sqrt{\varphi_\infty})$. The φ functions rise more steeply than the error functions near the origin, go through a maximum deviation, then approach the error function as a limit.

The value of φ_∞ is uniquely related to the derivative at the origin, φ_0'. This relation is shown in Fig. 3. The derivative φ_0' is equivalent to a dimensionless heat flux at the boundary, whereas the normalizing function $1 + \sqrt{\pi/4}\,\varphi_0'$ is the value which φ_∞ would have if diffusivity were a constant. We shall return to this relation between φ_∞ and φ_0' after considering the case of the chemically reacting gas.

Heat Diffusion in a Chemically Reacting Gas

A chemical reaction in the gas behaves as a reservoir which soaks up heat as temperature is increased, and liberates heat when temperature drops. Consequently, the specific heat is very large if the heat of reaction is large compared to RT. Hirschfelder (6) has shown that the coefficient of thermal conductivity, for gases in local equilibrium, is also very large; in fact it is approximately proportional to the specific heat. Thus, the Prandtl number is relatively constant and the diffusivity is a function of temperature which is not greatly affected by the chemical reaction. The integral of thermal conductivity, on the other hand, is greatly increased as a result of the reaction. This situation is illustrated in Fig. 4.

The diffusivity increases linearly with φ up to the point where the chemical reaction occurs; there it flattens out until the reaction is about complete, and then it increases again in a more or less linear manner. The solid lines are theoretical estimates, calculated from results in (7) for the case of air in which oxygen dissociation occurs. The pressure dependence of the curve for φ less than $2\varphi_c$ has been removed by normalizing both ordinate and abscissa with the factor

$$\varphi_e = (T_e/T_0)^{n+1} \qquad [12]$$

where

T_0 = boundary temperature
T_e = temperature where thermal conductivity is a maximum, i.e., where diffusivity is most nearly independent of the conductivity integral

The temperature T_e may be calculated from equations derived by Butler and Brokaw (8) for the thermal conductivity of reacting gas mixtures.

It should be noted that the calculation of the relation between diffusivity and the conductivity integral does not depend on precise numerical values of the transport coefficients. For example, the estimate shown for air in Fig. 4 is based on simple kinetic theory and very approximate collision cross sections (7). However, the corrections introduced by more exact calculations affect both the diffusivity and the conductivity simultaneously in such a way that the functional relation between the two is maintained.

The relation for reacting gases in general will be similar to that for air. The dashed curve on Fig. 4 is a limit which is approached as the heat of reaction becomes very large. This limiting relation has been used in the integrations which follow; that is, a is assumed to equal φ up to the point φ_e and thereafter is taken to be constant. Up to the point φ_e then, the solutions are the stretched out error functions which were discussed earlier, and which are shown in Fig. 2. At φ_e these solutions are joined by the solution for constant diffusivity which has a matching slope at the junction $(d\varphi/dy)_e$

$$\varphi = \varphi_c + \sqrt{\frac{\pi\varphi_c}{4}}\left(\frac{d\varphi}{dy}\right)_c \left(\exp\frac{y^2}{\varphi_c}\right) \times \left(\operatorname{erf}\frac{y}{\sqrt{\varphi_c}} - \operatorname{erf}\frac{y_e}{\sqrt{\varphi_c}}\right) \qquad [13]$$

In Fig. 5, the limit of the potential φ_∞ is shown for a reacting gas as a function of the boundary heat flux φ_0'. The solution now depends on the value of φ_c, which in turn depends on the boundary temperature, the pressure and the chemical reaction being considered. For example, in the case of air and a boundary temperature of zero deg C, the values 20, 40 and 60 for φ_c correspond to pressures about 10^{-4}, 10^{0} and 10^{2} atm, respectively. The solutions for values of φ_c corresponding to other pressures and different boundary temperatures can be obtained fairly accurately by interpolation between the numerically integrated solutions, such as the curves plotted in Fig. 5. The inert gas solution (Fig. 3) corresponds to φ_c equal to infinity (Fig. 5). It should be noted that these solutions can only be used up to the point where the chemical reaction goes to completion. Beyond this, the increase in diffusivity must again be taken into account. The domain of validity is a characteristic of each specific reaction. Within this limitation, the curves of Fig. 5 apply to chemically reacting gases in general.

Fig. 4 Diffusivity function

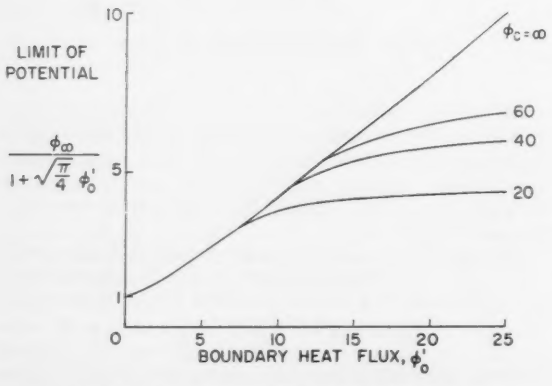

Fig. 5 Chemical equilibrium heat diffusion

Heat Flux Potentials for Air

The foregoing solutions (Fig. 5) have been put to use, in conjunction with experiment, to evaluate the heat flux potential for air as a function of temperature (3). In this experiment, a plane shock wave is reflected from the end wall of a shock tube. The heat flux to the wall is measured, and this fixes the abscissa for the graphical solution in Fig. 5. The temperature at the wall and the pressure of the gas after the shock reflection determine the value of φ_c (see Eq. [12]). Hence the value of the ordinate in Fig. 5 is fixed, and the value of φ_∞ is determined. The temperature of the gas associated with this heat flux potential is taken to be the equilibrium temperature after the shock reflection, and this is a known function of the measured shock velocity. This procedure, of course, implies that the experiments are conducted under conditions where the chemical relaxation times are short compared to the test interval.

Results of the experiments and calculations are shown in Fig. 6. The heat flux potential is shown divided by the inert gas value, where the coefficient n is taken to be $\frac{1}{2}$

$$\varphi_{inert} = \frac{2}{3}k_0T_0\left(\frac{T}{T_0}\right)^{3/2} = 3.2 \times 10^{-6}T^{3/2}\,\frac{\text{cal}}{\text{cm sec}} \qquad [14]$$

and T is in deg K. Thus the ratio φ/φ_{inert} should be unity if the coefficient of thermal conductivity is proportional to the one half power of temperature. This appears to be approximately true up to the temperature where oxygen dissociation begins. At the pressures involved in the present shock tube experiments, this occurred at about 2500 K. At higher temperatures, the heat flux potential becomes more than twice as large as the inert gas value as a result of the dissociation of oxygen. The solid curve on Fig. 6 shows a theoretical estimate of the heat flux potential, based on the coefficients of thermal conductivity presented in (7). The experimental points were obtained by the method described in (3), except that somewhat better instrumentation has been used to improve the reliability of the data. The small departure from ideal gas values which occurs at low temperatures is a result of the effect on thermal conductivity of vibrational energy excitation and of the formation of nitric oxide. However, the oxygen dissociation process has the large heat of reaction required to produce a sizable increase in the heat flux potential. The theory and experiment clearly show the same behavior owing to this effect.

It will be of interest next to examine an application of the heat flux potential to some problems of heat transfer in hypersonic flow.

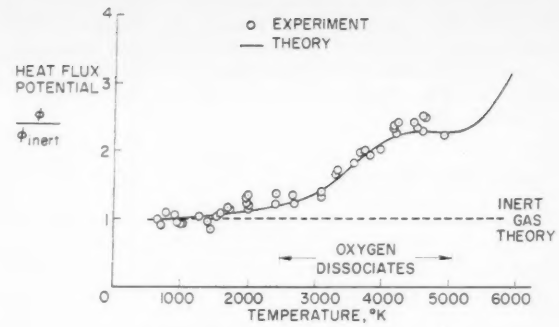

Fig. 6 Heat flux potential for air

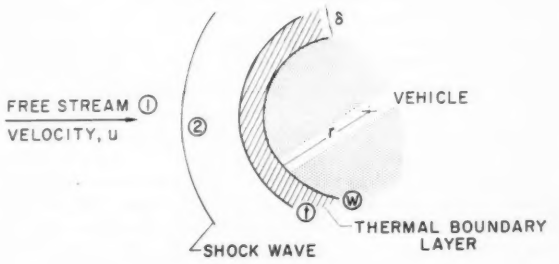

Fig. 7 Stagnation region nomenclature

Applications to Hypersonic Flow

Normally, heat transfer in fluid flow exhibits a complex interdependence between conduction and convection processes. However, at the stagnation region of hypersonic vehicles, it has been shown (9) that, to a first approximation, the conduction and convection effects are separable, and solutions can be expressed in a form which has a simple physical interpretation in terms of the heat flux potentials. The heat flux at the wall is given by the difference between the potential at stagnation conditions φ_t and its value at the wall φ_w all divided by a characteristic length δ

$$q = (\varphi_t - \varphi_w)/\delta \qquad [15]$$

The quantity δ can be interpreted as a thermal boundary layer thickness defined such that the gas temperature at the edge of the layer is a maximum, approximately the stagnation temperature (Fig. 7). According to this model then, the heat transfer at the stagnation region occurs essentially by a diffusion process, although the mass convection processes are responsible for establishing the magnitude of δ. For an axially symmetric stagnation region, for example, the thickness δ is approximately given by [see (9)]

$$\frac{1}{\delta} \simeq \frac{\sqrt{Re}}{r}\left(\frac{\rho_2}{\rho_1} - 1\right)^{1/4}\left(\frac{\mu_1}{\mu_t}\right)^{1/2} \qquad [16]$$

where the subscript t refers to stagnation conditions and the subscripts 1 and 2 refer, respectively, to the free stream and to conditions just following the shock wave (see Fig. 7). The Reynolds number Re is based on free stream conditions and on a length equal to the effective radius of curvature of the body.

None of the factors in the expression for the thermal boundary layer thickness (Eq. [16]) is strongly influenced by chemical reaction. In the integral φ_t however, the integrand k is greatly increased, and the upper limit of the integral T_t is greatly decreased by the reaction

$$\varphi_t = \int_0^{T_t} k dT \qquad [17]$$

It can be shown that these two effects almost compensate one another, and to a first approximation φ_t is just a function of the vehicle velocity, the Prandtl number and a weighted average coefficient of viscosity

$$\varphi_t \simeq u^2\bar{\mu}/2Pr \qquad [18]$$

where

$$\bar{\mu} = \int_0^{T_t} \mu C_p dT \Big/ \int_0^{T_t} C_p dT \qquad [19]$$

The viscosity coefficient, however, is not strongly influenced by chemical reactions, unless a high percentage ionization is produced [see (7)]. Consequently, stagnation region heating is relatively insensitive to dissociation effects, and is not a good quantity to measure for the purpose of evaluating transport properties or real gas effects in dissociating gases. It also becomes clear why calculations based on ideal gas properties have been observed to have the correct magnitude in spite of the unrealistically high stagnation temperature predicted by this method. Another method, found to give reasonable results where chemical reactions occur, assumes heat flux proportional to the enthalpy gradients. This is, of course, consistent with the fact that thermal conductivity is approximately proportional to the specific heat in the domain of the reaction, so that the integral φ is approximately proportional to enthalpy.

The heat transfer to cylindrical stagnation regions can likewise be expressed in terms of the heat flux potentials. Equation [15] applies to this case without change, except that δ is slightly larger than for the axially symmetric case [see (9)].

$$\frac{1}{\delta} \simeq \frac{\sqrt{Re}}{r}\left(\frac{3}{4}\right)^{1/4}\left(\frac{\rho_2}{\rho_1} - 1\right)^{1/4}\left(\frac{\mu_1}{\mu_t}\right)^{1/2} \qquad [20]$$

The analysis can also be extended to yawed cylindrical stagnation regions, such as the leading edge of a swept hypersonic wing. It is found that the chemical reaction effects are canceled in somewhat the same manner as in the stagnation heating of axially symmetric bodies. In the limit as the stagnation temperature becomes large compared to the wall temperature, the ratio of heat flux at angle of yaw $q(\lambda)$ to the value at zero yaw $q(0)$ is approximately given by

$$\frac{q(\lambda)}{q(0)} = \cos\lambda\left(\cos^2\lambda + \left(\frac{3}{4}\right)Pr\sin^2\lambda\right) \qquad [21]$$

For a Prandtl number of $\frac{3}{4}$ and yaw angles up to 70 deg, this is very close to the $\cos^{3/2} \lambda$ relation proposed by Goodwin, Creager and Winkler (10) for the total heat transfer to yawed cylinders. This effect has been checked experimentally in hypersonic flow (9,11).

Concluding Remarks

Although the preceding solutions are based on some decidedly first-order approximations to the Navier-Stokes equations, it is felt that the essential functional relationships which influence stagnation region heat transfer are probably retained, inasmuch as the results compare favorably with more rigorous calculations which are now available, such as those performed by Fay and Riddell (12). Perhaps the principal value of these approximations, at least in domains where the rigorous solutions have been worked out, lies in providing a somewhat simplified physical insight into the problems. It may be noted, however, that the concept of the heat flux potential is free of restrictions concerning the behavior of the Lewis number, and it can be applied to problems where multiple diffusion coefficients are involved in the heat transfer process. This situation exists, for example, where ionization or two or more simultaneous chemical reactions occur. However, at ionization temperatures the effects of emission and adsorption of radiation in the gas may be difficult to analyze separately from heat diffusion. In this case, temperature again becomes the normal dependent variable to use in the problem, and the functional dependence of thermal conductivity on temperature becomes important. This function could be approximately obtained from values of the integral φ, but the differentiation of the data involves a considerable loss of accuracy. It is advisable to treat a favorable comparison between theoretical and experimental values of φ as satisfying merely a necessary but not sufficient check of the theory.

In summary, some solutions have been presented for the nonsteady diffusion of heat through a semi-infinite gas having constant initial and boundary conditions. It is found that the heat flux potential function φ is a natural parameter to use as the dependent variable for problems involving heat diffusion through media in which thermal conductivity is a function of temperature. This potential has been evaluated by experiment for air up to 5000 K, including the influence of oxygen dissociation, and the results agree reasonably well with theoretical estimates. Finally, some relations between the heat flux potentials and heat transfer at the stagnation region of high speed vehicles have been discussed.

References

1 Carslaw, H. S. and Jaeger, J. C., "Conduction of Heat in Solids," Oxford University Press, England, 1947.

2 Jacob, M., "Heat Transfer," vols. I and II, John Wiley and Sons, Inc., N. Y., 1949.

3 Hansen, C. F., Early, R. A., Alzofon, F. E. and Witteborn, F. C., "Theoretical and Experimental Investigation of Heat Conduction in Air Including Effects of Oxygen Dissociation," NASA Rep. 27, 1959.

4 Boltzmann, L., "Zur Integration der Diffusionsgleichung bei Variabeln Diffusionscoefficienten," *Annalen der Physik*, vol. 53, 1894, pp. 959–964.

5 Kennard, E. H., "Kinetic Theory of Gases," McGraw-Hill Book Co., Inc., N. Y., 1938, chap. IV.

6 Hirschfelder, J. O., "Heat Transfer in Chemically Reacting Mixtures. I," *J. Chem. Phys.*, vol. 26, no. 2, Feb. 1957, pp. 274–281.

7 Hansen, C. F., "Approximations for the Thermodynamic and Transport Properties of High Temperature Air," NASA Rep. 50, 1959.

8 Butler, J. N. and Brokaw, R. S., "Thermal Conductivity of Gas Mixtures in Chemical Equilibrium," *J. Chem. Phys.*, vol. 26, no. 6, June 1957, pp. 1636–1643.

9 Eggers, A. J., Jr., Hansen, C. F. and Cunningham, B. E., "Theoretical and Experimental Investigation of the Effect of Yaw on Heat Transfer to Circular Cylinders in Hypersonic Flow," NACA RM A55E02, 1955.

10 Goodwin, G., Creager, M. O. and Winkler, E. L., "Investigation of Local Heat-Transfer and Pressure Drag Characteristics of a Yawed Circular Cylinder at Supersonic Speeds," NACA RM A55H31, 1956.

11 Cunningham, B. E. and Kraus, S., "Experimental Investigation of the Effect of Yaw on Rates of Heat Transfer to Transverse Circular Cylinders in a 6500-Foot-per-second Hypersonic Air Stream," NACA RM A58E19, 1958.

12 Fay, J. A. and Riddell, F. R., "Theory of Stagnation Point Heat Transfer in Dissociated Air," Avco Res. Rep. no. 1, Everett, Mass., June 1956.

1960-61 ARS Meeting Schedule

Date	Meeting	Location	Abstract Deadline
Oct. 10–12	Anatomy of Manned Space Operations Conference	Dayton, Ohio	Past
Nov. 3–4	Electrostatic Propulsion Conference	Monterey, Calif.	Past
Dec. 5–8	ARS Annual Meeting and Astronautical Exposition	Washington, D.C.	Past
1961			
Feb. 1–3	Solid Propellant Rocket Conference	Salt Lake City, Utah	Past
March 13–16	Testing Conference	Los Angeles, Calif.	Oct. 17
April 5–7	Lifting Re-Entry Vehicles: Structures, Materials, and Design Conference	Palm Springs, Calif.	Oct. 31
April 26–28	Detonation and Deflagration Phenomena Conference	Palm Beach, Fla.	Nov. 28
May 22–24	National Telemetering Conference	Chicago, Ill.	Dec. 1
June 7–9	ARS Semi-Annual Meeting	Los Angeles, Calif.	Feb. 1
Aug. 21–23	International Hypersonics Conference	Cambridge, Mass.	April 21
Aug. 23–25	Biennial Gas Dynamics Symposium	Evanston, Ill.	April 25
Oct. 9–13	ARS SPACE FLIGHT REPORT TO THE NATION	New York, N.Y.	May 2

Send all abstracts to Meetings Manager, ARS, 500 Fifth Ave., New York 36, N.Y.

Gradient Theory of Optimal Flight Paths

HENRY J. KELLEY[1]

Grumman Aircraft Engineering Corp.
Bethpage, N. Y.

An analytical development of flight performance optimization according to the method of gradients or "method of steepest descent" is presented. Construction of a minimizing sequence of flight paths by a stepwise process of descent along the local gradient direction is described as a computational scheme. Numerical application of the technique is illustrated in a simple example of orbital transfer via solar sail propulsion. Successive approximations to minimum time planar flight paths from Earth's orbit to the orbit of Mars are presented for cases corresponding to free and fixed boundary conditions on terminal velocity components.

THE PAST decade has seen considerable progress in techniques for the determination of flight paths which are optimal in the sense of various performance criteria. Treatments have employed almost exclusively the classical "indirect" method of the calculus of variations which is based on the reduction of variational problems to differential equations. A number of works on this subject are listed in (1 through 9).[2] An excellent bibliography is presented in the survey paper of (10).

Although many interesting results have been forthcoming from analytical solutions of the Euler-Lagrange differential equations governing optimal flight, the idealizing assumptions usually invoked limit their applicability in practical situations. Under more realistic assumptions, a numerical attack on these equations is required, and in this approach a serious difficulty may arise in the satisfaction of two-point boundary conditions. [See, for example, (11, 12 and 13).] This difficulty becomes a limiting factor where the order of the differential equations governing the basic system is four or higher.

Attention is directed in the present work to one of the direct methods of the calculus of variations, namely the method of gradients or "method of steepest descent," which offers circumvention of the two-point boundary value difficulty. The method also possesses the attractive feature of simultaneous optimization with respect to configuration parameters.

The notion of descent along the gradient direction was originally introduced by Hadamard in connection with mathematical existence proofs (14). Only in recent years has it found practical application to multivariable minimum problems of ordinary calculus (15) and to solution of systems of algebraic equations (16, 17) and integral equations (18).

The main idea of the present treatment stems from material presented by Prof. R. Courant in a 1941 address to the American Mathematical Society (19). An application of the gradient method to fixed end-point variational problems has been given by Stein (20). Our extension of the gradient idea to the case which includes differential equations as subsidiary conditions is heuristic in character.

Problem Formulation

For present purposes it will be assumed that the system of differential equations to be satisfied along the flight path is given in first-order form

$$\dot{x}_m = g_m(x_1, \ldots, x_n, y, t) \qquad m = 1, \ldots, n \qquad [1]$$

These equations relate velocities and positions, forces and accelerations, mass and flow of propellants and coolants, and the like. x_m may be termed problem variables, and y the control variable. Differentiation with respect to the independent variable, time t, is denoted by a superscribed dot.

An important class of problems is that in which the performance quantity to be minimized is expressed as a function of the final values of the variables x_m and t

$$P = P(x_{1f}, \ldots, x_{nf}, t_f) \qquad [2]$$

At a specified initial time t_0 as many as n boundary conditions on the x_m may be stipulated. Since an entire function $y(t)$ is at our disposal, we may reasonably consider problems in which numerous conditions are imposed upon the x_m at various subsequent t values. In the following we will restrict attention to conditions imposed at the terminal point of the flight path. Among the $n + 1$ quantities consisting of the n final values of the x_m plus the final time t_f, no more than n relations may be specified in order that the value of P not be predetermined.

Neighboring Solutions—Variations

We now assume that a solution of Equations [1] is available which satisfies the boundary conditions but which does not minimize P. Denoting the solution by $x_m = \bar{x}_m(t)$, $y = \bar{y}(t)$, we examine behavior in the neighborhood of this solution by setting $x_m = \bar{x}_m + \delta x_m$, $y = \bar{y} + \delta y$ and linearizing

$$\dot{\delta x}_m = \sum_{j=1}^{n} \frac{\partial g_m}{\partial x_j} \delta x_j + \frac{\partial g_m}{\partial y} \delta y \qquad m = 1, \ldots, n \qquad [3]$$

The partials of g_m are evaluated along $x_m = \bar{x}_m$, $y = \bar{y}$ and are therefore known functions of the independent variable t. The functions δx_m and δy are the *variations* of x_m and y in the neighborhood of $\bar{x}_m$, $\bar{y}$.

A formal solution of Equations [3] may be written in the form

$$\delta x_m = \sum_{p=1}^{n} \delta x_{p_0} \xi_{mp}(t) + \int_{t_0}^{t} \mu_m(\tau, t - \tau) \delta y(\tau) d\tau \qquad m = 1, \ldots, n \qquad [4]$$

where the first member represents solution of the homogeneous system of equations and the second a superposition of control variable effects. The functions μ_m are Green's functions or in-

---

Presented at the ARS Semi-Annual Meeting, May 9–12, 1960, Los Angeles, Calif.

[1] Section Leader, Systems Research. Member ARS.

[2] Numbers in parentheses indicate References at end of paper.

fluence functions; $\mu_m(\tau, t - \tau)$ may be thought of as the solution for δx_m corresponding to δy a unit impulse (Dirac delta function) introduced at time τ (21).

Since interest centers on final values of x_m, we evaluate the expressions [4] at $t = t_f$; however, to cover the possibility of a variable end point, $t_f = \bar{t}_f + \delta t_f$, a first-order correction term must be included

$$\delta x_{m_f} = \sum_{p=1}^{n} \delta x_{p_0} \xi_{mp}(\bar{t}_f) + \int_{t_0}^{\bar{t}_f} \mu_m(\tau, \bar{t}_f - \tau)\delta y(\tau)d\tau + \dot{\bar{x}}_{m_f}\delta t_f$$
$$= \sum_{p=1}^{n} \delta x_{p_0} \xi_{mp}(\bar{t}_f) + \int_{t_0}^{\bar{t}_f} \mu_m(\tau, \bar{t}_f - \tau)\delta y(\tau)d\tau + \bar{g}_{m_f}\delta t_f$$
$$m = 1, \ldots, n \quad [5]$$

where $\bar{g}_{m_f} = g_m(\bar{x}_{1_f}, \ldots, \bar{x}_{n_f}, \bar{y}_f, \bar{t}_f)$.

Computation of the Functions μ_m

Since computation of the functions $\mu_m(\tau, t - \tau)$ over a complete range of both arguments is unnecessary, only their evaluation at $t = \bar{t}_f$ required for subsequent calculations, it is reasonable to seek a means for performing the special computation which avoids the labor of the more general one. The following development relates the functions $\mu_m(\tau, \bar{t}_f - \tau)$ to solutions of a system of equations adjoint to the system [3] through an application of Green's theorem. The scheme employed is due to Bliss, as reported by Goodman and Lance (22).

We rewrite Equations [3] employing a subscript notation suitable to our immediate purpose

$$\delta \dot{x}_i = \sum_{j=1}^{n} \frac{\partial g_i}{\partial x_j} \delta x_j + \frac{\partial g_i}{\partial y} \delta y \qquad i = 1, \ldots, n \quad [6]$$

and write the system of equations adjoint to this system

$$\dot{\lambda}_i = -\sum_{j=1}^{n} \frac{\partial g_j}{\partial x_i} \lambda_j \qquad i = 1, \ldots, n \quad [7]$$

which is obtained by transposing the matrix of coefficients and changing the sign.

The solutions of the two systems are related by

$$\frac{d}{dt} \sum_{i=1}^{n} \lambda_i \delta x_i = \sum_{i=1}^{n} \lambda_i \frac{\partial g_i}{\partial y} \delta y \quad [8]$$

After integration of both left and right members between definite limits t_0 and $\bar{t}_f$, we find

$$\sum_{i=1}^{n} \lambda_i(\bar{t}_f)\delta x_i(\bar{t}_f) - \sum_{i=1}^{n} \lambda_i(t_0)\delta x_i(t_0) = \int_{t_0}^{\bar{t}_f} \sum_{i=1}^{n} \lambda_i \frac{\partial g_i}{\partial y} \delta y \, dt \quad [9]$$

This is the one-dimensional form of Green's theorem (22).

We now consider numerical solutions of the adjoint system with all boundary values specified at $t = \bar{t}_f$. To the special solutions corresponding to

$$\lambda_i(\bar{t}_f) = 0 \qquad i \neq m$$
$$\lambda_i(\bar{t}_f) = 1 \qquad i = m$$
$$\ldots\ldots\ldots\ldots\ldots\ldots\ldots\ldots\ldots\ldots\ldots\ldots [10]$$

we assign the symbols $\lambda_i^{(m)}(t)$. In this fashion n expressions for the values of the $\delta x_m(\bar{t}_f)$ are obtained from [9]

$$\delta x_m(\bar{t}_f) = \sum_{i=1}^{n} \lambda_i^{(m)}(t_0)\delta x_i(t_0) + \int_{t_0}^{\bar{t}_f} \sum_{i=1}^{n} \lambda_i^{(m)} \frac{\partial g_i}{\partial y} \delta y \, dt$$
$$m = 1, \ldots, n \quad [11]$$

By comparison with Equations [5] it may be seen that the desired relation between the $\mu_m(\tau, \bar{t}_f - \tau)$ and the $\lambda_i^{(m)}$ is the following one

$$\mu_m(\tau, \bar{t}_f - \tau) = \sum_{i=1}^{n} \lambda_i^{(m)} \frac{\partial g_i}{\partial y} \qquad m = 1, \ldots, n \quad [12]$$

and, also, that the $\xi_{mp}(\bar{t}_f)$ of Equations [5] is equal to $\lambda_p^{(m)}(t_0)$.

In the preceding development the choice of symbols λ for the variables of the adjoint system is deliberate, for Equations [7] are precisely those governing the Lagrange multiplier functions of the "indirect" theory. We note the important distinction, however, that the coefficients of [7] employed in the "indirect" theory are evaluated along a minimal solution of Equations [1], whereas in gradient computations they correspond to nonminimal paths.

Descent Parameter

Following Courant (19), we now introduce a parameter σ as a second independent variable, and seek a functional dependence of the control variable $y(t, \sigma)$ on this parameter such that the derivative of the performance quantity $dP/d\sigma$ is negative. In fact, within the restrictions imposed by the boundary conditions and the system equations, we shall attempt to make the slope of descent $dP/d\sigma$ "as steep as possible."

To enable operation within the restrictions just mentioned, we break down the control variable y as follows

$$y(t, \sigma) = \phi(t, \sigma) + \sum_{q=1}^{r} a_q(\sigma) f_q(t) \quad [13]$$

Here the $f_q(t)$ are a set of known linearly independent functions of t. Our intention is that the coefficients a_q of the second member of [13] be sacrificed to the fulfillment of boundary conditions, the number r being chosen appropriately for this purpose. This will leave the function ϕ free for the minimization of P.

We now take the derivatives of various quantities with respect to σ and evaluate them at $\sigma = \bar{\sigma}$, corresponding to the nonminimal solution $x_m(t, \bar{\sigma}) = \bar{x}_m$, $y(t, \bar{\sigma}) = \bar{y}$ introduced in the preceding section. For $\sigma - \bar{\sigma} = \Delta\sigma$ small, the variations appearing in Equations [5] may be identified as

$$x_{m_0} = \bar{x}_{m_0} + \delta x_{m_0} = \bar{x}_{m_0} + (dx_{m_0}/d\sigma)\Delta\sigma$$
$$m = 1, \ldots, n \quad [14]$$

$$x_{m_f} = \bar{x}_{m_f} + \delta x_{m_f} = \bar{x}_{m_f} + (dx_{m_f}/d\sigma)\Delta\sigma$$
$$m = 1, \ldots, n \quad [15]$$

$$t_f = \bar{t}_f + \delta t_f = \bar{t}_f + (dt_f/d\sigma)\Delta\sigma \quad [16]$$

$$y = \bar{y} + \delta y = \bar{y} + (\partial y/\partial\sigma)\Delta\sigma$$
$$= \bar{\phi} + \sum_{q=1}^{r} \bar{a}_q f_q(t) + \left[\frac{\partial\phi}{\partial\sigma} + \sum_{q=}^{r} \frac{da_q}{d\sigma} f_q(t)\right] \Delta\sigma \quad [17]$$

Equations [5] then take the form

$$\frac{\partial x_{m_f}}{\partial\sigma} = \sum_{p=1}^{n} \frac{dx_{p_0}}{d\sigma} \xi_{mp}(\bar{t}_f) + \int_{t_0}^{\bar{t}_f} \mu_m(\tau, \bar{t}_f - \tau) \frac{\partial\phi}{\partial\sigma} d\tau +$$
$$\sum_{q=1}^{r} \frac{da_q}{d\sigma} \int_{t_0}^{\bar{t}_f} \mu_m(\tau, \bar{t}_f - \tau) f_q(\tau) d\tau + \bar{g}_{m_f} \frac{dt_f}{d\sigma}$$
$$m = 1, \ldots, n \quad [18]$$

Boundary Conditions

We consider boundary conditions of the separated type, i.e., equations relating either initial values or final values. Boundary values may be variable on a surface, typified by

$$\mathfrak{z}(x_{u_f}, x_{v_f}, t_f) = 0 \quad [19]$$

in which case the following linear combination of derivatives must vanish

$$\frac{d\mathfrak{z}}{d\sigma} = \frac{\partial\mathfrak{z}}{\partial x_u} \frac{dx_{u_f}}{d\sigma} + \frac{\partial\mathfrak{z}}{\partial x_v} \frac{dx_{v_f}}{d\sigma} + \frac{\partial\mathfrak{z}}{\partial t_f} \frac{dt_f}{d\sigma} = 0 \quad [20]$$

In this expression the partial derivatives of $\Im$ are evaluated at $x_{uf} = \bar{x}_{uf}$, $x_{vf} = \bar{x}_{vf}$ and $t_f = \bar{t}_f$.

In the case of fixed boundary conditions of the form $x_{uf} = \bar{x}_{uf} = \text{constant}$, $t_f = \bar{t}_f = \text{constant}$, the relations to be satisfied take the simple form

$$\frac{dx_{uf}}{d\sigma} = 0 \quad \text{or} \quad \frac{dt_f}{d\sigma} = 0 \tag{21}$$

As many as n final conditions, fixed or of the form [19] may be specified, as mentioned earlier. Where fewer than this number are specified, we speak of "free" or "open" boundary values.

At the initial point similar freedom of choice may exist among the n initial values of the x_m, the only difference here being that t_0 will usually be fixed.

Gradient of P

Upon inspection it may be noted that there are n equations of the form [18] and at most $2n$ equations for boundary values, making a possible total of $3n$ equations. These relate $2n + 1$ derivatives of the x_{m_0}, x_{m_f} and t_f, the r derivatives of the a_q and integrals containing $\partial\phi/\partial\sigma$. We accordingly choose the number r of the a_q as $r = n - 1 - s$, where s is the number of open boundary conditions. Thus the system of equations will be determinate for arbitrary $\partial\phi/\partial\sigma$.

These equations may be arranged as a linear simultaneous system

$$AZ = B \tag{22}$$

where Z has $3n - s$ elements consisting of the derivatives with respect to σ of x_{m_0}, x_{m_f}, t_f and a_q. The matrix A is square and contains among its elements the quantities ξ_{m_p}, $\bar{y}_{m_f}$, the $\Im$ partials, and integrals of products $\mu_m f_q$, all of which are known. The column B includes integrals containing $\partial\phi/\partial\sigma$ in their integrands. The solution

$$Z = A^{-1}B \tag{23}$$

may be obtained through matrix inversion or equivalent processes. The matrix A expresses the relationship between small shifts in boundary values and small adjustments in the control function (through the a_q) to deal with them. Hence in normal circumstances A will be nonsingular.

The derivative with respect to σ of the quantity P to be minimized

$$\frac{dP}{d\sigma} = \frac{\partial P}{\partial x_{1_f}}\frac{dx_{1_f}}{d\sigma} + \ldots + \frac{\partial P}{\partial x_{n_f}}\frac{dx_{n_f}}{d\sigma} + \frac{\partial P}{\partial t_f}\frac{dt_f}{d\sigma} \tag{24}$$

may now be expressed in terms of known quantities and integrals containing $\partial\phi/\partial\sigma$ according to the solution [23]. It will take the form of a linear combination of the integrals

$$\frac{dP}{d\sigma} = \sum_{m=1}^{n} C_m \int_{t_0}^{\bar{t}_f} \mu_m(\tau, \bar{t}_f - \tau)\frac{\partial\phi}{\partial\sigma}\,d\tau \tag{25}$$

which may be expressed as a single integral

$$\frac{dP}{d\sigma} = \int_{t_0}^{\bar{t}_f}\left[\sum_{m=1}^{n} C_m\mu_m(\tau, \bar{t}_f - \tau)\right]\frac{\partial\phi}{\partial\sigma}\,d\tau \tag{26}$$

By analogy with a characteristic property of a vector gradient, we are now prepared to identify the gradient of P with respect to the function ϕ. [See p. 222 of the Courant-Hilbert English edition, (23), also (19).] If ϕ were a vector possessing a finite number of components ϕ_i, $i = 1, \ldots, j$, the derivative of P with respect to σ

$$\frac{dP}{d\sigma} = \sum_{i=1}^{j}\frac{\partial P}{\partial\phi_i}\frac{d\phi_i}{d\sigma} \tag{27}$$

could be expressed as

$$\frac{dP}{d\sigma} = \text{grad } P \cdot \frac{d\phi}{d\sigma} \tag{28}$$

If $\phi(t, \sigma)$ is a continuous function, and P a functional of ϕ, as in the case of present interest

$$\frac{dP}{d\sigma} = \int [P]_\phi \frac{\partial\phi}{\partial\sigma}\,d\tau \tag{29}$$

and the function occurring in product with $\partial\phi/\partial\sigma$, which we denote $[P]_\phi$, may be regarded as the gradient of P by extended definition.

Thus for the problem at hand it is evident from Equation [26] that

$$[P]_\phi = \sum_{m=1}^{n} C_m\mu_m(\tau, \bar{t}_f - \tau) \tag{30}$$

is the gradient of P.

Were the solution $x_m = \bar{x}_m$, $y = \bar{y}$ such as to minimize P, contrary to our assumption, the gradient $[P]_\phi$ would vanish. If our development were to parallel the classical or "indirect" approach, the construction of a solution would be sought from the vanishing of $[P]_\phi$ for which P is stationary and possibly a minimum. Thus $[P]_\phi$ is in some sense an Euler expression and the equation $[P]_\phi = 0$ and the relations [23] have an equivalence to the Euler-Lagrange equations and transversality conditions of the "indirect" theory.

Descent Process

Returning momentarily to the elementary geometric concept of a vector gradient, we regard $P(\phi_1, \ldots, \phi_i)$ as a surface, and starting from $P(\phi_1, \ldots, \phi_i)$ we move a point along this surface so that P and ϕ_i become functions of a time parameter σ. Then the velocity of ascent or descent along a line on the surface is as given by Equations [27 and 28]. We now choose the line along which the descent is as steep as possible, characterized by

$$\frac{d\phi_i}{d\sigma} = k\frac{\partial P}{\partial\phi_i} \tag{31}$$

where k positive corresponds to ascent and k negative to descent.

It is clear that in this continuous process, wherein the point moves according to the system of ordinary differential equations [31], the process will for $\sigma \to \infty$ approach a position for which grad $P = 0$, if P is bounded below.

This elementary idea may be generalized to the present variational problem according to the extended interpretation of the gradient of P, Equation [29]. We set

$$\frac{\partial\phi}{\partial\sigma} = k[P]_\phi = -[P]_\phi \tag{32}$$

and starting from the nonminimal solution $\sigma = \bar{\sigma}$, $\phi = \bar{\phi}$, $x_m = \bar{x}_m$, $a_q = \bar{a}_q$, re-evaluate these quantities on a continuous basis as the parameter σ increases.

Thus the continuous version of descent along the gradient requires numerical treatment of a partial differential equation for $\phi(t, \sigma)$ with determination of $\phi(t, \infty)$ the ultimate objective.

Stepwise Version

As an alternative to the continuous procedure given by Equation [32], we may elect to proceed stepwise, correcting a set of approximations to the solution $[P]_\phi = 0$ by corrections proportional to the negative of the gradient

$$\phi^{(i+1)} = \phi^{(i)} - [P]_\phi\Delta\sigma \tag{33}$$

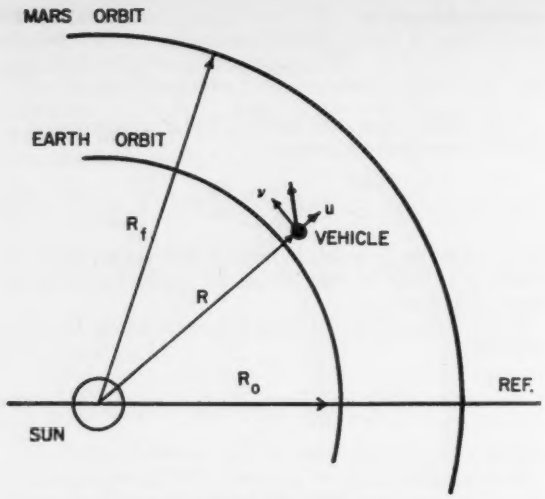

Fig. 1 Orbital transfer schematic

After choice of step size $\Delta\sigma$ and evaluation of $\phi^{(i+1)}$ and the $a_q^{(i+1)}$, the functions $x_m^{(i+1)}$ would be obtained from numerical integration of the basic system Equations [1] and $P^{(i+1)}$ determined from the values at $t_f^{(i+1)}$.

Since the determination of the gradient $[P]_\phi$ is expensive in terms of volume of numerical computations, it would seem desirable to exploit each calculation of local gradient direction of the utmost, taking $\Delta\sigma$ as large as possible. A procedure employed in some applications (17) is to follow the local gradient direction until the function P reaches a minimum. Such a procedure could be implemented by numerical integration of Equations [1] for a number of values of $\Delta\sigma$ and selection of the value of $\Delta\sigma$ for minimum P.

A possible pitfall of such a scheme of operation is that the boundary conditions, having been satisfied only in linearized version (Eq. [20]), may long since have been violated before minimum P is reached (24). Thus the choice of $\Delta\sigma$ involves a compromise which must be decided in the particular applition at hand. If the minimum P rule is employed for choice of $\Delta\sigma$, the boundary conditions must be restored by a correction cycle designed to recover from the departures.

After such restoration has been accomplished, for example via the coefficients a_q, the solution so obtained takes on the role of $\bar{x}_m$, $\bar{y}$ for the computation of a new local gradient direction.

Convergence

The convergence of the descent process has been investigated by Stein for a case not complicated by subsidiary conditions (20); his conclusion was that the process will converge if the functional whose minimum is sought is bounded below. In the process described in the preceding sections, the question of convergence is intimately related to the success of the technique for maintaining or correcting the boundary values at the terminal point.

The possibility of correcting small departures in terminal values of the x_m through small changes in the coefficients a_q can be shown to hinge on the nonvanishing of the determinant of the matrix A of Equation [22]. In certain cases a tendency of this determinant to become small may be observed as a minimum of P is approached. Where the difficulty is acute, the behavior may be likened to breakdown of a first-order differential correction scheme for guidance along the trajectory.

This type of behavior is a close relative of the conjugate end-point phenomenon of classical variational theory. If an extremal through point 1 has on it a contact point 2 with the envelope of a family of extremals through 1, then point 2 is said to be conjugate to point 1. The term *conjugate end points* refers to specification of boundary values at two such points as 1 and 2. The reader is advised to consult the text of Bliss (25) for the analytical basis of conjugate point theory.

The relevant test of the classical theory, *the necessary condition of Jacobi*, employs a determinant as a criterion. The requisite analysis amounts to investigation of *optimal* differential corrections of terminal values. Thus a matrix which is the optimal correction analog of the matrix A is set up, and the criterion of the Jacobi test is the nonvanishing of the determinant of this matrix at points along the extremal *up to* the terminal point of interest. Vanishing *at* the terminal point indicates that the end points are conjugates, and the necessary condition is fulfilled in borderline fashion. Computational procedures for applying the Jacobi test are of some interest; however, the acquisition of a "test specimen" solution requires that any convergence difficulty encountered in the descent process first be overcome.

Thus a possibility of convergence difficulty arises in conjugate end-point cases if the functions f_q selected happen to resemble the optimal correction functions of the indirect theory. There are certainly other possibilities for unfortunate choice of correction functions. Computational experience will be required to establish guidelines on this matter.

Configuration Parameters

In many practical engineering applications, optimal performance is sought not only in terms of flight path selection but also in terms of parameters influencing vehicle configuration. We have, for clarity, avoided complicating the preceding analytical work by such considerations. It is an easy matter, however, to add terms to Equations [5] of the form $(\partial x_{m_f}/\partial e_i)\delta e_i$ and to carry them through along with constraints relating e_i, thus forming a basis for simultaneous optimization of configuration and flight path. The slopes $\partial x_{m_f}/\partial e_i$ are probably best determined by numerical integration of Equations [1] for small changes in e_i.

Solar Sailing Example

For the purpose of exploring the computational aspect of the gradient optimization technique, we have chosen a planar case of transfer between planetary orbits by means of the interesting solar sailing scheme. The potential capabilities of solar sail propulsion have been investigated in the papers of Garwin (26), Cotter (27), Tsu (28) and London (29). This problem has the simplicity appropriate to an exploration of method, yet sufficient complexity to render analytical solution quite difficult unless drastic simplifications are introduced.

The equations of motion and kinematic relations are given in a notation nearly the same as that of Tsu (28). With reference to the schematic of Fig. 1, these are as follows:

Radial acceleration

$$\dot{u} = g_1 = \frac{v^2}{R} - A_0\left(\frac{R_0}{R}\right)^2 + \alpha\left(\frac{R_0}{R}\right)^2 |\cos^3\theta| \qquad [34]$$

Circumferential acceleration

$$\dot{v} = g_2 = -\frac{uv}{R} - \alpha(R_0/R)^2 \sin\theta\cos^2\theta \qquad [35]$$

Radial velocity

$$\dot{R} = g_3 = u \qquad [36]$$

Circumferential angular velocity

$$\dot{\psi} = v/R \qquad [37]$$

Since the heliocentric angle ψ does not appear in the first three equations, and will not appear in the statements of boundary conditions to be considered, Equation [37] may be ignored for purposes of gradient optimization. This amounts to the assumption that terminal matching of the heliocentric angles of vehicle and "target" planet is accomplished by selection of launch time.

Seeking minimum-time transfer, we identify the functional P as

$$P = t_f \qquad [38]$$

The functions u, v, R are the variables x_m of the theoretical development, and the sail angle θ appears in the role of the control variable y.

As initial conditions we specify velocity components u, v and radius R corresponding to motion in Earth's orbit approximated as a circle

$$t_0 = 0 \qquad [39]$$

$$u(0) = u_0 = u_E = 0 \qquad [40]$$

$$v(0) = v_0 = v_E \qquad [41]$$

$$R(0) = R_0 = R_E \qquad [42]$$

We consider terminal conditions corresponding to arrival at the orbit of the planet Mars (also taken as a circle) with prescribed velocity components

$$u(t_f) = u_f \qquad [43]$$

$$v(t_f) = v_f \qquad [44]$$

$$R(t_f) = R_f = R_M \qquad [45]$$

For fixed boundary values of u, v and R, the equations corresponding to Equations [5] of the preceding theoretical development are

$$\delta u_f = \int_0^{\bar{t}_f} \mu_1 \delta\theta \, d\tau + \bar{g}_{1f}\delta t_f = 0 \qquad [46]$$

$$\delta v_f = \int_0^{\bar{t}_f} \mu_2 \delta\theta \, d\tau + \bar{g}_{2f}\delta t_f = 0 \qquad [47]$$

$$\delta R_f = \int_0^{\bar{t}_f} \mu_3 \delta\theta \, d\tau + \bar{g}_{3f}\delta t_f = 0 \qquad [48]$$

In this case the number of functions f_q and coefficients a_q required is

$$r = n - 1 - s = 3 - 1 - 0 = 2 \qquad [49]$$

We select the functions f_q as

$$f_1(t) = t \qquad [50]$$

$$f_2(t) = t^2 \qquad [51]$$

and the control function $\theta(t)$ is broken down as

$$\theta = \phi + a_1 t + a_2 t^2 \qquad [52]$$

The system of equations corresponding to Equation [22] simplifies to

$$\left(\int_0^{\bar{t}_f} \tau\mu_1 d\tau\right)\frac{da_1}{d\sigma} + \left(\int_0^{\bar{t}_f} \tau^2\mu_1 d\tau\right)\frac{da_2}{d\sigma} + \bar{g}_{1f}\frac{dt_f}{d\sigma} = -\int_0^{\bar{t}_f} \mu_1 \frac{\partial\phi}{\partial\sigma}\, d\tau \qquad [53]$$

$$\left(\int_0^{\bar{t}_f} \tau\mu_2 d\tau\right)\frac{da_1}{d\sigma} + \left(\int_0^{\bar{t}_f} \tau^2\mu_2 d\tau\right)\frac{da_2}{d\sigma} + \bar{g}_{2f}\frac{dt_f}{d\sigma} = -\int_0^{\bar{t}_f} \mu_2 \frac{\partial\phi}{\partial\sigma}\, d\tau \qquad [54]$$

$$\left(\int_0^{\bar{t}_f} \tau\mu_3 d\tau\right)\frac{da_1}{d\sigma} + \left(\int_0^{\bar{t}_f} \tau^2\mu_3 d\tau\right)\frac{da_2}{d\sigma} + \bar{g}_{3f}\frac{dt_f}{d\sigma} = -\int_0^{\bar{t}_f} \mu_3 \frac{\partial\phi}{\partial\sigma}\, d\tau \qquad [55]$$

This 3×3 case may conveniently be inverted analytically. There seems little point in listing the inverse elements here, however.

$$\begin{bmatrix} \frac{da_1}{d\sigma} \\ \frac{da_2}{d\sigma} \\ \frac{dt_f}{d\sigma} \end{bmatrix} = -\begin{bmatrix} & C & \end{bmatrix}\begin{bmatrix} \int_0^{\bar{t}_f} \mu_1 \frac{\partial\phi}{\partial\sigma}\, d\tau \\ \int_0^{\bar{t}_f} \mu_2 \frac{\partial\phi}{\partial\sigma}\, d\tau \\ \int_0^{\bar{t}_f} \mu_3 \frac{\partial\phi}{\partial\sigma}\, d\tau \end{bmatrix} \qquad [56]$$

The slope of descent $dt_f/d\sigma$ is given by

$$\frac{dt_f}{d\sigma} = -\int_0^{\bar{t}_f} (C_{31}\mu_1 + C_{32}\mu_2 + C_{33}\mu_3)\frac{\partial\phi}{\partial\sigma}\, d\tau \qquad [57]$$

and the gradient of P by

$$[P]_\phi = -(C_{31}\mu_1 + C_{32}\mu_2 + C_{33}\mu_3) \qquad [58]$$

Accordingly we set

$$\partial\phi/\partial\sigma = -[P]_\phi = C_{31}\mu_1 + C_{32}\mu_2 + C_{33}\mu_3 \qquad [59]$$

and proceed with stepwise descent as in Equation [33].

A particularly suitable case for a first illustration of computational technique is the one in which terminal velocity components are unspecified—"free" boundary conditions. Here Equations [46 and 47] may be deleted and

$$r = n - 1 - s = 3 - 1 - 2 = 0 \qquad [60]$$

so that no functions f_q are needed. Hence

$$\theta = \phi$$

and

$$\frac{\partial\phi}{\partial\sigma} = \frac{\mu_3}{\bar{g}_{3f}} \qquad [61]$$

$$\frac{dt_f}{d\sigma} = -\frac{1}{\bar{g}_{3f}^2}\int_0^{\bar{t}_f} \mu_3^2\, d\tau \qquad [62]$$

in this case.

Computations have employed numerical values of the various constants from Tsu's paper, with

$$\alpha = 0.1 \text{ cm/sec}^2 = 3.28 \times 10^{-3} \text{ fps}^2$$

This value corresponds to about 10^{-4} g thrust acceleration developed by the sail when oriented broadside to the sun ($\theta = 0$) at Earth's orbit radius, or about 17 per cent of the sun's gravitational attraction.

Results of descent computations for the case of "open" terminal velocity components are shown in Figs. 2 through 4. The control program of the original flight path (Figs. 2 and 3), chosen arbitrarily, was far from optimal in that the radial velocity component at crossing of Mars' orbit was small. The greatest reduction in flight time—more than half of the original—is seen to be obtained in the course of the first descent (Fig. 4). In three descents minimum flight time has been attained for practical purposes, although small changes in the detailed structure of the control program are still in evidence.

Results for the case of terminal velocity components matched to the target planet

$$u_f = u_M \qquad v_f = v_M$$

are presented in Figs. 5 through 8. The tendency of the terminal values to depart from the prescribed values is shown in Fig. 5. These were restored via an iterative correction process employing increments in the coefficients a_1 and a_2 of Equation [52]. Typically, two or three iteration cycles were required to correct each point. Descent curves are shown in Fig. 6. The approach to the minimum-time solution is depicted in Figs. 7 and 8.

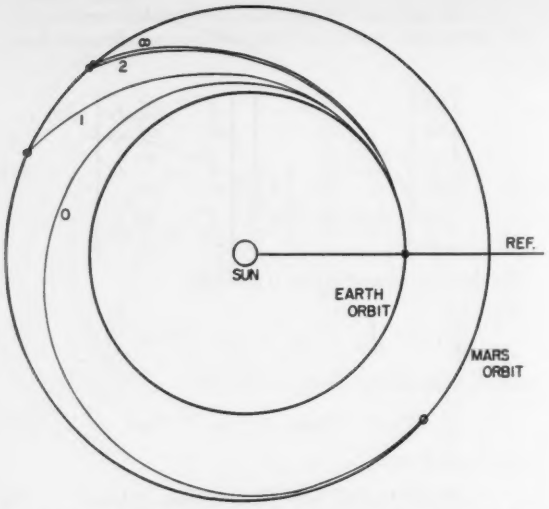

Fig. 2 Successive approximations to optimal transfer path, terminal velocity components open

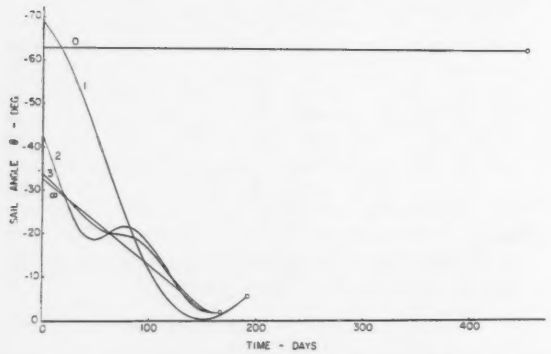

Fig. 3 Successive approximations to optimal sail angle program, terminal velocity components open

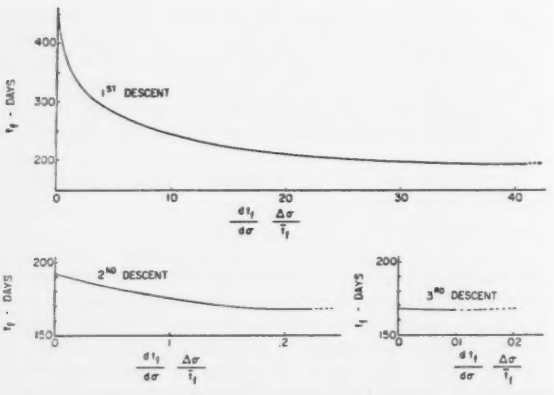

Fig. 4 Descent curves—solar sail transfer, terminal velocity components open

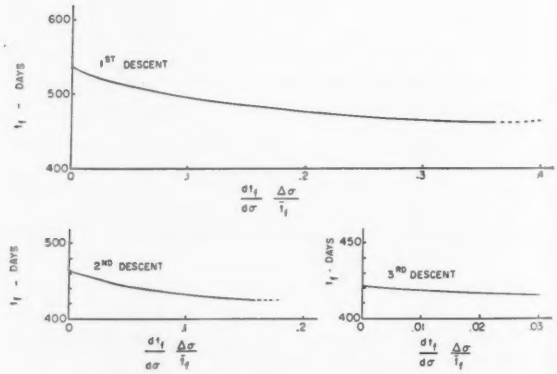

Fig. 5 Departure of terminal values, "matched" terminal velocity components

Fig. 6 Descent curves—solar sail transfer, "matched" terminal velocity components

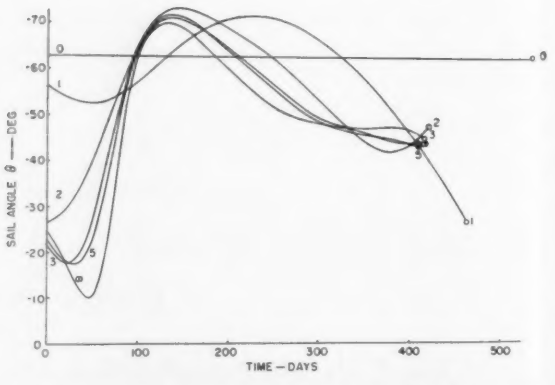

Fig. 7 Successive approximations to optimal sail angle program, "matched" terminal velocity components

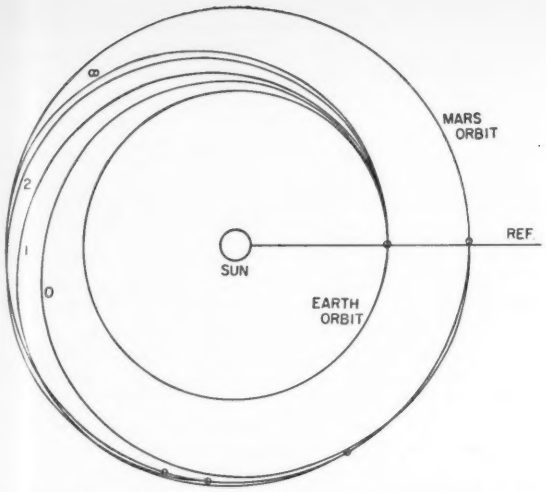

Fig. 8 **Successive approximations to optimal transfer path, "matched" terminal velocity components**

The first attempt at computations for this "matched velocity" case employed functions f_q constant and linear with time. This met with near zero determinant difficulty of the type discussed earlier. The combination of linear and square-law corrections indicated in the foregoing was successfully used to avoid this difficulty.

Concluding Remarks

Attention has been confined in the preceding development to the main ideas of the gradient technique. The extension to cases involving several control variables offers no particular difficulty. The limited computational experience reported here suggests that the gradient technique may be a useful one in applications, and particularly in those presenting difficulty when the classical "indirect" approach—numerical integration of the Euler-Lagrange equations—is used. Apart from the feature of surmounting the two-point boundary value difficulties of such cases, the gradient method may be particularly appropriate in distinguishing between minimal solutions of the Euler-Lagrange equations and those which are merely stationary.

Acknowledgments

The writer is pleased to acknowledge the contributions of Messrs. William P. O'Dwyer and H. Gardner Moyer of Grumman's Computation Facility in handling the computational phase of this study on the IBM 704, and of Mrs. Agnes Zevens of the Systems Research Section in checking and preparing the numerical results for publication.

Nomenclature

x_m = problem variables
y = control variable
g_m = functions of x_m and y appearing in basic system equations
t = time
P = function of final values of x_m to be minimized
δx_m, δy = variations of x_m and y
ξ_{mp} = functions appearing in the solution of Equations [3]
μ_m = Green's functions in the solution of Equations [3]
τ = variable of integration
λ = variables of the adjoint system, Equation [7]
σ = descent parameter
ϕ = auxiliary control variable, Equation [13]
f_q = known linearly independent functions of t
a_q = coefficients of the functions f_q
$\Delta\sigma$ = increment in σ
$\mathfrak{Z}$ = function relating boundary values of x_m and t
A = matrix of coefficients, Equation [22]
Z = column matrix having $dx_{m_0}/d\sigma$, $dx_{m_f}/d\sigma$, $dt_f/d\sigma$ and $da_q/d\sigma$ as elements, Equation [22]
B = column matrix containing integrals of $\mu_m(\partial\phi/\partial\sigma)$ products, Equation [22]
C_m = coefficients of the linear combination of μ_m, Equation [26]
$[P]_\phi$ = gradient of P, Equation [30]
k = proportionality constant of descent
e_i = configuration parameters
u = radial velocity component (see Fig. 1)
v = circumferential velocity component (see Fig. 1)
R = radial distance to sun (see Fig. 1)
ψ = heliocentric angle
A_0 = acceleration due to sun's gravitational attraction at Earth's radial distance
α = thrust acceleration of radially oriented solar sail at Earth's radial distance
θ = sail angle measured from radial orientation

Subscripts

f = denotes final value
0 = denotes initial value
m, p, i, j / q, r, u, v = general indexes
E = Earth
M = Mars
$(\cdot)$ = denotes time derivative
$(^-)$ = denotes nonminimal solution
(i) = denotes value at ith step
(m) = denotes special functional notation, explained by Equation [10]

References

1 Hestenes, M. R., "A General Problem in the Calculus of Variations with Applications to Paths of Least Time," Rand RM-100, March 1950.

2 Garfinkel, B., "Minimal Problems in Airplane Performance," *Quart. Appl. Math.*, vol. 9, no. 2, 1951.

3 Cicala, P., "Le Evoluzioni Ottime di un Aereo," Atti della Accademia delle Scienze di Torino, Classe di Scienze Matematiche, Fisiche e Naturali, vol. 89, 1954–1955. (Translated as NASA Technical Translation TTF-4, Oct. 1959.)

4 Miele, A., "An Extension of the Theory of the Optimum Burning Program for the Level Flight of a Rocket-Powered Aircraft," Purdue University School of Aeronautical Engineering, Rep. no. A-56-1, Technical Note no. AFOSR-TN-56-302, June 1956; *also J. Aeron. Sci.*, vol. 24, no. 12, Dec. 1957.

5 Breakwell, J. V., "The Optimization of Trajectories," North American Aviation, Inc., Rep. AL-2706, Aug. 1957; *also J. Soc. Ind. Appl. Math.*, vol. 7, no. 2, June 1959.

6 Okhotsimskii, D. E. and Eneev, T. M., "Some Variation Problems Connected with the Launching of Artificial Satellites of the Earth," *Uspekhi Fizicheskikh Nauk*, Sept. 1957. (Translated in *J. Brit. Interplanet. Soc.*, vol. 16, no. 5, Jan.-Feb. 1958.)

7 Miele, A., "General Variational Theory of the Flight Paths of Rocket-Powered Aircraft, Missiles and Satellite Carriers," Purdue University School of Aeronautical Engineering, Rep. no. A-58-2, Technical Note no. AFOSR-TN-58-246, Jan. 1958; *also Astronautica Acta*, vol. IV, fasc. IV, Dec. 1958.

8 Kelley, H. J., "An Investigation by Variational Methods of Flight Paths for Optimum Performance," Sc.D. thesis, Guggenheim School of Aeronautics, New York University, May 1958. (Published in part as "An Investigation of Optimal Zoom Climb Techniques," *J. Aero/Space Sci.*, vol. 26, no. 12, Dec. 1959.)

9 Leitmann, G., "On a Class of Variational Problems in Rocket Flight," Lockheed Missile and Space Systems Division Rep. 5067, September 1958; *also J. Aero/Space Sci.*, vol. 26, no. 3, Sept. 1959.

10 Leitmann, G., "The Optimization of Rocket Trajectories—A Survey," in "Progress in the Astronautical Sciences," S. F. Singer, Ed., to appear in 1961.

11 Mengel, A. S., "Optimum Trajectories," Proceedings of Project Cyclone Symposium 1 on REAC Techniques, Reeves Instrument Corp. and USN Special Devices Center, N.Y., March 15–16, 1951.

12 Irving, J. H. and Blum, E. K., "Comparative Performance of Ballistic and Low-Thrust Vehicles for Flight to Mars," in "Vistas in Astronautics," vol. II, Pergamon Press, N. Y., 1959, pp. 191–218.

13 Faulders, C. R., "Low-Thrust Steering Program for Minimum Time Transfer Between Planetary Orbits," SAE National Aeronautic Meeting, Los Angeles, Calif., Sept. 29–Oct. 4, 1958.

14 Hadamard, J., "Mémoire sur le Problèm d'Analyse Relatif à l'Équilibre des Plaques Élastiques Encastrées," Mémoires presentés par divers savants éstrangers à l'Académie des Sciences de l'Institut de France (2), vol.

33, no. 4, 1908.
15 Curry, H. B., "The Method of Steepest Descent for Non-Linear Minimization Problems," *Quart. Appl. Math.*, vol. II, no. 3, Oct. 1944.
16 Hestenes, M. R. and Stiefel, E., "Method of Conjugate Gradients for Solving Linear Systems," *Nat. Bur. Standards, J. Research*, vol. 49, 1952, pp. 409–436.
17 Forsythe, A. I. and Forsythe, G. E., "Punched-Card Experiments with Accelerated Gradient Methods for Linear Equations," Nat. Bur. Standards, Applied Mathematics Series 39, Sept. 1954, pp. 55–69.
18 Müller, C., "A New Method for Solving Fredholm Integral Equations," New York University Institute of Mathematical Sciences, Division of Electromagnetic Research Rep. no. BR-15, 1955.
19 Courant, R., "Variational Methods for the Solution of Problems of Equilibrium and Vibrations," *Bull. Amer. Math. Soc.*, vol. 49, no. 1, Jan. 1943.
20 Stein, M. L., "On Methods for Obtaining Solutions of Fixed End-Point Problems in the Calculus of Variations," *Nat. Bur. Standards, J. Research*, vol. 50, no. 5, May 1953.
21 Friedman, B., "Principles and Techniques of Applied Mathematics," John Wiley and Sons, Inc., N. Y., 1956.
22 Goodman, T. R. and Lance, G. N., "The Numerical Integration of Two-Point Boundary Value Problems," *Mathematical Tables and Other Aids to Computation*, vol. 10, no. 54, April 1956.
23 Courant, R. and Hilbert, D., "Methoden der Mathematischen Physik," Julius Springer, Berlin, vol. 1, 1924, 1931. (Translated and revised edition of vol. 1, Interscience Publishers, N. Y., 1953.)
24 Tompkins, C. B., "Methods of Steep Descent," in "Modern Mathematics for the Engineer," E. F. Beckenbach, Ed., McGraw-Hill Book Co., Inc., N. Y., 1956, chap. 18.
25 Bliss, G. A., "Lectures on the Calculus of Variations," University of Chicago Press, Chicago, 1946.
26 Garwin, R. L., "Solar Sailing—A Practical Method of Propulsion Within the Solar System," JET PROPULSION, vol. 28, no. 3, March 1958.
27 Cotter, T. P., "Solar Sailing," Sandia Research Colloquium, April 1959.
28 Tsu, T. C., "Interplanetary Travel by Solar Sail," ARS JOURNAL, vol. 29, no. 6, June 1959.
29 London, H. S., "Some Exact Solutions of the Equations of Motion of a Solar Sail With Constant Sail Setting," ARS JOURNAL, vol. 30, no. 2, Feb. 1960.

Optimum Thrust Programming of Electrically Powered Rocket Vehicles in a Gravitational Field

C. R. FAULDERS[1]

North American Aviation, Inc.
Downey, Calif.

The general problem of optimum thrust programming of an electrically powered rocket under the condition of constant jet power is considered. The thrust vector is assumed to be parallel to the instantaneous velocity vector at all times. The various optimization problems possible under these restrictions are shown to be equivalent to maximization of the change in velocity for specified propellant mass and arbitrary range, maximization of range for specified propellant mass and arbitrary change in velocity, and maximization of the change in velocity for specified range and specified propellant mass. The calculus of variations is employed to obtain analytical expressions for the thrust acceleration program for the foregoing problems with a constant gradient of the tangential component of gravitational force. Limiting values of this gradient for which the tangential component of gravity can be assumed constant in the derivation of optimum thrust programs are determined.

ELECTRICALLY powered rocket engines, such as the ion rocket and the plasma rocket, are characterized by a power source that is separate from the propellant. For a fixed power setting, therefore, the rate of propellant expenditure and the exhaust velocity can be varied over wide ranges, and a variety of thrust programs can be achieved. Electrical rockets are presently limited to very low thrust levels of the order of 10^{-3} or 10^{-4} Earth g's per unit mass of the complete space vehicle. For this reason, an entire mission would generally be carried out under power, with operating times measured in days or weeks.

The various possible requirements for optimum thrust programs are summarized in Table 1, assuming that the total time of powered flight is a specified parameter, and that the thrust is always in the tangential direction. The change in vehicle velocity is indicated by ΔV, the change in position, or range, by Δs, and the propellant mass by m_p.

Table 1 Optimum thrust program requirements (total time specified)

Case	ΔV	Δs	m_p
1	maximum	arbitrary	specified
2	specified	arbitrary	minimum
3	arbitrary	maximum	specified
4	arbitrary	specified	minimum
5	maximum	specified	specified
6	specified	maximum	specified
7	specified	specified	minimum

Received Dec. 8, 1959.
[1] Research Specialist, Aero-Space Laboratories, Missile Division.

It is to be noted, incidentally, that instead of specifying time, the variable to be maximized or minimized in any of these cases could be specified and time could be minimized. Case 1, for example, thus would be altered to the problem of specifying velocity and propellant mass, leaving range arbitrary and minimizing the time required to achieve the established objectives.

Since only first variations of the appropriate functions are to be taken to obtain solutions to these problems, sufficiency conditions for true maxima or minima will be omitted from the mathematical formulation. In this sense, Case 2 is equivalent to Case 1, Case 4 to Case 3, and Cases 6 and 7 to Case 5. Also, minimum time problems become equivalent to the corresponding reciprocal problems with time fixed. Therefore, three distinct sets of requirements can be designated as in Table 2.

Case I corresponds to the classical problem of maximizing the burnout kinetic energy with a fixed total energy and propellant mass. A practical application might involve the attainment of escape velocity with minimum propellant utilization. Fox, Michielsen and Irving (1–3)[2] have analyzed Case I for zero gravity and found the required thrust program to be one of constant thrust acceleration. Case II can be likened to sending a scientific probe a maximum distance from Earth or from the sun, with arbitrary final velocity. Thrust programming for maximum range is also discussed briefly by Irving in (3), again for zero gravity. A version of Case III wherein the increments in velocity and range are specified and the propellant is to be minimized is applicable to such problems as a change in position within a satellite orbit of specified radius or transfer between planets with combined acceleration and deceleration.

Analytical expressions are derived here for the thrust programs corresponding to the three cases discussed, with the influence of gravity taken into account. The jet power is held constant at the maximum limit for reasons noted in (3). Although the analysis is restricted to trajectories where the thrust vector is always parallel to the velocity vector, the results are applicable to a large number of practical trajectories, as indicated in (4, 5, 6 and 10). In particular, Earth escape and some orbital transfer missions can be carried out with tangential thrust; normal components of thrust become significant only when steering requirements are controlling factors, as in certain Earth-Mars missions (7–9). For convenience in the analysis, the gravity force will be split into normal and tangential components (Fig. 1) with the normal component controlling the change of direction of the flight path and the tangential component adding, in algebraic sense, to the thrust. The variation of this tangential component of gravity with distance along the flight path enters directly into the optimization problem. Although the total gravitational force varies inversely with the square of the radius from the center of mass, no a priori statement can be made as to the variation of the tangential component of gravity. An inverse square variation of this component would appear only if the trajectories were logarithmic spirals, and in general they are not. The assumption is made in this paper that the tangential component of gravity varies linearly with distance. An examination of digital computer data for powered trajectories between Earth and the moon with constant tangential thrust acceleration (4) indicates that actual variations of the tangential gravity component agree quite closely with this assumption.

Variational Differential Equation and End Conditions

Denoting the thrust per unit mass by a and the component of gravity force along the flight path by the derivative of the gravitational potential U with respect to distance, the equation of motion can be written

$$\dot{V} = a + dU/ds \quad [1]$$

$$\dot{s} = V \quad [2]$$

where dU/ds is a function of s only, and s is positive in the direction of the thrust vector. The propellant mass rate is related to the thrust acceleration by

$$a = c\dot{m}/(M_0 - m) \quad [3]$$

and the constant jet power is given by

$$P = (c^2/2)\dot{m} \quad [4]$$

Combining Equations [3 and 4] to eliminate c and integrating

$$\frac{1}{M_0 - m} - \frac{1}{M_0} = \frac{1}{2P}\int_0^t a^2 dt \quad [5]$$

According to Equation [5], the propellant mass is uniquely determined by the function

$$\psi = 2P/(M_0 - m) \quad [6]$$

where

$$\dot{\psi} = a^2 \quad [7]$$

Adopting the Mayer formulation, the general problem defined by Cases I, II and III can be stated as one of determining the thrust program $a(t)$ for which the function

$$F = G(V_T, s_T, \psi_T, T) + \int_0^T \left[\nu_1\left(\dot{V} - a - \frac{dU}{ds}\right) + \nu_2(\dot{s} - V) + \nu_3(\dot{\psi} - a^2)\right]dt \quad [8]$$

is stationary. ν_1, ν_2 and ν_3 are unspecified functions of time, and G is that function of the variables at time T which is to be maximized or minimized. The three terms in the integrand that are set off by parentheses represent the constraints on

Table 2 Distinct optimum thrust program requirements (total time specified)

Case	ΔV	Δs	m_p
I	maximum	arbitrary	specified
II	arbitrary	maximum	specified
III	maximum	specified	specified

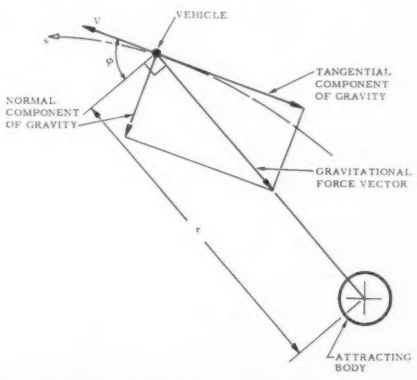

Fig. 1 Schematic sketch indicating force components

[2] Numbers in parentheses indicate References at end of paper.

the problem, Equations [1, 2 and 7]. Writing the Euler-Lagrange equations

$$\frac{\partial f}{\partial x_j} - \frac{d}{dt}\frac{\partial f}{\partial \dot{x}_j} = 0 \qquad x_j = V, s, a, \psi \qquad [9]$$

for the integrand of Equation [8] results in

$$\nu_2 + \dot{\nu}_1 = 0 \qquad [10]$$

$$\nu_1(d^2U/ds^2) + \dot{\nu}_2 = 0 \qquad [11]$$

$$\nu_1 + 2\nu_3 a = 0 \qquad [12]$$

$$\dot{\nu}_3 = 0 \qquad [13]$$

Combining Equations [10 through 13]

$$\ddot{a} = (d^2U/ds^2)a \qquad [14]$$

Boundary conditions for which the function F is stationary can be deduced by setting the total variation of F equal to zero. Thus, holding time T fixed and recalling Equation [9]

$$\left(\frac{\partial G}{\partial V_T} + \nu_1\right)_T \delta V_T + \left(\frac{\partial G}{\partial s_T} + \nu_2\right)_T \delta s_T + \left(\frac{\partial G}{\partial \psi_T} + \nu_3\right)_T \times \delta\psi_T = 0 \qquad [15]$$

For Case I, where velocity is to be maximized while range is unspecified, G becomes V_T and δs_T is nonzero. Thus, from Equation [15], $(\nu_2)_T$ is zero or, from Equations [10 and 12]

$$\dot{a}_T = 0 \qquad [16]$$

In addition, δV_T is nonzero. The requirement that the coefficient of δV_T be zero, however, contributes no useful information.

For Case II, maximum range and arbitrary velocity, G becomes s_T and δV_T is nonzero. Again from Equation [15], $(\nu_1)_T$ is zero and, from Equation [12]

$$a_T = 0 \qquad [17]$$

In Case III, G again becomes V_T, but only the coefficient of δV_T can be equated to zero owing to the specified range. As with Case I, however, the stipulation that $(\nu_1 + 1)_T$ equals zero does not impose any end condition on $a(t)$. This result would be expected, for Equations [1,2,7 and 14] comprise a fifth-order set of equations. Sufficient boundary conditions for the solution follow from V, s and ψ at time zero and the specified s and ψ at time T.

Linear Variation of Tangential Component of Gravity

Case I

Defining

$$\alpha^2 = d^2U/ds^2 \qquad [18]$$

Equation [14] becomes

$$\ddot{a} = \alpha^2 a \qquad [19]$$

Recognizing the appropriate end condition for Case I, namely Equation [16], the solution of Equation [19] is

$$\frac{a}{a_0} = \frac{\cosh \alpha T(1 - t/T)}{\cosh \alpha T} \qquad [20]$$

Substituting Equation [20] in Equation [5] and solving for the initial acceleration

$$\frac{a_0}{\sqrt{\frac{P^2}{EM_T}}} = \frac{\sqrt{4\alpha T\,[(\omega - 1)/\omega]}}{\sqrt{\frac{\sinh \alpha T}{\cosh \alpha T} + \frac{\alpha T}{\cosh^2 \alpha T}}} \qquad [21]$$

According to Equation [18], a constant tangential component of gravity corresponds to α of zero. Taking the limits of Equations [20 and 21] as α approaches zero

$$a/a_0 = 1 \qquad [22]$$

$$\frac{a_0}{\sqrt{P^2/EM_T}} = \sqrt{2\left(\frac{\omega - 1}{\omega}\right)} \qquad [23]$$

The equation of motion can be obtained from Equations [1 and 2] in the form

$$\ddot{s} - \alpha^2 s = a + (dU/ds)_0 - \alpha^2 s_0 \qquad [24]$$

With the thrust acceleration given by Equation [20], the solution to Equation [24] can be obtained by means of standard techniques applicable to linear differential equations. The velocity can then be obtained by taking the derivative of s with respect to time. Thus

$$\frac{\Delta V}{(a_0/2\alpha)} = \left(\sinh \alpha T + \frac{\alpha T}{\cosh \alpha T}\right) + \frac{V_0}{(a_0/2\alpha)} \times (\cosh \alpha T - 1) + \frac{(dU/ds)_0}{(a_0/2)} \sinh \alpha T \qquad [25]$$

$$\frac{\Delta s}{(a_0/2\alpha^2)} = \left(\frac{\cosh^2 \alpha T - 1}{\cosh \alpha T}\right) + \frac{V_0}{(a_0/2\alpha)} \sinh \alpha T + \frac{(dU/ds)_0}{(a_0/2)} (\cosh \alpha T - 1) \qquad [26]$$

where a_0 is given by Equation [21].

Case II

With the end condition given by Equation [17], the solution of Equation [19] applicable to Case II is

$$\frac{a}{a_0} = \frac{\sinh \alpha T(1 - t/T)}{\sinh \alpha T} \qquad [27]$$

From Equation [5]

$$\frac{a_0}{\sqrt{\frac{P^2}{EM_T}}} = \frac{\sqrt{4\alpha T\,[(\omega - 1)/\omega]}}{\sqrt{\frac{\cosh \alpha T}{\sinh \alpha T} - \frac{\alpha T}{\sinh^2 \alpha T}}} \qquad [28]$$

With an α of zero, Equations [27 and 28] reduce to

$$\frac{a}{a_0} = \left(1 - \frac{t}{T}\right) \qquad [29]$$

$$\frac{a_0}{\sqrt{P^2/EM_T}} = \sqrt{6\left(\frac{\omega - 1}{\omega}\right)} \qquad [30]$$

The solution of Equation [24] and subsequent differentiation of the solution with respect to time leads to the expressions

$$\frac{\Delta V}{(a_0/2\alpha)} = \sinh \alpha T + \frac{V_0}{(a_0/2\alpha)} (\cosh \alpha T - 1) + \frac{(dU/ds)_0}{(a_0/2)} \sinh \alpha T \qquad [31]$$

$$\frac{\Delta s}{(a_0/2\alpha^2)} = \left(\cosh \alpha T - \frac{\alpha T}{\sinh \alpha T}\right) + \frac{V_0}{(a_0/2\alpha)} \sinh \alpha T + \frac{(dU/ds)_0}{(a_0/2)} (\cosh \alpha T - 1) \qquad [32]$$

where a_0 is given by Equation [28].

A comparison of the first two terms of Equation [25] with the first term of Equation [31] indicates that, for zero initial velocity and zero initial tangential gravity force, the velocity

increment for Case I is greater than that for Case II by the ratio

$$\frac{\Delta V_I}{\Delta V_{II}} = \frac{\sqrt{(\cosh^2 \alpha T)(\sinh^2 \alpha T) - (\alpha T)^2}}{\sinh^2 \alpha T} \quad [33]$$

where the values of a_0 for Cases I and II have been obtained from Equations [21 and 28], respectively. At αT of zero, Equation [33] indicates a ratio of velocities of $2/\sqrt{3}$, whereas at αT approaching infinity, the velocity increments for Cases I and II are the same. At large αT, therefore, maximum velocity increment and maximum range are realized simultaneously.

The ratio of the thrust contributions to the distance increments for Cases I and II is given by

$$\frac{\Delta s_I}{\Delta s_{II}} = \frac{\sinh^2 \alpha T}{\sqrt{(\cosh^2 \alpha T)(\sinh^2 \alpha T) - (\alpha T)^2}} \quad [34]$$

or the inverse of the ratio of velocity increments.

Case III

The general solution of Equation [19] is simply

$$a = C_1 \cosh \alpha T + C_2 \sinh \alpha T \quad [35]$$

which reduces to

$$a = C_1 + C_2 t \quad [36]$$

as α approaches zero. In this case, the constants of integration C_1 and C_2 are determined from the specified range and propellant mass. Equivalently, specified values of range and velocity increment could be used to determine the constants. A problem that would fall under the category of Case III is one wherein the velocity is to be maximized but the range is specified as some function of the velocity.

Selection of Typical Values of (αT)

Optimum thrust programs for the condition of a constant gradient of the tangential gravity component (Eqs. [20, 27 and 35]) are dependent on the dimensionless parameter αT. This parameter, essentially the square root of a nondimensional gravity gradient, is a function of the particular trajectory characteristics, such as the initial position and velocity vector, the initial thrust to weight ratio of the vehicle, the thrust acceleration program, and the time of flight or distance of travel. It is of interest to determine representative values of αT for some actual powered flight space trajectories.

For spiral trajectories from an Earth satellite orbit to the moon, or to Earth escape velocity, values of αT can be roughly estimated. For a constant thrust per unit mass that is small compared with the local acceleration of gravity, the initial tangential component of gravity is twice the initial thrust per unit mass, and the final tangential component of gravity is approximately zero (4). Therefore

$$\alpha^2 T^2 = \left(\frac{\Delta g_s}{\Delta s}\right)_{avg} T^2$$

or

$$\alpha^2 T^2 \cong 2 \frac{a_0}{(\mu/r_0^2)} \frac{V_{s0}^2 T^2}{r_0 \Delta s} \quad [37]$$

where V_{s0} is the initial satellite velocity. Range is related to V_{s0} by

$$V_{s0} T \cong 2\Delta s$$

and the increment in radius is

$$\Delta r \cong \Delta s (\sin \phi)_{avg}$$

Table 3 Values of αT for Earth escape

$\frac{a_0}{(\mu/r_0^2)}$	$(\Delta r/r_0)_{escape}$	$(\alpha T)^a$
10^{-4}	100	0.1
10^{-3}	30	0.5
10^{-2}	10	1.0
10^{-1}	5	3.0

[a] Approximate value.

Table 4 Values of αT for small radius ratios

(r_2/r_1)	$(\alpha T)^a$
1.25	0.4
1.5	0.5
2.0	0.75

[a] Approximate value.

Again from (4), sin ϕ varies between approximately zero at takeoff from a satellite orbit and approximately unity at escape. With an average value of sin ϕ of the order of one half, Equation [37] becomes

$$\alpha^2 T^2 \cong 16 \frac{a_0}{(\mu/r_0^2)} \frac{\Delta r}{r_0} \quad [38]$$

Current estimates of the thrust acceleration of electrically powered rockets lead to values of the order of 10^{-4} to 10^{-3} Earth g's. The ratio appearing in Equation [38], however, is a function not only of the ratio of thrust to sea-level weight, but also of the radius of the initial satellite orbit. For values of $a_0/(\mu/r_0^2)$, estimates of $\Delta r/r_0$ for escape were obtained from (4). Values of αT computed from Equation [38] are indicated in Table 3.

Estimates of αT can also be obtained for a tangential thrust trajectory extending from the Earth orbit to other nearby orbits, such as that of Mars, and with only the solar gravitational field considered. The initial thrust to mass ratio is assumed to be 10^{-4} Earth g's, corresponding to a thrust to mass ratio of the order of one tenth the local solar gravity. In this case, the initial tangential component of gravity is again of the order of twice the initial thrust per unit mass. However, the final tangential component of gravity may be as large as one half this value, assuming that the thrust is always directed away from the starting point. Thus, following the development of Equation [37]

$$\alpha^2 T^2 \cong \frac{a_0}{(\mu/r_0^2)} \frac{V_{s0}^2 T^2}{r_0 \Delta s} \quad [39]$$

The expressions for range and increment in radius become, in this case

$$V_{s0} T \cong \Delta s \qquad \Delta r \cong \Delta s (\sin \phi)_0$$

From (4), for small thrust to weight ratios

$$(\sin \phi)_0 \cong 2a_0/(\mu/r_0^2)$$

Finally, therefore

$$\alpha^2 T^2 \cong \frac{1}{2} \frac{\Delta r}{r_0} \quad [40]$$

On the basis of the foregoing analysis, the correspondence between values of αT and radius ratios of the order of unity was taken to be that shown in Table 4.

In Fig. 2, the optimum nondimensional thrust programs for Case I, computed from Equation [20], is plotted for values of αT from 0 to 3.0. Thrust programs for Case II, Equation [27], are plotted in Fig. 3 for the same values of αT. Initial thrust accelerations are given in terms of powerplant characteristics by Equations [21 and 28].

A worthwhile comparison can be made of the velocity increment resulting from the use of the optimum thrust acceleration program with the velocity increment that would be obtained with simply a constant thrust acceleration. Similarly, the range obtained with the optimum program can be compared with that for constant thrust acceleration. Power level, operating time and mass ratio will be assumed to be the same in each case. The results of such comparisons are indicative of the importance of determining an optimum thrust program. Integration of Equation [24] with a constant thrust acceleration leads to

$$\frac{\Delta V}{(a_0/2\alpha)} = 2 \sinh \alpha T + \frac{V_0}{(a_0/2\alpha)} (\cosh \alpha T - 1) + \frac{(dU/ds)_0}{(a_0/2)} \sinh \alpha T \quad [41]$$

$$\frac{\Delta s}{(a_0/2\alpha^2)} = 2(\cosh \alpha T - 1) + \frac{V_0}{(a_0/2\alpha)} \sinh \alpha T + \frac{(dU/ds)_0}{(a_0/2)} (\cosh \alpha T - 1) \quad [42]$$

where a_0 is given by Equation [23]. For zero initial velocity and initial tangential gravity force, Equations [21, 23, 25, 28, 32, 41 and 42] can be combined to give

$$\frac{\Delta V_I}{\Delta V_{a=a_0}} = \sqrt{\frac{\alpha T}{2}} \frac{\sqrt{(\sinh \alpha T)(\cosh \alpha T) + \alpha T}}{\sinh \alpha T} \quad [43]$$

$$\frac{\Delta s_{II}}{\Delta s_{a=a_0}} = \sqrt{\frac{\alpha T}{2}} \frac{\sqrt{(\sinh \alpha T)(\cosh \alpha T) - \alpha T}}{\cosh \alpha T - 1} \quad [44]$$

These two ratios are plotted in Fig. 4. With an αT of 2.0, Fig. 4 indicates a 9 per cent increase in velocity and a 24 per cent increase in range owing to replacement of a constant thrust acceleration with the optimum program. At large values of αT, both ratios approach $\sqrt{\alpha T/2}$.

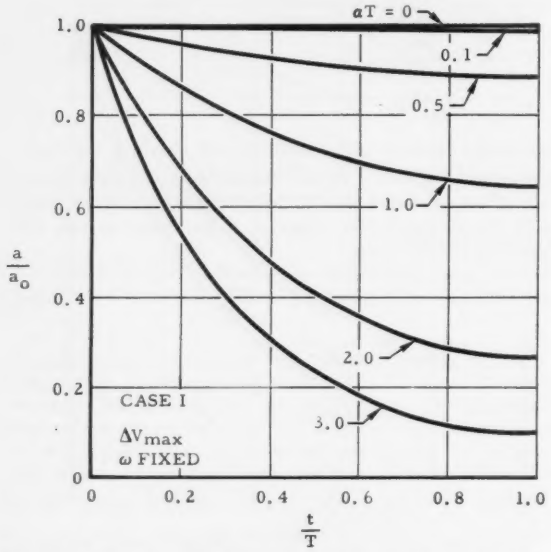

Fig. 2 Optimum thrust acceleration programs for Case I (maximum velocity increment)

Fig. 3 Optimum thrust acceleration programs for Case II (maximum range)

Discussion of Results

According to Fig. 2, the assumption of a constant tangential component of gravity is adequate for determination of the optimum thrust program for Case I when αT is less than 0.1. With Case II, however, it can be seen from Fig. 3 that the same assumption is valid for αT up to about 0.5. Optimum thrust curves for Case III might be expected to follow the same general variation with αT as that exhibited in Figs. 2 and 3. A safe estimate for the maximum value of αT for which the gravity force gradient can be neglected might be, therefore, of the order of 0.1 for Case III.

Fig. 4 Velocity increments and range obtained with optimum thrust program compared with values resulting from use of constant thrust acceleration, $V_0 = (dU/ds)_0 = 0$

The parameter α is real, and Figs. 2 and 3 are applicable when the gravity force is in opposition to the thrust and decreases in the positive direction of motion, or when the gravity force adds to the thrust and increases in the positive direction of motion. The latter condition would arise, for example, if a vehicle were to be accelerated toward the origin of a central force field. With a gravity force opposing the thrust but increasing in the direction of flight, or adding to the thrust but decreasing in the direction of flight, α would be imaginary and the thrust variations with time would be sinusoidal with a period of $2\pi/\alpha$. There are no obvious situations, however, other than the oscillatory phase of low thrust takeoff from a satellite orbit, where an imaginary α would be encountered with gravity steering alone.

The decrease in thrust acceleration to zero corresponding to maximum range (Fig. 3) is accompanied by an increase in the exhaust velocity to infinity, as can be seen from Equations [3 and 4]. In practice, a limiting exhaust velocity will exist, the value depending upon the design of the rocket engine. The thrust acceleration program to be used when account is taken of the minimum thrust limitation is, therefore, of interest. A complete analysis of this problem is beyond the scope of this paper. It can be shown, however, that a stationary solution is obtained with the thrust acceleration given by Equation [14] and the end condition, Equation [17], up to the time when the limiting exhaust velocity is reached and then holding constant exhaust velocity to burnout at total time T. The end condition would apply at the end of flight, not at the time when the limiting curve is reached. That is, the curve of thrust acceleration prior to reaching maximum exhaust velocity would, if extended past the limiting curve, go through zero at the time maximum range is to be achieved. Still greater range could probably be obtained by suddenly changing the power to zero or some reduced level at the time the limiting exhaust velocity is reached. Even with a discontinuity in power, however, the foregoing remarks concerning the variable exhaust velocity portion of the thrust acceleration curve are still applicable.

A requirement more common than maximizing distance of travel, or range, would be that of maximizing the change in radial position from the center of the gravitational field. When the flight path extends out beyond the radius where escape velocity is attained, a correspondence can be expected between maximum radius and maximum length of flight path. For flights that begin and end deep within the gravitational field, however, the reduction in thrust acceleration to zero that is necessary for maximum range may result in a tightening of the spiral trajectory to the point where the radius increment is much less than could be obtained with some other thrust program. A brief analysis of the latter case is given in the Appendix. It is shown there that when the thrust acceleration is small compared with the total gravitational acceleration at all times, and when the vehicle is initially in a circular satellite orbit, maximum change in radius is obtained with a constant thrust acceleration.

The assumption of a constant gradient of the tangential gravity component does not apply, certainly, to all possible trajectories that can be generated with tangential thrust. For more complex variations of the tangential gravity component with distance (e.g., parabolic, exponential), analytical solutions can be obtained for specific cases by expansion of Equations [1 and 14] in powers of some appropriate nondimensional parameter. Regardless of the actual variation of the tangential gravity component, the second derivative of thrust acceleration with time is positive as long as the thrust remains in the positive direction and α is real, as indicated by Equation [14]. End conditions for Cases I and II, furthermore, are independent of the gravitational force. On this basis, the thrust programs of Figs. 2 and 3 would be expected to be reasonable approximations for nonlinear variations of the tangential gravity component as long as the average slope is used in the determination of αT.

To obtain an exact solution, numerical integration of Equations [1, 2 and 14] would be necessary. For this purpose, an iterative scheme might be used wherein a trajectory would first be computed with an assumed thrust program, the resulting variation of the tangential gravity component would be used in the computation of a revised thrust program, and the process repeated until convergence was realized. The results presented here should prove useful in determining the thrust program to be assumed for the first iteration.

Conclusions

The optimum thrust acceleration program for the case of maximum velocity increment with a specified propellant mass and arbitrary range is constant thrust acceleration when the tangential component of gravity is constant. With a variable gravity component, the variation of the thrust acceleration involves a zero time derivative at burnout.

For maximum range, arbitrary velocity increment and a specified propellant mass, the thrust acceleration decreases linearly to zero when the tangential gravity component is constant. For arbitrary variation of the gravity component, the burnout thrust is zero.

The assumption of zero gravity in the determination of the optimum thrust program is valid for most engineering purposes as long as the gravity component variation can be represented by a straight line with the square root of the nondimensional gradient (αT) of the order of 0.1 or less.

Appendix: Thrust Acceleration Program for Maximum Change in Radius

If the thrust acceleration is small compared with the total gravitational force at all times, and if the vehicle is initially in a circular satellite orbit, the equations of motion can be linearized and the solution averaged over a single revolution (4) to give

$$\dot{V} = -a \qquad [A\text{-}1]$$

$$\frac{dr}{ds} = 2\frac{a}{(\mu/r^2)} \qquad [A\text{-}2]$$

From Equation [A-2], maximum change in radius is obtained when the integral

$$I = \int_0^T aV dt \qquad [A\text{-}3]$$

is maximized. With a specified mass of propellant, the integral

$$J = \int_0^T a^2 dt \qquad [A\text{-}4]$$

must be held constant, according to Equation [5]. From Equation [A-1]

$$I = -\int_0^T V\dot{V} dt \qquad [A\text{-}5]$$

$$J = \int_0^T \dot{V}^2 dt \qquad [A\text{-}6]$$

The function

$$f = V\dot{V} + \lambda\dot{V}^2$$

must satisfy the Euler-Lagrange equation. Thus

$$\frac{\partial f}{\partial V} - \frac{d}{dt}\frac{\partial f}{\partial \dot{V}} = 0$$

or

$$2\lambda\ddot{V} = 0$$

From Equation [A-1] therefore

$$\dot{a} = 0 \qquad [A\text{-}7]$$

and the thrust acceleration is a constant.

Nomenclature

a	=	thrust per unit mass of vehicle
c	=	exhaust velocity, measured with respect to vehicle
E	=	total energy expended, $E = PT$
f	=	integrand for which Euler-Lagrange equations are written
F	=	stationary function
G	=	function of dependent variables at time T
I	=	integral defined by Equation [A-3]
J	=	integral defined by Equation [A-4]
m	=	mass of propellant expended at time t
m_p	=	total mass of propellant
M_0	=	initial mass of vehicle plus propellant
M_T	=	final mass of vehicle, $M_0 = M_T + m_p$
P	=	jet power
r	=	radius measured from center of attracting body
s	=	distance measured along flight path
t	=	time
T	=	total time of flight
U	=	gravitational potential
V	=	velocity of vehicle
V_{s0}	=	satellite velocity at initial radius
α	=	$\sqrt{d^2 U/ds^2}$
λ	=	Lagrangian multiplier
μ	=	constant of a particular gravitational field
ν_1, ν_2, ν_3	=	unspecified functions of time t
ϕ	=	flight path angle measured from circumferential direction
ψ	=	$2P/(M_0 - m)$
ω	=	mass ratio, $\omega = M_0/M_T$

Subscripts

0	=	initial value at $t = 0$
T	=	final value at $t = T$
I	=	Case I
II	=	Case II

References

1 Fox, R., "Optimum Exhaust Velocity Programming and Propulsion Efficiency," *J. Astron. Sci.*, vol. VI, no. 1, Spring 1959, pp. 13–16.

2 Michielsen, H. F., "Minimum Weight and Optimum Flight Path of Low-Acceleration Space Vehicles," in "Advances in Astronautical Sciences," vol. 3, Plenum Press, Inc., N. Y., 1958.

3 Irving, J. H., "Low Thrust Flight: Variable Exhaust Velocity in Gravitational Fields," in "Space Technology," John Wiley and Sons, Inc., N. Y., 1959.

4 Perkins, F. M., "Flight Mechanics of Low Thrust Space Craft," in "Vistas in Astronautics II," Pergamon Press, Inc., N. Y., 1959.

5 Benney, D. J., "Escape From a Circular Orbit Using Tangential Thrust," JET PROPULSION, vol. 28, no. 3, March 1958, pp. 167–169.

6 Fox, R. H., "Powered Trajectory Studies for Low Thrust Space Vehicles," ARS preprint 879-59, June 1959.

7 Faulders, C. R., "Low Thrust Rocket Steering Program for Minimum Time Transfer Between Planetary Orbits," Society of Automotive Engineers, Paper 88A, Oct. 1958.

8 Rodriguez, E., "A Method of Determining Steering Programs for Low Thrust Interplanetary Vehicles," ARS JOURNAL, vol. 29, no. 10, Oct. 1959, pp. 783–788.

9 Copeland, J., "Interplanetary Trajectories Under Low Thrust Radial Acceleration," ARS JOURNAL, vol. 29, no. 4, April 1959, pp. 267–271.

10 Fox, R., "Ionic Propulsion," *Astron. Sci. Rev.*, vol. I, no. 3, July-Sept. 1959, pp. 7–12.

Solid Propellant Detonability

ADOLPH B. AMSTER,[1] EVAN C. NOONAN[2] and GEORGE J. BRYAN[3]

U. S. Naval Ordnance Laboratory
Silver Spring, Md.

Using a shock sensitivity test, it has been possible to formulate broad patterns of behavior for propellants under certain conditions. Conventional double-base propellants have a sensitivity somewhat less than that of conventional insensitive military explosives. This sensitivity increases slightly with an increase in temperature and markedly with decreasing density. Pore type is important; samples with nonconnected pores increase in sensitivity as temperature decreases. Many composite propellants containing conventional rubber-like binders are not easily detonated. Composites containing high energy binders are readily detonated. An investigation of the attenuation of shock by Lucite has been made. The results of this study make it possible to determine the pressure required to initiate detonation in a propellant under the conditions of the booster sensitivity test.

AS THE quantity of solid propellants used in individual rockets, particularly in guided missile propulsion systems, grows larger and larger, the safety of such motors with respect to accidental explosion or detonation becomes of considerable concern. Because of the confines of shipboard usage, the Navy must give special attention to this aspect of safety.

Early in the Polaris program projects to study propellant safety were established with a number of organizations, among them the Naval Ordnance Laboratory. One aim of the NOL project was to determine the shock sensitivity of solid propellants.

Experience with explosives has shown a good correlation of

Received March 16, 1960.

[1] Present address: Combustion Research Department, United Technology Corp., Sunnyvale, Calif. Member ARS.

[2] Chief, Physical Chemistry Division.

[3] Present address: Space Technology Laboratories, Inc., Patrick Air Force Base, Fla.

impact test results with field handling experience and also with the results of shock sensitivity tests, also known as booster or gap tests (1).[4] The simple and inexpensive nature of impact testing has been an advantage in the preliminary screening of explosives. Application of the test to propellants has failed to produce results which can be correlated with handling experience or with shock sensitivity tests. As a matter of fact, since the impact sensitivities of most propellants imply that they are more sensitive than most booster explosives, it is apparent that the use of these results as a basis for screening would have denied the Armed Forces most, if not all, of its propellants.

For this reason and, in addition, to evaluate directly the shock induced detonability of solid propellants, we have used a gap test which is a modification of one generally used for liquid monopropellants and developed by Edwards at this Laboratory (2). Briefly, gap testing is a procedure by which a high energy shock wave is transmitted from a "donor" to an "acceptor." In its usual form, using a standardized donor, the distance between the two is varied and the results are reported in terms of that distance or "gap" at which there is a 50 per cent probability of detonation of the acceptor.

Fig. 1 represents, schematically, the fashion in which the tests are conducted at NOL (3). The gap cards are of cellulose acetate and are each 0.0254-cm (0.01 in.) thick and 5.08 cm (2 in.) in diameter. For gaps greater than 1.27 cm (0.50 in.) the cards can be replaced by a combination of 1.27-cm (0.50 in.) Lucite disks and 0.0254-cm (0.01 in.) cards to give the desired thickness. We have found no discernible difference in substituting 1.27 cm (0.5 in.) of solid Lucite for 50 cards. The charge diameter exceeds the critical diameter[5] for most explosives.

The damage to the plate is used to determine whether a detonation has occurred. With most explosives a detonation very neatly punches a hole into the center of the plate; the diameter of the hole is close to that of the charge. The remainder of the plate is essentially undamaged. In the absence of a detonation, no damage to the plate occurs. With propellants, the critical diameter appears often to approach or to exceed that of the charge used. In such systems misleading (false positive) results may be produced by an unstable detonation. For such systems it is good practice to measure shock velocities. Methods for doing this are described elsewhere in detail (4). Briefly, thin wires are inserted into the charge at predetermined points. Connected to these wires are units which measure the time required for the shock or detonation to travel between pins. The stability of detonation is judged by the constancy of the velocity as the shock propagates along the charge. We have been able to correlate the plate damage very nicely with the shock velocity at the plate. For velocities over about 4000 m per sec, the damage is essentially the same as with high explosives. With increasing detonation velocity, the hole size increases up to about $2\frac{1}{2}$ in. with Composition B, which has a detonation velocity of about 7800 m per sec. Within the range 3000–4000 m per sec, the edges of the plate around the hole will show an outward bulge. From 1200 to 1300 m per sec there will be a derby hat-like bulge instead of a hole, the depth being larger for higher velocities. At less than 1200 m per sec there is no discernible effect. Since for all safety purposes the detonation velocity is secondary, all stable detonations are reported as "goes."

The test procedure is roughly as follows: A test is run at zero gap. If detonation occurs, the next test is made at eight cards, and the number of cards is doubled with each additional test until the sample gives a negative result. Each successive shot is then made half way between the closest "go" and "no-go" card values. This procedure is continued until a positive and negative test have been obtained which differ by only one card. Without going into further detail, it takes only two to four more shots to ascertain within one half card what the 50 per cent point is. It is our feeling that the results reported herein are precise within one to two cards.

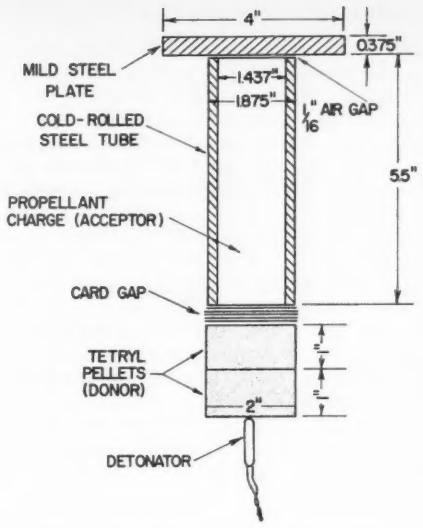

Fig. 1 Shock sensitivity test apparatus

Test Results

Impact vs. Gap Testing

Let us now examine some of the results which have been obtained. First let us take a look at a comparison between the impact sensitivities of explosives and of some typical propellants. Bearing in mind that Tetryl and pure RDX are considered to be too sensitive for use as high explosives, it is seen immediately from Table 1 that none of the propellants tested would have been accepted by this standard. Double-base and, by now, many composite propellants have a history of safe use and freedom of accidents. There do not seem to be any reports of trouble during handling of these materials after they are through the manufacturing stages. Safety records of this sort are hard to reconcile with the impact data; it is well not to place too much reliance upon them. There is, however, one important area in which impact data may be very useful. Research at this laboratory has shown a good correlation between impact data and ignitibility test results (5).

Table 1 Approximate order of impact sensitivities of some common explosives and propellants

Explosive	Propellant
PETN (11-16[a])	composite high energy binder (11)
	composite polysulfide rubber (15)
RDX (16-33)	composites polyurethane binder (16-41)
	polyvinyl chloride binder
	polyester-styrene binder
Tetryl (26-50)	double-base Type I (28)
Composition B (45-82)	
TNT (150-215)	

[a] Numbers in parentheses indicate height in cm, using Bruceton Type 12 tools, 2.5 kg weight.

[4] Numbers in parentheses indicate References at end of paper.
[5] I.e., that diameter below which a detonation will not propagate.

Shock Sensitivity of Nondefective Solid Propellants

A number of different types of double-base and composite propellants have been examined for shock sensitivity. The results are listed in Table 2; values for some better known military explosives are given for comparison. It is seen that conventional composites (polyurethane, polyvinyl chloride or polysulfide rubber binders) cannot be detonated in the diameters tested. The double-base propellants detonate readily, and the use of an explosive binder increases the sensitivity almost to that of our common insensitive high explosives.

The data in Table 2 were taken at or close to 24 C. It is interesting to examine the effects of temperature. Typical data are presented in Table 3. Obviously marked changes in temperature do not induce any comparable change in sensitivity, and such change as does occur is generally in the expected direction; i.e., rising temperatures increase detonability. All propellants which failed to detonate at 24 C also failed at −59 C and +66 C. Furthermore, repeated temperature cycling between these extremes had no apparent effect on any of the propellants. An indication of the insensitivity of at least two of the composites is indicated by the failure of two polyurethane binder systems to propagate a detonation in a modified gap test, i.e., a charge 50.8 cm (20 in.) in diameter and 203-cm (80 in.) long confined in a 0.635-cm (0.25 in.) thick steel tubing and boostered by a 340.5-kg (750 lb) Composition B charge 50.8 cm (20 in.) in diameter and 101.6-cm (40 in.) long (6).

Table 2 Shock sensitivity of selected solid propellants and standard military explosives (temperature = 24 C = 75 F)

Material	Sensitivity (cards at 50% point)	Remarks
Propellant		
polysulfide rubber binder	<0[a]	...
polyvinyl chloride binder	<0	...
polyurethane binder	<0	...
polyester-styrene binder	<0	...
double-base Type I (medium energy)	9½	...
double-base Type II (high energy)	35	...
composite with high energy binder	72	...
hybrid (double base plus inorganic oxidizer)	88	...
Explosive		
ammonium nitrate	<0	pressed 1.61 g/cc
Tritonal	114	cast
TNT	139½	cast
Explosive D	150½	pressed 1.59 g/cc
Composition B	179½	cast
Tetryl	272	pressed 1.63 g/cc

[a] Did not detonate.

Table 3 Effect of temperature on propellant sensitivity

Propellant	Sensitivity[a] (−59 C)	(−32 C)	(−4 C)	(24 C)	(38 C)
double-base Type I	<0	<0	2½	9½	12½
double-base Type II	26½	28	34	35	37½
composite with high energy binder	49	...	...	72	97½
hybrid (double base plus inorganic oxidizer)	57	...	...	88	82

[a] In cards 0.0254-cm (0.01 in.) thick.

Shock Sensitivity of Porous Solid Propellants

Defective grains (containing pores, cracks, etc.) are notorious for exploding during or subsequent to ignition (7). In order to further our understanding of the process so that control might be accomplished, the shock sensitivities of a number of porous propellants were measured. Two types of pores were treated: Connected and nonconnected.

The connected pores were made in either of two ways. With the double-base propellants small cylindrical granules (1 × 4 mm and 2 × 8 mm) were extruded, and these were poured into the steel gap test tube until, after moderate shaking, the tube was filled. For the composite propellants, charges were prepared by pressing fine lathe turnings into the steel tube. In each case the charge density was determined simply by weighing the charge used and knowing its dimensions. The result was compared with the density of a solid charge and expressed as "% M.D.," i.e., percentage manufactured density.

For double-base and composite charges containing nonconnected pores, samples were obtained by manufacturing under conditions conducive to bubble formation.

The results for a typical double-base propellant (Type I, see Table 2) are shown in Fig. 2. It is seen that sensitivity increases with increasing porosity (i.e., decreasing % M.D.). At ambient temperature and above, pore type does not seem to be important. As the temperature is lowered pore type becomes increasingly significant. For samples with connected porosity, sensitivity decreases with temperature. For those with nonconnected pores, sensitivity increases remarkably with decreasing temperature.

A different type of behavior is noted with the composite propellants so far tested. Here, as with the double-base systems,

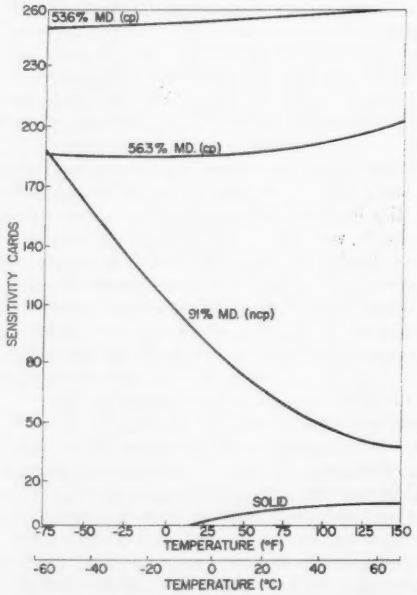

Fig. 2 Effect of porosity and temperature on the shock sensitivity of a medium energy double-base propellant (cp = connected pores; ncp = nonconnected pores)

the introduction of connected porosity increases sensitivity; temperature changes have a secondary effect—increasing temperature increases sensitivity slightly. Samples containing nonconnected pores are, within the range tested, nondetonable regardless of % M.D. or temperature. Although they have not yet been tested, one would expect that porous composites containing an inherently explosive binder would behave in the same fashion as the double-base systems.

Is there an explanation for the marked increase in sensitivity induced by decreasing the temperature of the foam-like double-base propellants containing nonconnected pores? Can this behavior be reconciled with the insensitivity of the foam-like composites even at low temperatures? We believe both these questions can be answered. Let us examine a postulated mechanism for the shock induced transition to detonation in a confined granular material (8). Presumably a deflagration begins at the exposed surfaces of the propellant fragments. Since the sample is confined, the product gases do not escape, and the rising pressure causes an increase in the linear burning rate. The process continues until a stable detonation develops. Obviously the rate at which the pressure rises depends upon the total area of the propellant exposed to the hot gases initially present. In a system containing connected pores the gases can diffuse readily and a large area can ignite; the result is an easily propagated deflagration; i.e., the sample is sensitive. If the pores are nonconnected, the hot gases do not readily diffuse forward (away from the reaction zone into unreacted material), and, until high pressure gases rupture the interpore membrane, the reaction is restricted. If, however, the sample is brittle the same shock which serves to initiate the deflagration may be strong enough to produce an almost immediate rupture of these membranes, and the sample will now behave in an extremely sensitive fashion. For now, not only is gas flow possible, but the total surface area available for combustion is increased manyfold. The brittleness of any viscoelastic material (such as a propellant) is known to increase with decreasing temperature and/or with increasing rate of stress application (9). The double-base systems tested are much less elastic at ambient temperature and slow rates of stress application than are the composites tested. This brittleness apparently is the cause for the sensitivity.

Absolute Scale for Expressing Sensitivity

As convenient as the card gap values are for expressing detonability on a relative scale, it certainly is more desirable to be able to express sensitivity in terms of a more fundamental scale, e.g., rate at which energy must be transferred to an explosive to initiate detonation. Prerequisite to the complete determination of these data, and perhaps the most significant portion thereof, is knowledge of the pressure at the leading edge of the shock wave. Although it has not yet been possible to measure such high pressures directly, some indirect techniques do exist (10). One such method has been applied to our gap test where we were interested in determining the pressure in the leading edge of the shock wave as it left the Lucite gap (attenuator) and was about to enter the acceptor. The following steps are involved:

1 High speed photographic studies are used to obtain the particle velocity (u) vs. shock velocity (U) relation for Lucite.

2 Using the same donor-attenuator geometry as in the gap test, simple probe measurements are used to measure the shock velocity as a function of the distance the shock has travelled from the tetryl-Lucite interface.

3 Using the relation for shock pressure

$$P = \rho_0 uU$$

where ρ_0 is the density of the unshocked material, and the data from steps 1 and 2, we can then calculate the shock pressure as a function of distance into the gap.

The data required for step 1 are available (11), and those for step 2 have been obtained at this laboratory and will be reported in detail at a future date. Of particular interest and importance to the propellant sensitivity problem are the data from the completed calculations. These are shown in Fig. 3, in which the pressure is shown as a function of distance into the attenuator. The sensitivities of typical materials are indicated.

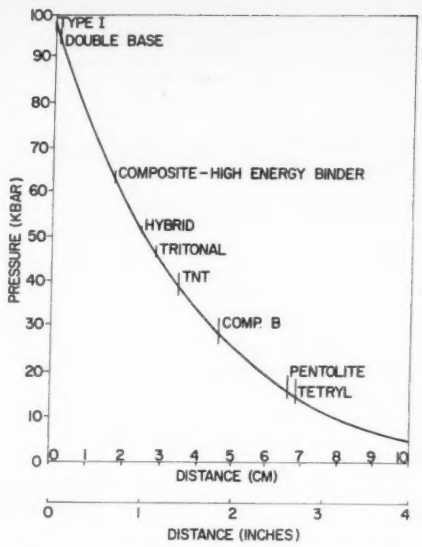

Fig. 3 Pressure vs. attenuator thickness in the shock sensitivity test

Conclusion

It is demonstrated that impact test data do not correlate with detonability measurements. Despite the inexpensive and, therefore, attractive nature of the test, impact test results should not be used as criteria for the rejection of interesting systems.

Shock sensitivity data demonstrate that propellants tend to be detonable with relative ease (approaching that for high explosives) if they contain a continuous matrix which is itself explosive. For a given class of high energy matrix, sensitivity tends to increase with energy. The search for more energetic propellants of that type will be complicated by this fact.

Propellants with high energy matrixes presently seem to have a small specific impulse advantage over those with low energy binders. Perhaps careful formulation studies with medium energy binders might partially bridge this specific impulse gap and retain the valuable insensitivity of the low energy binder types.

Defects, which are of such a nature as to permit the flow of gaseous combustion products through the matrix, significantly increase the shock sensitivity. A shock, or rapid pressure rise such as may accompany an improper ignition, can convert an otherwise satisfactory brittle propellant into an easily detonable system. The possibility must be considered in evaluating the viscoelastic behavior of interesting formulations.

References

1 Military Explosives Department of the Army Technical Manual TM 9-1910, April 1955.

2 Card Gap Test for Shock Sensitivity of Liquid Monopropellants, Test no. 1, Liquid Propellant Test Methods, recommended by the JANAF Panel on Liquid Propellant Test Methods, Liquid Propellant Information Agency, Silver Spring, Md.

3 Amster, A. B., Beauregard, R. L., Bryan, G. J. and Lawrence, E. K., "Detonability of Solid Propellants I. Test Methods and Instrumentation," NavOrd Rep. 5788, U. S. Naval Ordnance Laboratory, Silver Spring, Md., 3 February 1958.

4 Taylor, J., "Detonation in Condensed Explosives," Clarendon Press,

Oxford. England, 1952.
5 Bryan, G. J., private communication.
6 Amster, A. B., Beauregard, R. L., Harrell, B. W. and Jaffe, I., "Detonability of Propellants III. Shock Sensitivity of Solid Confined Large Diameter Charges of Polaris Propellants," NavOrd Rep. 6289, U. S. Naval Ordnance Laboratory, Silver Spring, Md., 16 March 1959. (*Confidential*)
7 Ley, W., "Rockets, Missiles, and Space Travel," The Viking Press, N. Y., 1957, revised edition, p. 169.
8 Kistiakowsky, G. B., "Initiation of Detonation of Explosives" in "Third Symposium on Combustion, Flame, and Explosions," Williams and Wilkins Co., Baltimore, 1959, p. 560.
9 Hopkinson, B., "Collected Scientific Papers," Cambridge University Press, England, 1921, p. 423.
10 Deal, W. E., "Measurement of the Reflected Shock Hugoniot and Isentrope for Explosive Reaction Products," *Phys. Fluids*, vol. 1, 1958, p. 523; *see also* Holton, W. C., "The Detonation Pressures in Explosives as Measured by Transmitted Shocks in Water," NavOrd Rep. no. 3968, U. S. Naval Ordnance Laboratory, Silver Spring, Md., 1 December 1954. (*Confidential*)
11 Coleburn, N., private communication; *also* Buchanan, J. S. et al., "Dynamic Compression of Perspex," Memo (MX) 20/59 Armaments Research and Development Establishment, England, April 1959.

Servo Control of a Variable Thrust Rocket

J. J. RODDEN[1] and R. J. POLLAK[2]

Lockheed Aircraft Corp.
Sunnyvale, Calif.

Completed tests of a variable thrust engine operated in a closed loop formed by feeding back a voltage proportional to chamber pressure to an electrohydraulically actuated injector are described. In effect, a "thrust" servomechanism was created which produces thrust proportional to a voltage input. These tests were conducted at the Naval Ordnance Test Station, China Lake, Calif. They demonstrated closed loop thrust response to a voltage command equivalent to a second-order system flat to about 6 cps. It was determined that through proper mechanical design a continuously controlled engine with full-range-throttlability could be produced with a bandpass limited only by the chemical reaction time for fuel ignition.

AN INCREASING need is apparent today for variable thrust liquid rocket engines. Requirements exist for controllable power to propel aircraft, spacecraft and missiles and for reaction controls in all of these (1).[3] Engines with shutoff and restart capability and with two levels of non-zero thrust are in operation at present. The continuously variable thrust engine is being developed by many agencies (2,3).

A variation in thrust is achievable practically by varying: Propellant flow rate, injector pressure differential, and nozzle throat area either singly or in combinations (4). When such an engine is operated in an unmanned vehicle or in an automatic system in a manned vehicle, some form of feedback signal is mandatory to indicate when the thrust is at its commanded level. This signal, compared to the command, generates the error signal characteristic of a servomechanism and may be electrical, mechanical or pressure in nature. Convenient feedback parameters (other than thrust itself) are combustion chamber pressure, fuel flow rate and the position of a moving part, such as a flow regulator or injector. Reference (5) describes a design of a servo controlled bipropellant rocket utilizing two feedbacks, chamber pressure and mixture ratio. This motor successfully demonstrated the ability to accurately maintain the pre-set commanded levels of these parameters.

Over the past two years, NOTS at China Lake, Calif., has developed a variable thrust liquid rocket engine utilizing UDMH and RFNA (5,6). It employs only one moving part, a variable area injector, and has a demonstrated capability to operate at any level from zero to rated thrust upon demand. Its basic simplicity renders it particularly applicable to storable systems.

Received June 16, 1960.
[1] Mathematical Engineer, Missiles and Space Division.
[2] Research Specialist, Missiles and Space Division.
[3] Numbers in parentheses indicate References at end of paper.

Description of Injector Operation

A simplified schematic of the variable thrust injector is shown in Fig. 1. The flow of both the fuel and oxidizer, maintained essentially at a constant ratio, is controlled within the injector assembly by the movement of a single part, a cylindrically chaped pintle. The fuel flows along the inner surface of this pintle, and the oxidizer around the outer surface. The oxidizer to fuel ratio is established by the relative diameters of the two annular passages and the angles of the conical surfaces at the orifices. The basic elements of this design are the following:

1 Hydraulic pressure input which acts against the pintle.
2 The pintle, whose movement permits the mixing of fuel and oxidizer and meters the flow rate of the mixture.
3 The spring which opposes the pintle movement.
4 The combustion chamber and nozzle.

The 100 per cent throttlable characteristic of the motor is attained by utilization of the hypergolic fuel UDMH with RFNA oxidizer which ignites on mixing. The sliding pintle regulates the variable orifice through which the fuel and oxidizer flow.

Chamber pressure is a conveniently available indication

of engine thrust and was used as the feedback in the servo. A block diagram of the servo configuration tested is shown in Fig. 2. It consists of the injector and combustion chamber, hydraulic pressure control servo valve and pressure supply, an operational d-c analog amplifier, and a pressure transducer.

The NOTS injector used in these tests has a rated fuel flow rate corresponding to 3500 lb generated thrust. For the purpose of these tests, the injector pintle travel was restricted mechanically to limit the thrust level to 400 lb, and the injector was used with a 400-lb combustion chamber.

Operating at this reduced thrust level conserved fuel and thus allowed more firings per test stand fueling. The results gained from operating at this low thrust level are applicable to larger rocket motors, since the operation of the servo feedback depends on the variation of the chamber pressure and not the generated thrust. Thrust is proportional to the product of chamber pressure, the thrust coefficient and nozzle throat area, or

$$T = C_F A_t P_C$$

The coefficient and area are dependent on the combustion chamber design. With different motor chambers different thrust can be attained even with no change in maximum chamber pressure.

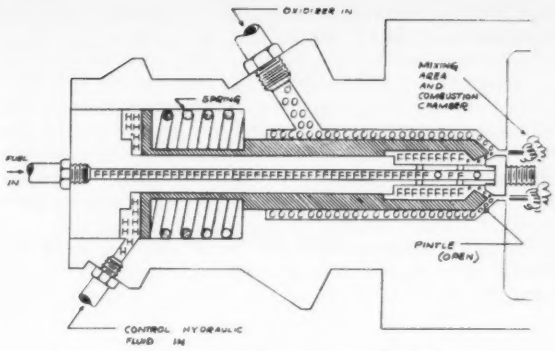

Fig. 1 Schematic of NOTS variable thrust injector

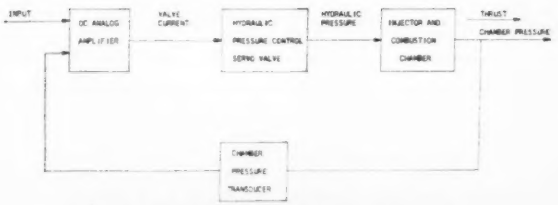

Fig. 2 Block diagram of servo configuration

Results of Injector Tests

The open loop tests consisted of determining the transfer function of chamber pressure to hydraulic control pressure inputs. The response was determined for ramp, step and sinusoidal inputs. For ramp inputs there was a high sensitivity of the chamber pressure and thrust to changes in the input current and hydraulic pressure. This open loop touchiness severely hampered testing, since a very small change in input current would swing the injector full open or closed. From these tests an approximate injector transfer function was estimated as a low frequency (about 1 cps) first-order lag. Further refinement of the injector function data was later found from the closed loop runs.

Prior to closing the loop, tests of the pressure control valve were taken to determine the hydraulic system's influence on closed loop operation. The frequency response of the valve indicated that the hydraulic pressure supply system would limit performance, since the pump had the characteristic of a 6-cps second-order system. It was unfortunate that the pressure supply limited the closed loop response, but this did not detract from the objective of the servo demonstration.

After determining estimates of the injector and hydraulic transfer functions, an amplifier gain for closing the loop was estimated for stable closed loop runs.

Comparison of closed loop response to ramp input with the open loop data showed improved sensitivity and linearity achieved with the stabilized system. The feedback also reduced burning roughness.

Response to a sinusoidal input is shown in Fig. 3. The limitation in frequency response results from the pump dynamics. The frequency response of the closed loop injector to sinusoidal inputs was taken about an operating thrust level of about 200 lb. The experimental data from those runs for amplitude response of chamber pressure, hydraulic pressure and error current are shown in Fig. 4.

These responses were combined to find the hydraulic and injector transfer functions. By curve-fitting the latter functions with templates, idealized linear transfer functions were found. The results indicated the injector to be a first-order lag with a break frequency at 1.6 cps. With these linear transfer functions, a calculated closed loop response was determined which is shown with the experimental points. It is felt that reasonable agreement was found.

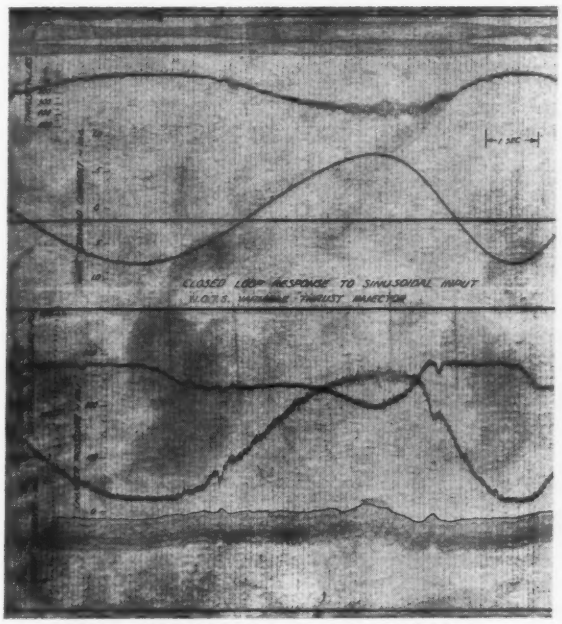

Fig. 3 Closed loop response to sinusoidal input

Analysis of Injector

A theoretical analysis was performed to obtain a mathematical representation of the injector. The validity of this model is confirmed by the experimental results. The model is to serve for greater understanding and as an aid for design. The block diagram of Fig. 5 is shown in order to correlate the experimental results with the mechanical design of the injector. The net force resulting from the hydraulic pressure, damping, spring force and chamber pressure acts to move the pintle. There are basically two kinds of damping: Stiction or coulomb and viscous. The coulomb friction adds or subtracts an offset force to the hydraulic input dependent on the direction of pintle travel. This effects a hysteresis in the closed loop operation. The force from the

chamber pressure is regenerative, since an increase in chamber pressure forces the pintle open further to increase flow rate and thus produce more thrust. The pintle spring tends to balance this chamber force. The chemical reaction time between the pintle displacement and the formation of the thrust and chamber pressure was found to be small (of the order of 50 millisec) compared to the dynamic time constants of the rest of the loop, and can be neglected here. This reaction time can be further reduced with the use of splash plates to aid fuel oxidizer mixing.

With the assumption that the ratio of pintle mass to viscous damping M/B is small, the injector transfer function can be approximated to

$$\frac{P_C}{P_H} = \frac{-A_H K_C/B}{S + (K - K_C A_C)/B}$$

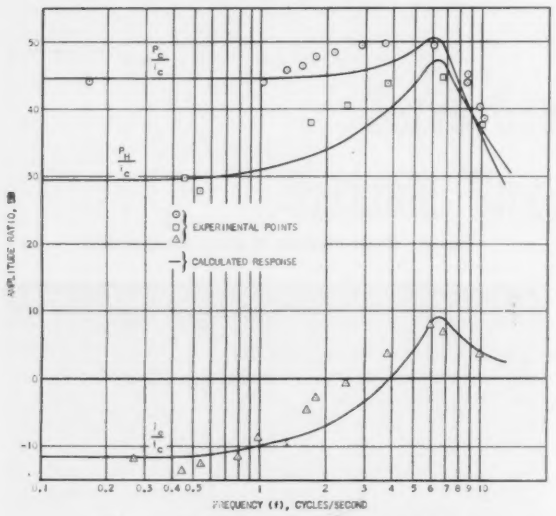

Fig. 4 Closed loop frequency response

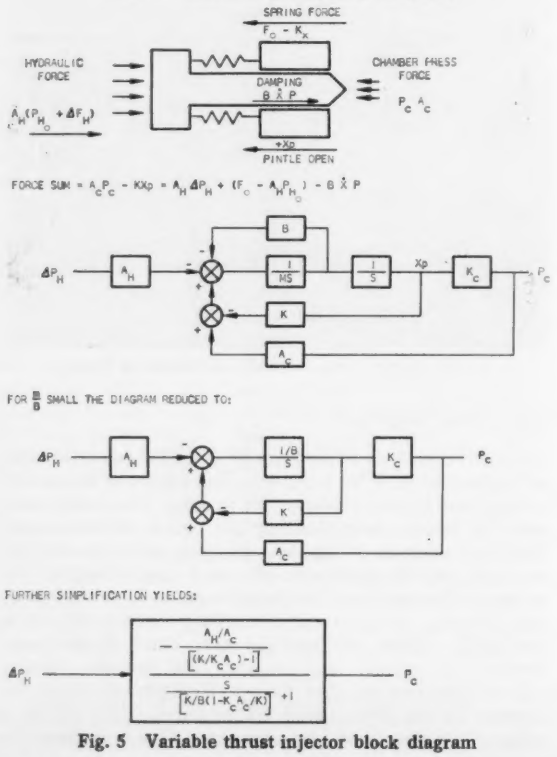

Fig. 5 Variable thrust injector block diagram

where

P_C = chamber pressure
P_H = input hydraulic pressure
A_C = effective chamber pressure
A_H = hydraulic pressure active area
K_C = slope of chamber pressure vs. pintle displacement function
B = viscous damping coefficient
K = pintle spring constant

This first-order system agrees with the form of the experimentally found transfer function.

Some of the injector parameters shown were determined readily. The measurements of the hydraulic and chamber pressure areas A_H and A_C, were taken from an assembly drawing of the injector. The effective chamber pressure area A_C acting on the pintle had to be estimated, since the fluid fuel and oxidizer have influence in modifying the effective area. The pintle spring constant K was measured experimentally on the "cold" injector.

A numerical check of the gain and break frequency of the injector frequency response cannot be made directly, since there was no measured data for damping coefficient B and the chamber pressure vs. pintle displacement slope K_C.

In an effort to estimate the injector gain K_C, the approximate chamber pressure vs. pintle position function was constructed from oxidizer and fuel flow rate data. Examination of the slope of this function showed that K_C varies over a range of 10.1 (from 17,000 to less than 1400 psi per in.). From the injector transfer function it can be seen that this nonlinearity changes the injector's first-order break frequency and gain.

An estimate of the viscous damping coefficient was found with the frequency response data. From the injector transfer function the steady-state gain and break frequency can be found. These expressions can be solved for the damping coefficient as a function of break frequency and gain

$$\text{Damping coefficient } B = \frac{K/W_B}{(A_C/A_H G + 1)}$$

Substituting the measured and estimated parameter values of:

Spring constant	K	= 11,000 lb/in.
Hydraulic pressure area	A_H	= 3.68 in.^{2}
Chamber pressure area	A_C	= 1.32 in.^{2}
Gain (from freq. resp.)	G	= 5.6 psi/psi
Break freq. (from freq. resp.)	W_B	= 1.6 cps − 10 rad/sec

into the foregoing expressions gives an approximate damping coefficient of

$$B = 366 \text{ lb-sec/ft}$$

This viscous friction force is distributed between O-rings and fuel, oxidizer and hydraulic fluid film surfaces. At 1.6 cps, the peak viscous force on the pintle is of the order of 10 to 20 lb at maximum amplitude.

The characteristic root of the injector first-order lag changes as the injector gain K_C varies. At the critical value of $K_C = K/A_C$ the injector root crosses to the unstable region. For the injector tested at NOTS the critical value was about $K_C = 8000$ psi per in. which occurred at about half full thrust. The shifting of the injector root is not readily detected in the frequency response, since the average K_C value of the thrust excursion determines the basic response. The effect of this root's presence near the origin was noted in the open loop response to a ramp input in that the chamber pressure and thrust went from 100 per cent to zero with practically no change in hydraulic pressure input showing the "integrator" effect of the injector transfer function. The presence of an unstable root was evident during open loop tests in the difficulty of trying to operate between saturated and zero thrust.

In the NOTS test a control loop was formed by connecting the output of the chamber pressure transducer to the servo amplifier which regulates the hydraulic servo valve. The dynamics of this loop is strongly influenced by pintle gain. The range of closed loop for the gains and parameters of the NOTS test if pump dynamic effects could be neglected would be from 6 to 10 cps. Unfortunately, the pressure supply pump used in these tests limited the overall response.

Design Recommendations

The foregoing analysis is useful in determining considerations for future design of servo controlled injectors. In a high performance servo the break frequency is as large as possible. Examination of the injector closed loop break frequency expression can indicate how to improve performance. The closed loop break frequency is

$$W_B = \frac{K}{B} + \frac{K_C A_H}{B}\left(K_P K_H - \frac{A_C}{A_H}\right)$$

where

K_P = amplifier gain, v/psi chamber pressure
K_H = servo gain, psi hydraulic pressure per volt

It is to be noted that this expression is valid only when the bandpass of the other elements of the closed loop, such as the hydraulics and electronics, is large compared to the overall closed loop break frequency.

The first term of the frequency of both the open and closed loop injector is the ratio of spring constant K to viscous damping coefficient B. This term can be increased by stiffening the spring and minimizing damping. The maximum spring rate is limited by the amount of force available from the control pressure source to deflect the pintle open. The damping can be reduced by limiting the sliding surface area to the pintle and minimizing O-ring seals.

To reduce the effect of chamber pressure feedback which lowers the natural frequency, the ratio of net area of the pintle exposed to the chamber pressure A_C to the net active hydraulic pressure area A_H should be made a minimum.

The feedback gain consisting of the product of the gains of the chamber pressure transducer, electronic and hydraulic systems $K_P K_H$ should be made large. The limit of these gains must be determined from considerations of the pintle gain K_C and any dynamic lags in the system for stability. Noise considerations are also influential in determining limits of the feedback gain.

Further need to eliminate O-ring seals exists to reduce hysteresis in the closed loop system which is due to stiction forces on the sliding pintle. This hysteresis effect can be partially compensated, at least at low frequency, by incorporating an integral-lead network in the servo loop.

The injector gain K_C is probably the most difficult parameter to design, since the chamber pressure vs. pintle opening will be fundamentally quite nonlinear. Attempts should be made to make the slope of the flow characteristic near-linear and the magnitude of the slope K_C as large as is feasible, while maintaining the mixing ratio and flow rates required for combustion. This consideration might be achieved by minimizing the total travel of the pintle from open to close.

The injector design discussed here requires control of the absolute value of input hydraulic pressure to provide actuation force. This generally requires the hydraulic supply system to circulate large flow rates of fluid—which involves considerable power consumption. It was this taxing of the hydraulic pump that limited the performance in these tests of the NOTS injector. A pintle design that can be actuated by a differential in hydraulic pressure would eliminate any large pump flow requirement. In addition such a design would allow elimination of the restraining spring, since the feedback loop would regulate the actuation force to position the pintle.

Commonly available high performance servo valves which produce differential pressure or flow would be readily adaptable to this alternate pintle design.

Conclusions

The feasibility of incorporating the NOTS variable injector into a servo controlled system was demonstrated. It was found that the servo control effectively linearized the injector nonlinear characteristic in addition to augmenting stability.

The analysis of the injector indicated a number of considerations applicable to design of injectors for fast response servo systems.

Since the servo controlling of an injector of the NOTS type is not dependent on the thrust produced, it appears that the thrust capability of such a servo controlled injector is limited only by the size of fuel and oxidizer flow rates that can be satisfactorily mixed for combustion.

Acknowledgment

The authors are indebted to E. Rutkowski, T. Preston and D. Klein of NOTS, China Lake, for their assistance in this project.

References

1 Reichel, R. H., "Importance and Application of Thrust Control for Liquid Propellant Rockets," ARS preprint 348-56, Nov. 1956.

2 DeBottari, L., "Chamber Pressure Control for a Liquid Rocket Engine," ARS preprint 546-57, Nov. 1957.

3 Reardon, F. H., "An Automatic Chamber Pressure and Mixture Ratio Control System for Liquid Propellant Rocket Motors," ARS preprint 571-57, Nov. 1957.

4 Meyer, M., "Throttling Thrust Chamber Control," ARS preprint 26-50, Dec. 1950.

5 Klein, D. M., "Design and Preliminary Evaluation of a Variable Thrust Rocket Motor," U. S. Naval Ordnance Test Station, China Lake, Calif., Nov. 1959 (NOTS IDP-567). (*Confidential*)

6 Rutkowski, E. V., "Variable Thrust Rocket Engines," ASTRONAUTICS vol. 4, no. 10, Oct. 1959.

Technical Notes

Effect of Different Types of Video Filters on PDM/FM Radio Telemetry[1]

A. T. BUBLITZ[2] and M. H. NICHOLS[2]

University of Michigan, Ann Arbor, Mich.

UGLOW (1)[3] has compared analytical results of PDM/FM telemetry based on two different video filter characteristics. The results compared by Uglow were taken from Feldman and Bennett's analysis (2) with a Gaussian video filter (the model used by Feldman and Bennett for PPM/FM applies equally well to PDM/FM) and from Nichols and Rauch (3) with an ideal sharp cutoff low pass filter hereafter abbreviated by ILPF. This paper corrects the method of optimization used in chapter 11 of the book by Nichols and Rauch, and extends the analysis of Feldman and Bennett.

Comparison of Filters

Both the Gaussian and the ILPF characteristics are impossible to realize. In practice, the ILPF is usually approximated by a maximally flat gain or Butterworth type of filter characteristic; the Gaussian low pass filter is most often approximated by a maximally flat phase or Thomson type of filter characteristic. See, e.g., reference list in (4). From the point of view of using such a filter at the output of the demodulator in a PDM/FM system, three characteristics of the filter performance are of interest:

1 The rate of decay of the transient in the response to a step input, which determines the amount of cross-talk between adjacent pulses.

2 The rate of rise (slope) of the response to a step input at the slicing level.

3 The equivalent noise bandwidth of the filter (using as basis of comparison an ILPF).

When a low pass filter is used at the output of an FM demodulator, the portion of the noise power spectrum intercepted by the filter will be proportional to the cube of the bandwidth of the filter; i.e., the rms video noise voltage at the output of the filter will be proportional to the three halves power of the filter bandwidth. For any low pass filter other than the ILPF, a definition of bandwidth F_c has to be chosen—such as the 3-db point of the amplitude response curve which is used in this paper. The rms output signal to noise ratio of a PDM/FM system using a particular low pass filter is proportional to the ratio of the slope of the step response of the video filter at the slicing level to the rms noise voltage at the output of the filter (which includes the second and third of the three criteria for low pass filters).

The response of an ideal vertical cutoff low pass filter has an initial overshoot of 9 per cent to a unit step input, and the oscillations die off approximately inversely proportional to time (3), a slope of 2.0 F_c at the slicing level (slicing level taken equal to half height), where F_c is the cutoff frequency and the equivalent noise bandwidth is F_c. A Gaussian filter has *no* overshoot in its response to a unit step input; it has an effective noise bandwidth of 1.34 F_c with an FM video noise spectrum, where F_c is the 3-db frequency of the Gaussian filter, and the slope of the step response is 3.0 F_c at the slicing level. The ratio of the maximum slope of the step response to the three halves power of the equivalent noise bandwidth of an ILPF (used in a PDM/FM system) is 2.0 $F_c^{-1/2}$, and for the Gaussian filter it is 1.94 $F_c^{-1/2} \cong 2.0\ F_c^{-1/2}$. As shown later in a numerical illustration, the use of the Gaussian filter in practice eliminates the problem of cross-talk in PDM/FM.

Output Signal to Noise Ratio of a PDM/FM System

The rms output signal to noise ratio S/N of a PDM/FM system when well above threshold is, approximately[4]

$$\frac{S}{N} = \frac{(\text{rms full modulation time})\ (\text{pulse slope at slicing level})}{\text{rms fluctuation noise voltage in video}} \left(\frac{F}{2f_m}\right)^{1/2} \qquad [1]$$

where

F = number of samples per channel per sec
f_m = cutoff frequency of the low pass output filter in each channel

$$\frac{\text{pulse slope at slicing level}^5}{\text{rms fluctuation noise voltage in video}} = \frac{4\sqrt{3}\,k_s S F_c f_D}{k_1 B_N^{3/2}}$$

where

S = rms value of signal in IF, in volts (referred to output)
k_s = constant defined so that the slope of the unit step response of the filter is 2 $k_s F_c$ at the slicing level
F_c = 3-db point of filter, cps
k_1 = rms fluctuation noise voltage per root unit bandwidth in IF channel (referred to output)
B_N = equivalent noise bandwidth of video filter for FM = $k_e F_c$, where k_e is a constant
f_D = peak frequency swing of FM link when fully modulated

$$\text{rms full modulation time}^6 = \frac{1}{2^{3/2}}\left(\frac{1}{nF} - \tau\right)$$

where

n = number of channels

Presented at the ARS 14th Annual Meeting, Washington, D. C., Nov. 16–20, 1959.

[1] Part of this work was carried out under Air Force Contract AF 33(616)-5796 with the Flight Control Laboratory, Wright Air Development Center.

[2] College of Engineering.

[3] Numbers in parentheses indicate References at end of paper.

[4] See, for example (3), p. 60.

[5] Slicing level assumed to occur at half steady-state pulse height.

[6] The factor $1/2^{3/2}$ appears, since this derivation assumes sinusoidal modulation; thus the rms value is $1/2^{3/2}$ of the peak-to-peak swing.

EDITOR'S NOTE: The Technical Notes and Technical Comments sections of ARS Journal are open to short manuscripts describing new developments or offering comments on papers previously published. Such manuscripts are usually published without editorial review within a few months of the date of receipt. Requirements as to style are the same as for regular contributions (see masthead page).

τ = guard time = spacing between pulses to reduce cross-talk plus minimum pulse length

The factor $(F/2f_m)^{1/2}$ in Equation [1] takes into account the frequency components of the noise lying between $F/2$ and f_m taken out by the individual channel low pass output filter which is assumed to cut off sharply at f_m.

By substitution into Equation [1], the rms individual channel output signal to noise ratio at carrier threshold $(S/N)_t$ is obtained

$$\left(\frac{S}{N}\right)_t = \sqrt{\frac{3}{2}} F_c \left(\frac{1}{nF} - \tau\right)\left(\frac{B_0}{F_c}\right)^{3/2} \frac{\delta k_7}{p} \left(\frac{F}{2f_m}\right)^{1/2} \quad [2a]$$

where

B_0 = IF channel noise bandwidth
p = constant = $B_0/2f_D$
k_7 = $k_5/k_6^{3/2}$

The constant δ is the FM carrier threshold factor given by[7]

$$S_t = \delta k_1 B_0^{1/2} \quad [2b]$$

when S_t is the rms value of the carrier at threshold.

The constant p can be estimated from the calculations of Salinger (6) on the response of an ideal vertical cutoff band pass filter to a step change in frequency. In a PDM/FM system, the carrier frequency f_0 is modulated by shifting it from $f_0 - f_D$ to $f_0 + f_D$ which, according to the results of Salinger, gives a pulse at the output of the discriminator approximately of the form $Si(\pi B_0 t)$ plus a damped ringing oscillation equal in frequency to $2f_D$. The apparent damping as well as the magnitude of this ringing is dependent on the value of the ratio $B_0/2f_D = p$, and as the value of p approaches 1.0, the magnitude of the ringing approaches a maximum and the damping approaches zero. For deviation ratios $f_D/F_c = D$ greater than 0.5, this ringing oscillation will be attenuated to an amount depending on the actual characteristics of the IF bandpass and of the video low pass filter. Curves giving the time response of the carrier frequency to a sudden shift are given in Salinger's paper and also in Appendix 13 of (3). From these curves it appears as though $p = 1.4$ would be a conservative choice. If the deviation ratio is greater than 0.5 and the action of the video low pass filter is considered, then the value of p can be allowed to approach closer to 1.0. [See (3), p. 65.]

Output Signal to Noise Ratio of a PDM/FM System With a Gaussian Video Filter

The guard time τ depends on the characteristic of the video filter and must be chosen to satisfy cross-talk criteria and the minimum allowable pulse height. The minimum allowable pulse height determines the minimum pulse length, and the minimum pulse gap between the end of a fully modulated pulse and the beginning of the next pulse. Since the step response of a Gaussian filter has no overshoot, it turns out that τ is controlled by the minimum pulse height requirement. Fig. 1 illustrates schematically the pulse height effect for a particular spacing with a Gaussian filter where $\tau = \tau_1 + \tau_2$. If $\tau_1 = \tau_2$, then $h_1 \cong h_2$. The values of h_1 and h_2 determine the leeway for noise discrimination at minimum modulation and full modulation, respectively. For, if the instantaneous video noise voltage exceeds h_2, the pulse plus noise will exceed the slicing level for the long pulse, and if the instantaneous video noise voltage is less than $-h_1$, the short pulse plus noise will not reach the slicing level. Thus h_2 and h_1 determine the video threshold for minimum and maximum modulation.[8] Also, Fig. 1 shows that the slopes at the slicing levels are reduced, which increases the output noise at full and minimum modulation when above threshold.[9] These considerations determine the minimum permissible values of τ_1 and τ_2. The quantities τ_1 and τ_2 so determined can be written as

$$\tau_1 = \frac{k_3}{F_c} \qquad \tau_2 = \frac{k_4}{F_c}$$

where k_3 and k_4 are constants. Equation [2a] then becomes for this case

$$\left(\frac{S}{N}\right)_t = k_7 \sqrt{\frac{3}{2}} \left(\frac{F_c}{nF} - k_3 - k_4\right)\left(\frac{B_0}{F_c}\right)^{3/2} \frac{\delta}{p} \left(\frac{F}{2f_m}\right)^{1/2} \quad [3]$$

Following the procedure of Feldman and Bennett (2), $(S/N)_t$ can be maximized by varying F_c, holding the other variables constant, i.e., for constant IF bandwidth B_0 and constant nF. This gives

$$F_c/nF = 3(k_3 + k_4) \quad [4]$$

Substitution of Equation [4] into Equation [3] gives

$$\left(\frac{S}{N}\right)_{t\,\max} = k_7 \left(\frac{2nF}{3F_c}\right)^{1/2} \left(\frac{B_0}{nF}\right)^{3/2} \frac{\delta}{p} \left(\frac{F}{2f_m}\right)^{1/2} \quad [5]$$

The required IF bandwidth B_0 to give $(S/N)_{t\,\max}$ at carrier threshold is obtained from Equation [5]

$$\frac{B_0}{nF} = \left[\frac{1.22}{k_7}\left(\frac{p}{\delta}\right)\left(\frac{2f_m}{F}\right)^{1/2}\left(\frac{F_c}{nF}\right)^{1/2}\left(\frac{S}{N}\right)_{t\,\max}\right]^{2/3} \quad [6a]$$

For purposes of illustration, we will assume that $\tau_1 = \tau_2$, which makes $h_1 = h_2$, and that the threshold requirement is that $h_1 = h_2 = h/4$. The total guard time is $\tau = \tau_1 + \tau_2$. Writing the transfer function of the Gaussian filter as $\exp(-c^2f^2/F_c^2)$, where F_c is the frequency for 3-db attenuation and $c^2 = 0.35$, the guard time τ for this case is computed by use of error function tables to be $0.61/F_c$ sec. From Equation [4], $F_c/nF = 1.8$, and from the discussion of the comparison of filters, $k_7 \cong 1.0$, so Equation [5] becomes

$$\left(\frac{S}{N}\right)_{t\,\max} = 0.6 \left(\frac{B_0}{nF}\right)^{3/2} \frac{\delta}{p} \left(\frac{F}{2f_m}\right)^{1/2} \quad [6b]$$

It is now necessary to check to see that cross-talk is at a tolerable level under the modulation condition illustrated in Fig. 1. This is done by dividing the value of the "tailoff" of the long pulse at the time the trailing edge of the short pulse crossed the slicing level by the slope of the short pulse at that time.

[7] This assumes for purposes of analysis that a well-defined threshold exists for all deviation ratios. Some idea of the validity of this assumption can be obtained by reference to the results published by Stumpers (5).

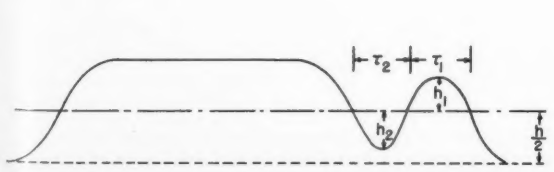

Fig. 1 Schematic showing reduction of pulse height

[8] Assuming that the leading edges of the pulses are fixed, the modulation sensitivity near full modulation will decrease because of the presence of the leading edge of the next pulse. This effect can be calibrated out.

[9] It is conceivable that in some cases the reduction of the slope at the slicing level is of more concern than the reduction of the pulse height, so that a minimum allowable slope becomes the criterion for minimum allowable pulse width. The general procedure is the same in either case.

To obtain the cross-talk relative to full modulation, we divide by the full modulation time, that is, by $(1/nF - \tau)$. For this illustration, the relative cross-talk is approximately 0.4×10^{-6}, which is certainly adequate! It is also necessary to check to see that the video threshold is satisfied when the carrier is above threshold, i.e., for Equation [6b] to be valid, $S_t > S_v$, where S_t is the rms value of the carrier required for carrier threshold and S_v is the rms value of the carrier required for video threshold. Using the principles for video threshold from (3), p. 66, and the expression for carrier threshold from Equation [2b] and substituting for B_0 from Equation [6a] and F_c from Equation [4], using the relation $2pf_D = B_0$, the ratio of the two threshold values of S becomes

$$\frac{S_v}{S_t} = \frac{11.3k_5(k_3 + k_4)}{(2f_m/F)^{1/2}(S/N)_{t\ \max}}$$

Using this numerical illustration, $k_5 = 1.5$ and $k_3 + k_4 = 0.61$; also $(2f_m/F)^{1/2}$ is the order of unity, and we choose $(S/N)_{t\ \max} = 100$. With these values

$$\frac{S_v}{S_t} \cong \frac{1}{10}$$

Thus for reasonable values of the variables, the video threshold is satisfied for a lower signal strength than the carrier threshold and the results are valid.

Output Signal to Noise Ratio of a PDM/FM System With an ILPF

In the case of the Gaussian filter, the consideration of minimum allowable pulse height determines the guard time τ required. Since the envelope of the step function response of an ILPF dies off approximately inversely with the time, it turns out that cross-talk reduction rather than minimum pulse height determines the guard time τ required. Following the procedure in (3), p. 245, the maximum relative cross-talk γ is given by

$$\gamma = 0.023\ nF/F_c^2\tau(1 - nF\tau) \qquad [7]$$

Solving for τ and choosing the root which gives $\tau \to 0$ as $F_c \to \infty$

$$\tau = \frac{1}{2nF} - \left[\left(\frac{1}{2nF}\right)^2 - \frac{0.023}{\gamma F_c}\right]^{1/2} \qquad [8]$$

Following the same procedure as in the previous section, this value of τ is substituted into Equation [2a] and $(S/N)_t$ maximized against F_c, holding nF and B_0 constant, giving

$$\frac{F_c}{nF} = 2\sqrt{\frac{0.041}{\gamma}} \qquad \tau = \frac{1}{6nF} \qquad [9]$$

This is the same result as obtained in (3), p. 105.

Substitution of these values and $k_7 = 1$ into Equation [2a] gives

$$\left(\frac{S}{N}\right)_{t\ \max} = 1.6\ \gamma^{1/4}\left(\frac{B_0}{nF}\right)^{3/2}\frac{\delta}{p}\left(\frac{F}{2f_m}\right)^{1/2} \qquad [10]$$

Thus if 60-db cross-talk suppression (relative to full modulation)[10] is required under the modulation conditions of Fig. 1, the factor $1.6\gamma^{1/4}$ becomes 0.3, which may be compared with 0.6 in Equation [6b]. The required IF bandwidth B_0 to give $(S/N)_{t\ \max}$ at carrier threshold is obtained from Equation [10]

$$\frac{B_0}{nF} = \frac{0.73}{\gamma^{1/6}}\left(\frac{2f_m}{F}\right)^{1/3}\left[\frac{p}{\delta}\left(\frac{S}{N}\right)_{t\ \max}\right]^{2/3} \qquad [11]$$

It is necessary to check to see that the video threshold is satisfied when the carrier is above threshold. Using the same procedure as with the Gaussian filter, one obtains

$$\frac{S_v}{S_t} = \frac{1.9}{\gamma^{1/2}\left(\frac{S}{N}\right)_{t\ \max}\left(\frac{2f_m}{F}\right)^{1/2}} \qquad [12]$$

Using $\gamma = 10^{-3}$, $(S/N)_{t\ \max} = 100$ and $(2f_m/F)^{1/2} \sim 1$, this relation gives

$$S_v/S_t = 0.6$$

This shows that for these values, the video threshold is satisfied. Equation [10] is valid only for values of $(S/N)_{t\ \max} > 60$ if $\gamma = 10^{-3}$, etc. For values such that $S_t < S_v$, the value of S/k_1 obtained from the video threshold expression must be used instead of Equation [2b] and the optimization carried forward.

Conclusion

Based on the special numerical examples, the output signal to noise ratio for the Gaussian type of video filter is approximately twice that for the ILPF. Also, in practice, it is possible to approximate very closely the Gaussian or maximally flat phase behavior (4). For example, a tenth-order low pass Bessel filter has a step function response very close to that of a Gaussian filter with only 0.12 per cent overshoot. A tenth-order Butterworth filter has nearly 20 per cent overshoot, or twice the overshoot of the step function response of an ILPF.

References

1 Uglow, K. M., "Noise and Bandwidth in PDM/FM Radio Telemetering," IRE Trans. on Telemetry and Remote Control, vol. TRC-3, Paper no. 7.5, April 1957, 10 pp.

2 Feldman, C. B. and Bennett, W. R., "Bandwidth and Transmission Performance," *Bell Sys. Tech. J.*, vol. 28, July 1949, pp. 490–498.

3 Nichols, M. H. and Rauch, L. L., "Radio Telemetry," John Wiley and Sons, Inc., N. Y., 1956, 2nd ed.

4 Henderson, K. W. and Kautz, W. H., "Transient Responses of Conventional Filters," IRE Trans. on Circuit Theory, vol. CT-5, Dec. 1958, pp. 333–347.

5 Stumpers, F. L. H. M., "Theory of Frequency-Modulation Noise," Proc. IRE, vol. 36, Sept. 1948, pp. 1081–1092.

6 Salinger, H., "Transients in Frequency Modulation," Proc. IRE, vol. 30, Aug. 1942, pp. 378–383.

[10] It might be argued that 60 db is overly stringent, since cross-talk of this sort occurs only when one channel is near full modulation and the following channel is near minimum modulation. Questions of this sort can be settled only by detailed analysis of a particular measurement program.

Gyro Time Constants

ALLEN LANGE[1]

Bendix Corp., Systems Div., Ann Arbor, Mich.

IN (1),[2] page 89, a discrepancy between the computed and measured values of an integrating rate gyro time constant is noted. It is suggested in (1) that the elastic compliance of the gimbal creates a time delay which may contribute to this observed discrepancy. The purpose of this note is to suggest an additional reason for this discrepancy, namely, the use of a familiar approximation for the angular momentum of the gyro rotor. Two expressions for the gyro transfer function are developed, one using the familiar approximation for the angular momentum and one using a more exact relation. It is shown that the gyro time constants associated with these two transfer functions are different, and an attempt is made to estimate the numerical difference in the two time constants.

Angular Momentum of the Gyro Rotor[3]

Let a gyro rotor be contained in a single gimbal which is mounted on a platform rotating with respect to a Newtonian frame. The application of Newton's second law to the spinning rotor may be expressed in vector form as follows

$$\bar{M}_r = D_i(J_r\bar{W}_{ir}) \qquad [1a]$$

where

$\bar{M}_r$ = moment applied to the gyro rotor
$D_i(\ )$ = vector operator indicating the time rate of change of the vector with respect to a Newtonian frame
J_r = inertia tensor of the gyro rotor = $\begin{vmatrix} J & 0 & 0 \\ 0 & J & 0 \\ 0 & 0 & J_{SP} \end{vmatrix}$
$\bar{W}_{ir}$ = angular velocity of the gyro rotor with respect to the Newtonian frame

Equation [1a] may be written as

$$\bar{M} = D_i(\bar{H}_r) \qquad [2a]$$

where $\bar{H}_r = J_r\bar{W}_{ir}$ is the angular momentum vector of the gyro rotor.

J_r is invariant only with respect to a set of coordinates rotating with the rotor. Consequently, Equations [1a] or [2a] may be expressed as

$$\bar{M}_r = D_r(J_r\bar{W}_{ir}) + \bar{W}_{ir} \times (J_r\bar{W}_{ir}) \qquad [1b]$$

$$\bar{M}_r = D_r(\bar{H}_r) + \bar{W}_{ir} \times \bar{H}_r \qquad [2b]$$

$D_r(\ )$ is a vector operator indicating the time rate of change of the vector with respect to the rotor coordinates r. Now, $\bar{H}_r$ may be expressed as follows, in terms of components in a coordinate set g attached to the gimbal on which the gyro rotor is mounted

$$\bar{H}_r{}^g = H_{SP}\begin{vmatrix} \frac{J}{J_{SP}}\left(\frac{W_1 + DG}{\omega}\right) \\ \frac{J}{J_{SP}}\left(\frac{W_2}{\omega}\right) \\ 1 + \frac{W_3}{\omega} \end{vmatrix} \qquad [3a]$$

where

H_{SP} = $J_{SP}\omega$
ω = rotational speed of the gyro rotor with respect to the gimbal
DG = rotational speed of the gimbal with respect to the platform on which it is mounted
W_1, W_2, W_3 = x, y and z components, respectively, of the rotational speed of the platform with respect to the Newtonian frame i, in gimbal coordinates

The superscript g indicates that the vectors are to be expressed in terms of their components in gimbal coordinates. Similarly, the superscripts r and p will be used to indicate rotor and platform coordinates, respectively.

In a practical gyro, ω is a large number, so that

$$W_3/\omega \ll 1 \qquad J/H_{SP} \to 0$$

Then Equation [3a] may be written as

$$\bar{H}_r{}^g \approx H_{SP}\begin{vmatrix} 0 \\ 0 \\ 1 \end{vmatrix} \qquad [3b]$$

Consequently, it is common practice to consider that the term $D_r(\bar{H}_r)$ in Equation [2b] is zero. The assumptions leading to the approximate Equation [3b] are physically reasonable; however, it is demonstrated in the following that the use of Equation [3b] leads to an expression for the gyro reaction torque different from that resulting from the use of Equation [3a]. The two expressions resulting from the use of Equations [3a and 3b] are developed and compared in the following section.

Gyro Rotor Kinetics

Combining Equations [2b and 3b] leads to the following result

$$\bar{M}_r{}^g = \begin{vmatrix} M_1 \\ M_2 \\ M_3 \end{vmatrix} = H_{SP}\left(\begin{vmatrix} W_1 + DG \\ W_2 \\ W_3 + \omega \end{vmatrix} \times \begin{vmatrix} 0 \\ 0 \\ 1 \end{vmatrix}\right) = H_{SP}\begin{vmatrix} W_2 \\ -(W_1 + DG) \\ 0 \end{vmatrix} \qquad [4]$$

The first component of Equation [1b] may be expanded as follows

$$D_r(J_r\bar{W}_{ir}{}^g) = J_rD_i(\bar{W}_{ir}{}^g)$$

But

$$D_r\,\bar{W}_{ir}{}^g = D_i\,\bar{W}_{ir}{}^g + \bar{W}_{ri}{}^g \times \bar{W}_{ir}{}^g = D_i\,\bar{W}_{ir}{}^g$$

Now, $\bar{W}_{ir}$ may be written as the vector sum $\bar{W}_{ir} = \bar{W}_{ip} + \bar{W}_{pg} + \bar{W}_{gr}$ so that

$$D_i\bar{W}_{ir}{}^g = D_i(T_{gp}\bar{W}_{ip}{}^p) + D_g(\bar{W}_{pr}{}^g) + \bar{W}_{ig}{}^g \times \bar{W}_{pr}{}^g \qquad [5]$$

where T_{gp} is a scalar operator transforming $\bar{W}_{ip}{}^p$ into $\bar{W}_{ip}{}^g$. For purposes of the present analysis, let the gyro output axis be aligned with the x axis of the platform. Then

$$T_{gp} = \begin{vmatrix} 1 & 0 & 0 \\ 0 & \cos G & \sin G \\ 0 & -\sin G & \cos G \end{vmatrix}$$

and the first term on the right-hand side of Equation [5] becomes

$$D_i(T_{gp}\bar{W}_{ip}{}^p) = D(T_{gp})\bar{W}_{ip}{}^p + T_{gp}D_i(\bar{W}_{ip}{}^p) = \begin{vmatrix} A_1 \\ A_2 + DG\,W_3 \\ A_3 - DG\,W_2 \end{vmatrix} \qquad [6]$$

Received April 6, 1960.

[1] Supervisory Engineer.

[2] Numbers in parentheses indicate References at end of paper.

[3] The relations presented in this and the following sections have been abstracted from a more detailed treatment given in (2).

where A_1, A_2 and A_3 represent the x, y and z components, respectively, of the rotational acceleration of the platform with respect to the Newtonian frame i as expressed in gimbal coordinates.

The second and third terms on the right-hand side of Equation [5] may be expressed as

$$D_g(\bar{W}_{gr}{}^g) + \bar{W}_{ig}{}^g \times \bar{W}_{gr}{}^g = \begin{vmatrix} D^2G + W_2\omega \\ W_3DG - (W_1 + DG)\omega \\ -W_2DG \end{vmatrix} \quad [7]$$

Note that the synchronous motor driving the gyro rotor has the characteristic that $D\omega = 0$. Then the first component of Equation [1b] can be written by combining Equations [6 and 7] to give

$$D_r(J_r\,\bar{W}_{ir}{}^g) = \begin{vmatrix} J(A_1 + D^2G + W_2\omega) \\ J(A_2 + 2DG\,W_3 - [W_1 + DG]\,\omega) \\ J_{SP}(A_3 - 2\,DG\,W_2) \end{vmatrix} \quad [8]$$

The second component of Equation [1b] may be written

$$\bar{W}_{ir}{}^g \times (J_r\,\bar{W}_{ir}{}^g) = \begin{vmatrix} (J_{SP} - J)(W_3 + \omega)W_2 \\ -(J_{SP} - J)(W_1 + DG)(W_3 + \omega) \\ 0 \end{vmatrix} \quad [9]$$

so that, combining Equations [8 and 9], the exact expression for $D_r(\bar{H}_r{}^g)$ is given by

$$\begin{vmatrix} M_x \\ M_y \\ M_z \end{vmatrix} = \begin{vmatrix} J(A_1 + D^2G) + H_{SP}\,W_2 + (J_{SP} - J)W_2W_3 \\ J(A_2 + 2DG\,W_3) + (J - J_{SP})W_3(W_1 + DG) + H_{SP}(W_1 + DG) \\ J_{SP}(A_3 - 2DG\,W_2) \end{vmatrix} \quad [10]$$

We are concerned here with only the x component of Equations [4 and 10]. Denoting M_x from Equation [4] by M_a (approximate), and M_x from Equation [10] by M_e (exact), we have

$$M_e = J(A_1 + D^2G) + H_{SP}W_2 + (J_{SP} - J)W_2W_3 \quad [11]$$

$$M_a = H_{SP}W_2 \quad [12]$$

Equations [11 and 12] represent the effect of a torque about the gimbal axis on a spinning rotor treated as a free body. It follows that the reactive torque on the gimbal about its x axis due to the spinning rotor is given by $-M_e$ or $-M_a$. In the following section, the gimbal is treated as a free body, and its motion as the result of the net applied torque is computed.

Gyro Gimbal Kinetics

Newton's second law applied to the gyro gimbal may be expressed as

$$\bar{M}_g{}^g = \begin{vmatrix} M_{xg} \\ M_{yg} \\ M_{zg} \end{vmatrix} = D_i(J_g\bar{W}_{ig}{}^g) \quad [13]$$

where J_g is the inertial tensor of the gimbal, which may have the form

$$J_g = \begin{vmatrix} J_x & 0 & 0 \\ 0 & J_y & 0 \\ 0 & 0 & J_z \end{vmatrix}$$

We are interested here only in the x component; M_{xg} is given by

$$M_{xg} = M_c - C\,DG + M_r \quad [14]$$

where

M_c = applied control torque
$C\,DG$ = damping torque due to the product of C the damping factor and the relative angular velocity between the platform and the gimbal DG
M_r = gyroscopic reaction torque, where $M_r = -M_a$ or $-M_e$, corresponding to the use of the exact expression (Eq. [11]) or the approximate expression (Eq. [12]) for the gyro reaction torque

The right-hand side of Equation [13] can be examined in the same fashion as the right-hand side of Equation [1]. Performing this expansion, and equating the x component to Equation [14] gives

$$M_c - CDG + M_r = J_x(A_1 + D^2G) + (J_z - J_y)W_2W_3 \quad [15]$$

Rearranging, and denoting the terms resulting from the use of Equation [11] by the subscript e, and those resulting from the use of Equation [12] by the subscript a, we have

$$(DT_a + 1)\,G = \frac{1}{D}\left[\frac{M_c - H_{SP}W_2}{C} + \left(T_aA_1 + \frac{J_y - J_z}{C}\,W_2W_3\right)\right] \quad [16]$$

$$(DT_e + 1)G = \frac{1}{D}\left[\frac{M_c - H_{SP}W_2}{C} + \left(T_eA_1 + \frac{(J_y - J_z)(J_{SP} - J)}{C}\,W_2W_3\right)\right] \quad [17]$$

where

$$T_a = J_z/C$$

$$T_e = (J_z + J)/C$$

Equation [16] is identical to Equation [10] of Derivation Summary 2 of (1) with the following exceptions:

1 Equation [16] does not contain a torque due to uncertainty.

2 Equation [16] contains the term $[(J_y - J_z)/C]W_2W_3$, due to inertial coupling of the gimbal, which disappears if $J_y = J_z$, and in any case may be quite small if $J_y \approx J_z$ and the product W_2W_3 is small.

However Equation [17] differs from Equation [16], and hence from the equivalent expression developed in (1), by the inclusion of the inertia of the gyro rotor about an axis normal to the spin axis with the gimbal inertia. Therefore, the "exact" gyro time constant T_e is given by $(J_z + J)/C$, whereas the "approximate" gyro time constant T_a is given by J_z/C. (As before, the notation "exact" refers to the use of Eq. [11] for expressing gyro reaction torque, and the notation "approximate" refers to the use of Eq. [12].) On page 89 of (1), the observation is made that the *measured* gyro time constant is greater than the computed gyro time constant, which, presumably, is computed from an expression similar to Equation [16]. Since T_e is greater than T_a, it is pertinent to examine the possibility that the measured time constant exceeds the computed time constant, because the computed time constant is based on the reasonable approximation $D_r(\bar{H}_r) = 0$. A quantitative evaluation of this hypothesis, based on some simplifying assumptions, is given in the following section.

Rotor and Gimbal Inertias

The ratio of the exact to the approximate gyro time constant may be written as

$$\frac{T_e}{T_a} = 1 + \frac{J}{J_z} \quad [18]$$

From (1), we know that the ratio of T_m the measured time constant to T_c the computed value is greater than 1 or

$$T_m/T_c = 1 + \Delta \quad [19]$$

Using the values given on page 89 of (1)

$$T_m = 0.0027 \text{ sec} \qquad T_c = 0.0017 \text{ sec} \qquad \Delta = 0.59$$

The hypothesis is that T_m the measured time constant is to be associated with T_e the exact time constant, and T_c the computed time constant is to be associated with T_a the approximate time constant. Then $\Delta \sim J/J_z$, and we seek a numerical value for J/J_z. The ratio J/J_z may be written as

$$\frac{J}{J_z} = \left(\frac{J}{J_{SP}}\right)\left(\frac{J_{SP}}{J_z}\right)$$

Since J/J_z represents a degradation of the dynamic performance of the gyro (because it increases the gyro time constant), it is desirable to keep J/J_z small. Also, since a large J_{SP} corresponds to a highly sensitive gyro, and a small J_z corresponds to a gyro with good dynamic performance, J_{SP}/J_z should be large. Therefore J/J_{SP} should be as small as possible.

For a solid homogeneous spherical rotor, J/J_{SP} is equal to 1. For a solid homogeneous cylindrical rotor

$$\frac{J}{J_{SP}} = \frac{1}{6}(3 + n^2)$$

where $n = h/r$, the ratio of the height of the cylinder to its radius. In the case of a hollow cylindrical rotor

$$\frac{J}{J_{SP}} = \frac{1}{6}\left(3 + \frac{n^2}{1 + m^2}\right)$$

where m is the ratio of the inner to the outer radius, with $0 < m < 1$.

For $n = 1, m = 0, J/J_{SP} = 0.67$. Therefore, it seems reasonable to assume that $J/J_{SP} \leq 1.0$. From the table on page 76 of (1)

$$\frac{J_{SP}}{J_z} = \frac{11.97}{37.6} = 0.317$$

so that

$$J/J_z \leq 0.317$$

and it can be concluded, therefore, that the use of the approximation given by Equation [3b] accounts for only half, at most, of the observed discrepancy Δ between the measured and computed gyro time constant, the remainder, presumably, due to the elastic effects suggested in (1).

References

1 Draper, C. S., Wrigley, W. and Grohe, L. R., "The Floating Integration Gyro and Its Application to Geometrical Stabilization Problems on Moving Basis," IAS Preprint no. 503, Jan. 1955.

2 Lange, A., "Automatic Control of Three-Dimensional Vector Quantities, Part 3," IRE Trans. on Automatic Control, vol. AC-5, no. 2, June 1960, pp. 106–117.

Satellite Librations

C. F. BERNINGER[1]

Aveo Research and Advanced Development Div., Wilmington, Mass.

THE PREVIOUSLY published work on satellite librations assumes the mass center of the satellite to be traveling on a Keplerian orbit. The "librations" or oscillations of the vehicle about its center of mass are due to differences in the gravitational and centrifugal forces acting on the various mass elements of the satellite—the centrifugal force terms determined from the specified Keplerian orbit. Coupling between the orbital and libration motions, which appears obvious from considerations of conservation of momentum or energy, may be illustrated by writing the equations of motion in general form.

For simplicity, the equations of motion are written for a dumbbell-shaped satellite consisting of two point masses connected by a weightless rigid rod of length $2l$. The radius between the center of mass of the dumbbell system and center of Earth is denoted as ρ (Fig. 1). The radii from the center of Earth to each mass are r_1 and r_2. The angular position to the center of mass of the satellite is given by θ measured from a fixed reference line $0A$ and the angular attitude of the satellite is specified by ϕ.

By employing Lagrange's equations with ρ, θ and ϕ as the generalized coordinates one obtains

$$2m\ddot{\rho} - 2m\rho\dot{\theta}^2 = R$$

$$\frac{d}{dt}(2m\rho^2\dot{\theta}) = \Theta$$

$$\frac{d}{dt}(2ml^2\dot{\phi}) = \Phi \qquad \ldots\ldots [1]$$

where R, Θ and Φ are the generalized forces.

The gravitational forces acting on the masses are designated as G_1 and G_2 and are given by

$$G_1 = -\frac{\mu m}{r_1^2} = -\frac{\mu m}{\rho^2(1 + \delta^2 + 2\delta\cos\Omega)}$$

$$G_2 = -\frac{\mu m}{r_2^2} = -\frac{\mu m}{\rho^2(1 + \delta^2 - 2\delta\cos\Omega)} \qquad \ldots\ldots [2]$$

where

$\delta = l/\rho$

$\Omega = \phi - \theta$

$\mu =$ positive gravitational constant

The gravitational force system G_1 and G_2 may be resolved into components acting at the center of mass of the satellite consisting of a radial force R, a force T perpendicular to R, and a torque Φ acting about the mass center.

The sum of the radial components of G_1 and G_2 parallel to ρ is given by

$$R = -\mu m\left\{\frac{\cos\left[\sin^{-1}(l\sin\Omega/r_1)\right]}{r_1^2} + \frac{\cos\left[\sin^{-1}(l\sin\Omega/r_2)\right]}{r_2^2}\right\} \qquad [3]$$

The torque Φ is readily determined by resolving G_1 and G_2 into components parallel and perpendicular to the longitudinal axis of the dumbbell (Fig. 2). The perpendicular components are

$$F_1 = G_1\cos\lambda_1$$

$$F_2 = G_2\cos\lambda_2$$

and, from trigonometric relationships

$$\cos\lambda_1 = \rho\sin\Omega/r_1$$

$$\cos\lambda_2 = \rho\sin\Omega/r_2$$

Received March 28, 1960.

[1] Project Manager.

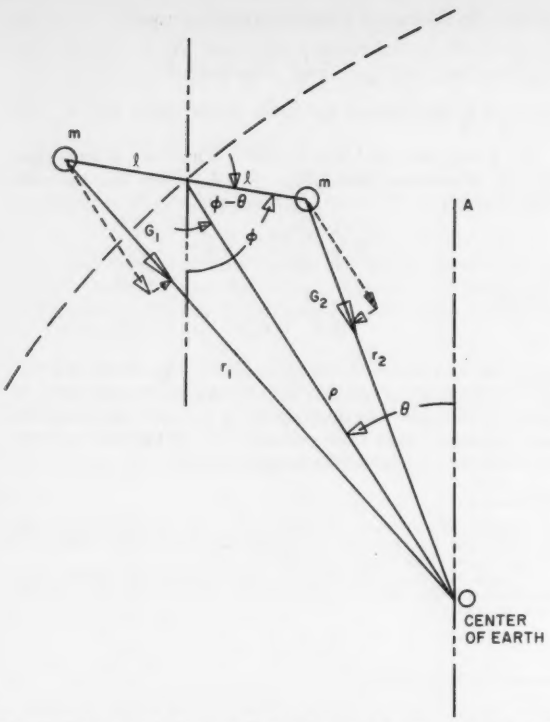

Fig. 1 Force resolution parallel and perpendicular to radius of satellite center of mass

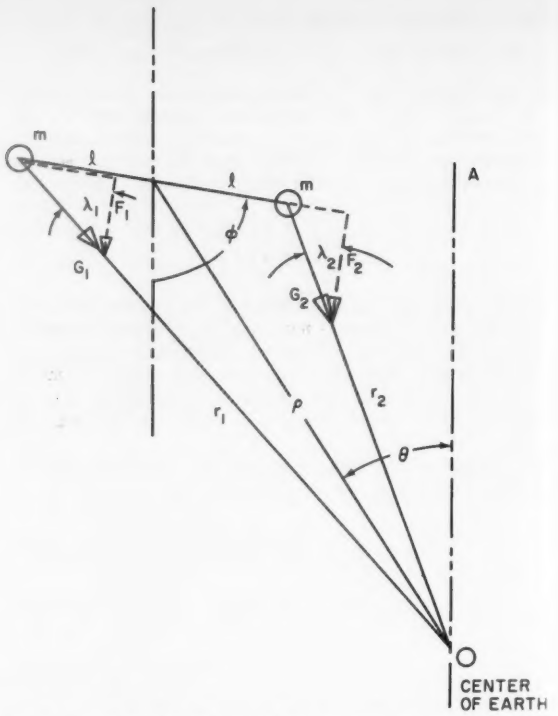

Fig. 2 Force resolution parallel and perpendicular to dumbbell axis

The torque about the dumbbell center of mass is then given by

$$\Phi = \mu m \rho l \sin \Omega \left(\frac{1}{r_1^3} - \frac{1}{r_2^3}\right) \qquad [4]$$

The generalized force Θ corresponds to the torque about the center of Earth. Since G_1 and G_2 pass through 0

$$\Theta = 0 \qquad [5]$$

Substitution of Equations [3, 4 and 5] into Equations [1] yields

$$\ddot{\rho} - \rho\dot{\theta}^2 = -\mu m \left\{\frac{\cos\left[\sin^{-1}(l \sin \Omega/r_1)\right]}{r_1^2} + \frac{\cos\left[\sin^{-1}(l \sin \Omega/r_2)\right]}{r_2^2}\right\} \qquad [6]$$

$$(d/dt)(\rho^2\dot{\theta}) = 0 \qquad [7]$$

$$\frac{d}{dt}(2ml^2\dot{\phi}) = \mu m l \rho \sin \Omega \left(\frac{1}{r_1^3} - \frac{1}{r_2^3}\right) \qquad [8]$$

Expansion of the trigonometric expressions of Equation [6] and expansion of the sums and differences of the reciprocal powers of r_1 and r_2 permit Equations [6 and 8] to be written as

$$\ddot{\rho} - \rho\dot{\theta}^2 = -(\mu/2\rho^2)[2 + \delta^2(-2 + 8\cos^2\Omega - 2\sin^2\Omega)] \qquad [9]$$

$$\frac{d}{dt}(2\,ml^2\dot{\phi}) = \frac{6\delta^2\,\mu\,ml \sin\Omega\cos\Omega}{\rho} \qquad [10]$$

wherein powers of δ greater than 2 are discarded.

Differentiation of the left side of Equation [10] enables one to rewrite the equation

$$\rho\ddot{\phi} = 3\mu\delta \sin\Omega\cos\Omega/\rho^2 \qquad [11]$$

In this form a comparison of Equations [11 and 9] reveals that the left sides of both equations are "of the order ρ." The right side of Equation [11] is proportional to δ, whereas the non-Keplerian term in Equation [9] is proportional to δ^2. Since δ is, for reasonable Earth satellites, very small compared to unity, a reasonable approximation is given by neglecting the δ^2 terms. Equations [9 and 7] then become Kepler's equations of motion. Equation [10] is an auxiliary equation giving the librations and is equivalent to the equation used in (1, 2 and 3).[2] It should be noted, however, that (4), in effect, uses Equation [8] for the investigation of the librations. The increased accuracy afforded by the use of this equation is questionable, since it includes terms comparable in magnitude to those neglected by the approximation of Equations [6 and 7].

References

1 Klemperer, W. B. and Baker, R. M., Jr., "Satellite Librations," *Astronautica Acta*, vol. III, 1957.

2 Klemperer, W. B., "Satellite Librations of Large Amplitude," ARS JOURNAL, vol. 30, no. 1, Jan. 1960, pp. 123–124.

3 Baker, R. M., Jr., "Librations on a Slightly Eccentric Orbit," ARS JOURNAL, vol. 30, no. 1, Jan. 1960, pp. 124–126.

4 Schindler, G. M., "On Satellite Librations," ARS JOURNAL, vol. 29, no. 5, May 1959, pp. 368–371.

[2] Numbers in parentheses indicate References at end of paper.

Dynamic Stabilization of a Small Body Between Two Equal Rotating Masses[1]

HOWARD D. GREYBER[2]

Aerosciences Laboratory, General Electric Co., Philadelphia, Pa.

AN INTERESTING and simple illustration of the systems concept of dynamic stabilization is the stability of a small body lying on the line of centers and equidistant from two equal rotating masses which interact by gravitation but are held at some arbitrary distance by a weightless bar. Elsewhere, we have applied the dynamic stabilization concept to problems of hydrodynamic and hydromagnetic instabilities (1).[3] Other applications of dynamic stabilization are the upside down pendulum with an oscillating support and strong focusing in charged particle accelerators.

Let us consider uniformly rotating frames of reference, $\sum$ and $\sum'$, the origins of which coincide. The acceleration in unprimed system is related to that in the primed rotating system by (2)

$$\frac{d^2\mathbf{r}}{dt^2} = \frac{d^2{}'\mathbf{r}}{dt^2} + 2\boldsymbol{\omega} \times \frac{d'\mathbf{r}}{dt} + \boldsymbol{\omega} \times (\boldsymbol{\omega} \times \mathbf{r}) \qquad [1]$$

Consider two equal masses as in Fig. 1 with ω as shown, and the x, y coordinate system rotating with the masses. Examining the forces on a small body m, close to the "ridge point" 0 in Fig. 1, we may write

$$F_y = m\ddot{y} + 2m\omega\dot{x} - m\omega^2 y \qquad [2a]$$

also

$$F_y = GMm\left[\frac{1}{(R-y)^2} - \frac{1}{(R+y^2)}\right]$$

Assuming x and y small, we have

$$F_y = G(Mm4y/R^3) \qquad [2b]$$

Similarly

$$F_x = m\ddot{x} - 2m\omega\dot{y} - m\omega^2 x = -2(GMmx/R^3) \qquad [3]$$

Gathering terms

$$\ddot{y} + 2\omega\dot{x} + y(-\omega^2 - 4GM/R^3) = 0 \qquad [4a]$$

$$\ddot{x} - 2\omega\dot{y} + x(-\omega^2 + 2GM/R^3) = 0 \qquad [4b]$$

Letting $x = ae^{\alpha t}$ and $y = be^{\alpha t}$ and $S = GM/R^3$, we obtain

$$b\alpha^2 + a(2\omega\alpha) + b(-\omega^2 - 4S) = 0 \qquad [5a]$$

$$a\alpha^2 - b(2\omega\alpha) + a(-\omega^2 + 2S) = 0 \qquad [5b]$$

If these are considered as a set of linear equations in a and b, they may be solved by setting the determinant equal to zero and obtaining

$$\alpha^2 = S - \omega^2 \pm$$

$$(1/2)\sqrt{4(\omega^2 - S)^2 - 4(\omega^2 - 2S)(\omega^2 + 4S)} \qquad [6]$$

We note that taking the negative sign means that α^2 is more in the stable region, and thus to find stable regions we consider only the plus sign case.

Our criterion for stability is the usual mathematical definition that stability is implied when the dependent variables (in this case the coordinates of the test particle) remain finite, i.e., bounded, as time goes to infinity. In addition, here we claim stability only if both solutions remain finite for the parameters assumed. The reason for this is the belief that the physical system follows the unstable solution if one exists.

Reducing Equation [6] we find

$$\alpha^2 = S - \omega^2 + \sqrt{S(9S - 4\omega^2)} \qquad [7]$$

We now wish to discover if the unstable equilibrium of the particle on the "ridge point" with no rotation can be made stable for some value of ω. Three cases are to be distinguished.

Case I

ω^2 is less than S, α^2 is greater than 0, and α is real. Hence, the system is unstable.

Case II

S is less than ω^2, and ω^2 is less than $9/4\ S$. In this region α^2 changes so that the system changes from an unstable regime to a stable one. To find the boundary between stable and unstable regions, we set $\alpha^2 = 0$, and find $\omega^2 = 2S, -4S$. Since the negative value for ω^2 is meaningless physically, $\omega = \sqrt{2S}$ is the boundary between stable and unstable regions. Thus, stability is from $2S < \omega^2 < 2.25\ S$. Thus, we see that a small body m near point 0 can be stable against small perturbations if ω^2 is properly chosen.

Case III

ω^2 is greater than $9/4\ S$. Here one can show that ω^2 is complex; one finds a real part for α so that we have instability throughout.

One should be careful to distinguish our problem from the usual problem treated in books on celestial mechanics, such as Moulton's (3). In the celestial mechanics problem, the rotational frequency and distance of the two heavy bodies is determined, i.e., $\omega^2 = S/4$, so no weightless bar is required.

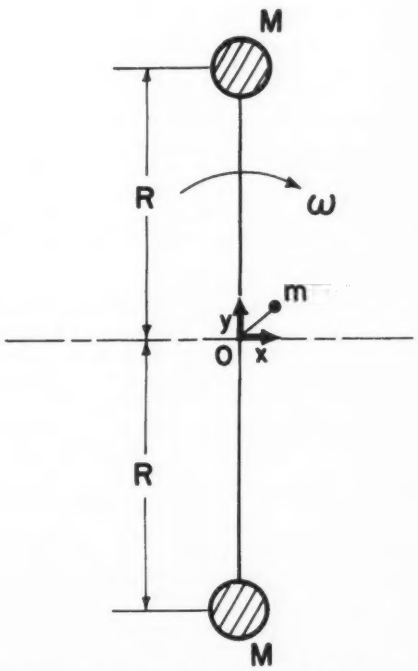

Fig. 1 Relative positions of the small body m and the rotating masses M

Received March 31, 1960.

[1] Preliminary version of this work is given in Aerophysics TM-121, General Electric Co., Missile and Space Vehicle Dept., April 1959.

[2] Now at Geophysics Corporation of America, Boston, Mass.

[3] Numbers in parentheses indicate References at end of paper.

Case I shows that for $\omega^2 = S/4$, the solution is unstable, which agrees with the result in celestial mechanics for the straight-line solutions for the centers of libration.

It is amusing to note that the two equilateral triangle point solutions are stable if μ is less than 0.0385. Since for the Earth-moon system, $\mu = 0.0121$, the equilateral triangle points for the Earth-moon system are stable (4). If one ignores the many perturbing effects, one may anticipate finding a relatively high density of interplanetary dust at these equilateral triangle points for the Earth-moon system. It appears worthwhile to design an experiment with a space vehicle to travel to and investigate the space in the region of these points.

Conversations with W. A. Newcomb, who suggested this illustrative problem, are gratefully acknowledged.

References

1 Greyber, H. D., "Dynamic Stabilization of Hydrodynamic and Hydromagnetic Instabilities," MSVD Aerophysics Operation, General Electric Co., Philadelphia, Research Memo no. 7. (To be published in *Phys. Fluids.*)

2 Joos, G., "Theoretical Physics," Hafner Co., 1934, chap. X.

3 Moulton, F., "Celestial Mechanics," MacMillan Co., Inc., N.Y., 1912, chap. 6.

4 Bucheim, R. W., Rand Corp., Santa Monica, Calif., RM-1726, June 4, 1956.

Fifth Harmonic of Earth's Gravitational Field

HERMAN F. MICHIELSEN[1]

Lockheed Aircraft Corp.,
Missiles and Space Div., Palo Alto, Calif.

Available information on the changes in perigee height of 1958 Delta Two seem to indicate an effect opposite to that which would result from the third harmonic of the gravitational field, as it was determined from observations on 1958 Beta. This effect is tentatively explained by the assumption of a fifth harmonic of slightly lower magnitude than the third. The available evidence is not conclusive but indicates the need for further study.

IN REFERENCE (1),[2] O'Keefe et al. arrive at the conclusion that certain long period oscillations of the orbit elements of Vanguard I, specifically of the eccentricity, clearly indicate the presence of an odd harmonic in Earth's gravitational field. Assuming, tentatively, this to be the lowest possible harmonic, that is, the third one, a specific coefficient for this anomaly was derived. Higher odd harmonics were surmised to be considerably lower in magnitude and insignificant.

In this note, it is proposed to consider a fifth harmonic on top of the third. The words "proposed" and "consider" are used here intentionally, since from the information available to the author, he is not able to prove conclusively the existence of a sizable fifth harmonic. But the indications are considered sufficiently strong to warrant dissemination of the findings. In addition, it is shown analytically that a fifth or higher harmonic of such a magnitude that the orbit elements of *certain* satellites are substantially affected cannot be discarded a priori.

It is well known (1) that the third harmonic causes the perigee of a satellite to move up and down, concurrently with the latitude of the perigee. In the case of Vanguard, this motion amounts to about 5 miles and in such a fashion that it always reaches its highest location at extreme southern latitude and its lowest location at extreme northern latitude. Because of the slow decay of the Vanguard orbit, the motion could be observed very clearly and repeatedly and substantiated beyond doubt.

An interesting feature of the effect of the third harmonic on the perigee radius is that, for all practical purposes, the rate of change of this parameter is proportional to the rate of change of the argument of perigee. Both are strongly dependent on the orbit inclination, but in essentially the same fashion. As a result, the cumulative effect of the third harmonic on the perigee radius is independent of the inclination and only a function of the instantaneous latitude of the perigee. This is true whether the inclination is greater or smaller than the critical inclination of 63°4, at which the argument of perigee is stationary.

Such a proportionality does not exist, however, between the rate of change of the perigee radius which results from any *higher* odd harmonic in the gravitational field, and the rate of change of the argument of perigee. The cumulative effect of such higher odd harmonics on the perigee radius can, therefore, be surprisingly high, if the orbit inclination happens to be close to 63°4, when the perigee changes extremely slowly in latitude and, as a result, accumulation continues in one direction for a considerable length of time.

This fact was recognized when an effort was made to account for certain indications that the perigee of 1958 Delta Two (Sputnik III, satellite) was lower than expected in southern latitudes, an effect opposite to the one caused by the third harmonic, as established from 1958 Beta (Vanguard I). Assuming the third harmonic to exist beyond doubt, it was conceived that an additional effect existed, which would be very small in the case of Vanguard, but relatively large in the case of Sputnik, so that it could override the effect of the third harmonic. The fifth harmonic was found to fulfill this requirement.

Neglecting terms in ϵ^2 and short period terms, the perigee height can be expressed as

$$\mu_p = \mu_{p,0} + \left[\frac{3}{10}\left(\frac{A_3}{A_2}\right) + \Phi_\gamma\left(\frac{A_5}{A_2\rho_\beta^2}\right)\right]\cdot\sin\delta_p \quad [1]$$

where

$$\Phi_\gamma = \frac{5}{42}\cdot\frac{8 - 28\sin^2\gamma + 21\sin^4\gamma}{4 - 5\sin^2\gamma} \quad [2]$$

where

$\mu_p = (r_p/r_e) - 1$
$\rho_\beta = r_\beta/r_e$
r_e = equatorial radius of Earth
r_p = perigee radius
r_β = semilatus rectum
δ_p = latitude of perigee
γ = orbit inclination

A_2, A_3 and A_5 are gravitational constants in the following expression for the gravitational potential

$$-E = g_e\cdot r_e\left[\frac{1}{\rho} + \frac{A_2}{\rho^3}\left(\frac{1}{3} - \sin^2\varphi\right) + \frac{A_3}{\rho^4}\left(\frac{3}{5}\sin\varphi - \sin^3\varphi\right) + \frac{A_4}{\rho^5}\left(\frac{3}{35} - \frac{6}{7}\sin^2\varphi + \sin^4\varphi\right) + \frac{A_5}{\rho^6}\left(\frac{5}{21}\sin\varphi - \frac{10}{9}\sin^3\varphi + \sin^5\varphi\right)\right] \quad [3]$$

Received May 2, 1960.
[1] Staff Scientist. Member ARS.
[2] Numbers in parentheses indicate References at end of paper.

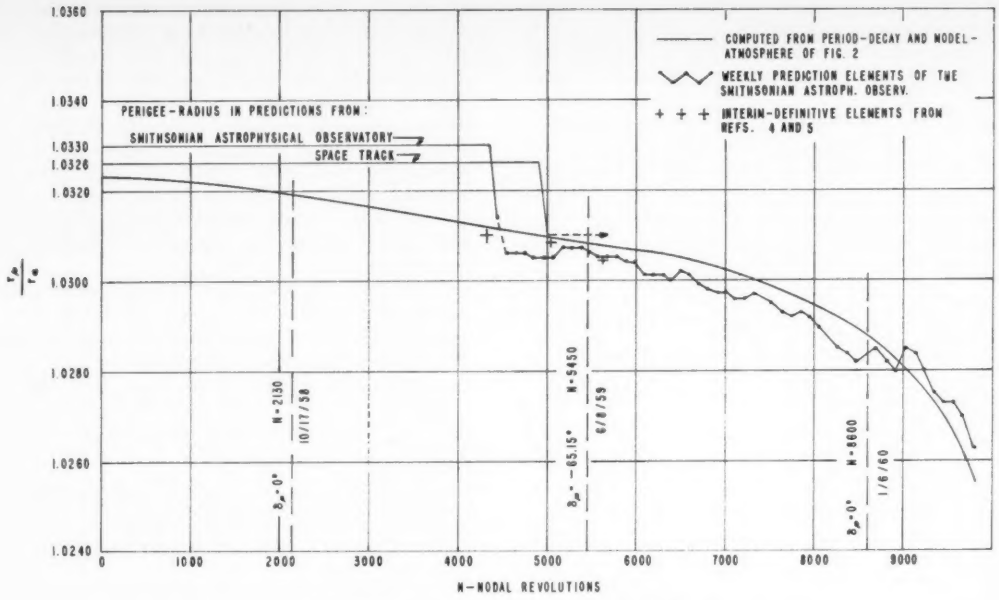

Fig. 1 Perigee radius vs. number of revolutions

Numerical evaluation of Equation [2] then yields

$$\Phi_\gamma = +0.061 \text{ for } \gamma = 33°25 \text{ (in the case of Vanguard)}$$
$$\Phi_\gamma = +0.832 \text{ for } \gamma = 65°15 \text{ (in the case of Sputnik)} \quad \ldots\ldots [4]$$

Consequently, the effect of a fifth harmonic of Earth's gravitational field on the perigee height is more than 10 times stronger on the Sputnik than it is on the Vanguard.

Fig. 1 shows the change in perigee radius of 1958 Delta Two according to the best information known to the author at the time of writing. Unfortunately, hardly any values are yet published on the first 4000 revolutions of this satellite. The initial perigee radius, however, seems to have been at least 1.0326 r_e and possibly considerably more. The solid line represents values for r_p, computed from the known period decay and a model atmosphere which satisfactorily fits current satellite data (see Fig. 2). In this computation neither the third nor a fifth harmonic was considered. The points and crosses are the best available actual data. Even if considerable allowance is made for uncertainties in these data, the impression is gained that the perigee tends to be *lower* in southern latitudes and higher in the northern ones. A satisfactory fit could be obtained in the second half of the satellite's lifetime if a somewhat lower scale height is used in the atmospheric model. The initial value for r_p would then, however, be approximately 1.0315 r_e, which is very much lower than any published value. Of course, the possibility that the scale height was considerably higher during the first 5000 revolutions and lower during the last, cannot be excluded, but there does not seem to be any specific reason for such an assumption.

A critical evaluation of the period decay, as derived from Space Track bulletins, indicated a higher relative decay in those time periods when the perigee was in moderate southern latitudes (2). This indicates that the perigee was relatively low in southern latitudes. Again, explanations based on atmospheric changes are fully admissible, but not specifically indicated.

Some numerical considerations with respect to the third and fifth harmonic may now follow. Assuming $A_2 = 1.6234 \cdot 10^{-3}$ and $r_\beta = 1.312\ r_e$ for the Vanguard and $1.110\ r_e$ for the Sputnik (as an average), it is found that the displacements $\Delta\mu$ of the perigee height in the southern apex are

$$\Delta\mu = +0.000624 \text{ for Vanguard}$$
$$\Delta\mu = +0.001006 \text{ for Sputnik}$$

if $A_3 = -6.0 \cdot 10^{-6}$ and $A_5 = 0$, in accordance with present-day assumptions. If, however, we would assume tentatively

$$A_3 = -6.5 \cdot 10^{-6} \qquad A_5 = +4.5 \cdot 10^{-6} \qquad [5]$$

then the values of $\Delta\mu$ are

$$\Delta\mu = +0.000621 \text{ for Vanguard}$$
$$\Delta\mu = -0.000609 \text{ for Sputnik}$$

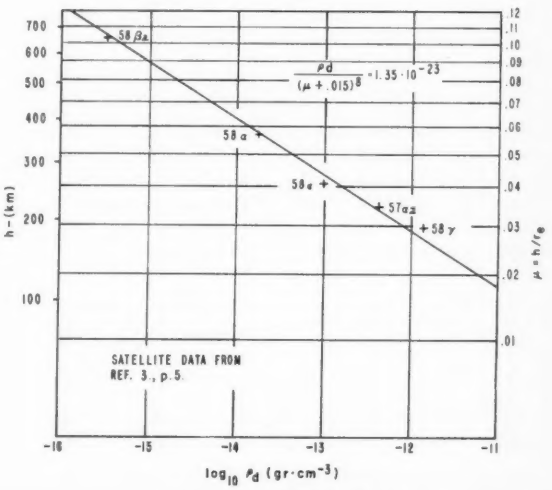

Fig. 2 Atmospheric model

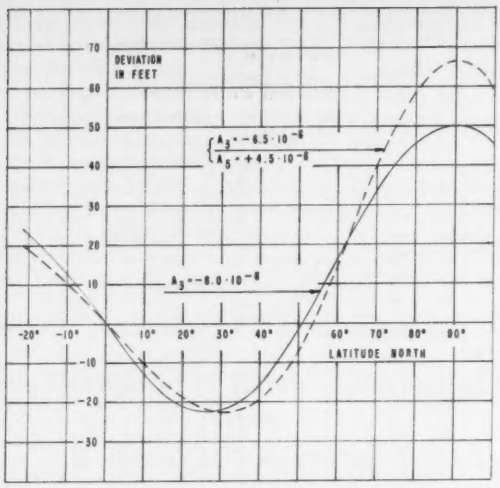

Fig. 3 Deviations of equipotential at sea level

Consequently, the assumption [5] would fit both the observed perigee motion of the Vanguard and the suspected inverse motion in the perigee of the Sputnik.

Finally, then, one may ask how this fifth harmonic would affect the equipotential surface of Earth, the so-called "pear-shape." Fig. 3 shows the radial displacements, due to $A_3 = -6.0 \cdot 10^{-6}$ and to $A_3 = -6.5 \cdot 10^{-6}$ and $A_5 = 4.5 \cdot 10^{-6}$. The difference is surprisingly small. In fact, it is so small that it is almost harder to believe that a *random* anomaly in the potential would exactly follow the solid line, than that it would deviate from it by an amount of the order of the difference indicated by the dotted line. The conclusion must be then that there may be a number of harmonics of order higher than four, slowly decreasing in magnitude with increasing order number, which substantially affect the long period orbit changes of satellites, inclined at angles reasonably close to 63°4. The purpose of this note is primarily to emphasize this finding and stimulate further investigation of higher harmonics and their effects.

Observations between June and September 1960 on 1960 Epsilon One (Sputnik IV) yielded a confirmation of the findings reported here. In addition, however, observations on 1960 Gamma One (Transit I, rocket) seem to indicate that also higher order odd harmonics (seventh or higher) are involved.

References

1 O'Keefe, J. A., Eckels, A. and Squires, R. K., "Vanguard Measurements Give Pear-Shaped Component of Earth's Figure," *Science*, vol. 129, 1959, p. 565; *see also* Harvard Announcement Card no. 1420, Dec. 29, 1958.

2 Michielsen, H. F., "The Fifth Harmonic of the Earth's Gravitational Field," Lockheed Missiles and Space Div., Palo Alto, Calif., Rep. no. 312307, March 1960.

3 Whitney, C. A., "The Structure of the High Atmosphere, Part I," in "Research in Space Science," Special Rep. no. 21, Smithsonian Institution, Astrophysical Observatory, Feb. 1959.

4 Smithsonian Institution, Astrophysical Observatory, "Operational Information," in "Research in Space Science," Special Rep. no. 26, May 1959.

5 Smithsonian Institution, Astrophysical Observatory, "Operational Information," in "Research in Space Science," Special Rep. no. 28, Sept. 1959.

High Temperature Equilibria Involving Metallic Halides

L. J. GORDON[1]

Aerojet-General Corp., Solid Rocket Plant, Sacramento, Calif.

WHEN high temperature equilibria are calculated for a system containing a multivalent metal, such as Be, Mg, B, Al, C, Si, Ti, etc., and more than one halide, F, Cl, etc., a considerable number of mixed halides must be assumed as products. It is shown here that the mixed halides need not be considered individually, as they may be included in the equilibrium gas composition simply as multiplicity factors of the primary halides. Depending on the iterative technique and on the memory limitations of the automatic computer used for the calculation, this method can provide a saving of calculating efforts. The method is illustrated as follows: For a trivalent metal M and the halides F and Cl, regardless of what other elements are present, the metal halide vapors which normally would be assumed are

$$\left.\begin{matrix} MF_3 \\ MF_2Cl \\ MFCl_2 \\ MCl_3 \end{matrix}\right\} \text{ molecular species} \qquad \left.\begin{matrix} MF_2 \\ MCl_2 \\ MFCl \\ MF \\ MCl \end{matrix}\right\} \text{ dissociation products}$$

One can safely assume, and in fact the data for the mixed halides were probably obtained from the assumption, that ΔH and ΔF for the following reactions are zero

$$\tfrac{2}{3}\, MF_3 + \tfrac{1}{3}\, MCl_3 \rightleftharpoons MF_2Cl \qquad [1a]$$

$$\tfrac{1}{3}\, MF_3 + \tfrac{2}{3}\, MCl_3 \rightleftharpoons MFCl_2 \qquad [1b]$$

Therefore, the quantity of MF_2Cl and $MFCl_2$ present can be written as functions of the quantities of primary halides

$$MF_2Cl = (MF_3)^{2/3}\,(MCl_3)^{1/3} \qquad [2a]$$

$$MFCl_2 = (MF_3)^{1/3}\,(MCl_3)^{2/3} \qquad [2b]$$

But now as for the contribution of the mixed halides to the H and S sums as well as to the number of moles of gas present, Equations [1] may be taken as if the equilibrium signs were equal signs, yielding

$$\overline{MF_3} = MF_3 + \tfrac{2}{3}\,(MF_3)^{2/3}\,(MCl_3)^{1/3} + \tfrac{1}{3}\,(MF_3)^{1/3}\,(MCl_3)^{2/3} \qquad [3]$$

where

MF_3, MCl_3 = quantities of these species calculated from other equilibria

$\overline{MF_3}$ = effective total quantity of that species

Writing a similar expression for MCl_3 and then rearranging terms yield

$$\overline{MF_3} = MF_3\left[1 + \frac{2}{3}\left(\frac{MCl_3}{MF_3}\right)^{1/3} + \frac{1}{3}\left(\frac{MCl_3}{MF_3}\right)^{2/3}\right] \qquad [4a]$$

$$\overline{MCl_3} = MCl_3\left[1 + \frac{2}{3}\left(\frac{MF_3}{MCl_3}\right)^{1/3} + \frac{1}{3}\left(\frac{MF_3}{MCl_3}\right)^{2/3}\right] \qquad [4b]$$

Similarly for the divalent dissociation products one obtains

Received April 6, 1960.

[1] Senior Engineer, Thermodynamics Section, Solid Propellant R&D Laboratory. Member ARS.

the expressions

$$\overline{MF_2} = MF_2\left[1 + \frac{1}{2}\left(\frac{MCl_2}{MF_2}\right)^{1/2}\right] \quad [5a]$$

$$\overline{MCl_2} = MCl_2\left[1 + \frac{1}{2}\left(\frac{MF_2}{MCl_2}\right)^{1/2}\right] \quad [5b]$$

It is not immediately obvious that calculation of the complicated expressions within the brackets presents savings over straightforward calculation of $MFCl_2$ and MF_2Cl, etc., but since in most computer programs H − S data and equilibrium constants are calculated as needed from stored $C_p - T$ data, the saving is obtained by eliminating both storage space and mathematical integration of the C_p data for the mixed halides. When more than one multivalent metal is considered in the system, the expressions within the brackets may be written as generalized computer sub-routines realizing that the expressions used for a bivalent metal are the same as those used for the dissociation products of tri- and tetravalent metals, etc.

Development of expressions for cases such as that of a tetravalent metal with three halides is left to the reader.

Heat Storage System for Satellite Powerplants

C. L. WALKER,[1] J. D. MATCHETT[2] and R. J. HANOLD[3]

Allison Div., General Motors Corp., Indianapolis, Ind.

In satellites using a solar energy source, the energy must be stored for use during the shaded portion of the orbit. A system has been designed for storing energy as heat, making use of the high heat of fusion of lithium hydride. This heat storage system, for use specifically with heat engines or thermoelectric energy conversion systems, will potentially store enough energy to supply up to 75 w-hr of usable electrical power per pound of storage system weight.

AN EARTH satellite may spend a large portion of orbital time shaded from the sun. This is also true of satellites orbiting other planets in our solar system. Several studies (1–4)[4] have shown that for satellite power requirements up to a few kilowatts, solar energy provides the best energy source for long missions. Thus it is imperative that energy be stored for use during the time the vehicle is shaded from the sun.

The conventional energy storage device has been the electrical storage battery (5,6). Other concepts have included regenerative fuel cells (7) and even flywheels. However, many of the solar powered satellite designs use a thermal to electrical energy conversion device, such as a heat engine or thermoelectric converter. Therefore, it seemed feasible that heat storage might be used rather than some other method of energy storage. An obvious advantage would be that a heat engine could run continuously without stops and starts. This study has not only verified the feasibility but also has indicated that a decided weight advantage also exists over other energy storage components.

The storage of energy as heat is, of course, not a new idea; a considerable amount of work has been conducted in conjunction with solar home heating research. Nevertheless, until recently heat storage as applied to space vehicles has received only slight attention in the literature (2,3). However, heat storage is not without its problems. Thermal energy may be stored and released by several mechanisms: Sensible heat, heat of fusion, heat of vaporization and heat of transformation. These possibilities must be balanced against system requirements which include high storage capacity per unit weight, operating temperature in a range compatible with conversion system, thermal stability, materials compatibility, etc.

The heat of fusion method was chosen as the most desirable because it avoided the bulk of vaporizing and condensing but still accepted and rejected energy at a constant temperature. This choice was strengthened when an investigation of several elements and compounds disclosed that the compound lithium hydride had a heat of fusion higher per pound than any other substance. In addition, its melting temperature was usable with several thermodynamic cycles. Data on the properties of lithium hydride have been obtained from the survey reports of Gibb and Messer (8), and from communications with the Lithium Corporation of America (9,10). A summary of the thermal properties of lithium hydride are shown in Table 1.

The heat reservoir — conceived as a group of individually encased capsules of LiH — takes heat from a transfer fluid (probably one of the alkali metals or their alloys) as it comes from the solar collector and rejects the fluid at nearly a constant temperature. During the shaded portion of the orbit this heat will be returned to the fluid, so as to maintain a constant fluid temperature or a constant heat rejection rate. A proposed solar absorber, heat reservoir and heat transfer loop are shown in Fig. 1.

The individual capsules were designed with a conical shape and were placed so that the thickest portion was exposed to the fluid inlet where heat transfer rates would be the greatest. With this arrangement the fusion front will approach the centerline of the capsule uniformly for maximum utilization of the storage material. Subsequent theoretical calculations have supported this hypothesis, although the cone angle will be smaller than expected. Initially it was feared that, in the absence of gravity, the hydrogen "bubble" which is necessary to prevent dissociation would locate itself in such a way as to impede heat flow. It was also feared that cracking upon solidification would also interfere with the heat flow. Fortunately, recent casting tests indicate that the void locates itself in the center of the capsule in the presence of gravity, apparently from surface tension. Very few cracks developed, and those were in a radial direction.

In the design shown in Fig. 1 the lithium hydride accounts for approximately 60 per cent of the total heat reservoir weight. The energy storage capacity of the LiH is 310

Table 1 Properties of lithium hydride

Melting point	1256F
Heat of fusion	1065 ± 135 Btu/lb
Density at 20 C	48.5 lb/ft³
Density of melt	36.1 lb/ft³
Specific heat	1.0 Btu/lb F
Thermal conductivity	4.2 Btu/hr ft F

Presented at the ARS 14th Annual Meeting, Nov. 16–20, 1959.

[1] Section Chief, Fluid Dynamics and Heat Transfer. Member ARS.

[2] Project Engineer.

[3] Research Engineer. Member ARS.

[4] Numbers in parentheses indicate References at end of paper.

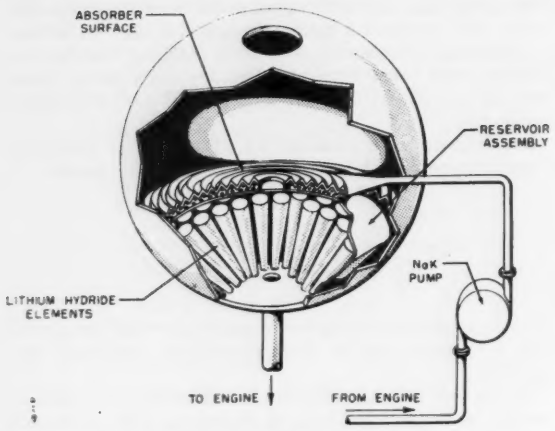

Fig. 1 A proposed heat reservoir system

w-hr per lb but the effective capacity of the reservoir is then only 190 w-hr per lb. A typical mercury vapor turbine engine may have an efficiency of 10 per cent, whereas a recently developed heat engine operating on the Stirling cycle has exhibited efficiencies as high as 40 per cent. Therefore, in this range of conversion system efficiencies a heat reservoir will store from 19 to 75 w-hr of usable energy per pound of reservoir weight.

References

1 Rosenblum, L., "Small Power Plants for Use in Space," *Aero/Space Engng.*, vol. 17, no. 7, July 1958, p. 30.
2 von Doenhoff, A. E. and Hallissy, J. M., Jr., "Systems Using Solar Energy for Auxiliary Space Vehicle Power," IAS Report 59-40, Jan. 1959.
3 Stem, J. M., "Solar-Mechanical Power Plant Design Problems," AIEE Paper CP 59-903, June 1959.
4 Huth, J. H., "Power for Satellites," ASME Paper 59-AV-3, Mar. 1959.
5 Vinal, G. W., "Primary Batteries," John Wiley and Sons, Inc., N. Y., 1950.
6 "Yardney Silvercel," Technical Bulletin, Yardney Electric Corp., N. Y., 1953.
7 Eisenberg, M., "Electrochemical Energy Sources for Space Flight Applications," ARS preprint 866-59, 1959.
8 Gibb, T. R. P., Jr. and Messer, C. E., "A Survey Report on Lithium Hydride," AEC Rep. no. NYO-3957, 1954.
9 "A Compendium of Data on Lithium and Selected Compounds of Lithium," Lithium Corp. of America, Inc., Feb. 1958.
10 Private communication from C. E. Messer, Tufts University, regarding value of latent heat, Lithium Corp. of America, Feb. 1960.

Shock Tube Design for Producing High Gas Temperatures

HUGH N. POWELL[1]

Cornell University, Ithaca, N. Y.

The ideal performance of a new shock tube design is analyzed on an ideal gas constant c_p basis and compared to the standard design. It is shown that within the same experimental limitations, the shock temperature may be increased by factors up to 3, or the shock density by factors of 10 or larger with smaller but sizable gains in both temperature and density under most conditions of interest. Most standard shock tube modifications are also applicable to the new design.

SINCE the paper in 1952 by Resler, Lin and Kantrowitz (1)[2] which demonstrated the feasibility of using shock tubes to produce high temperatures, the shock tube has become an essential tool for high temperature gasdynamic and physical chemical research. Experimentally, the maximum shock strength (and therefore shock temperature) which is attainable with any particular driver and driven gas combination is limited—via the driver to driven gas acoustic velocity ratio—by the means of generating and sustaining a reasonably uniform high temperature in the driver gas chamber; and—via the driver to driven gas pressure ratio—by the chamber's pressure limitations. The latter also directly limits the attainable shock density at a given shock T. One or more of the following techniques are frequently used to augment the performance within a given set of experimental limitations:

1 An area contraction between the driver and driven gas sections.

2 The ignition of a combustible mixture to produce the desired high T and p driver gas.

3 The use of multiple diaphragms and a buffer gas between driver and driven gases.

Reference (2) gives a convenient set of ideal performance curves for the basic shock tube and the foregoing modifications.

The purpose of this paper is to outline a new shock tube configuration which permits quite substantial increases in the values of shock T and ρ to be achieved without increasing the driver T or p. For the sake of simplicity, ideal performance is assumed and ideal, constant specific heat driver and driven gases are used. Although not completely accurate, this basis does provide a good measure of the energies involved and constitutes a simple means of comparative performance evaluation.

Figs. 1 (a) and (b) show schematically the conventional basic shock tube design, termed configuration I, which will be used as a basis of comparison. Fig. 1 (c) shows the proposed configuration II *before* the diaphragm has ruptured. The test (i.e., driven) gas flows isentropically through a converging-diverging nozzle from state (0) to state (1) where it has a Mach number M_1^*. An asterisk denotes quantities which are defined relative to laboratory (shock tube) coordinates. Before entering the exhaust line (say to a dump tank), it passes through an oblique shock attached to the crown formed by the edges of two metal flaps which are held together, say by a small piece of adhesive. These flaps are hinged on their left edges near the diaphragm. When the diaphragm ruptures, the expanding driver gas blows apart the flaps which then close off the exhaust ducts. The driver gas then drives a shock into the oncoming test gas as is shown in Fig. 1 (d). An alternative picture of the transition from Fig. 1 (c) to (d) is to assume that the flaps part and close off the exhaust ducts shortly before the diaphragm ruptures. Then the test gas stagnates between the diaphragm and a shock moving into the state (1) gas stream. When the diaphragm ruptures, a second shock is formed which overtakes and coalesces with the first one, again yielding the situation pictured in Fig. 1 (d). Insofar as shock formation is concerned, the flaps act somewhat like a second weak diaphragm in a multiple diaphragm tube; other mechanical arrangements are possible.

Received May 23, 1960.
[1] Associate Professor, Sibley School of Mechanical Engineering.
[2] Numbers in parentheses indicate References at end of paper.

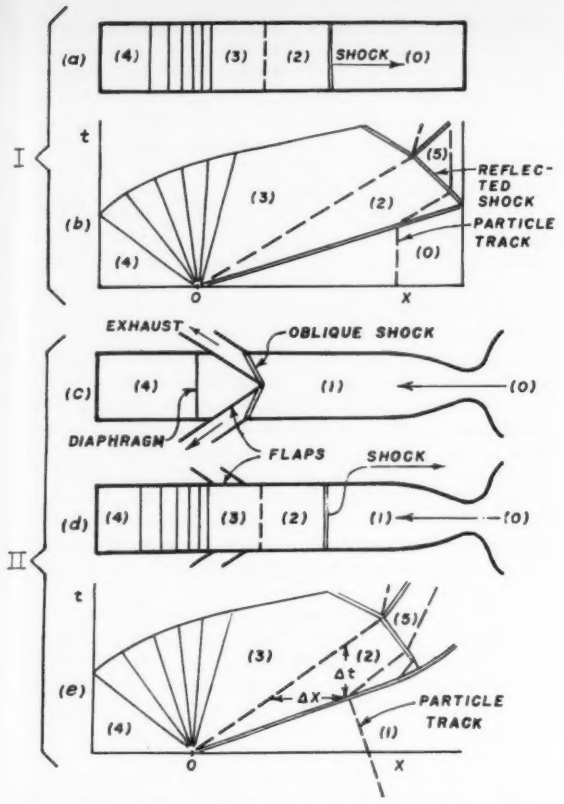

Fig. 1 Schematic representations of configurations I and II

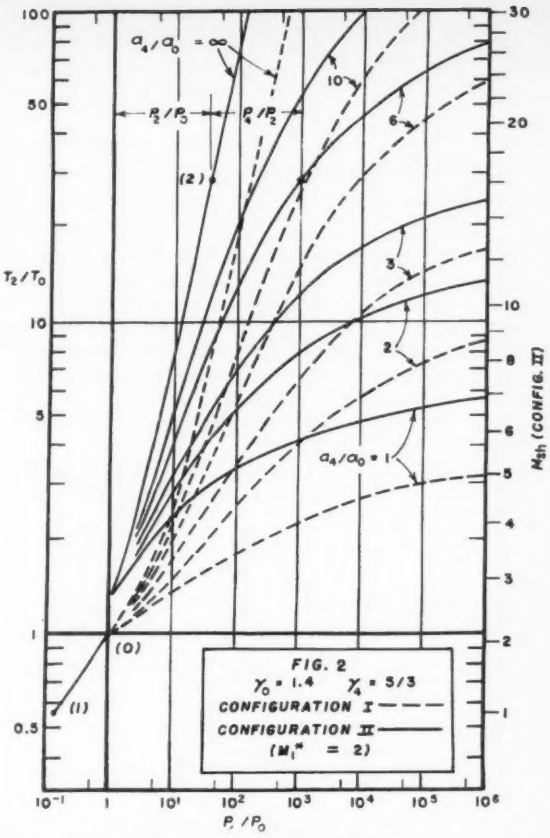

Fig. 2 Comparison of configurations I and II with respect to shock temperature. Quantities pertinent to a representative shock state (2) are also shown

For convenience let the subscripts *is* and *sh* identify the isentropic and normal shock steady-state flow functions of the stream and shock Mach numbers, M_1^* and M_{sh}, respectively. A combination of these functions with the equation for isentropic unsteady flow in a constant area duct yields

$$\frac{p_4}{p_0} = \frac{(p_1/p_0)_{is}\,(p_2/p_1)_{sh}}{\left\{1 - \frac{\gamma_4 - 1}{2(a_4/a_0)}\sqrt{\left(\frac{T_1}{T_0}\right)_{is}}\left[\frac{2}{\gamma_0 + 1}\left(M_{sh} - \frac{1}{M_{sh}}\right) - M_1^*\right]\right\}^{\frac{2\gamma_4}{\gamma_4 - 1}}} \quad [1]$$

which expresses the overall pressure ratio p_4/p_0 as a function of M_{sh} and M_1^*, the driver to driven gas acoustic velocity ratio a_4/a_0, and the driven and driver gas specific heat ratios γ_4 and γ_0, respectively. Equation [1] reduces to the standard equation for configuration I when $M_1^* = 0$.

Fig. 2 shows T_2/T_0 as a function of p_4/p_0 with a_4/a_0 as a parameter for the case $\gamma_0 = 1.4$ and $\gamma_4 = \frac{5}{3}$ with $M_1^* = 2$ in the two configurations. The configuration II curves originate at the p_4/p_0 such that the $M_1^* = 2$ stream is just stagnated. In the steeper portions of the a_4/a_0 curves, configuration II is seen to increase T_2/T_0 by factors up to 2 or so relative to configuration I for the same experimental (T_0, p_0) and (T_4, p_4) states. At $p_4/p_0 = \infty$, the degree of improvement can be determined from the denominator of Equation [1] which then becomes zero. The resulting values of T_2/T_0 are shown in Fig. 3 as a function of M_1^*. It is seen that the degree of improvement is substantially less than at normal (p_4/p_0).

An expression for the shock density ρ_2 can be obtained

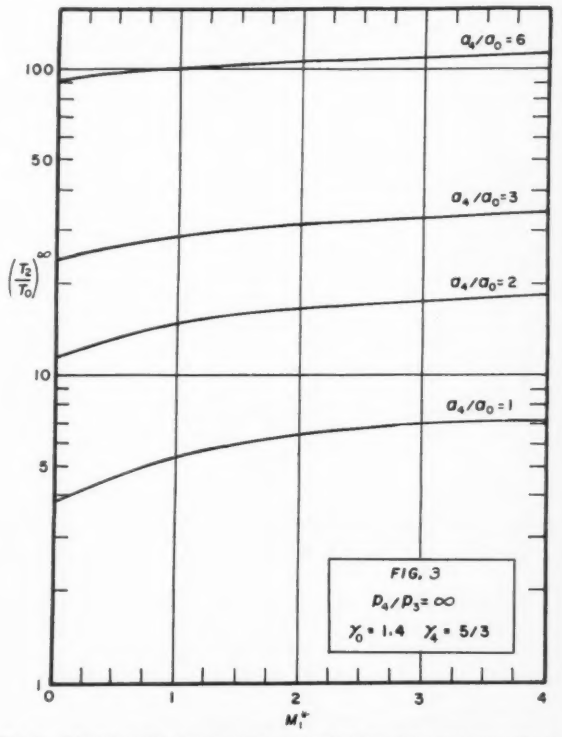

Fig. 3 Limiting shock temperature (at infinite driver pressure) as a function of driven gas nozzle Mach number

from Equation [1] and the gas law

$$\frac{\rho_2 R_0 T_0}{p_4} = \left(\frac{p_2}{p_4}\right)\left(\frac{T_0}{T_2}\right) =$$

$$\frac{\left\{1 - \frac{\gamma_4 - 1}{2(a_4/a_0)}\sqrt{\left(\frac{T_1}{T_0}\right)_{is}}\left[\frac{2}{\gamma_0 + 1}\left(M_{sh} - \frac{1}{M_{sh}}\right) - M_1^*\right]\right\}^{\frac{2\gamma_4}{\gamma_4 - 1}}}{T_1/T_0} \qquad [2]$$

The T_2/T_0 values follow from M_{sh} and M_1^* via Equation [1]. Fig. 4 shows T_2/T_0 vs. $(\rho_2 R_0 T_0)/p_4$ with a_4/a_0 and p_4/p_0 as parameters for configurations I and II with $M_1^* = 2$. It is seen that configuration II may also yield substantially greater shock densities, ρ_2 for the same experimental (T_0, p_0) and (T_4, p_4) states or alternatively, a markedly increased ρ_2 at the same T_2. This feature is especially useful in connection with optical measurements, the sensitivity of which are limited by density.

The general increase in accessible T_2 and ρ_2 is the result of two effects, both of which stem directly from the use of a nozzle.

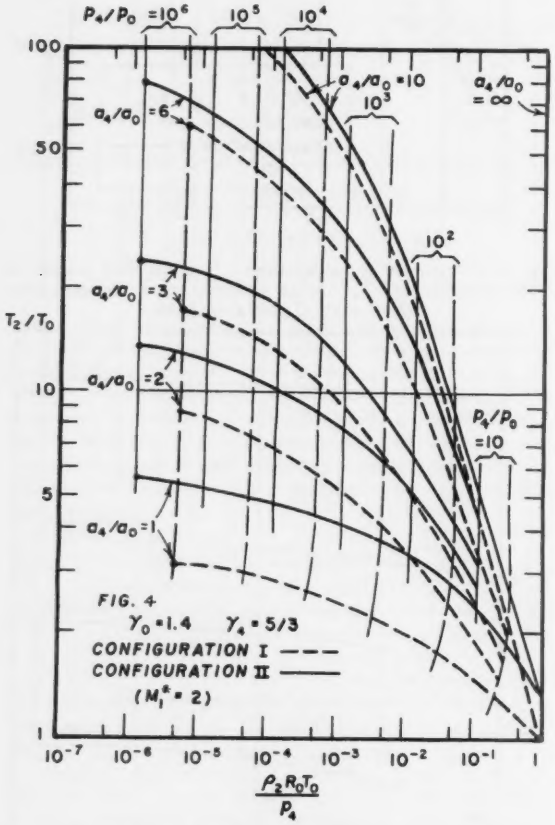

Fig. 4 Comparison of configurations I and II with respect to shock temperature and density

The first effect is simply that beginning with any given (p_0, T_0) state a nozzle expansion followed by a shock to a given T_2 is more irreversible than a shock by itself to T_2 (as can be clearly seen on a T-S diagram). Consequently, for the same $T_{2(I)} = T_{2(II)}$, $p_{2(II)}$ is less than $p_{2(I)}$. Alternatively, for the same $p_{2(I)} = p_{2(II)}$, $T_{2(II)}$ is greater than $T_{2(I)}$. Therefore, *less driver pressure is needed for* the same T_2, or the same driver pressure gives a higher T_2.

The second effect stems from the strong cooling effect of the expansion on the acoustic velocity of the state (1) gas as compared with the corresponding state (0) gas in configuration I. The increase in M_{sh} which is necessary to compensate the cooling to attain a given shock T_2 is largely offset by the $-M^*$ term in the denominator of Equation [1] so that the $\sqrt{(T_1/T_0)_{is}}$ factor still causes a net increase in the quantity within the braces. Although this increase is not large, the effect on p_4/p_0 is considerably amplified by the high power, $2\gamma_4/(\gamma_4 - 1) = 5$, to which this quantity is raised. Because of these effects, both T_2 and especially ρ_2 are markedly greater than if the driven gas pressure in configuration I were merely reduced by a factor equal to the pressure ratio across the nozzle, $p_1/p_2 = 0.128$; i.e., regardless of the p_0 value, performance can always be increased by a nozzle expansion from p_0 (assuming that p_0 is not so low that boundary layer effects are dominant).

If M_1^* is increased, the corresponding Fig. 2 plots continue to show sizable increases in T_2/T_0 relative to configuration I (e.g., by factors of 3 for $M_1^* = 3$), but these gains are increasingly at the expense of ρ_2, so that the matching Fig. 4 plots show only small improvements in density over those already given for $M_1^* = 2$.

Certain additional factors should be noted:

1 It can be shown that the highly disruptive type of shock-boundary layer interaction caused by spillage of high pressure shock gas into the boundary layer will not occur when $M_{sh} \geq 5.98$ (for $M_1^* = 2$)—a condition which is satisfied under most conditions when such a tube would be used.

2 If the tube L/D is large so that it must be made slightly divergent to allow for frictional effects on the supersonic stream, then the shock experiences a converging cross section, and a compensating effect for frictional attenuation of the shock is also realized.

3 Configuration II introduces no modifications in the operation of the driver gas; hence, the standard shock tube modifications mentioned at the beginning of this note are equally adaptable to configuration II with equivalent increases in performance.

In summary, it is concluded that for the same driven and driver gas states, the configuration II design permits sizable increases in T_2 or ρ_2 or both to be achieved relative to configuration I. In effect, these performance increases are purchased by the use of more apparatus, e.g., configuration II can be regarded as a combination of a shock tube driver with a small supersonic blowdown wind tunnel. However, there appear to be no outstanding difficulties of principle or practice in applying such a design.

References

1 Resler, E. L., Lin, S. C. and Kantrowitz, A., "The Production of High Temperature Gases in Shock Tubes," *J. Appl. Phys.*, vol. 23, no. 12, Dec. 1952, pp. 1390–1397.

2 Russo, A. L. and Hertzberg, A., "Modifications of the Basic Shock Tube to Improve Its Performance," Cornell Aeronautical Laboratory, Inc. Ithaca, N. Y., Rep. no. AD-1052-A-7, Aug. 1958.

Optimum Contours for Propulsion Nozzles[1]

ELDON L. KNUTH[2]

The Marquardt Corp., Van Nuys, Calif.

OPTIMUM designs of missiles and space vehicles frequently require maximum thrust to weight ratios for the nozzles. Foelsch (1)[3] describes an approximate method of constructing the shortest nozzle producing maximum thrust for a given area ratio; Guderley and Hantsch (2) present an exact method for designing the nozzle giving maximum thrust for a given length; whereas Rao (3,4) gives an exact method for constructing the nozzle producing maximum thrust for a given length and a given throat contour. Although Rao (3) states "length is a fair indication of nozzle weight," the decision of these authors to use a fixed length as a constraint was influenced also by the difficulty of exactly formulating the problem, using the methods of the variational calculus, if some other constraint (such as fixed surface area) were used. In the present paper, relatively simple approximate methods for constructing nozzles producing maximum thrust for a given length and nozzles producing maximum thrust for a given surface area are developed. It is believed that, in many cases, surface area supersedes length as a measure of weight.

If the fluid flow distribution at a given cross section of a nozzle is independent of the wall contours at all other cross sections of this nozzle (a condition satisfied most nearly by slender nozzles), then the optimum contour at the given cross section also is independent of the contours at other cross sections, and the optimum contour of the nozzle may be obtained by optimizing independently the contour for each differential element of a nozzle. Since the thrust contribution $d\tau$ by an element of the nozzle is given by

$$d\tau = (p_w - p_a)\, 2\pi R \tan\theta\, dx$$

one may write for thrust per unit length

$$d\tau/dx = (p_w - p_a)\, 2\pi R \tan\theta$$

and for thrust per unit surface area

$$d\tau/(2\pi R \sec\theta\, dx) = (p_w - p_a) \sin\theta$$

with

p_w = pressure at nozzle wall
p_a = ambient pressure
R = radius
θ = angle between nozzle wall and axial direction
x = distance along axis

The thrust per unit length (or per unit surface area) is a maximum if its variation with respect to a change in θ vanishes, i.e., if for thrust per unit length

$$(dp_w/d\theta) \tan\theta + (p_w - p_a) \sec^2\theta = 0$$

and for thrust per unit area

$$(dp_w/d\theta) \sin\theta + (p_w - p_a) \cos\theta = 0$$

The variation $dp_w/d\theta$ may be written

$$\frac{dp_w}{d\theta} = \left(\frac{dp_w}{dM_w}\right)\left(\frac{dM_w}{d\theta}\right)$$

with M_w = Mach number adjacent to nozzle wall. For the case in which the flow is isentropic and the isentropic exponent γ is constant

$$\frac{dp_w}{dM_w} = -\left(\frac{p_w}{M_w}\right)\left(\frac{\gamma M_w^2}{1 + [(\gamma - 1)/2]M_w^2}\right)$$

If the slope of a differential wall element is altered, then the Mach number corresponding to this differential wall element is changed according to the Prandtl-Meyer relation

$$\frac{dM_w}{d\theta} = \frac{M_w\{1 + [(\gamma - 1)/2]M_w^2\}}{(M_w^2 - 1)^{1/2}}$$

Substituting into the equations describing conditions necessary for thrust maxima, one finds that maximum thrust per unit length is obtained if

$$\sin 2\theta = 2\left(\frac{p_w - p_a}{p_w}\right)\left[\frac{(M_w^2 - 1)^{1/2}}{\gamma M_w^2}\right] \qquad [1a]$$

and that maximum thrust per unit surface area is obtained if

$$\tan\theta = \left(\frac{p_w - p_a}{p_w}\right)\left[\frac{(M_w^2 - 1)^{1/2}}{\gamma M_w^2}\right] \qquad [1b]$$

Equation [1a] is the same equation obtained by Guderley and Hantsch (2) and by Rao (3) for the differential element at the downstream end of the nozzle; Equation [1b] is believed to be new.

The wall slope immediately downstream of the nozzle throat may be computed exactly for the case in which the Mach number is uniform across the throat section and equal to unity. Then, immediately downstream of the throat, the angle turned by the fluid since leaving the point at which the Mach number is unity is given by the Prandtl-Meyer function

$$\theta = \left[\frac{(\gamma + 1)}{(\gamma - 1)}\right]^{1/2} \tan^{-1}\left[\frac{(M_w^2 - 1)(\gamma - 1)}{(\gamma + 1)}\right]^{1/2} - \tan^{-1}(M_w^2 - 1)^{1/2} \qquad [2]$$

Solving this equation simultaneously with one of the two forementioned equations describing conditions necessary for thrust maxima, one obtains the wall slope immediately downstream of the throat. (E.g., for the case in which the thrust per unit surface area is maximized, if $\gamma = 1.230$ and $p_a = 0$, then immediately downstream of the throat, M_w will be equal to 1.723 and θ will be 21.0 deg.)

To the approximation that fluid properties are constant over any given cross section of the nozzle, an extremely simple and yet useful, approximate procedure for the rapid design of optimum contours for propulsion nozzles results. The following steps are found to be convenient:

1 Compute values of wall slope and Mach number immediately downstream of the throat, using Equations [1 and 2].

2 For several values of M greater than the Mach number immediately downstream of the throat, compute corresponding values of R, using the relation for one-dimensional flows in nozzles, and corresponding values of p, using the isentropic relation.

3 For the several values of M, compute corresponding values of the wall slope R', using Equations [1].

4 Compute distances between the cross sections corresponding to the several values of M, using the relation $\Delta x = \Delta R/R'_{avg}$.

Several optimum contours calculated by this procedure are presented in Fig. 1. Curves A and B indicate the dependence of the optimum contour on the isentropic exponent, whereas curves B and C compare the result of optimizing thrust per unit length with the result of optimizing thrust per unit surface area. Curve B appears to agree with the curve given by Guderley and Hantsch (2) in their Fig. 8.

Submitted Nov. 1959, revised May 1960.

[1] This paper presents the results of one phase of research carried out at ASTRO Division of The Marquardt Corp., under Contract no. AF 33(600)-37921.

[2] Research Consultant. Also Associate Professor of Engineering, University of California, Los Angeles. Member ARS.

[3] Numbers in parentheses indicate References at end of paper.

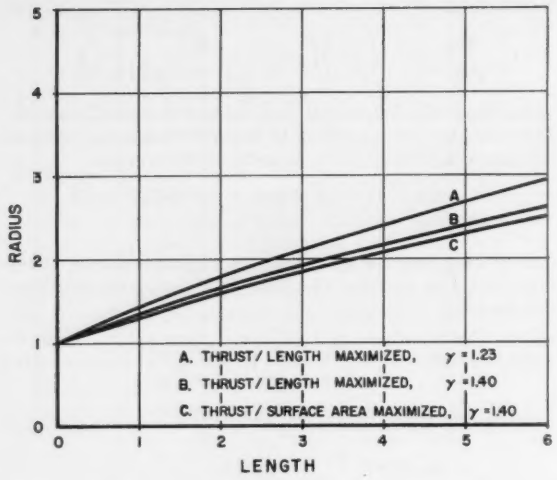

Fig. 1 Optimum nozzle contours for two isentropic exponents and two constraints (ambient pressure = zero)

This design procedure may be used also for nozzles with plugs. If one desires to use a throat with a given contour, then it is suggested that one begin with a contour calculated by the design procedure described and replace the sharp throat by the desired throat, the throat section and the remainder of the nozzle being joined with continuous slope. For cases involving real fluids, Equations [1] are unchanged, but Equation [2] and the area-Mach number relation used in step 2 must be replaced by the appropriate differential equations; wall contours are calculated using numerical integrations.

Acknowledgments

The author appreciates the stimulating technical discussions held with Dr. Kuno Foelsch, Dr. Artur Mager and Dr. G. V. R. Rao.

References

1 Foelsch, K., "The Analytical Design of an Axially Symmetric Laval Nozzle for a Parallel and Uniform Jet," *J. Aeron. Sci.*, vol. 16, March 1949, pp. 161–167.

2 Guderley, G. and Hantsch, E., "Beste Formen für Achsensymmetrische Überschallschubdüsen," *Zeitschrift für Flugwissenschaften*, vol. 3, Sept. 1955, pp. 305–313.

3 Rao, G. V. R., "Exhaust Nozzle Contour for Optimum Thrust," Jet Propulsion, vol. 28, no. 6, June 1958, pp. 377–382.

4 Rao, G. V. R., "Contoured Rocket Nozzles," presented at the Ninth Annual IAF Congress, Amsterdam, Aug. 25–30, 1958.

Book Reviews

Ali Bulent Cambel, Northwestern University, *Associate Editor*

Thermodynamics, by Herbert B. Callen, John Wiley and Sons, Inc., New York, 1960, 376 pp. $8.75.

Reviewed by Serge Gratch
Northwestern University

It is a pleasure to find a textbook in thermodynamics which combines clarity of presentation and logical rigor with a modern point of view. Dr. Callen has been extremely successful in demonstrating that his subject can be presented in a mature, rigorous manner without an unusual amount of mathematical complexity.

This textbook develops thermodynamics from a few basic postulates, chosen on the basis of the resulting simplicity in the subsequent derivations. The first postulate essentially establishes the existence of equilibrium states and the existence of internal energy. The ideas usually expressed in the statement of the first law of thermodynamics are then developed easily as part of the discussion of the measurability of energy. The second postulate is essentially the second law of thermodynamics, stated in the form of the entropy maximum principle. The third postulate completes the usual content of the second law by asserting the additivity of the entropy of composite systems and by requiring entropy to be a monotonically increasing function of energy, thus ruling out negative temperatures. The fourth postulate is essentially the third law of thermodynamics.

Dr. Callen's presentation is essentially deductive. The postulates are not derived inductively from experimental observations, but rather their validity is established a posteriori by demonstrating that they invariably lead to conclusions consistent with experimental observations. This approach leads to a considerable simplification of the mathematics and to a sharper emphasis on fundamental ideas.

Dr. Callen is extremely careful to rest the quantitative development of the theory completely on macroscopic arguments, thus preserving "thermodynamics as a self-contained macroscopic discipline, autonomous and distinct from statistical mechanics." However he uses the ideas of statistical mechanics to advantage by very lucid elementary qualitative discussions designed to make the postulates of thermodynamics intuitively more attractive.

The first part of the book is devoted to the presentation of the postulates and the derivation of some of their most general consequences. In particular, in this part are discussed some of the general relations among properties of typical substances, some of the basic considerations on processes, an excellent coverage of equilibrium and stability of thermodynamic systems, and a rigorous and clear discussion of phase transitions. The second part of the book covers representative applications to chemical thermodynamics, elasticity, and magnetic and electric systems. The third part is devoted to fluctuations and irreversible thermodynamics. The elegance, clarity and thoroughness of this section is not surprising in view of Dr. Callen's many original contributions in this field.

There is no doubt that the method of presentation of thermodynamics followed in this book is a tremendous improvement over the traditional Carnot-Clausius-Kelvin approach. Dr. Callen's postulational approach unquestionably leads to a more straightforward, logical and simple presentation. The usual conclusions concerning efficiencies of cycles are obtained very easily as corollaries of the basic postulates. This reviewer, however, disagrees with Dr. Callen's veiled implication, on page 43 of his book, that the same weaknesses of the conventional treatments are shared by Caratheodory's method. I believe that the latter method leads to just as logical and straightforward a presentation of thermodynamics as the postulational approach chosen by Dr. Callen. However, at present, there are no books on thermodynamics from Caratheodory's point of view comparable in scope to Dr. Callen's book. Thus the latter is unique in removing all the hocus

pocus traditionally found in books on the subject. This book is admirably suited for the advanced undergraduate students or first-year graduate students for whom it is intended, and, with appropriate omissions and with the addition of a little introductory material, it is also an excellent textbook for elementary courses.

AGARD Flight Test Manual, edited by Courtland D. Perkins and Enoch J. Durbin, Pergamon Press, New York, 1959, 2865 pp., 4 vols. $100.

Reviewed by Eino K. Latvala and Associates
ARO, Inc.

This, the second edition of the "AGARD Flight Test Manual," is another outstanding example of the North Atlantic Treaty Organization (NATO) technical cooperation. Over 60 authors representing Canada, France, the Netherlands, the United Kingdom and the United States have contributed to make a comprehensive handbook covering performance, stability and control, and instrumentation related to flight testing of aircraft. Previously published for official restricted distribution only, this new edition has been revised and enlarged and made available for public sale. The manual is published in four loose-leaf volumes in special binders with annual supplements to be made available in 1960. Due to the diversity of subjects covered in the volumes, this reviewer enlisted the aid of four of his associates to review the volumes individually.

Volume I "Performance" contains 12 chapters on the test and analysis procedures for performance flight testing of piloted aircraft. The opening chapter is devoted to the important topics of the definition of standard terms and quantities (such as standard atmosphere, altitude and air speed) and methods of measurement of pressure and temperature. Means for minimizing the effects of non-ideal instrument time response are discussed, and correction and calibration techniques are shown. Throughout this initial chapter and, in fact, throughout the entire volume, very careful attention is given to explicit definitions of quantities. When it is realized that the published material may be used in several different languages, the absolute necessity for clear and non-ambiguous definitions is obvious.

Determination of the inflight thrust and power produced by turbojet, turboprop, ramjet and reciprocating engines is discussed in Chapter 2. Several methods of determining aircraft powerplant performance are given. These include direct measurement of thrust or torque, calculation of thrust based on measurement of gas properties, and determination of engine performance based on climb performance of an aircraft. The errors in overall powerplant performance resulting from typical values of instrumentation errors are shown for a wide variation of engine operating conditions.

The important problem of establishing methods for determining aircraft performance at "standard conditions" from data obtained on the aircraft operating at nonstandard conditions is discussed in Chapter 3. Both analytical and experimental methods for reducing test data to standard conditions are discussed.

With Chapters 1 through 3 as an appropriate background, the data reduction techniques and performance test methods for turbojet, turboprop and reciprocating engine powered aircraft are discussed in Chapters 4, 5 and 6, respectively. Methods for the determination of such characteristics as level flight performance, range and endurance, rate-of-climb and descent are presented. The procedures for the determination of the performance of turbojet and reciprocating engine powered aircraft are much better developed than those dealing with the turboprop powered aircraft. The development of test procedures for flight tests of turboprop powered aircraft has been hampered because only relatively few such planes have been tested and also because the power is produced both by a propeller and by direct jet thrust. Throughout these chapters, as well as throughout the entire volume, the applicable equations are derived in detail, and final equations are clearly presented. For all aircraft, performance testing recommended instrumentation requirements are shown, and test pilot technique is discussed.

Optimum climb theory and the techniques of determining climb schedules from flight tests are discussed in Chapter 7. Three separate analyses of the optimum energy climb schedule are presented; however, the analyses do arrive at the same fundamental conclusions.

The takeoff and landing performance of aircraft weighing more than 4400 lb operating from hard surface runways is considered in Chapter 8. The organization of this chapter is similar to the earlier chapters in that, after the terms are defined and the methods of measurement discussed, the basic equations for the process are given, and the methods of determining performance at standard conditions are shown.

Several unrelated special test techniques are discussed in Chapter 9. These special techniques include: Inflight air flow visualization, calibration of angle-of-attack and sideslip angle measuring systems, and airbrake evaluation.

Flight test techniques for helicopters are discussed in Chapters 10 through 12. The test techniques to establish level flight performance, climb and descent performance, and takeoff and landing performance are presented. In addition to these, the specialized performance characteristics of helicopters relating to ground effect and transition performance following a sudden loss of power are analyzed for single rotor and tandem rotor helicopters. Theoretical analysis of ground effects and of performance following sudden loss of power are presented and are compared to experimental data.

Several appendixes, which contain frequently used tables of atmospheric properties and graphs of some of the more frequently needed relationships of Mach number, calibrated air speed and altitude, are included in this volume.

The value of this volume is somewhat reduced by the fact that most of the material is based on information published no later than 1953. A great many of the present-day high performance turbojet powered aircraft operate at conditions for which the assumptions given in this manual are not completely valid. Care should be exercised to re-evaluate the assumptions made if these techniques are to be applied to aircraft operating at Mach numbers of 2 and 3. Undoubtedly the primary reason for reliance on reference material which is several years old was to avoid the use of classified data. The unique provisions made for ease of revision and addition of material to the volume should minimize the time required to incorporate newer techniques for high performance aircraft as soon as such techniques are available.

The authors and editors have provided complete listings of symbols at the beginning of each chapter in all four volumes to facilitate reading and understanding. Unfortunately, however, the symbols for several parameters vary from chapter to chapter. Since the manual is designed to serve primarily as a reference text for the study of individual sections, the nomenclature variation may not create as much confusion as when the manual is read cover-to-cover.

—Robert E. Smith

Volume II "Stability and Control" is divided into 14 chapters as follows: Introduction, Airplane Motions, Static Longitudinal Stability and Control, Flight Testing Aircraft for Longitudinal Maneuvering Characteristics, Lateral and Directional Control and the Measurement of Aerodynamic Coefficients in Steady Asymmetric Flight and in Flight on Asymmetric Power, Flight Techniques Used to Determine Adequacy of Lateral Control, Stalling and Measurement of Maximum Lift, Spinning, High Speed Stability and Control Problems, Dynamic Response Techniques, Measurement and Interpretation of Flight Test Data for Dynamic Stability and Control, Routine Handling Tests for Helicopters, Study of the Handling Characteristics of Helicopters by Harmonic Methods, A Survey of Flight Flutter Testing Techniques.

Each chapter includes the flight test procedure and the basic equations from which it was derived, the pilot's procedure, the required instrumentation, the data reduction method and the data analysis method. Typical flight test data are presented in graphical form. Detailed mathematical derivations are avoided throughout. Criteria representing desirable stability and control characteristics are stated, and numerous references are included at the end of each chapter.

The technical content of this volume requires that the reader be at least generally familiar with the technique of stability and control analysis. Thus, the volume would be useful to the engineer having limited experience in this field and of lesser value to the more experienced engineer except as a reference.

—Robert C. Bauer

Volume III "Instrumentation Catalog" is intended to serve only as a guide in the preliminary design of flight test instrumentation systems. Although it contains well

over 600 pages, this "catalog" will definitely not serve as a detail design handbook. It was desired that current general usage be reflected in this compilation, and to this end material was solicited from users rather than manufacturers.

The material is organized under the following broad categories: Sensing devices, electromechanical indicators, recorders, radio link systems, timing devices, electrical signal modifiers, power suppliers, ground tracking systems, calibration equipment and data reduction aids. The information presented for each item is arranged in a concise format on a single loose-leaf page, which will facilitate the revisions which are expected at regular intervals. On one side of this page is a photograph of the particular item and on the other side are tabulated the technical characteristics, which include mode of operation, ranges, types of output, sensitivity, accuracy, linearity, resolution, dynamic response, cost, availability, power requirements, size, special features and typical applications.

The most comprehensive coverage is given sensing devices, recorders and calibration equipment. The rather sparse coverage of telemetry and radio control equipment indicates the book was intended mainly for the aircraft field rather than the missile field. Obviously, a tremendous amount of information has been sorted, condensed and organized by the compilers of this volume, yet it should be stressed that it will find its greatest usefulness as a source of leads to more detailed information.

—William N. MacDermott

Volume IV "Instrumentation System" rounds out the series by bridging the gap between methods of flight testing (Vols. I and II) and the instrumentation catalog (Vol. III). Volume IV is devoted to the concept of the total data systems, i.e., data acquisition, data storage, data processing and data analysis systems. The material is divided into four parts. Part I discusses the importance of systems planning considering the type of data required, number of channels, dynamic response, storage, data reduction capabilities, and accuracy and reliability problems with only a brief mention of cost problems of manpower, time and hardware.

Part II is a very excellent and comprehensive survey of the various types of data collection systems used in aircraft and missile flight testing. Every major type of data system is described and analyzed. These include displacement, temperature, pressure, acceleration, force, altitude, flow and icing systems, including signal modification, telemeter techniques and data storage. The manual describes in detail various French telemeter systems. Since the basic techniques described are similar to those used in the United States, the reviewer feels that the description given carries too much detail. Similarly detailed descriptions are given for recorder systems though a majority of these products described are manufactured in the USA.

Part III describes data reduction systems, i.e., data handling and processing. There follows a brief description of the various systems and hardware available with a passing glimpse into analog computer techniques. This is followed by a reasonably thorough description of digital computers and their application to data handling.

Part IV starts with a good description of the various types of errors that are incurred in the overall systems, and methods of defining and eliminating these various errors. The second portion of Part IV brings forth the very important concept that all data is merely a sampling of occurrences and that the data must and should be treated statistically. Although some examples of data fairing and distribution are given, the basic concepts of data distribution, systematic error, random error, sigma and confidence levels could be expounded further.

Taken in its entirety, Volume IV is an excellent reference covering the broad ranges of instrument systems.

—Ira R. Heimlich

The excellent manner in which the contributions of many authors have been integrated into a single, well-organized reference work demands that credit be given to the editors. If the manual serves to provide a uniform basis for standardizing flight test techniques and for quoting of aircraft performance characteristics among the member nations of NATO, the tremendous amount of time and effort which has been expended to prepare the manual will have been well spent. The broad scope of flight testing technology which is covered should make the manual a valuable reference to the engineer working in this and related fields.

—Eino K. Latvala

Symposium of Plasma Dynamics, General editor, Francis H. Clauser, Addison-Wesley Publishing Co., Inc., Reading, Mass., 1960, 369 pp. $12.50.

Reviewed by Robert A. Gross
Columbia University

This book is a forerunner of what promises to be a flood of books concerning the newly popular subject of electrically conducting gases interacting with electromagnetic fields. This large subject is literally exploding now with new results in many fields of science and engineering. Recognizing the interdisciplinary nature and rapid growth of this subject, the Air Force Office of Scientific Research and the National Academy of Sciences organized a symposium in June of 1958 which brought together many leading scientists and engineers working in this field. The four-day meeting at Woods Hole, Mass., had no formal papers presented, but, instead, introductory speakers on each topic and then informal and often provocative discussions. A transcript of the discussion was taken, and 10 technical section editors put the proceedings in book form.

The technical material covered is very broad and reflects the many disciplines represented at the meeting. High temperature plasma experimental research results are described and concern mostly thermonuclear fusion efforts. Sections on gaseous electronics and electron beams present the experience and viewpoint of electrical engineers. Sections on the statistical and continuum approach to analytically describing the behavior of plasmas show the power and limitations of each approach. Applications to high speed flight are briefly covered. Solar and finally cosmical magnetohydrodynamics are presented to complete the readers' picture of the subject.

This book offers a broad and advanced view of the field of plasma dynamics. It is not for the beginner in this field, since it shows specialists describing and defending their work before other experts in the field. Nomenclature is varied and frequently unexplained, and the text often lacks detail which would be expected in informal blackboard-type discussions. This reviewer found it difficult reading at times, but when augmented by work and supplementary reading, it was often rewarding. The book does bring the experienced reader nearly up to the present (i.e., to mid 1958) and gives him a glimpse of other areas of this big subject. One very unusual and worthwhile feature is an extensive bibliography which takes 68 pages and includes many references from the "subliterature" of industrial and government reports. This book is not recommended for the technical reader who wants to learn for the first time what plasma dynamics is about. It does present a remarkable chance for the specialist to learn what other experts in his own and allied fields are presently doing and thinking. Hence it should provide a stimulus for persons engaged in plasma research.

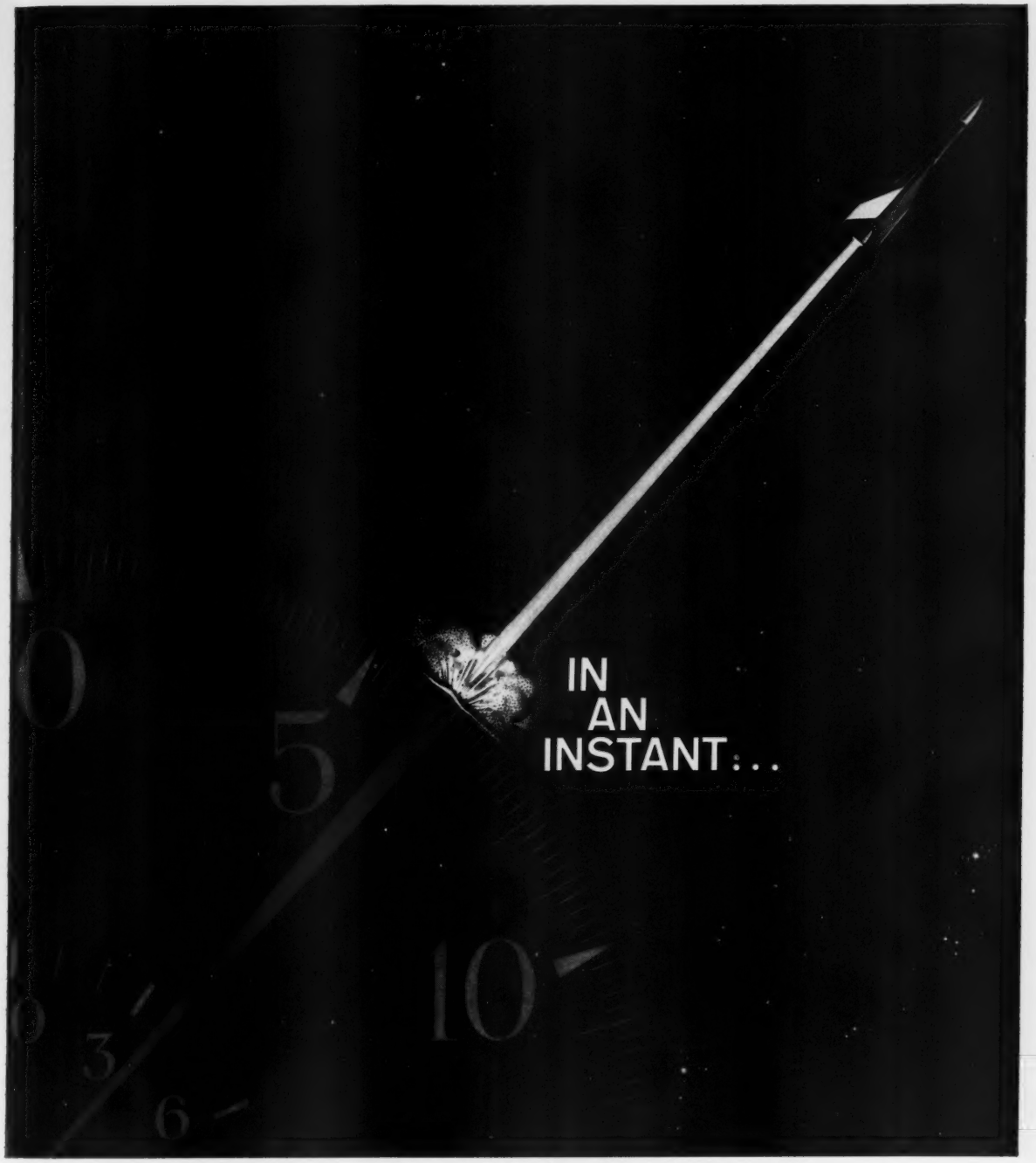

because this oxidizer's stored aboard

Nitrogen Tetroxide provides immediate, hypergolic ignition with amine fuels. Even after 9 years of storage, nitrogen tetroxide is ready for instant use. Combustion efficiencies closely approach the theoretical 99%.

N_2O_4—Requires no refrigeration—can be stored indefinitely in missiles at launching sites.—**Can be used with most fuels**—including those containing carbon.—**Eliminates rough starts**—fast reaction prevents accumulation of propellants in thrust chambers.—**Allows throttleable control** of motors.

We'll gladly supply technical literature, including: a 59-page Product Bulletin, and a brochure entitled "Large Scale Handling of Nitrogen Tetroxide."

For specifications and local offices, see our insert in Chemical Materials Catalog, pages 475-482 and in Chemical Week Buyers Guide, pages 37-44.

BASIC TO AMERICA'S PROGRESS

Allied Chemical

NITROGEN DIVISION
Dept. NT14-21-2, 40 Rector Street, New York 6, N.Y.

2819

Technical Literature Digest

M. H. Smith, *Associate Editor*
The James Forrestal Research Center, Princeton University

Propellants and Combustion

Polymerization of Solid Propellants, by W. H. Groetzinger III, ARS JOURNAL, vol. 30, no. 5, May 1960, pp. 498–499.

Propagation of Flames Supported by a Zeroeth-order Chemical Reaction, by Joseph O. Hirshfelder and Sara S. Van Domelen, *Phys. Fluids,* vol. 3, March-April 1960, pp. 210–215.

Shock-initiated Detonations, by Roger A. Strehlow and Arthur Cohen, *Phys. Fluids,* vol. 3, March-April 1960, p. 319.

Mass-spectrometric Studies of Ionization in Flames, I: The Spectrometer and Its Application to Ionization in Hydrogen Flames, by P. F. Knewstubb and T. M. Sugden, *Proc., Royal Soc., London,* vol. 225, no. 1283, May 10, 1960, pp. 520–537.

The Formation of a Detonation Wave During the Combustion of Gas in Pipes, by G. D. Salamandra, T. V. Bazhenova, *Soviet Physics-Tech. Phys.,* vol. 4, no. 11, May 1960, pp. 1244–1249.

The Interaction of Weak Shock Waves with the Flame Front, by G. D. Salamandra and I. K. Sevast'yanova, *Soviet Physics-Tech. Phys.,* vol. 4, no. 11, May 1960, pp. 1250–1257.

Propellant Vaporization as a Design Critierion for Rocket-engine Combustion Chambers, by Richard J. Priem and Marcus F. Heidmann, *NASA Tech. Rep.* R-67, 1960, 127 pp.

The Interactions Between Nitrogen and Oxygen Molecules, by Willard E. Meador Jr., *NASA Tech. Rep.* R-68, 1960, 52 pp.

American Chemical Society, **Literature of the Combustion of Petroleum** (*Advances in Chemistry Series, no. 20*), Washington, D. C., The Society, 1958, 295 pp.

Cool Flames and the Organic Reaction Mechanisms Involved in Their Formation, by Cecil E. Boord, pp. 5–14.

Fundamental Principles of Flammability and Ignition, by Bernard Lewis and Guenther von Elbe, pp. 15–21.

Application of Chemical Reactor Theory to Combustion Processes, by E. C. Woodward, pp. 22–38.

Detonative and Deflagrative Combustion, by Richard B. Morrison, Thomas C. Adamson Jr. and Alexander Weir, pp. 69–84.

Explosion Limit Phenomena and Their Use in Elucidation of Reaction Mechanisms, by Walter Roth and Milton Scheer, pp. 85–103.

Role of Vaporization Rate in Combustion of Liquid Fuels, by Gilbert S. Bahn, pp. 104–115.

Burning of a Liquid Droplet, by Henry Wise and George A. Agoston, pp. 116–135.

Production and Measurement of Single Drops, Sprays, and Solid Suspensions, by James A. Browning, pp. 136–154.

Drop-size Distributions of Fuel Sprays, by J. Mason Pilcher and Ralph E. Thomas, pp. 155–165.

Flame Propagation in Premixed Gases, by Frank E. Belles, pp. 166–186.

Combustion of Atomized Liquid Propellants, by C. C. Miesse, pp. 243–262.

Nitrogen Oxide Formation in Autoignition of Liquid Fuel Sprays, by G. J. Mullaney, *Ind. Engng. Chem.,* vol. 52, June 1960, pp. 529–532.

American Society for Testing Materials, **Symposium on Materials Research Frontiers,** Boston, June 25, 1958, Philadelphia, The Society, 1959, 48 pp. (*ASTM Special Technical Publication 243.*)

Modern Liquid Fuels, by Arthur L. Lyman, pp. 17–31.

Materials and Structures

Puncture Problem at Cosmic Velocities, by M. A. Lavrent'ev, ARS JOURNAL, vol. 30, no. 4, April 1960, *Russian Suppl.,* pp. 386–388. (Also *NASA Tech. Transl.* F-40, May 1960, 6 pp.)

Satellite Pressure Losses Caused by Meteoroid Impacts, by M. Kornhauser, ARS JOURNAL, vol. 30, no. 5, May 1960, pp. 475–479.

Procedures for Electroplating Coatings on Refractory Metals, by John G. Beach and John A. Gurklis, *Battelle Mem. Inst., Defense Metals Info. Center, DMIC Memo* 35, Oct. 1959, 26 pp.

Temperature Flexure of Elastic Elements, by G. A. Slomyanskii, *NASA Tech. Transl.* F-34, May 1960, 20 pp. (Translated from *Some Questions Relating to Modern Instrumentation Technology,* edited by Poliakov, pp. 5–21.)

An Investigation of Metal-ceramic Composites for High-temperature Applications, by Sherwood W. McGee, *Armour Res. Found., ARF* 2175–1, May 15, 1959, 6 pp. (*ASTIA AD* 217, 445.)

Oxidation of Tungsten and Tungsten Based Alloys, by E. A. Gulbransen, K. F. Andrew, P. E. Blackburn et al., *Westinghouse Electric Corp., Res. Labs.,* Sept. 1959, 78 pp.

Application of Rate-temperature Parameters to Tensile Data for Magnesium Alloys and a Relation Between the Larson-Miller Constant and the Activation Energy, by Charles R. Manning Jr., *NASA TN* D-172, May 1960, 23 pp.

American Society for Testing Materials, **Symposium on Materials Research Frontiers,** Boston, June 25, 1958, Philadelphia, the Society, 1959, 48 pp. (*ASTM Special Technical Publication 243.*)

Materials in the Nuclear Age, by John J. Antal, pp. 7–16.

Some New Types of Neutron-shielding Materials, by Anthony N. Fasano, *Wright Air Dev. Center, WADC-TN-59-227,* June 1959, 12 pp.

Vibration and Near-field Sound of Thin-walled Cylinders Caused by Internal Turbulent Flow, by Paul F. R. Weyers, *NASA TN* D-430, June 1960, 58 pp.

Creep Bending and Buckling of Thin Circular Cylindrical Shells, by Burton Erickson, Francis W. French, Sharad A. Patel, N. J. Hoff and Joseph Kempner, *NASA TN* D-429, June 1960, 49 pp.

Strength Properties of Reinforced Plastic Laminates at Elevated Temperatures, by K. H. Boller and K. E. Kimball, *Wright Air Dev. Center TR* 59–229, Aug. 1959, 54 pp.

Temperature Distribution and Thermal Stresses in Structures with Contact Resistances, by Frederick V. Pohle, T. J. Lardner and Francis W. French, *Brooklyn Polytechnic Inst., Dept. Aeron. Engng. & Appl. Mech., PIBAL Rep.* 557, May 1960, 23 pp.

An Improved First - approximation Theory for Thin Shells, by J. Lyell Sanders Jr., *NASA Tech. Rep.* R-24, 1959, 11 pp.

A Design Philosophy for Repeated Thermal Loading, by E. W. Parkes, *NATO, AGARD Rep.* 213, 1958, 24 pp.

Buckling of Conical Shells Under External Pressure and Thermal Stresses, by Josef Singer and Nicholas J. Hoff, *Technion Res. and Dev. Foundation, Haifa, Israel, Tech. Final Rep.,* Dec. 1959, 78 pp.

Some Experiments Concerning Subsequent Yield Surfaces in Plasticity, by Harvey G. McComb Jr., *NASA TN* D-396, June 1960, 33 pp.

Missile Structures and Materials, by E. Z. Gray, *NATO AGARD Rep.* 218, 1958, 22 pp., 8 refs.

Some Effects of Internal Heat Sources on the Design of Flight Structures, by G. E. A. Thomann and R. B. Erb, *NATO, AGARD Rep.* 208, 1959, 62 pp., 7 refs.

Yield Conditions for Rotationally Symmetric Shells Under Axisymmetric Loading, by P. G. Hodge Jr., *J. Appl. Mech.* (*ASME Trans.*), vol. 82E (vol. 27, no. 2), June 1960, p. 323.

Integral-differential and Integral Equations for the Equilibrium of Thin Elastic Shells, by N. A. Kiltschewskij, *Zeitschrift für Angewandte Math. und Mech.,* vol. 40, April 1960, pp. 153–160. (In German.)

Symposium on Surface Effects on Spacecraft Materials, Palo Alto, Calif., May 1959, ed. by Francis J. Clauss, John Wiley & Sons, N. Y., 1960, 404 pp.

Effect of Surface Thermal-radiation Characteristics on the Temperature-control Problem in Satellites, by Walter G. Camack and Donald K. Edwards, pp. 3–54.

Temperature Control of the Explorers and Pioneers, by T. O. Thostesen, A. R. Nibbs and E. P. Buwalda, pp. 55–91.

Coatings for Space Vehicles, by Joseph C. Richmond, pp. 92–116.

Spectral Reflectance Measurements, by Robert V. Dunkle, pp. 117–140.

Emissivity of Materials Near Room Temperature, by Ralph McDonough, pp. 141–151.

Vanguard Emittance Studies at NRL, by Louis F. Drummeter Jr. and E. Goldstein, pp. 152–163.

Emissivity, Absorptivity, and High-temperature Measurement at Armour

EDITOR'S NOTE: Contributions from Professors E. R. G. Eckert, J. P. Hartnett, T. F. Irvine Jr. and P. J. Schneider of the Heat Transfer Laboratory, University of Minnesota, are gratefully acknowledged.

Research Foundation, by O. H. Olson and Sidney Katz, pp. 164–181.

Some Methods Used at the National Bureau of Standards for Measuring Thermal Emittance at High Temperatures, by Joseph C. Richmond, pp. 182–194.

A Method for Measuring Total Hemispherical Emissivity of Metals, by C. P. Butler and Edward C. Y. Inn, pp. 195–211.

High-temperature Emissivity Measurements at The Martin Company, by Melvin Crompton, pp. 212–219.

Apparatus for the Measurement of Spectral and Total Emittance of Opaque Solids, by Clyde C. Shaw, pp. 220–246.

Materials Sublimation and Surface Effects in High Vacuum, by G. F. Vanderschmidt and J. C. Simons Jr., pp. 247–262.

Vacuum Volatility of Organic Coatings, by Lt. George F. Matacek, pp. 263–285.

Effects of High Vacuum on Mechanical Properties, by M. R. Achter, pp. 286–306.

Surface Phenomena and Friction, by T. Bruce Daniel, pp. 307–318

Panel Discussion: High-vacuum Environmental-test Chambers and Equipment, by M. R. Achter, T. B. Daniel, R. L. Jepsen, Lt. G. F. Matacek, N. Milleron, E. Perkins, J. P. Reynolds, J. C. Simons and G. F. Vanderschmidt, pp. 319–346.

Measurement of Extreme Ultraviolet Solar Radiation and Associated Photoelectric Emissions from Solids, by Hans E. Hinteregger, pp. 347–363.

The Effects of Ultraviolet Radiation on Organic Film-forming Polymers, by J. E. Cowling, A. Alexander, F. Noonan, R. Kagarise and S. Stokes, pp. 364–377.

Interplanetary Dust Distribution and Erosion Effects, by David B. Beard, pp. 378–390.

Atomic and Molecular Sputtering, by Robert P. Stein, pp. 391–404.

Fluid Dynamics, Heat Transfer and MHD

Plasma Turbulence, by Leslie S. G. Kovasznay, *Space Tech. Labs., Inc., Phys. Res. Lab., STL/TR-60-0000-AE038,* Feb. 1960, 22 pp.

Transverse Pinch Oscillations, by Burton D. Fried, *Space Tech. Labs., Inc., Phys. Res. Lab., STL/TN-60-0000-09059,* March 1960, 8 pp.

Hardness of the Axially-symmetric Magnetic Piston, by Allan B. Schaffer, *Space Tech. Labs. Inc., Phys. Res. Lab., STL/TR-60-0000-09011,* Jan. 1960, 14 pp.

Surface Disturbances in Magnetohydrodynamics, by S. I. Syrovatskiy, *NASA Tech. Transl.* F-23, May 1960, 45 pp.

Compressible Flow Tables, k = 1.30, Isentropic Process, by C. Hoebich, *Army Rocket & Guided Missile Agency, Ordn. Missile Labs. Div., Design & Dev. Lab., Redstone Arsenal, ARGMA TN* 1H1N-10, April 1960, 87 pp.

Calculation of the Heating of Shells at High Speeds, by I. N. Sokolova, ARS JOURNAL, vol. 30, no. 4, April 1960, *Russian Suppl.,* pp. 375–379.

Concerning the Problem of the Influence of Internal Degrees of Freedom of Particles on the Transport Coefficients of a Multi-component Mixture of Gases, by E. V. Samuilov, ARS JOURNAL, vol. 30, no. 4, April 1960, *Russian Suppl.,* pp. 388–393.

Method of Calculation of the Transport Coefficients of Air at High Temperatures, by E. V. Stupochenko, B. V. Dotsenko, I. P. Stakhanov and E. V. Samuilov, ARS JOURNAL, vol. 30, no. 4, April 1960, *Russian Suppl.,* pp. 394–402.

Investigation of a Stationary Discontinuity Surface in an Electro-magnetic Field with a Gas Conductivity Jump, by G. A. Lyubimov, ARS JOURNAL, vol. 30, no. 4, April 1960, *Russian Suppl.,* pp. 416-420.

Heat and Mass Transfer in Aeronautical Engineering, by D. B. Spalding, *Aeron. Quarterly,* vol. 11, May 1960, pp. 105–136.

Recent Progress in Rarefied Gasdynamics, by S. A. Schaaf, ARS JOURNAL, vol. 30, no. 5, May 1960, pp. 443–447.

Hypersonic Shock Wave - Boundary Layer Interaction and Leading Edge Slip, by H. T. Nagamatsu and R. E. Sheer Jr., ARS JOURNAL, vol. 30, no. 5, May 1960, pp. 454–462.

International Symposium on Rarefied Gas Dynamics, Nice, 1959, Rarefied Gas Dynamics: Proceedings, edited by F. M. Devienne, Pergamon Press, N. Y., 1960, 442 pp.

Techniques of Measurement in Rarefied Gases, by I. Estermann, pp. 38–54.

Techniques of Measurements, Flow Visualization, by F. C. Hurlbut, pp. 55–68.

The Application of Supersonic Beam Sources to Low Density, High Velocity Experimentation, by Hermon M. Parker, A. R. Kuhlthau, Richardo Zapata and John E. Scott, pp. 69–79.

Theory of Rarefied Gases, by Harold Grad, pp. 100–138.

Recent Investigations of the Boltzmann Equation, by Eugene P. Gross, pp. 139–150.

The Boltzmann-Maxwell Equation as the Fundamental Equation of Gas Dynamics, by Toyoki Koga, pp. 151–160.

Experiment Versus Kinetic Theory for Rarefied Gases, by F. S. Sherman and L. Talbot, pp. 161–191.

Contributions to the Theory of Almost-free-molecule Flows, by V. C. Liu, pp. 239–245.

Theoretical Solutions to Some Nearly Free Molecular Problems, by D. R. Willis, pp. 246–257.

Aerodynamics of Rarefied Gases, by Ronald F. Probstein, pp. 258–275.

The Study of Boundary Conditions in Slip-flow Aerodynamics, by Robert E. Street, pp. 276–292.

Slip Flow over a Short Flat Plate, by J. A. Laurmann, pp. 293–316.

The Drag of a Sphere Which Moves at High Speed Through a Rarefied Gas, by Pierre Welander, pp. 317–328.

Aerodynamic Coefficients of a Pointed Cone at Angles of Attack in Rarefied Gas Flow, by V. A. Langelo and A. Lengyel, pp. 329–351.

On the Fundamental Aspects of Free Molecule Flow, by M. Z. Krzywblocki, pp. 352–366.

General Considerations on the Aerothermodynamics of Rarefied Gases, by Edmond A. Brun, pp. 367–382. (In French.)

Some Remarks on the Free Molecular Regime, by F. M. Devienne, pp. 383–386. (In French.)

Determination of Fundamental Atomic and Molecular Properties from Gas Dynamic Measurements, by Wayland C. Griffith, pp. 387–389.

Study of the Different Flow Regimes in Rarefied Gases by the Revolving Arm Method, by B. Crave, pp. 390–393. (In French.)

Plasma Dynamics—from Gas Dynamic Point of View, by Shih-I Pai, pp. 394–405.

A Discussion of Magnetic Boundary Layers with Boundary Conditions Assimilating Combustion, Blowing or Sublimation at the Wall, by Paul S. Lykoudis, pp. 407–415.

Continuum Theory and Rarefied Hypersonic Aerodynamics, by Ronald F. Probstein, pp. 416–431.

Numerical Comparison Between Exact and Approximate Theories of Hypersonic Inviscid Flow Past Slender Blunt Nosed Bodies, by Saul Feldman, ARS JOURNAL, vol. 30, no. 5, May 1960, pp. 463–468.

Solar Heating of a Rotating Cylindrical Space Vehicle, by A. Charnes and S. Raynor, ARS JOURNAL, vol. 30, no. 5, May 1960, pp. 479–484.

Flight Mechanics

The Long-time Satellite Rendezvous-Trajectory, by Louis W. Spradlin, *Aero/-Space Engng.,* vol. 19, June 1960, pp. 32–37.

Orbits for Planetary Satellites from Doppler Data Alone, by Armin J. Deutsch, ARS JOURNAL, vol. 30, no. 6, June 1960, pp. 536–542.

Angular Displacement of a Magnetized Sphere by the Terrestrial Magnetic Field During Vertical Descent, by Marvin H. Hewitt, ARS JOURNAL, vol. 30, no. 6, June 1960, p. 558.

An Approximate Analytic Solution of Re-entry Trajectory with Aerodynamic Forces, by Kenneth Wang and Lu Ting, ARS JOURNAL, vol. 30, no. 6, June 1960, pp. 565–566.

Elliptical Orbit Characteristics, by G. S. Gedeon and B. J. Greer, ARS JOURNAL, vol. 30, no. 6, June 1960, pp. 570–572.

The Orbits of Cosmic Rockets Towards the Moon, by L. I. Sedov, *Astronautica Acta,* vol. 6, no. 1, 1960, pp. 16–31.

Vehicle Design, Testing and Performance

Manned Space Flight—Present and Future Steps, by Robert R. Gilruth and H. Kurt Strass, *Aero/Space Engng.,* vol. 19, May 1960, pp. 16–17, 88.

The Military Test Space Station, by Col. Lowell B. Smith, *Aero/Space Engng.,* vol. 19, May 1960, pp. 18–19.

Atmospheric Entry of Manned Vehicles, by Carl Gazley, *Aero/Space Engng.,* vol. 19, May 1960, pp. 22–23, 90.

Design Criteria and Their Application to Economical Manned Satellites, by H. Hermann Koelle, Erich E. Engler and John W. Massey, *Aero/Space Engng.,* vol. 19, May 1960, pp. 24–25, 90.

Manned Scientific Orbital Laboratory, by M. Stoiko, G. G. Kayten and J. W. Dorsey, *Aero/Space Engng.,* vol. 19, May 1960, pp. 26–27, 92–93.

Some Factors Influencing the Selection of a Manned Space Station Concept, by Joseph H. Doss and Leo J. Montague, *Aero/Space Engng.,* vol. 19, May 1960, pp. 28–29, 94.

A Modular Concept for a Multimanned Space Station, by Saunders B. Kramer and Richard A. Byers, *Aero/Space Engng.,* vol. 19, May 1960, pp. 30–31, 90.

Man's Contribution to an Operational Space Station Concept, by M. A. Grodsky

and R. D. Sorkin, *Aero/Space Engng.*, vol. 19, May 1960, pp. 80–81.

The Australian Sounding Rockets Long Tom and Aeolus, by D. A. H. Bird, *J. Roy. Aeron. Soc.*, vol. 64, May 1960, pp. 277–289.

Studies on Dynamics and Instrumentation of the Holloman Track, *Air Force Missile Dev. Center, Holloman AFB, New Mexico, AFMDC-TR-59-8*, April 1959, 624 pp., 84 refs.

Calculation of the Flexural Rigidity of the Holloman Track, by Alfred W. Simon, pp. 1–8.

A Method of the Experimental Determination of the Parameters of the Holloman Track, by Alfred W. Simon, pp. 9–22.

The Experimental Determination of the Fundamental Parameters of the High-speed Test Track (Supplementary Report), by Alfred W. Simon, pp. 23–34.

Calculations Pertaining to a Moving Load on a Beam on an Elastic Foundation, by Alfred W. Simon, pp. 35–54.

Dynamic Analysis of a High-speed Track, by Stephen H. Crandall, pp. 55–78.

The Timoshenko Beam on an Elastic Foundation, by Stephen H. Crandall, pp. 79–106.

Deflection of the Holloman Track Under Static Load, by F. J. Calkum and Ray L. Larkins, pp. 107–122.

The Relation Between the Bending Strain and the Load for a Beam on an Elastic Foundation, by Alfred W. Simon, pp. 123–138.

Vibrations Set up by Moving Load in Track on Elastic Foundation, by Frank W. Bubb, pp. 139–200.

Track Vibration Study in Controlled Excitation, by Thomas P. Rona, pp. 201–232.

Vibration Level Measurements in the Supersonic Test Track, by Thomas P. Rona, pp. 233–246.

Transverse Beam Vibrations in Accelerated Rocket Sleds, by Thomas P. Rona, pp. 247–272.

Recommendations for the Strain Measurement Program at the Holloman Track, by Thomas P. Rona, pp. 273–280.

Statistical Analysis of Markings: Sled Run of 12 July 1956, by Paul R. Rider, pp. 281–292.

High Accuracy Velocity Measurements, by Thomas P. Rona, pp. 293–324.

Notes on Design of Sled Slippers for the High-speed Track, by S. Kyropoulos and M. E. Shank, pp. 325–334.

Some Considerations Concerning Lubrication of Slippers for the High-speed Track, by M. E. Shank, pp. 335–356.

Performance Characteristics of Lubrication for High-speed Tracks, by S. Kyropoulos, pp. 357–370.

A Study of the Aerodynamics of High-speed Sleds, by Joe R. Foote and S. Hoyer, pp. 371–402.

Some Remarks on the Optimum Speed Attainable with a Two-stage Sled, by Joe R. Foote, pp. 403–422.

Ram Wind Tunnel, by Harry L. Gephart, pp. 423–448.

Preliminary Investigation of the Aerodynamic Effects of Linear Acceleration as Related to the High-Speed Track, by Ray Holland Jr. and J. R. Foote, pp. 449–572.

Parameters for Rocket Sled Propulsion Systems, by H. J. Weigand and Ferdinand F. Kuhn, pp. 573–612.

Some Requirements for the Efficient Attainment of Range by Air-borne Vehicles, by M. Arens, *Technion, Israel Inst. Tech., Dept. Aeron. Engng., Haifa, Rep.* 3, Sept. 1959, 26 pp.

Investigation of the Low-subsonic Flight Characteristics of a Model of an All-wing Hypersonic Boost-glide Configuration Having Very High Sweep, by *Robert E. Shanks, NASA TN* D-369, June 1960, 21 pp.

The Tiros System on the Ground, by John E. Kiegler and Charles B. Oakley, ASTRONAUTICS, vol. 5, June 1960, pp. 44–45, 100–102.

Guidance and Control

On Automatic Controls, by S. Lefschetz, *RIAS, Baltimore, Md., Tech. Rep.* 60–9, March 1960, 6 pp.

Comparison of Some Actuation Methods for Attitude Control of Space Vehicles, by Walter Haeussermann, *Aero/Space Engng.*, vol. 19, May 1960, pp. 64–65.

Attitude Control of a Space Vehicle by a Gyroscopic Reference Unit, by Marvin L. Chatkoff and Lewis G. Lynch, *Aero/Space Engng.*, vol. 19, May 1960, pp. 66–67.

Attitude and Flight Path Control System for a Space Station Supply Vehicle, by J. Stalony-Dobrzanski and O. Imai, *Aero/-Space Engng.*, vol. 19, May 1960, pp. 68–69, 100, 102.

Orbital Rendezvous and Guidance, by Ernst A. Steinhoff, *Aero/Space Engng.*, vol. 19, May 1960, pp. 70–71, 106.

Rendezvous in Space—Effects of Launch Conditions, by Norman V. Petersen and Robert S. Swanson, *Aero/Space Engng.*, vol. 19, May 1960, pp. 72–73, 106–107.

Ascent Guidance for a Satellite Rendezvous, by T. B. Garber, *Aero/Space Engng.*, vol. 19, May 1960, pp. 74–75, 108.

A Guidance Technique for Achieving Rendezvous, by Philip G. Felleman and Norman E. Sears Jr., *Aero/Space Engng.*, vol. 19, May 1960, pp. 76–77.

Manned Control of Orbital Rendezvous, by E. Levin and J. Ward, *Aero/Space Engng.*, vol. 19, May 1960, pp. 78–79.

Longitudinal Range Control During the Atmospheric Phase of a Manned Satellite Reentry, by Arthur Assadourian and Donald C. Cheatham, *NASA TN* D-253, May 1960, 46 pp.

On the Analysis of the Stability of the Periodic Modes of Operation in Nonlinear Control Systems with Many Degrees of Freedom, by V. A. Taft, *Automation & Remote Control* (*trans. of Avtomatika i Telemekhanika*), vol. 20, no. 9, Sept. 1959, pp. 1132–1140.

On Designing Correcting Circuits for Automatic Control Systems in Accordance with the Mean Square Error Criterion, by V. I. Kukhtenko, *Automation & Remote Control* (*trans. of Avtomatika i Telemekhanika*), vol. 20, no. 9, Sept. 1959, pp. 1151–1160.

Experimental Determination of Automatic Control System Links' Transfer Functions by Means of Standard Electronic Models, by L. N. Darovskikh, *Automation & Remote Control* (*trans. of Avtomatika i Telemekhanika*), vol. 20, no. 9, Sept. 1959, pp. 1180–1187.

Frequency Elements of Remote Control, by I. N. Listiskaya, V. N. Mikhailovskii, K. D. Nadtochii and V. N. Okhotskva, *Automation & Remote Control* (*trans. of Avtomatika i Telemekhanika*), vol. 20, no. 9, Sept. 1959, pp. 1230–1234.

The Principles Involved in the Construction of an Automatic Radio Direction Finder, by Iu. A. Ierumhimovich, *Radio Engng.* (*trans. of Radiotekhnika*), vol. 14, no. 6, 1959, pp. 86–94.

The Transient Behavior of Nonlinear Systems, by Francis H. Clauser, *The Johns Hopkins University, Dept. Aeron.*, April 1960, 56 pp.

Self-adaptive Control Systems, by George J. Thaler, *Naval Postgrad. School, Tech. Rep.* 18, April 1960, 32 pp.

Dynamic Programming and Numerical Experimentation as Applied to Adaptive Control Systems, by M. Aoki, *Univ. Calif., Los Angeles, Dept. Engng., Rep.* 60–16, Feb. 1960, 215 pp.

Investigation of Third-order Contactor Control Systems with Two Complex Poles Without Zeros, by Irmgard Flügge-Lotz and Tomo Ishikawa, *NASA TN* D-428, June 1960, 69 pp.

The Theory of Correctional Manoeuvres in Interplanetary Space, by D. F. Lawden and R. S. Lang, *Astronautica Acta*, vol. 6, no. 1, 1960, pp. 48–60.

On Evaluating the Quality of Nonlinear Automatic Systems with Random Interference, by E. P. Popov, *Automation & Remote Control* (*trans. of Avtomatika i Telemekhanika*), vol. 20, no. 10, Oct. 1959 (June 1960), pp. 1281–1287.

L. S. Pontryagin Maximum Principle in the Theory of Optimum Systems, by L. I. Rozonoer, *Automation & Remote Control* (*trans. of Avtomatika i Telemekhanika*), vol. 20, no. 10, Oct. 1959 (June 1960), pp. 1288–1302; and vol. 20, no. 11, Nov. 1959 (June 1960), pp. 1405–1421.

The Problem of Optimizing Systems which Contain Essentially Non-linear Elements, by E. P. Merkulova, *Automation & Remote Control* (*trans. of Avtomatika i Telemekhanika*), vol. 20, no. 10, Oct. 1959 (June 1960), pp. 1303–1313.

Optimal Control of an Object with Two Controlling Stimuli, by E. A. Rozenman, *Automation & Remote Control* (*trans. of Avtomatika i Telemekhanika*), vol. 20, no. 10, Oct. 1959 (June 1960), pp. 1314–1318.

A Method of Synthesizing Linear Sampled-data Automatic Control Systems to Accord with Dynamic Criteria, by L. N. Vongin, *Automation & Remote Control* (*trans. of Avtomatika i Telemekhanika*), vol. 20, no. 10, Oct. 1959 (June 1960), pp. 1319–1328.

AC Servo Systems in Which the Signal Depends on the Error and Its Derivative, by N. P. Vlasov, *Automation & Remote Control* (*trans. of Avtomatika i Telemekhanika*), vol. 20, no. 10, Oct. 1959 (June 1960), pp. 1329–1334.

Graphicoanalytic Method of Computing Steady-state Speeds of Pneumatic Drives, by V. N. Dmitriev and V. I. Chernyshev, *Automation & Remote Control* (*trans. of Avtomatika i Telemekhanika*), vol. 20, no. 10, Oct. 1959 (June 1960), pp. 1335–1341.

Experimental Determination of Power Positioning Servo System Characteristics, by M. B. Tumarkin, *Automation & Remote Control* (*trans. of Avtomatika i Telemekhanika*), vol. 20, no. 10, Oct. 1959 (June 1960), p. 1396.

Instrumentation and Communications

Methods for the Control of Interfering Currents Originating at the Input of an Electrostatic Fluxmeter During Its Operation in a Conducting Medium, by I. M. Imyanitov and Ya. M. Shvarts, *NASA Tech. Transl.* F-16, May 1960, 10 pp.

Methods of Combatting Interfering Currents That Arise at the Input of an Electrostatic Fluxmeter Operating in a Conducting Medium, by I. M. Imyanitov and Ya. M. Shvartz, ARS JOURNAL, vol. 30, no

4, April 1960, *Russian Suppl.*, pp. 403–406.

Telebit—An Integrated Space Navigation and Communication System, by George E. Mueller, ASTRONAUTICS, vol. 5, May 1960, pp. 26–27, 88, 90, 92, 94, 96.

How Good Is the Lunik III Photography?, by Merton E. Davies, ASTRONAUTICS, vol. 5, May 1960, pp. 28–29, 112–113.

A Solid-state UHF Radar Transponder, by Lincoln Cartledge and G. Bradford Tiffany, ASTRONAUTICS, vol. 5, May 1960, pp. 30–31, 114–115.

A Recoverable Interplanetary Space Problem, by Milton B. Trageser, ASTRONAUTICS, vol. 5, May 1960, pp. 32–35, 116, 118–120.

Television Cameras for Space Exploration, by M. H. Mesner and J. R. Staniszewski, ASTRONAUTICS, vol. 5, May 1960, pp. 36–37, 126–130.

Maser, Iraser, and Laser, by Harold Lyons, ASTRONAUTICS, vol. 5, May 1960, pp. 38–39, 100–104.

Space Age Electronic Materials, by John W. Buttrey, ASTRONAUTICS, vol. 5, May 1960, pp. 40–41, 121–130.

Project Mercury Tape Recorder, by G. W. Boyer, ASTRONAUTICS, vol. 5, May 1960, pp. 44–45, 72, 74–75.

X-15 Operations: Electronics and the Pilot, by Neil A. Armstrong, ASTRONAUTICS, vol. 5, May 1960, pp. 42–43, 76, 78.

Signal Transmission Through Ionized Media; How Man-made Ionization Affects Communications, by W. A. Greenhow, *Electronics*, vol. 33, May 20, 1960, pp. 81–85.

Spectrometric Analysis of Missile Flights; Rapid-scan Spectrometer Provides Function-of-time Chart, by J. N. Day Jr., *Electronics*, vol. 33, May 20, 1960, pp. 86–88.

Measuring the Temperature of a Gas Downstream from a Shock Wave, by S. A. Losev and N. A. Generalov, *Instruments & Experimental Techniques* (*trans. of Pribory i Tek. Eksper.*), no. 3, May-June 1959 (published April 1960), pp. 454–455.

A Theory of Radar Scattering by the Moon, by T. B. A. Senior and K. M. Siegel, *J. Res., Nat. Bur. Standards, D. Radio Propagation*, vol. 64D, May-June 1960, pp. 217–230.

Theory of the Stagnation-point Langmuir Probe, by Lawrence Talbot, *Phys. Fluids*, vol. 3, March-April 1960, pp. 289–298.

The Design of Automatic Gain Control in Transistor Amplifiers, by Ye. P. Dement'ev, *Radio Engng.* (*trans. of Radiotekhnika*), vol. 14, no. 6, 1959, pp. 51–59.

Some Questions on the Dispersion of Radiowaves in the Ionosphere, by V. D. Gusev, *Radio Engng. & Electronics* (*trans. of Radiotekhnika i Elektronika*), vol. 4, no. 1, 1959 pp. 15–22.

The Investigation of Winds and Nonuniformity in the Ionosphere by a Radio Astronomical Method, by V. V. Vitkevich and Ia. L. Kokurin, *Radio Engng. & Electronics* (*trans. of Radiotekhnika i Elektronika*), vol. 4, no. 1, 1959, pp. 23–29.

Signal Detection Against a Background of Normal Noise and Random Reflections, by V. D. Zubakov, *Radio Engng. & Electronics* (*trans. of Radiotekhnika i Elektronika*), vol. 4, no. 1, 1959, pp. 42–59.

Maximum Noise-proofing of the Radioreception of Signals with Amplitude Frequency and Phase Manipulation, by N. P. Teplov, *Telecommunications* (*trans. of Elektrosvyaz'*), no. 1, 1959, pp. 34–47.

Bulletin of Stations for Optical Observations of Artificial Earth Satellites, *NASA Tech. Transl.* F-19, May 1960, 50 pp. (Translated from *Iskusstvennye Sputniki Zemli*, no. 7, Moscow, Acad. Sci. USSR, 1959.)

Artificial Earth Satellites, vols. I & II, ed. by I. V. Kurnosova, transl. from Russian, Plenum Press, N. Y., 1960, 120, 107 pp.

Optical Methods for the Observation of Artificial Earth Satellites, by I. S. Shklovskii, vol. I, pp. 56–63.

Use of the Doppler Effect for Determining Orbit Parameters of an Artificial Earth Satellite, by V. A. Kotel'nikov, V. M. Durbrovin et al., vol. I, pp. 64–78.

An Acoustical Method for the Measurement of the Mechanical Parameters of Meteorites, by M. A. Isakovich and N. A. Roi, vol. II, pp. 105–107.

Pulsating Flow Measurement—Today, Part II, by P. H. Stirling and Henry Ho, *Ind. Engng. Chem.*, vol. 52, June 1960, p. 75–76A.

Variable Capacitance Liquid Level Sensors, by L. Bruce Wilner, *Rev. Sci. Instr.*, vol. 31, May 1960, pp. 501–507.

Satellite Astronomical Observatories, by Nancy G. Roman, *Aero/Space Engng.*, vol. 19, May 1960, pp. 86–87.

Atmospheric and Space Physics

Some Results of the Determination of the Structural Parameters of the Atmosphere Using the Third Soviet Artificial Earth Satellite, by V. V. Mikhnevich, B. S. Danilin, A. I. Repnev and V. A. Sokolov, *NASA Tech. Transl.* F-13, May 1960, 20 pp. *Also* ARS JOURNAL, vol. 30, no. 4, April 1960, *Russian Suppl.*, pp. 407–413.

Analysis of the Moon's Surface by Nuclear Reactions, by E. F. Martina and Carlton D. Schrader, *Space Tech. Labs., STL/TR-60-0000-00078*, April 1960, 31 pp.

International Geophysical Year Bibliography of Literature in the Russian Language for 1958, compiled by R. F. Zatrutina and Z. M. Mikhaylova, edited by B. I. Silkin, *NASA Tech. Transl.* F-12, May 1960, 75 pp.

Some Aspects of Lunar Geology, by J. Green, *Astronaut. Sci. Rev.*, vol. 2, no. 1, Jan.–March 1960, pp. 9–12, 16.

Ice in Space, by Donald H. Robey, *J. Brit. Interplanet. Soc.*, vol. 17, Jan.-Feb. 1960, pp. 205–215.

Energy Dependence of Transient Changes in the Primary Cosmic-ray Spectrum, by K. G. McCracken, *Phys. Rev.*, vol. 117, March 15, 1960, pp. 1570–1579.

Stability of an Idealized Atmosphere, I: Discussion of Results, by K. M. Case, *Phys. Fluids*, vol. 3, March-April 1960, pp. 149–154.

Stability of an Idealized Atmosphere, II: Zeros of the Confluent Hypergeometric Function, by Freeman J. Dyson, *Phys. Fluids*, vol. 3, March-April 1960, pp. 155–157.

Artificial Earth Satellites, vols. I & II, ed. by I. V. Kurnosova, transl. from Russian, Plenum Press, N. Y., 1960, 120, 107 pp.

Cosmic-ray Measurements with Artificial Earth Satellites, by S. N. Vernov, N. L. Grigorov et al., vol. I, pp. 5–9.

Determination of Atmospheric Density from the Observed Deceleration of the First Artificial Earth Satellites, by M. L. Lidov, vol. I, pp. 10–24.

Determination of Density of the Upper Atmosphere from Secular Variations of Orbital Elements of the First Two Artificial Earth Satellites, by P. E. El'yasberg, vol. I, pp. 25–29.

Rocket Measurement of Electron Concentration in the Ionosphere by Means of an Ultra-short-wave Dispersion Interferometer, by K. I. Gringauz, vol. I, pp. 79–84.

Distribution of Electron Density as a Function of Height from Data of Experiments with Rockets and Artificial Earth Satellites: Effect on Propagation of Radio Waves, by L. A. Zhekulin, vol. I, pp. 85–101.

Some Results of Measurements of the Thermo-dynamic Parameters of the Stratosphere Obtained with the Aid of Meteorological Rockets, by E. G. Shvidkovskii, vol. II, pp. 12–19.

Disturbances Occurring in the Gaseous Medium During the Flight of a Satellite, by B. A. Mirtov, vol. II, pp. 20–31.

Preliminary Results of a Determination of the Density of the Atmosphere Above 100 km, by V. V. Mikhevich, vol. II, pp. 32–39.

An Investigation of the Ionic Composition of the Earth's Atmosphere Using Rockets and Satellites, by V. G. Istomin, vol. II, pp. 40–44.

Soviet Ionospheric Studies Using Rockets and Artificial Earth Satellites, by V. I. Krasovskii, vol. II, pp. 45–62.

Preliminary Report on Geomagnetic Measurements Carried out from the Third Soviet Artificial Earth Satellite, by S. Sh. Dolginov, L. N. Zhuzgov and N. V. Pushkov, vol. II, pp. 63–67.

Micrometeorite Studies Using Rockets and Satellites, by O. D. Komissarov, T. N. Nazarova et al., vol. II, pp. 68–74.

The Search for Corpuscles with the Help of the Third Artificial Earth Satellite, by V. I. Krasovskii, Yu. M. Kushnir et al., vol. II, pp. 75–77.

The Study of the Soft Component of Cosmic Rays Outside of the Earth's Atmosphere, by S. N. Vernov, P. V. Vakulov et al., vol. II, pp. 78–89.

The Heavy Nuclei of the Primary Cosmic Radiation, by L. V. Kurnosova and L. A. Razorenov, vol. II, pp. 90–95.

Human Factors and Bioastronautics

Selection of Personnel for Manned Space Stations, by Romney H. Lowry, *Aero/Space Engng.*, vol. 19, May 1960, pp. 32–33.

Work and Living Space Requirements for Manned Space Stations, by Fred A. Payne, *Aero/Space Engng.*, vol. 19, May 1960, pp. 34–35.

Gravity Problems in Manned Space Stations, by Carl C. Clark and James D. Hardy, *Aero/Space Engng.*, vol. 19, May 1960, pp. 36–39.

Atmosphere Control, by Carey B. Jackson, George R. Roush Jr. and Robert M. Bovard, *Aero/Space Engng.*, vol. 19, May 1960, pp. 40–41, 94, 96.

Design of an Operational Ecological System, by Eugene B. Konecci and Neal E. Wood, *Aero/Space Engng.*, vol. 19, May 1960, pp. 42–43, 96.

Space and Man, by W. M. Meyer, *Raketentechnik und Raumfahrtforschung*, vol. 4, no. 2, June 1960, pp. 37–40. (In German.)

Artificial Earth Satellites, vols. I & II, ed. by I. V. Kurnosova, transl. from Russian, Plenum Press, N. Y., 1960, 120, 107 pp.

Research on Animal Flight in an Artificial Earth Satellite, by V. N. Chernov and V. I. Yakovlev, vol. I, pp. 102–120.

Benvenuto Cellini (1500-1571), one of the world's most revered artists, was also a pioneer metallurgist. His scientific methods of casting bronze and alloys for his statues are nearly as well known as his great artistry.

But Cellini had his troubles with his furnace, or *manica*. In his autobiography he says, "...all of a sudden an explosion took place, as though a thunderbolt had formed and been discharged amongst us..."

Here at CEA, our scientists and engineers analyze advanced systems. For example, we supply missile and ground support equipment manufacturers with detail data on the response of their structures to thermal and aeroelastic environments. In our studies, we use an invention that would have deeply impressed Cellini: our Direct Analog Computer.

COMPUTER ENGINEERING ASSOCIATES, INC.
350 North Halstead Pasadena, California
ELgin 5-7121

Index to Advertisers

ACADEMIC PRESS, INC.....926, 927

AEROJET-GENERAL CORP.....
.....Back cover
D'Arcy Advertising Co., Los Angeles, Calif.

ALLIED CHEMICAL CORP., GENERAL CHEMICAL DIV...
.....Second cover
Kastor, Hilton, Chesley, Clifford & Atherton, Inc., New York, N. Y.

NITROGEN DIVISION..... 987
G. M. Basford Co. New York, N. Y.

AMERICAN GEOPHYSICAL UNION..... 921

COMPUTER ENGINEERING ASSOC..... 992
Guerin, Johnstone, Jeffries, Inc., Los Angeles, Calif.

CONVAIR, A DIV. OF GENERAL DYNAMICS CORP....Third cover
Lennen & Newell, Inc., Beverly Hills, Calif.

EXCELCO DEVELOPMENTS.... 925
Melvin F. Hall Advertising Agency, Inc., Buffalo, N. Y.

LOS ALAMOS SCIENTIFIC LABORATORY..... 924
Ward Hicks Advertising Agency, Inc., Albuquerque, N. Mex.

PHILOSOPHICAL LIBRARY..... 923
Franklin Spier, Inc., New York, N. Y.

PRECISION PRODUCTS DEPT., NORTRONICS DIV., NORTHROP CORP..... 922
S. Gunnar Myrbeck & Co., Inc., Quincy, Mass.